
Università degli Studi della Calabria
Facoltà di Scienze Matematiche Fisiche e Naturali
Dipartimento di Chimica

Dottorato di ricerca in Metodologie Chimiche Inorganiche
XXIII ciclo

AREA 03 -Scienze Chimiche, SSD-CHIM03/Chimica generale ed inorganica

Doctoral Dissertation

***On the roles of metal ions in
bioinorganic chemistry:
computational insights***

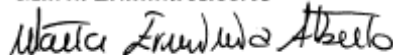
Supervisore e Coordinatore

Prof. Nino Russo



Candidata

Marta Erminia Alberto



A.A. 2009-2010

Preface

The importance of metal ions in many biological processes has become increasingly evident over the last twenty five years. The understanding of the multiple roles of metals within ever more complex biological pathways is one of the main goal of the modern biological inorganic chemistry. Metal ions have unique chemical properties that allow them to play diverse roles in cellular biochemistry.

A large number of metal ions are essential nutrients and indispensable for living organisms (Fe, Co, Cu, Mn, Mo, Zn etc.), promoting the catalysis of important chemical reactions and performing specific physiological functions acting as cofactors in *metalloenzymes*. The active sites of a significant fraction of all proteins and enzymes contain one or more metal ions, superbly and perhaps optimally conditioned by protein structure and environment toward accomplishment of evolutionarily directed function. The precise role of protein scaffold, catalytic or structural, is still not well defined, being it subject of a heated debate. More metals in enzyme's active site can work more or less independently, being required for distinct functions either structural or catalytic, or alternatively, catalyzing different steps in a multistep sequence. Therefore, one of the central challenge in this interdisciplinary field between inorganic chemistry and biochemistry is to deduce how metal ions and their scaffolds promote difficult biochemical reactions

On the other hand, many metal ions are becoming progressively more widespread as agents for diagnosis. Interest in metal-based radiopharmaceuticals as ^{99m}Tc , nowadays the most widely used radioisotope for diagnosing diseased organs, and magnetic resonance imaging contrast agents as Gd, is exceptionally strong. Perhaps the greatest benefit of medicinal bioinorganic chemistry has been the discovery of the therapeutic effect of some metals against a wide range of diseases and metabolic disorders. In this field,

the successful development of *platinum-containing drugs* for the treatment of cancer has played a major role in the rapid growth and development of biological inorganic chemistry over the last decades. Enormous progress has been made in the elucidation of the mode of action of cisplatin, on the detailed knowledge of the Pt-DNA adducts and on the kinetics of binding to protein and purine bases. Detailed knowledge of the reactions of new platinum and non-platinum compounds on their complicated route from injection or oral administration to the DNA of the tumor cell is crucial for the development of improved antitumor agents.

The proper description of metal containing systems remains a challenge for quantum chemistry. Computational transition metal chemistry today is almost synonymous with DFT for medium-sized molecules. In the fundamental fields of understanding mechanisms of reactions of transition metal complexes, it is generally accepted that these methods give a reliable descriptions of the geometries and relative energies. The opening section of this thesis, "*Theoretical Background*", briefly introduces the DFT approach to solving the many-electron problem. Several approximate functionals to calculate the exchange-correlation energy $E_{xc}[\rho]$ and basis sets available are discussed in the text. The computational protocols used for our works were also presented.

With the aim to move towards a broader understanding of how metals function within biological systems, our research has been planned with a twofold purpose: *i*) investigate the mechanism by which platinum-based drugs induce apoptosis in tumor cells and *ii*) explore the ability of binuclear metal ion center in enzymes in promoting important biochemical reactions.

The thesis is then structured in two main *Parts*.

The 3 chapters of the *Part1*, deal with the mechanism of action of Pt(II) anticancer drugs since their non-enzymatic conversion to active derivatives by hydrolysis to their subsequent binding to purine DNA bases. In particular, *Chapter 1* introduces the current understanding of the biochemical mechanisms of action of the world's best selling anticancer drug cisplatin. The steps of triggering cell death by cisplatin and its analogues are presented and

discussed. *Chapter 2* gives a topical account of the efforts made in order to overcome the drawbacks of cisplatin with a primary focus on the development of new derivatives with improved pharmacological properties. The classical structure-activity rules that directed the synthesis of these new derivatives and the description of the compounds currently registered for clinical use represent the early sections of this chapter. The purpose of our research concerning the so called *classical* Pt(II) anticancer drugs is then introduced followed by a brief description of each computational work performed.

Chapter 3 illustrates the recent strategy directed toward the rational design of unconventional complexes that violate the original structure-activity relationships, but yet showing antitumor activities. In this field, there is a considerable research focused on the marginalized trans Pt(II) derivatives and on the development of more effective non-platinum drugs. Together with the advances in this area, our computational studies on these novel drugs will be discussed along the chapter.

Attempts in the understanding how metal ions and their scaffolds can promote biochemical reactions are explored in the *Part 2* of this thesis (*Chapter 4*). One or more metal ions are optimally conditioned by protein structure and environment, in order to accomplish a specific biological function. The crucial requirement of binuclear center in metallohydrolases was explored by examining two related enzymes, purple acid phosphatases (PAPs) and prolidase. The quantum chemical modeling of such enzymes is discussed. Our work can contribute to the common effort to derive a better description of the steps involved in the hydrolytic reaction mechanisms and concerning the role of each metal ion in promoting important enzymatic reactions. Together with the elucidation of the catalytic mechanisms of these binuclear metallohydrolases, one of the main features addressed in this thesis is the evaluation of the effects of various bivalent ions into the enzyme's active site. Chapter 4 also canvasses a range of binuclear centers in prolidase enzyme, providing insights on how the identity of metal ions can modulate the catalytic efficiency.

List of Papers included in this thesis

- I. **The Second-Generation Anticancer Drug Nedaplatin: A Theoretical Investigation on the Hydrolysis Mechanism**
Marta E. Alberto, Maria F. Lucas, Matej Pavelka, and Nino Russo,
J. Phys. Chem. B **2009**, 113, 14473;
- II. **Neutral and Acidic Hydrolysis Reactions of the Third Generation Anticancer Drug Oxaliplatin**
Maria F. Lucas, Matej Pavelka, Marta E. Alberto and Nino Russo,
J. Phys. Chem. B **2009**, 113, 831;
- III. **The Degradation Pathways in Chloride Medium of the Third Generation Anticancer Drug Oxaliplatin**
Marta E. Alberto, Maria F. Lucas, Matej Pavelka and Nino Russo,
J. Phys. Chem. B **2008**, 112, 10765;
- IV. **Which one among the Pt-containing anticancer drugs forms more easily monoadducts with G and A DNA bases? A comparative study between oxaliplatin, nedaplatin and carboplatin**
Marta E. Alberto, Valeria Buteria and Nino Russo, *manuscript*;
- V. **Methionine Ligand selectively promotes monofunctional adducts between *Trans*-EE platinum anticancer drug and Guanine DNA base**
Marta E. Alberto and Nino Russo,
Chem. Commun. **2010**, DOI: 10.1039/c0cc03605f
- VI. **Rhenium(IV) Compounds act as Anticancer Agents**
José Martínez-Lillo, Teresa F. Mastropietro, Rosamaria Lappano, Antonio Madeo, Marta E. Alberto, Nino Russo, Marcello Maggiolini, and Giovanni De Munno, submitted;
- VII. **The Catalytic Mechanism of Fe(III)-Zn(II) Purple Acid Phosphatase: a Theoretical Investigation**
Marta E. Alberto, Tiziana Marino, Maria J. Ramos and Nino Russo,
J. Chem. Theory Comput. **2010**, 6, 2424;
- VIII. **Can human prolidase enzyme use different metals for full catalytic activity?**
Marta E. Alberto, Monica Leopoldini, Nino Russo, *submitted*

List of Papers not included in this thesis

IX. Absorption Spectra of Xantene Dyes and Analogues

Marta Alberto and Nino Russo

Science and Supercomputing in Europe, **2007**, 79-82, ISBN/ISSN: 978-88-86037-21-1;

X. The mutual influence of non-covalent interactions in π -electron deficient cavities: the case of anion recognition by tetraoxacalix[2]arene[2]triazine

Marta E. Alberto, Gloria Mazzone, Nino Russo and Emilia Sicilia

Chem. Commun., **2010**, 46, 5894.

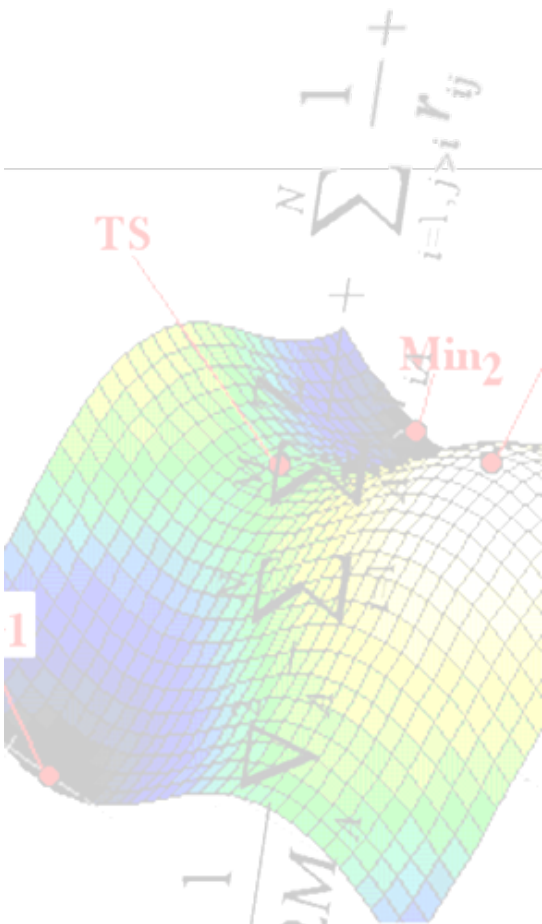
Table of Contents

Preface	iii
List of Papers included in this thesis	vi
List of Papers not included in this thesis	vii
Theoretical Background	1
Opening Remarks.....	3
Density Functional Theory.....	
Exchange-Correlation Functional	8
Hybrid Density Functionals employed in this thesis	9
Basis sets and pseudopotentials	11
Bibliography	15
<i>Part 1: Overview</i>	17
1 General Remarks on Pt(II) Anticancer Drugs	19
Introduction	21
1.1 Biochemical Mechanism of Action.....	23
1.1.1 Cellular Uptake	24
1.1.2 Drug Activation by Hydrolysis	24
1.1.3 DNA: A Primary target for Platinum Drugs.....	25
1.1.3 Inhibition of transcription by Pt(II) Antitumor Complexes.....	28
Bibliography	30
2 “Classical Pt(II) Anticancer Drugs”: <i>Understanding their mechanisms of action by Computational Studies</i>	33
Introduction	35
2.1 Second-Generation –Overcoming Toxicity-	36
2.1.1 Carboplatin.....	36
2.1.2 Nedaplatin	38
2.2 Third-Generation –Overcoming Cisplatin Resistance.....	38
2.1.2 Oxaliplatin	38
2.3 Study Aims	40
2.4 Common Mechanistic Details.....	41
2.5 Hydrolysis Mechanisms of the Second- and Third- Generation anticancer drugs Nedaplatin and Oxaliplatin.....	42
2.6 Chlorination Mechanism	44
2.7 Interaction of of the Second- and Third- Generation anticancer Drugs with DNA bases.....	45
Bibliography	46

3	“Non-Classical Anticancer Drugs”: Computational Studies on new-developed antitumor complexes.....	49
	Introduction	51
	3.1 Trans Compounds.....	52
	3.1.1 Computational Studies on <i>Trans-EE</i> and <i>Trans-EE/Met</i> reaction mechanisms.....	54
	3.2 Non-Platinum Compounds.....	56
	3.2.1 Promising Re(IV) complexes as anticancer drugs: an experimental and computational investigation	58
	Bibliography	60
	Appendix A	63
	Paper I.....	65
	Paper II	79
	Paper III	89
	Paper IV	95
	Paper V	111
	Paper VI	129
	<i>Part 2: Overview.....</i>	<i>149</i>
4	Metallohydrolases: On the functional roles of binuclear metal center in enzyme’s active site.....	151
	Introduction	153
	4.1 Binuclear Metallohydrolases.....	154
	4.2 Modeling enzymatic reaction: Cluster Models.....	155
	4.3 Purple Acid Phosphatases.....	157
	4.3.1 Computational Investigation on the catalytic mechanism of Fe(III)-Zn(II) PAP.....	158
	4.3.1.1 rkbPAP Active Site and Cluster Model	159
	4.3.1.2 Function of binuclear metal center in the catalytic process	160
	4.3.1.3 Energetic of reaction.....	162
	4.4 Prolidases.....	164
	4.4.1 Computational Investigation of human prolidase: can it use different metals for full catalytic activity?.....	165
	4.4.1.1 Prolidase Active Site and Cluster Model	167
	4.4.1.2 Function of binuclear metal center in the catalytic process	167
	Bibliography	170

Appendix B	173
Paper VII.....	175
Paper VIII.....	197

Theoretical Background



The important role of computational methods in contemporary inorganic chemistry and the ubiquitous character of metal ions in the environment and living organisms, led to the fast development of theoretical modeling of transition metal chemistry. Computational investigation have proven to be an essential tool for the study of chemical reactions involving transition metal complexes. Among these, not only the elementary reactions such as substitution, migratory insertion, hydrogen transfer, oxidative addition/reductive elimination, metathesis, and nucleophilic addition but also reactions concerning catalytic processes.

Many important chemical and physical properties of the chemical systems can be predicted from first principles by various computational techniques.

The density functional theory (DFT) methods can be considered the state of the art of the modern theoretical approaches, and fundamental tool for the understanding of transition metal reaction mechanisms. It provides an excellent compromise between accuracy of the results and the requested computational efforts. The relativistic effective core potentials (RECPs) generated from the relativistic HF atomic core are especially valuable for heavy transition metal complexes due to the incorporation of the most important relativistic effect as well as the reduction of computational cost through the replacement of core electrons by means of pseudopotentials, which elevates the research efficiency. The solvent effect, which was neglected in previous theoretical reaction studies, should also be considered in these basic solution reactions to simulate the true experimental reaction process, especially in cases where the solvent effect is eminent.

Opening remarks

A molecular system in a stationary state is fully characterized by the solution to the many-electron Schrödinger equation, which represents the fundamental postulate in quantum mechanics. The time-independent form of it is usually sufficient to be utilized for the ground state chemistry. The Schrödinger equation is an eigenvalue equation

$$H|\Phi\rangle = E|\Phi\rangle \quad (1)$$

where H is a hermitian operator called Hamiltonian, $|\Phi\rangle$ is the wavefunction and E is the energy. Quantum mechanical computation is based on solving that equation. Nevertheless, while the Schrödinger equation is powerful enough to describe almost all properties of systems, it is too complex to solve for all but the simplest systems. The equation is unique for each system as the Hamiltonian for different systems are different. For a general N electrons and M nuclei system, the Hamiltonian operator contains kinetic and potential energy

$$\hat{H} = -\sum_{i=1}^N \frac{1}{2} \nabla_i^2 - \sum_{A=1}^M \frac{1}{2M_A} \nabla_A^2 - \sum_{i=1}^N \sum_{A=1}^M \frac{Z_A}{r_{iA}} + \sum_{i=1, j>i}^N \frac{1}{r_{ij}} + \sum_{A=1, B>A}^M \frac{Z_A Z_B}{R_{AB}} \quad (2)$$

The first term in eq. (2) is the operator for the kinetic energy of the electrons while the second one is the analogue operator for the nuclei; the third term represent the coulomb attraction between electrons and nuclei; the last two terms represent the repulsion between electrons and between nuclei, respectively.^{1,2}

Unfortunately, the exact resolution of such equation is only possible for systems containing just one electron. Of course, the majority of chemical

species lie outside this reduced set, and the time-independent Schrödinger equation has to be solved under certain approximations. The principal one adopted in quantum chemistry is the Born-Oppenheimer approximation,³ whose mathematical consequence is that the total molecular wavefunction can be separated into a product of an electronic wavefunction and a nuclear one. The justification for this separation is that electrons are much lighter than nuclei and thus, under most circumstances, they may be considered as moving under the field of fixed nuclei. As a consequence, the kinetic energy of nuclei in eq. (2) can thus be ignored and the nucleus-nucleus repulsion can be considered to be constant for certain geometry. The description of the motion of N electrons in the field of M point charges is then described by the so-called electronic Hamiltonian:

$$\hat{H}_{\text{elec}} = -\sum_{i=1}^N \frac{1}{2} \nabla_i^2 - \sum_{i=1}^N \sum_{A=1}^M \frac{Z_A}{r_{iA}} + \sum_{i=1, j>i}^N \frac{1}{r_{ij}} \quad (3)$$

The solution of resulting Schrödinger equation involving the electronic Hamiltonian

$$H_{\text{elec}} \Phi_{\text{elec}} = E_{\text{elec}} \Phi_{\text{elec}} \quad (4)$$

is the electronic wavefunction, which describes the motion of the electrons depending explicitly on the electronic coordinates but parametrically on the nuclear coordinates, as well as the electronic energy.

For different arrangement of the nuclei, Φ_{elec} is a different function of the electronic coordinates. One important limitation of the Born-Oppenheimer separation is that the total wavefunction is limited to one electronic surface, i.e. a particular electronic state. It breaks down when two (or more) electronic states are close in energy at particular nuclear geometries. In such situations, a “non-adiabatic” wavefunction must be used. Moreover, in writing the Hamiltonian as sum of electronic kinetic and potential energy terms, relativistic effects have been ignored. These are normally negligible for lighter elements ($Z < 36$) but not for the 4th period of higher. Nevertheless, spin-dependent terms,

e.g. spin-orbit or spin-spin coupling may be calculated as corrections after the resolution of the electronic Schrödinger equation.

Once the electronic problem has been solved, it is possible to solve the motion of the nuclei under the same assumptions. The electronic coordinates can be reasonable replaced by their average values, averaged over the electronic wavefunction, since the electrons move much faster than the nuclei. This then generates a nuclear Hamiltonian for the motion of the nuclei in the average field of the electrons

$$\hat{H}_{\text{elec}} = -\sum_{A=1}^M \frac{1}{2M_A} \nabla_A^2 + E_{\text{elec}}(\{R_A\}) + \sum_{A=1, B>A}^M \frac{Z_A Z_B}{R_{AB}} \quad (5)$$

The solution of the corresponding nuclear Schrödinger equation

$$H_{\text{nucl}} \Phi_{\text{nucl}} = E \Phi_{\text{nucl}} \quad (6)$$

describes the vibration, rotation and translation of a molecule and E , which is the Born-Oppenheimer approximation to the total energy of the (1), includes electronic, vibrational, rotational and translational energy.

It is worth noting that the sum of $E_{\text{elec}}(\{R_A\})$ and the nucleus-nucleus repulsion, namely $E_{\text{tot}}(\{R_A\})$, provides a potential for nuclear motion. This function constitutes a **potential energy surface**.² Thus the nuclei in the Born-Oppenheimer approximation move on a potential energy surface obtained by solving the electronic problem. The concept of potential energy surfaces is fundamental in quantum chemistry, its topology determines the stability and reactivity of any chemical system and its detailed knowledge gives an understanding of the reaction mechanisms for a given chemical process.

Density Functional Theory

Ground-State DFT is a completely different approach to solving the many-electron problem than the traditional solution of Schrödinger equation since the electron density $\rho(r)$, a function of only 3 variables, is used as the descriptor of an electronic state. Employing the electron density to extract information about a given system can appear physically more intuitive than a wavefunction based approach since it is measurable. However, it is not obvious that there is a unique relationship between the electron density of a system and its properties. Such relation was introduced by Hohenberg-Kohn (1964)⁴ and it is the basic framework for modern density functional methods. The first Hohenberg-Kohn theorem states that every observable of a stationary quantum mechanical system can be calculated, in principle exactly, from the ground-state density $\rho(r)$, i.e., every observable can be written as a functional of the ground-state density. They concluded that the ground-state density $\rho(r)$ uniquely determines the external potential V_{ext} (up to an additive constant). The latter, in turn, uniquely determines the electronic Hamiltonian because the remaining operators, the kinetic energy operator (T) and the electron-electron repulsion operator (U_{ee}), depend exclusively on the coordinates of the electrons and their forms are the same for all systems, depending only on the number of electrons. For this reason, they are grouped together into the universal functional $F[\rho]$. Thus, the total electronic energy expressed as a functional of the density of the system depends only on the number of electrons, N, and the external potential.

$$E_{\text{tot}}[\rho(r)] = F[\rho(r)] + V_{\text{ext}}[\rho(r)] \quad (7)$$

Moreover, an energy variational principle for this functional, in analogy to the variational principle for wavefunctions, was established in the second HK theorem. This implies that any calculated energy is always higher than or equal to the true ground state energy.

The Hohenberg-Kohn theorems, although laid a rigorous foundation for DFT as it is known today, do not tell us how to calculate E_{tot} from ρ since the exact form of the functional $F[\rho(r)]$ is not known and represent the major part of complexities of the many-electron problems.

Kohn and Sham ⁵ invented an indirect approach to this functional and thereby turned DFT into a practical tool for rigorous calculations. They develop an orbital-based scheme in which the total kinetic energy (T) is divided into two parts, the kinetic energy (T_0) of a non-interacting system of N-electrons (with the same density as the real interacting system) and a residual part (T_u), which is the missing one to accurately describe the real interacting system ($T = T_0 + T_u$).

The second part of the $F[\rho(r)]$, the electron-electron repulsion consists of a classical Coulomb interaction (J) and a non-classical e-e contribution (V_q)

$$U_{ee}[\rho] = J[\rho] + V_q[\rho] \quad (8)$$

As a consequence, the $F[\rho(r)]$ functional can be written as:

$$F[\rho(r)] = T_0[\rho] + J[\rho] + T_u[\rho] + V_q[\rho] \quad (9)$$

The missing unknown part of the kinetic energy $T_u[\rho]$ and the non-classical electron-electron interaction energy $V_q[\rho]$ can be combined to form an exchange-correlation functional ($E_{xc}[\rho]$). The total energy can finally be presented as:

$$E[\rho(r)] = T_0[\rho] + J[\rho] + V_{\text{ext}}[\rho] + E_{xc}[\rho] \quad (10)$$

The first three terms, the kinetic energy of the non-interacting system, the classical Coulomb repulsion and the nuclear-electron attraction can be calculated explicitly. The exchange-correlation term, $E_{xc}[\rho]$ incorporates all unknown contributions to the total Energy (the non-classical effect of self-interaction correction, exchange and correlation). The main challenge of the

density functional theory is to find an appropriate way to accurately describe $E_{xc}[\rho]$.⁶

Up to now, there is no exact solution of this functional, nevertheless approximate functional have been proposed. One approach to calculate the exchange-correlation energy $E_{xc}[\rho]$ is based on assuming that the density ρ varies very slowly and locally with position and can thus be treated as a homogeneous electron gas. This is referred to as the Local Spin Density Approximation (LSDA).⁷ The exchange energy of an uniform electron gas $\epsilon_{xc}(\rho)$ can be computed exactly. An accurate expression for $\epsilon_{xc}(\rho)$ has been found by Vosko, Wilk and Nusair (VWN).⁸ However, while the assumed homogeneous electron distribution works well for certain systems, it is not useful for most molecules, where the density is far from being homogeneous.

To yield accurate chemical description, one usually has to add corrections by means of terms involving the gradient of ρ . These corrections are added to both exchange and correlation terms to form the so-called Generalized Gradient Approximation (GGA).

➤ Exchange-Correlation Functionals

The development of GGA methods, has followed two main lines. The first one, also credited as semiempirical approach, has been very successful in chemistry and it was initially proposed by Becke.⁹⁻¹⁴ The basic idea is to choose a flexible mathematical functional form depending on one or more parameters and then to perform a numerical fitting procedures of these parameters to molecular thermochemical data. Exchange functionals that follow this philosophy include Becke88 (B),¹⁵ Perdew-Wang (PW),¹⁶ modified-Perdew-Wang (MPW),^{16,17} OptX (O),¹⁸ and X.¹⁹

The second group of GGA methods, advocated by Perdew and also called nonempirical approach, considers that the development of exchange-correlation functionals should be anchored in basic principles derived from quantum mechanics, including scaling relations, correct limits for high and low

densities, correct LSDA limit for slowly varying densities, and the fulfillment of exact relations on the exchange and correlation holes. Among the exchange functionals based on this principle are Perdew 86 (P),²⁰ Perdew-Burke-Ernzerhof (PBE),²¹ and modified-Perdew-Burke-Ernzerhof (mPBE).^{21,22}

For the correlation functional, several different formulations have been developed. Examples of GGA correlation functional include Becke 88 (B88),²³ Perdew 86,²⁰ Perdew-Wang 91 (PW91),²⁴ and the extremely popular Lee-Yang-Parr (LYP),²⁵ which is constructed from the Colle-Salvetti correlation energy formula.²⁶ More recently, a new class of very promising DFT functional based on the GGA was developed by including additional semilocal information beyond the first-order density gradient contained in the GGAs. These methods, termed meta-GGA (M-GGA), depend explicitly on higher order density gradients, or typically on the kinetic energy density, which involves derivatives of the occupied Kohn-Sham orbitals. These methods represent a significant improvement in the determination of properties such as atomization energies. However, they are more technically challenging, with several difficulties in terms of numerical stability. Several M-GGA functionals for the exchange functional, correlation functional or both have been developed. Examples include B95,¹³ KCIS,²⁷ TPSS,²⁸ and VSXC.²⁹

➤ **Hybrid density functionals employed in this thesis**

Hybrid functionals have allowed a significant improvement over GGAs for many molecular properties. For this, they have become a very popular choice in quantum chemistry and are now widely used. A hybrid exchange-correlation functional is usually obtained as a linear combination of a percentage of Hartree-Fock exact exchange functional E_x^{HF} and the exchange-correlation of a conventional GGA method. The parameters determining the weight of each individual functional are typically specified by fitting these coefficients to experimental atomization energies, ionization potentials, proton

affinities, total atomic energies, and other data, for a representative set of small molecules.³⁰

The combination of the exchange functional of Becke (B88)¹⁵ with the popular gradient-corrected correlation developed by Lee, Yang and Parr (LYP),²⁵ added to a VWN local-density approximation⁸ to the correlation functional and a 20% of exact HF exchange lead to the popular **B3LYP** functional.

$$E_{XC}^{B3LYP} = (1-a)E_X^{LSDA} + aE_X^{HF} + bE_X^{B88} + cE_C^{LYP} + (1-c)E_C^{VWN} \quad (11)$$

The B3LYP is by far the most utilized functional in chemistry. Several benchmark studies tested its accuracy in the reproduction of several chemical properties, including bond lengths and angles, barrier heights, atomization energies, binding energies, ionization potentials, electron affinities, heats of formation, and several types of nonbonded interactions.³¹ It was concluded that the B3LYP is able to compete in accuracy with the most sophisticated density functional and often at a fraction of the CPU time associated. It performs well for the structure determination, for the calculation of atomization energies and other thermochemical quantities, still remaining the method of choice to obtain geometrical parameters.³¹ Considering the good trade-off between speed and accuracy for B3LYP, that functional was chosen in our works for structures optimization and to obtain energetic profiles. Nevertheless, in *Paper VII*, in which an enzymatic reaction mechanism was studied, different exchange correlation functionals were used in addition to B3LYP in order to estimate the energies of the stationary points on the reaction paths. The benchmark was planned with the purpose to test density functionals at different levels of sophistication nowadays available, in determining transition-state barriers, above all for enzymatic reaction mechanism for which a well-established computation protocol is still lacking. Actually, for some properties, several new density functional are suggested to outperform the popular B3LYP.^{31,32} The determination of barrier heights is one

of such cases, for which the hybrid-meta DF in particular showed great ability in the reproduction of the reaction kinetics with high accuracy.

The hybrid-meta GGA methods (HM-GGA) represent a new class of density functionals, based on a similar concept to the M-GGA functionals, and under active development. The difference lies in the fact that they start from M-GGAs instead of standard GGAs. Hence, these methods depend on the Hartree-Fock exchange, the electron density and its gradient, and the kinetic energy density. In order to test the improvement of these methods over the previous formalism, **BB1K**,^{13,15,33} **MPW1B95**,^{13,17,24,32} **MPWB1K** ^{13,17,24,32} were also employed in our work. The first one, is based on the exchange functional of Becke (B88), as well as B3LYP, but combined with the Becke's 1995 correlation functional. The MPW1B95 and MPWB1K are based on the modified Perdew and Wang exchange functional (MPW) and Becke's 1995 correlation functional. It was suggested that the modified Perdew-Wang exchange functional (MPW) performs better than the Becke 88 one in essentially all respects, and the Becke 95 correlation functional likewise performs better than the LYP one. This assessment should include noncovalent interactions, in addition to thermochemical data and barrier heights. Taking these aspects under consideration, in our investigation we examined the performances of these HM-GGA in the reproduction of barrier heights by comparing the obtained data with experimental ones. In addition, in our set of hybrid density functionals we include also the PBE1PBE,^{21,22} hybrid functional obtained combined the modified exchange Perdew, Burke ed Ernzerhof functional with the PBE correlation one.

➤ **Basis sets and pseudopotentials**

Historically, the quantum calculations for molecules were performed as LCAO MO, i.e. Linear Combination of Atomic Orbitals - Molecular Orbitals. This means that molecular orbitals are expressed as a linear combination of a finite number of known one-electron functions (atomic orbitals), centered at each

atomic nucleus within the molecule. Also KS orbitals are then expressed as a linear combination of basis functions

$$\Psi_i = \sum_{\mu=1}^n C_{\mu i} \varphi_{\mu} \quad (12)$$

where ψ_i is the i -th molecular orbital, $C_{\mu i}$ are the coefficients of linear combination, φ_{μ} is the μ th atomic orbital, and n is the number of atomic orbitals.

Basis sets were first developed by J.C. Slater who proposed as basis functions hydrogen-like exponentials of the form $e^{-\xi r}$, which are known as Slater-type orbitals. STOs have a number of attractive features primarily associated with the correct exponential decay with increasing r . The exponential dependence on distance from the nucleus is very close to the exact hydrogenic orbitals.⁷

That is why, the Gaussian Type Orbitals (GTOs) were introduced.

Although these do not produce optimal atomic orbitals, they enable the large number of multicenter integrals involved in molecular computations to be evaluated with much greater facility. Gaussian approximations to atomic orbitals are functions of the form $e^{-\alpha r^2}$. The main difference to the STOs is that the variable r in the exponential function is squared. This feature allows an analytical solution of the general four-index integral but, at the same time, the shape of the radial portion of the orbital is not a good, leading to a loss of accuracy. At the nucleus ($r=0$), the GTOs have zero slope instead of a cusp with finite slope. As a consequence, behavior near the nucleus is poorly represented. Moreover, GTOs fall off too rapidly for large r . This leads to an inadequate representation of the "functions tail". Nevertheless, Gaussian orbitals have the beneficial property that the product of two GTOs is a third Gaussian function centered between the original two. Known as the Gaussian Product Theorem, this property allows two-electron integrals to be written with respect to at most two centers.

In order to combine the best feature of GTOs in terms of computational efforts, with a STOs proper radial shape, the basis functions used for SCF calculations

were developed as a linear combination of GTOs properly combined to approximate the shape of the STO functions. Obviously, the more primitives that are employed, the more accurately a contracted function can be made to match a given STO.

The basis set can be divided into

- Minimal basis sets: Typically they give inaccurate results, but are computational faster than their counterpart. Examples are STO-3G.
- Split valence basis sets: They are typically X-YZG (double zeta basis). In this case, X refers to the number of primitive Gaussians comprising each core atomic orbital. The Y and Z indicate that each valence orbital is composed of the two set of basis functions, the first one composed of Y primitive Gaussian functions whereas the second composed of Z primitive Gaussian functions (6-31G). The split valence triple zeta X-YZWG is also used, e.g., 6-311G.

Although those basis sets are good approximations, a better approximation is to acknowledge and account for the fact that sometimes orbitals share qualities of 's' and 'p' orbitals or 'p' and 'd', etc. and not necessarily have characteristics of only one or the other. As atoms are brought close together, their charge distribution causes a polarization effect (the positive charge is drawn to one side while the negative charge is drawn to the other) which distorts the shape of the atomic orbitals. In this case, 's' orbitals begin to have a little of the 'p' flavor and 'p' orbitals begin to have a little of the 'd' flavor. One asterisk (*) at the end of a basis set denotes that polarization has been taken into account in the 'p' orbitals. Two asterisks (**) means that polarization has taken into account the 's' orbitals in addition to the 'p' orbitals. In addition, when an atom is in an anion or in an excited state, the loosely bond electrons, which are responsible for the energy in the tail of the wave function, become much more important. To compensate for this area, computational scientists use **diffuse** functions. These basis sets utilize very small exponents to clarify the properties of the tail. Diffuse basis sets are represented by the '+' signs. One '+' means that we are accounting for the 'p' orbitals, while '++' signals that we are looking at

both 'p' and 's' orbitals, (much like the asterisks in the polarization basis sets). Polarized split valence double zeta basis sets were used in the presented works to perform geometry optimization. More accurate energies were then obtained by performing single-point calculations with larger basis set including also diffuse functions.

More elaborated approach it is used for transition metals, for which relativistic effects are expected to become important. One basic consequence of the special theory of relativity is that mass increases towards infinity as a body's velocity approaches c , which can be expressed mathematically as $m = m_0 / \sqrt{1 - (v/c)^2}$.³⁴ Actually, for heavy elements the core electrons reach velocities sufficiently near the speed of light that they manifest relativistic effects. A non-relativistic Hamiltonian operator is incapable of accounting for such effects, which can be significant for many chemical properties. The use of relativistic pseudopotentials or effective core potential (ECPs) can overcome this difficulty and decrease the computational efforts. The pseudopotential is an attempt to replace the complicated effects of the motion of the core electrons of an atom and its nucleus with an effective potential, or pseudopotential, so that the Schrödinger equation contains a modified effective potential term instead of the Coulombic potential term for core electrons normally found in the Schrödinger equation. Among available ECP basis sets, the commonly used ones were formulated as LanL,³⁵ CEP,³⁶ and SDD.³⁷ They differ in the schemes of fitting the ECP to Gaussian functions. The way of treating light atoms and valence electrons is also varied in these three basis sets. First-row atoms are treated with all-electron basis sets of Dunning/Huzinaga full double- ζ (D95)³⁸ and Dunning/Huzinaga valence double- ζ (D95V)³⁸ and ECP basis sets for LanL, SDD, and CEP, respectively. The sizes of these basis sets are in the sequence of SDD > CEP-121G > LanL2DZ. In our works, both SDD and LANL2DZ were utilized to describe the metal ions.

Bibliografia

- [1] Levine, I. R. Quantum Chemistry, 5th ed.; Prentice Hall: New Jersey, **2000**
- [2] A. Szabo, N. S. Ostlund, Modern Quantum Chemistry: Introduction To Advanced Electronic Structure Theory, McGraw-Hill, Inc. **1989**.
- [3] M. Born, J. R. Oppenheimer, *Ann. Phys.* **1927**, 84, 457.
- [4] Hohenberg, P.; Kohn, W. *Phys. Rev.* **1964**, 136, B864.
- [5] Kohn, W.; Sham, L. *J. Phys. Rev.* **1965**, 140, A1133.
- [6] Parr, R. G.; Yang, W. Density Functional Theory of the Electronic Structure of Molecules; Oxford University Press: New York, **1989**.
- [7] Cramer, C.J. Essential of Computational Chemistry Theories and Models; Wiley, John & Sons, Incorporated: England, **2002**.
- [8] Vosko, S.H., Wilk, L. & Nusair, M. *Can. J. Phys.* **1980**, 58, 1200.
- [9] Becke, A. D. *J. Chem. Phys.* **1986**, 84, 4524.
- [10] Becke, A. D. *J. Chem. Phys.* **1992**, 96, 2155.
- [11] Becke, A. D. *J. Chem. Phys.* **1992**, 97, 9173.
- [12] Becke, A. D. *J. Chem. Phys.* **1993**, 98, 5648.
- [13] Becke, A. D. *J. Chem. Phys.* **1996**, 104, 1040.
- [14] Becke, A. D. *J. Chem. Phys.* **1997**, 107, 8544.
- [15] Becke, A. D. *Phys. Rev. A* **1988**, 38, 3098.
- [16] Perdew, J. P.; Wang, Y. *Phys. Rev. B* **1986**, 33, 8800.
- [17] Adamo, C.; Barone, V. *J. Chem. Phys.* **1998**, 108, 664.
- [18] Handy, N. C.; Cohen, A. *J. Mol. Phys.* **2001**, 99, 403.
- [19] Xu, X.; Goddard, W. A., III. *Proc. Natl. Acad. Sci. U.S.A.* **2004**, 101, 2673.
- [20] Perdew, J. P. *Phys. Rev. B* **1986**, 33, 8822.
- [21] Perdew, J. P.; Burke, K.; Ernzerhof, M. *Phys. Rev. Lett.* **1996**, 77, 3865.
- [22] Adamo, C.; Barone, V. *J. Chem. Phys.* **2002**, 116, 5933.
- [23] Becke, A. D. *J. Chem. Phys.* **1988**, 88, 1053.
- [24] Perdew, J. P. Unified Theory of Exchange and Correlation Beyond the Local Density Approximation. In Electronic Structure of Solids '91; Ziesche, P., Eschig, H., Eds.; Akademie Verlag: Berlin, Germany, **1991**; pp 11-20.
- [25] Lee, C.; Yang, W.; Parr, R. G. *Phys. Rev. B* **1988**, 37, 785.
- [26] Colle, R.; Salvetti, D. *Theor. Chim. Acta* **1975**, 37, 329.
- [27] Krieger, J. B.; Chen, J.; Iafrate, G. J.; Savin, A. Electron Correl. Mater. Prop. 1999, 463.
- [28] Tao, J.; Perdew, J. P.; Staroverov, V. N.; Scuseria, G. E. *Phys. Rev. Lett.* **2003**, 91, 146401.
- [29] Van Voorhis, T.; Scuseria, G. E. *J. Chem. Phys.* **1998**, 109, 400.
- [30] Becke, A. D. *J. Chem. Phys.* **1993**, 98, 1372.
- [31] Sousa S. F., Fernandes, P.A.; Ramos M. J.; *J. Phys. Chem. A*, **2007**, 111, 10439 and references therein
- [32] Zhao, Y.; Truhlar, D. G. *J. Phys. Chem. A* **2004**, 108, 6908.
- [33] Zhao, Y.; Lynch, B. J.; Truhlar, D. G. *J. Phys. Chem. A* **2004**, 108, 2715.
- [34] Gorin, D. J., Toste, F. D.; *Nature*, **2007**, 446, 395
- [35] Hay, P. J.; Wadt, W. R. *J. Chem. Phys.* **1985**, 82, 299.
- [36] Stevens, W.; Krauss, M.; Basch, H.; Jasien, P. G. *Can. J. Chem.* **1992**, 70, 612.
- [37] Leininger, T.; Nicklass, A.; Stoll, H.; Dolg, M.; Schwerdtfeger, P. *J. Chem. Phys.* **1996**, 105, 1052 and previous papers by the same group.
- [38] Dunning Jr., T. H.; Hay, P. J. In *Modern Theoretical Chemistry*; Schaefer, H. F., III, Ed.; Plenum: New York, **1976**; Vol. 3.



Part 1

Since the finding of the anticancer activity of cisDDP, platinum chemistry has become one of the most extensive and versatile area of chemistry. The increasingly importance in this field is demonstrated by the continuous interest in the mechanism of action of the anticancer drugs, in the kinetic studies of the hydrolysis and bases-platination reactions, in the nature of DNA adducts and so on, becoming a weighty part of contemporary medicinal inorganic chemistry.

With the development of computational transition metal chemistry, the necessity to obtain accurate mechanistic details of the single steps involved in the cell death induction by platinum(II) compounds is also increased. Nevertheless, the direct theoretical efforts in elucidating these phenomena based on high-level quantum chemical investigations are relatively more scarce than the experimental efforts.

The capability of reproducing the correct order of kinetic and thermodynamic parameters in the class of the substitution reactions for the square-planar cisplatin and its analogues is an important feature for an accurate candidate theory of the hydrolysis and bases platination mechanisms, which is of fundamental importance in the understanding of the mechanism of reaction of the anticancer drug and in the design of novel platinum complexes with activity in cisplatin-resistant tumors.

1

General Remarks on Pt(II) Anticancer Drugs

Introduction

The successful development of metal-containing anticancer drugs began with the serendipitous discovery of an inhibitory effect of a soluble platinum complex on the division of living cells.

In the early 1960s, during a study of the effects of electric fields on bacterial growth, Barnett Rosenberg et al. observed that when an electric field was applied across platinum electrodes immersed in an aerobic solution of *Escherichia coli* cells growing in the presence of NH_4Cl , the bacteria were unable to divide normally but grew into filaments up to 300 times their normal length.¹

They found that an electrolysis product from the platinum electrode, identified as $\text{cis-}[\text{Pt}(\text{NH}_3)_2\text{Cl}_4]$,² was responsible for this curious phenomenon. Subsequently, various other platinum group metal complexes were found to induce filamentous growth in bacteria. Interestingly, while the divalent compound $\text{cis-PtCl}_2(\text{NH}_3)_2$ and related neutral $\text{cis-bis(amine)platinum(II)}$ and -platinum(IV) complexes were active, the trans isomers were not. Instead, they suppressed bacterial growth at high concentrations.³

In a series of experiments to test the effects of the various platinum coordination complexes on human leukemias cells (L1210) and on sarcomas artificially implanted in rats, $\text{cis-PtCl}_2(\text{NH}_3)_2$ was the most effective out of this group. Clinical trials ensued in 1972, culminating in FDA approval in 1979. Cisplatin is currently used for the treatment of testicular cancer (for which it has a 90% cure rate), ovarian, bladder, melanoma, non-small cell lung cancer (NSCLC), small cell lung cancer (SCLC), lymphomas and myelomas.^{4,5}

Unfortunately, its therapeutic efficacy is somewhat compromised by the occurrence of serious dose-limiting side effect which arise from the indiscriminate uptake of the drug into all rapidly dividing cells (tumours, but also for example bone marrow) and the body's attempt to excrete the drug through the kidneys.⁶

These side effects include: nephrotoxicity (reduced kidney function and damage), neurotoxicity (nervous system damage), ototoxicity (hearing loss), and myelosuppression (reduction in bone marrow activity). Although the nephrotoxicity of cisplatin can be repressed through the development of special drug-dosing protocol making use of rescue agents, the intrinsic and acquired cellular resistance displayed by many tumor cells further limits its clinical application.

There are three main mechanisms of drug resistance:⁷

- Reduced drug uptake and/or increased drug efflux.
- Degradation and deactivation by intracellular thiols. In particular this may be due to raised glutathione levels which can be as high as 10 mM inside resistant cells.
- Improved repair or tolerance of DNA-cisplatin adducts.

The toxicity of cisplatin and the cellular resistance to it, have driven the development of improved platinum-based anticancer drugs that display fewer or more tolerable side effects and/or are able to overcome one or more resistance mechanisms. Over 3000 platinum compounds have been synthesized and screened for antitumor activity.⁸ In the 30 years since cisplatin's first approval for human use, only 23 other platinum-based drugs have shown enough pharmacological advantages relative to cisplatin to be tested in clinical trials.⁹ Among these, only three are currently registered for clinical use:

- ❖ *cis*-Diammine(1,1-cyclobutanedicarboxylato) platinum II (Carboplatin);
- ❖ *cis*-Diammine (glycolato) platinum II (Nedaplatin);
- ❖ *trans*-L-1,2-Diaminocyclohexaneoxalato platinumII (Oxaliplatin).^{10,11,12}

Recently, another two Pt(II) complexes gained marketing approval in individual nations (Lobaplatin, approved in China and Heptaplatin approved in the Republic of Korea).^{13,14}

1.1 Biochemical Mechanisms of Action

Much progress has been made in elucidating the cisplatin mode of action and many details of the mechanism by which platinum-based drugs kill cancer are now well established. The early steps of triggering cell death by platinum(II) compounds involve four stages. They are (1) cellular accumulation by both passive and active uptake; (2) activation of the platinum(II) complex; (3) binding to nucleic acids to form a variety of Pt-DNA adducts; and (4) the cellular response to DNA damage.¹⁵⁻¹⁷

Subsequent signal transduction pathways activated by this interaction between platinum-DNA damage and other nuclear proteins lead to cell-cycle arrest, attempts to repair the DNA lesions, and apoptosis or necrosis. The results of these processes decide the fate of treated cells.¹⁸

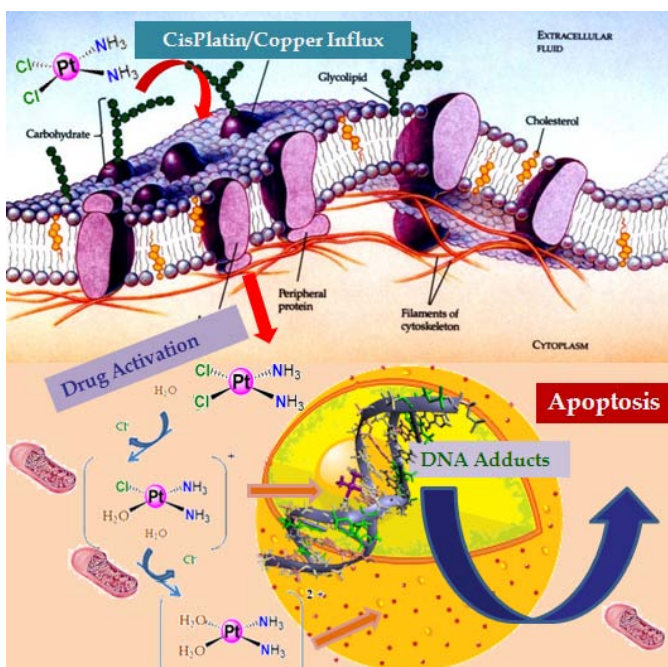


Figure 1.1 Illustration of the biochemical mechanism of action of cisplatin

1.1.1 Cellular Uptake

The delivery of platinum compounds across the cancer cell membrane is the first step toward successful therapy. Understand what happens outside of the cell and inside it, is important for the design of novel metal-based anticancer agents and suggest strategies for improving the effectiveness of cancer therapy with the existing drugs.

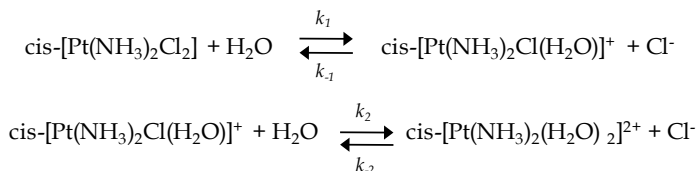
In the clinical protocols, the Pt(II) generation drugs are administered to the blood stream as an intravenous injection. The high concentration of physiological chloride in blood and extracellular body fluids (100 mM), is enough to allow the chloride ligands stay attached to the drug, hence maintaining a relatively stable neutral state until the drug enters the cell.

When it reaches the tumour, cisplatin is thought to be taken up into the cells by three possible mechanisms: passive diffusion, copper transporter proteins (*e.g.* CTR1) and/or organic cation transporters.¹⁹

For years it was thought that cisplatin entered cells primarily through passive diffusion, owing to data that showed platinum uptake was neither saturable nor inhibited by structural analogues.²⁰⁻²² However, a growing body of evidence suggests a role for active uptake by membrane proteins, such as the copper transporter CTR1, in cisplatin accumulation.^{23,25}

1.1.2 Drug Activation by Hydrolysis

As the compounds cross the cell membrane, the lower chloride concentration (4–20 mM) promotes the drug activation by hydrolysis mechanism. The loss of one or both of the chloride ligands leads to the formation of charged active species for subsequent interaction with cellular nucleophiles.^{26,27}



The rate constant k_1 and k_2 have been calculated to be approximately $2 \cdot 10^{-5}$ and $3 \cdot 10^{-5} \text{ s}^{-1}$, respectively. Coordination of water to platinum lowers its pKa, causing hydroxo products to form, as well. The acid dissociation constant for mono-aqua complex has been determined to be 6.56.²⁸ This means that at physiological pH the less reactive monohydroxo form could present.

The ultimate target for cisplatin inside the cell is DNA. Previous to binding to genomic or mitochondrial DNA the formation of aquo species is hence required. Such cationic molecules are rarely able to diffuse through the lipid bilayer that constitutes biological membranes. The aqua derivatives of cisplatin, therefore, may not readily diffuse back out of the cell before binding to intracellular targets. This behavior, conversion of cisplatin to a form trapped within the cell, may be a significant contributor to the potent cytotoxicity of the drug following its passive diffusion into cells without prior chemical modification. Moreover, hydrolysis step represent the limiting step for reaction of cis-DDP with DNA controlling the time-dependence of platinum binding to its biological target.^{29,30}

Nevertheless, many competitors for DNA binding are present in the cell as well as in the nucleus, such as small molecules and ions which compete for cisplatin binding [Cl^- , $(\text{HPO}_4)^{2-}$, OH^- , H_2O], amino acids, peptides, proteins, and polyphosphates.³¹⁻³³ Pt-protein binding is thought to play an important role in the toxicity and the mechanism of cisplatin-resistance.³⁴

1.1.3 DNA: A Primary Target for Platinum Drugs

It is generally accepted that binding of platinum (II) compounds to genomic DNA (gDNA) in the cell nucleus is largely responsible for its antitumor

properties. The induced structural distortions are key for the antitumor activity of cisplatin suppressing DNA transcription efficiently and ultimately leading to cell death.³⁵

The duplex has a hydrophobic core of the hydrogen bonded bases and as such the possible Lewis base sites available for coordination to the platinum are limited to the exposed portion of the nucleobases found in the major groove. Although the N1 and N7 of adenine and the N3 atom of cytosine are also suitable positions for platinum binding, the N7 position of the imidazole rings of guanine, located in the major groove of the double helix, is the most reactive nucleophilic site for platination.³⁶ This tendency results from the strong basicity of that position and from hydrogen bond interactions between ammine protons of cisplatin with O6 and group in guanine and their accessibility for the platinum complexes.

Cisplatin and related complexes bound to DNA have been thoroughly studied by both X-ray crystallography and NMR spectroscopy yielding abundant information about platinum modification of DNA structure.

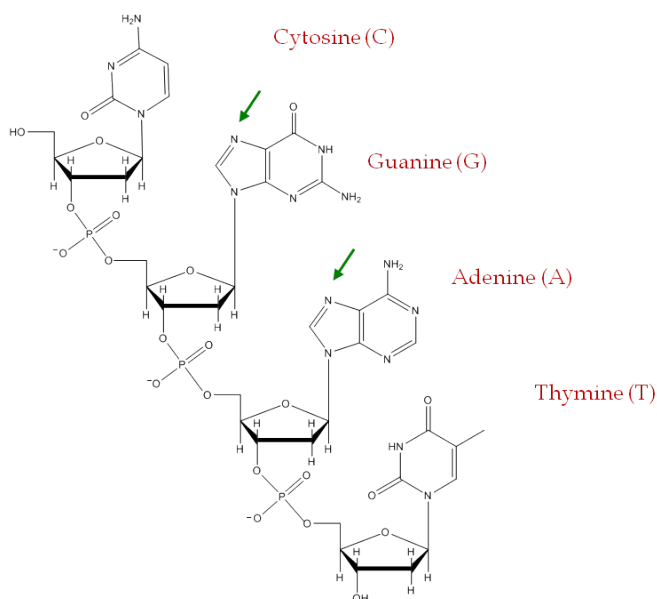


Figure 1.2: GN7 and AN7 binding sites in ds DNA.

A spectrum of intra- and inter-strand DNA cross-links have been identified both in vitro and in vivo.³⁷⁻⁴⁰

The 1,2-[Pt(NH₃)₂]²⁺-d(GpG) intrastrand crosslink was found to be the major adducts comprising ≈ 65% of total products. Other minor products include 1,2-d(ApG) (≈25%) and 1,3-d(GpNpG) (5-10%) intrastrand adducts, as well as a smaller number of interstrand cross-links (ICL) and monodentate adducts. Surprisingly, the 1,2-d(GpA) lesion is not observed either in vitro or in vivo.⁴¹

X-Ray structural investigation of Pt-DNA adducts initially focused on platinated di- or trinucleotides.⁴²⁻⁴⁴ However, it was not until a platinated DNA dodecamer duplex containing a site-specific 1,2-[Pt(NH₃)₂]²⁺-d(GpG) intrastrand cross-link was solved by X-ray crystallography that fine details of the structure of Pt-damaged DNA began to emerge (see Fig. 2.2 a).^{45,46}

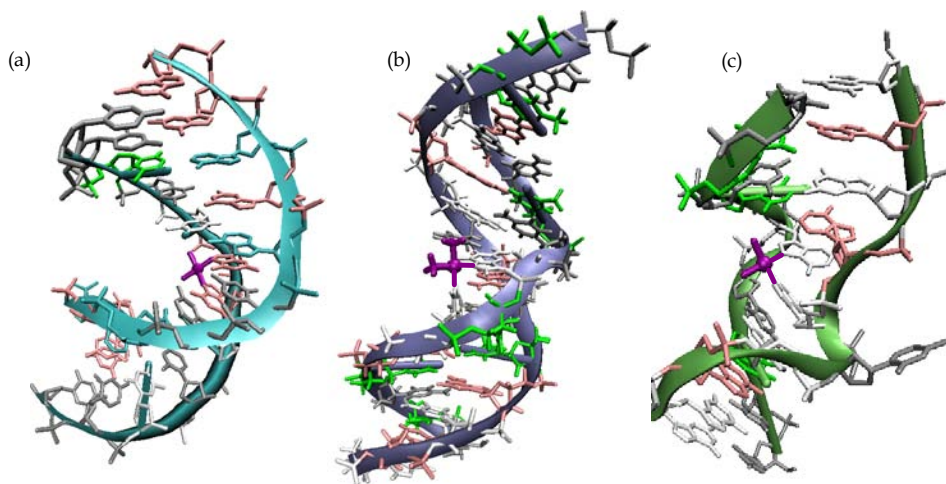


Figure 1.3: X-Ray crystal structures of double stranded DNA containing cisplatin different adducts (a) 1,2-d(GpG) intrastrand cross-link (1A1O); (b) 1,3-d(GpTpG) intrastrand cross-link (1DA4); (c) interstrand cross-link (1A2E). PDB accession codes are given in parentheses.

The X-ray crystal structure revealed that the Pt adduct induces a global bend in the DNA duplex and unwinds the double helix in the vicinity of the platination site, bending it toward the major groove and generating a widened and shallow minor groove. In addition to the structure of the 1,2-intrastrand cross-link, that of the 1,3-intrastrand cross-link on duplex DNA has also been solved

by NMR spectroscopy.^{47,48} This lesion, distorts double-stranded DNA in a different manner than the 1,2-d(GpG) cross-link (Fig. 2.2b). In this structure the duplex results less bent and the double helix displays local unwinding and widening of the minor groove, similarly to features of the structure of the 1,2-d(GpG) cross-link. Although the area of the duplex in the immediate vicinity of the 1,3-d(GpTpG) adduct is more severely distorted than in the 1,2-d(GpG) counterpart, the global effects of the 1,3-cross-link on the DNA duplex are more subtle than for the 1,2-lesion, with a less dramatic

bend angle. The structure of a DNA molecule containing a site-specific interstrand cisplatin cross-link was solved both by X-ray crystallography⁴⁹ (Fig. 2c) and by NMR spectroscopy.⁵⁰

This Pt-DNA adduct is structurally unique in many ways compared to the intrastrand cross-links. This kind of adducts bends the helix toward the minor groove in which the platinum moiety is now located. (Fig.2.3c). The double helix is severely unwound, with the result that the two cytosine bases opposite the bound guanines are pointed outward, away from the duplex.

1.1.4 Inhibition of transcription by platinum antitumor complexes

Following platinum-induced DNA modification, cellular repair systems act to recognize the damage and continuously function until the fate of drug-treated cells is decided. Knowledge of these repair mechanisms involving platinum damaged DNA provides essential clues to understanding the cellular responses to platinum-based anticancer drugs and for improving the efficacy of therapies. Many proteins participate in the damage recognition playing several roles in this process.¹⁶

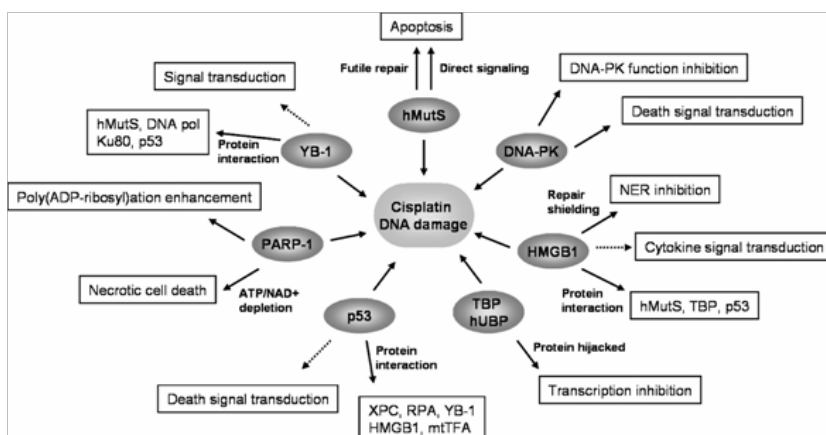


Figure 1.4: Roles of proteins that bind to DNA following cisplatin damage. Figure adapted from ref.16

The inhibition of DNA replication had been widely considered to be the key step in the mechanism of cisplatin cytotoxicity.⁵¹⁻⁵³ Nevertheless considerable evidence indicates transcription inhibition as a critical determinant in the pathway of apoptosis triggered by cisplatin. Since these reports, numerous systems employing both site-specifically and globally platinated DNA templates, with both recombinant proteins and living cells, have been designed to study inhibition of transcription by cisplatin and other platinum anticancer agents. Taken together, the data clearly demonstrate that the ability of a platinum complex to block RNA synthesis is directly associated with its efficacy as an antitumor agent⁵⁴ and that cisplatin-induced cell death does not correlate with inhibition of DNA synthesis.⁵⁵⁻⁵⁸ Inhibition of transcription induces a cellular response leading to the activation of p53, a tumor suppressor protein, through the ATR kinase.^{59,60} Induction of p53 connects blocked RNA polymerase with cell cycle checkpoints, DNA repair, and apoptosis. After a certain time point, if the transcription block persists, the cells will undergo apoptosis in either a p53-dependent or -independent manner. The mechanism of this process is not clearly understood, but several pathways have been proposed, as reviewed in detail elsewhere.⁶⁰

Bibliografia

- [1] Rosenberg, B.; Camp, L.; Krigas, T. *Nature* **1965**, 205, 698.
- [2] Rosenberg, B.; Camp, L.; Trosko, J.; Mansour, V. H. *Nature* **1969**, 222, 385.
- [3] Rosenberg, B. *In Nucleic Acid-Metal Zon Interactions*; Spiro, T. G., Ed.; Wiley: New York, **1980**; p 3.
- [4] Martindale: *The complete drug reference*, ed. S. C. Sweetman, Pharmaceutical Press, London, 35th edn, **2007**.
- [5] M. Watson, A. Barrett, R. Spence and C. Twelves, *Oncology*, Oxford University Press, Oxford, 2nd edn, **2006**.
- [6] Pil, P.; Lippard, S. J. *In Encyclopedia of Cancer*; Bertino, J. R., Ed.; Academic Press: San Diego, CA, **1997**; Vol. 1
- [7] K. Kehe and L. Szinicz, *Toxicology*, **2005**, 214, 198.
- [8] Weiss, R. B.; Christian, M. C. *Drugs* **1993**, 46, 360.
- [9] Lebwohl, D.; Canetta, R. *Eur. J. Cancer* **1998**, 34, 1522.
- [10] Fuentès, M. A.; Alonso, C.; Perez, J. M. *Chem. Rev.* **2003**, 103, 645.
- [11] Kelland, L. R.; Sharp, S. Y.; O'Neill, C. F.; Raynaud, F. I.; Beale, P. J., Judson, I. R. *J. Inorg. Biochem.* **1999**, 77, 111.
- [12] Wong, E.; Giandomenico, C. M. *Chem. Rev.* **1999**, 99, 2451.
- [13] I. Limited, *Drugs R&D*, **2003**, 4, 369.
- [14] D.-K. Kim, H.-T. Kim, J.-H. Tai, Y.-B. Cho, T.-S. Kim, K. H. Kim, J.-G. Park and W.-S. Hong, *Cancer Chemother. Pharmacol.*, **1995**, 37, 1.
- [15] D. Wang and S. J. Lippard, *Nat. Rev. Drug Discovery*, **2005**, 4, 307.
- [16] Y. Jung and S. J. Lippard, *Chem. Rev.*, **2007**, 107, 1387.
- [17] Jamieson, E. R.; Lippard, S. J. *Chem. Rev.* **1999**, 99, 246.
- [18] Siddik, Z. H. *Oncogene* **2003**, 22, 7265.
- [19] C. A. Puckett, R. J. Ernst and J. K. Barton, *Dalton Trans.*, **2010**, 39, 1159.
- [20] G. R. Gale, C. R. Morris, L. M. Atkins and A. B. Smith, *Cancer Res.*, **1973**, 33, 813.
- [21] S. P. Binks and M. Dobrota, *Biochem. Pharmacol.*, **1990**, 40, 1329.
- [22] Gately, D. P.; Howell, S. B., *Br. J. Cancer* **1993**, 67, 1171.
- [23] S. Ishida, J. Lee, D. J. Thiele and I. Herskowitz, *Proc. Natl. Acad. Sci. U. S. A.*, **2002**, 99, 14298.
- [24] K. Holzer, G. Samimi, K. Katano, W. Naerdemann, X. Lin, R. Safaei and S. B. Howell, *Mol. Pharmacol.*, **2004**, 66, 817.
- [25] T. Boulikas and M. Vougiouka, *Oncol. Rep.*, **2003**, 10, 1663.
- [26] L. Kelland, *Nat. Rev. Cancer*, **2007**, 7, 573.
- [27] Aprile, F.; Martin, D. S. *Inorg. Chem.* **1962**, 1, 551.
- [28] A. Andersson, H. Hedenmalm, B. Elfsson, H. Ehrsson, *J. Pharm. Sci.* **1994**, 83, 859.
- [29] J. Reedijk, *Inorg. Chim. Acta*, **1992**, 873, 198.
- [30] M. P. Goren, R. K. Wright, and M. E. Horowitz, *Cancer Chemoth. Pharm.*, **1986**, 18, 69.
- [31] Johnson, N. P.; Hoeschele, J. D.; Rahn, R. O. *Chem.-Biol. Interact.* **1980**, 30, 151.
- [32] Ushay, H. M.; Tullius, T. D.; Lippard, S. J. *Biochemistry* **1981**, 20, 3744.
- [33] F. A. Blommaert, H. C. M. van Dijk-knijnenburg, F. J. Dijt, L. den Engelse, R. A. Baan, F. Berends, and A. M. J. Fichtinger-Schepman, *Biochemistry*, **1995**, 34, 8474.
- [34] P. S. T. Yuen, L. K. Doolittle, and D. L. Garbers, *J. Biol. Chem.*, **1994**, 269, 791.
- [35] Mello, J. A.; Lippard, S. J.; Essigmann, J. M. *Biochemistry* **1995**, 34, 14783.
- [36] Yang, X.-L.; Wang, A. H.-J. *Pharmacol. Ther.* **1999**, 83, 181.
- [37] J. P. Caradonna, S. J. Lippard, M. J. Gait and M. Singh, *J. Am. Chem. Soc.*, **1982**, 104, 5793.

- [38] A. M. J. Fichtinger-Schepman, J. L. van der Veer, J. H. J. den Hartog, P. H. M. Lohman and J. Reedijk, *Biochemistry*, **1985**, 24, 707.
- [39] A. Eastman, *Biochemistry*, **1986**, 25, 3912.
- [40] P. M. A. B. Terheggen, B. G. J. Floot, E. Scherer, A. C. Begg, A. M. J. Fichtinger-Schepman and L. den Engelse, *Cancer Res.*, **1987**, 47, 6719.
- [41] Y. Mantri, S. J. Lippard and M.-H. Baik, *J. Am. Chem. Soc.*, **2007**, 129, 5023.
- [42] S. E. Sherman, D. Gibson, A. H.-J. Wang and S. J. Lippard, *Science*, **1985**, 230, 412.
- [43] G. Admiraal, J. L. van der Veer, R. A. G. de Graaff, J. H. J. den Hartog and J. Reedijk, *J. Am. Chem. Soc.*, **1987**, 109, 592.
- [44] S. E. Sherman, D. Gibson, A. H.-J. Wang and S. J. Lippard, *J. Am. Chem. Soc.*, **1988**, 110, 7368.
- [45] P. M. Takahara, A. C. Rosenzweig, C. A. Frederick and S. J. Lippard, *Nature*, **1995**, 377, 649.
- [46] P. M. Takahara, C. A. Frederick and S. J. Lippard, *J. Am. Chem. Soc.*, **1996**, 118, 12309.
- [47] C. J. Van Garderen and L. P. A. Van Houte, *Eur. J. Biochem.*, **1994**, 225, 1169.
- [48] J.-M. Teuben, C. Bauer, A. H.-J. Wang and J. Reedijk, *Biochemistry*, **1999**, 38, 12305.
- [49] F. Coste, J.-M. Malinge, L. Serre, W. Shepard, M. Roth, M. Leng and C. Zelwer, *Nucleic Acids Res.*, **1999**, 27, 1837.
- [50] H. Huang, L. Zhu, B. R. Reid, G. P. Drobny and P. B. Hopkins, *Science*, **1995**, 270, 1842.
- [51] H. C. Harder, R. G. Smith and A. F. Leroy, *Cancer Res.*, **1976**, 36, 3821.
- [52] N. P. Johnson, J. D. Hoeschele, N. B. Kuemmerle, W. E. Masker and R. O. Rahn, *Chem.-Biol. Interact.*, **1978**, 23, 267.
- [53] A. L. Pinto and S. J. Lippard, *Proc. Natl. Acad. Sci. U. S. A.*, **1985**, 82, 4616.
- [54] K. E. Sandman, S. S. Marla, G. Zlokarnik and S. J. Lippard, *Chem. Biol.*, **1999**, 6, 541.
- [55] C. M. Sorenson and A. Eastman, *Cancer Res.*, **1988**, 48, 4484.
- [56] C. M. Sorenson and A. Eastman, *Cancer Res.*, **1988**, 48, 6703.
- [57] C. M. Sorenson, M. A. Barry and A. Eastman, *J. Natl. Cancer Inst.*, **1990**, 82, 749.
- [58] A. Eastman, 'Cisplatin, Chemistry and Biochemistry of a leading Anticancer Drug', ed. B. Lippert, Wiley-VCH, **1999**, pp. 111
- [59] M. Ljungman, F. Zhang, F. Chen, A. J. Rainbow and B. C. McKay, *Oncogene*, **1999**, 18, 583.
- [60] F. A. Derheimer, C.-W. Chang and M. Ljungman, *Eur. J. Cancer*, **2005**, 41, 2569.

2

“*Classical*” Pt(II) Anticancer Drugs

Understanding their mechanisms of action

by Computational Studies

Introduction

For over three decades, continuous efforts have been made in order to overcome the drawbacks of cisplatin with a primary focus on the development of new derivatives with improved pharmacological properties. The challenge in designing metal-based drugs primarily lies in balancing the potential toxicity with the positive outcome. The reduction of the dose-limiting toxicities and the circumvention of intrinsic or acquired resistance to cisplatin represent the major goal in the search for new platinum anticancer agents.

Of the thousands of Pt compounds evaluated for antitumor activity, the majority of them adhered to the set of **structure-activity relationships** summarized by Cleare and Hoeschele.^{1,2} This relationship stress the necessity to take into consideration specific factors during the development of classical anticancer platinum (II) complexes [PtX₂-(Am)₂]. First of all *cis* geometry of the square-planar compounds was assumed to be necessary since early works. Furthermore, according to these general rules, two ammines with at least one N-H moiety on each ligand (symmetric, asymmetric, chelating or not), are required as “spectator group”. The leaving group instead, should be an anion with intermediate binding strength to platinum and have a weak trans effect to avoid labilizing the amine. Complexes with labile leaving groups are highly toxic, while complexes with inert leaving groups are generally inactive.

The structure-activity relationships dominated Pt drug design for over 20 years and remained valid until relatively recently. This is reflected in the fact that all Pt compounds that are currently registered for clinical use adhere to this set of guidelines: Carboplatin, Nedaplatin and Oxaliplatin.³⁻⁵

Since the toxicity of platinum-based drugs was directly related to the ease with which the leaving groups are substituted by water, second-generation platinum drugs contain less labile ligands such as bis-carboxylates and glycolate in the case of Carboplatin and Nedaplatin, respectively. The slower rates of aquation displayed by these compounds, are expected to be

responsible for the reduced side effects observed in patients compared with those treated with Cisplatin.⁶

Despite the side effects are significantly reduced, making high dose chemotherapy possible, these compounds have not solved the clinical limitation of resistance. Therefore it was necessary to design a drug able to overcome that resistance. The result of this research led the so-called third generation Pt(II) drugs. The approach was to modify the non-leaving spectator ligands, introducing chelating amino groups such as 1,2-Diaminocyclohexane in the case of Oxaliplatin. The different features of this kind of ligand has been proposed to contribute to the failure of DNA-oxaliplatin adduct detection by the mismatch recognition proteins in the cell response, together with different conformational distortions within the DNA strands.⁷⁻¹⁰

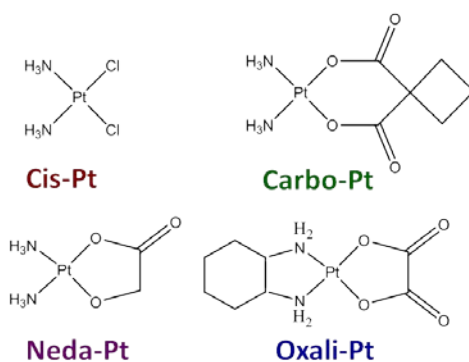


Figure 2.1: Chemical Structures of CisPt and its second and third generation analogues

2.1 Second Generation – overcoming toxicity

2.1.1 Carboplatin

Cis-Diammine(1,1-cyclobutanedicarboxylato) platinum II, has been a successful development designed to overcome the severe side effects associated with cisplatin treatment. It was the first derivative with a more tolerable toxicological profile in clinical trials.¹¹ The modification of the leaving group in carboplatin has proven to show an impressive impact on the properties and consequently the considerable outcome of an anticancer agent.

The observed pharmacokinetic differences between carboplatin and cisplatin arise from the slower rate of conversion of the first to the reactive species. Replacement of the chloride groups in cisplatin by cyclobutanedicarboxylate ligand significantly diminished the nephrotoxic effects of the formed carboplatin without affecting its antitumor activity and making high dose chemotherapy possible. The rate constant found for the substitution of the O,O ligand was found to be $5 \times 10^{-9} \text{ s}^{-1}$, compared with $2 \times 10^{-5} \text{ s}^{-1}$ for cisplatin.¹²⁻¹⁴

It has been suggested that carboplatin might function as a pro-drug of cisplatin by substitution of the cyclobutane dicarboxylate group by chloride groups. However, some studies report that reaction of carboplatin with chloride ions is too slow for the reported half-life of the drug in blood plasma,^{15,16} suggesting that the key activation step involves carboplatin by direct substitution of the O,O ligand by water. Nevertheless, whether or not carboplatin is a pro-drug for cisplatin, once aquated it yields the same active component as cisplatin and therefore, the biological mechanism of action of carboplatin appears to be entirely analogous to that of cisplatin and also the spectrum of cancers that can be treated is identical. Carboplatin is now the drug of choice for ovarian cancer, in preference to cisplatin, and has recently undergone additional Phase II and III trials for the treatment of salivary gland cancer¹⁷ and advanced mullerian cancer¹⁸ to further expand its clinical application.

Although carboplatin forms the same type of adducts as cisplatin, the product profile is markedly different in cells.¹⁹ The major carboplatin adduct identified was cis-[Pt(NH₃)₂(dG)₂] (36%), which could arise from 1,3-d(GpNpG) intrastrand cross-links. This lesion, the main adduct of carboplatin-DNA binding, distorts double-stranded DNA in a different manner than the 1,2-d(GpG) cross-link (Fig. 2.3b). Minor products included 1,2-d(GpG) (30%), 1,2-d(ApG) (16%), as well as a small number of interstrand (3–4%) cross-links and monofunctional adducts.

2.1.2 NedaPlatin

Nedaplatin (*cis*-Diammine (glycolato) platinum II) is a second-generation platinum derivative, with relevant antineoplastic activity.²⁰⁻²² It contains a novel ring structure in which glycolate is bound to the platinum by a bidentate ligand and forms reactive platinum complexes that bind to nucleophilic groups in DNA, resulting in intrastrand and interstrand DNA cross-links, apoptosis, and cell death.

This agent appears to be ten times more water soluble than cisplatin and then less nephrotoxic and neurotoxic compared to both cisplatin and carboplatin.²³

Preclinical and clinical studies demonstrated that nedaplatin has anticancer activity superior to that of carboplatin and equivalent to that of cisplatin.²⁴

Since its approval in 1995, it has been used in the treatment of NSCLC, SCLC, oesophageal cancer and head and neck cancers.²⁰⁻²² Recently, several Phase I and Phase II studies have shown promising results when nedaplatin is used in combination therapies.²⁵⁻²⁷

Two further clinical trials have been conducted to investigate the effect of replacing cisplatin with nedaplatin in patients normally treated with a regime of cisplatin and 5-FU for oesophageal squamous cell carcinoma,^{28,29} and locoregionally advanced nasopharyngeal carcinoma.³³ Despite no dramatic clinical benefits have been described for the use of nedaplatin over cisplatin, its use could be useful when treating cancer patients that also present with renal impairment.^{28,29}

2.2 Third Generation – overcoming cisplatin resistance

2.2.1. Oxaliplatin

Oxaliplatin (*trans*-1R,2R-Diaminocyclohexaneoxalato platinumII), has become the third to achieve worldwide clinical acceptance. It presents the two ammine ligands incorporated into a 1,2-diaminocyclohexane (dach) framework (R,R-dach).

The clinical advantage of oxaliplatin is that it was the first drug approved that was capable of overcoming cisplatin resistance. It has a different spectrum of activity and it is used for the treatment of adjuvant and metastatic colorectal cancers in combination with 5-FU and folinic acid.¹⁰ Recent clinical trials have tried to extend its spectrum of activity to include the treatment of metastatic gastric and oesophagogastric adenocarcinoma,³⁰ and to improve its effectiveness against colorectal cancers through its administration with different drugs such as irinotecan and capecitabine.³¹ Ongoing clinical trials as of April 2010 include examination for efficacy in gastric, fallopian tube and ovarian, breast, NSCLC, pancreatic cancers, acute myeloid leukaemia, indolent lymphoma, and hepatoma. The precise biological reasons for the difference in spectrum of activity and the ability of this agent to circumvent some cisplatin resistance mechanisms remain to be fully elucidated, but seems to hinge on the dach ligand and on the different adducts it forms with DNA.³²⁻³³ Whilst the predominant DNA adducts formed by oxaliplatin are 1,2-intrastrand GG adducts analogous to those formed by cisplatin, the bulky hydrophobic dach ligand points into the DNA major groove which prevents binding of DNA repair proteins.³⁴ The oxalate ligand also greatly reduces the severity of the side effects of the drug.³² It has been postulated that the conformational differences between the biologically active R,R-isomer of oxaliplatin- and cisplatin-DNA adducts may be responsible for differences in protein recognition and cellular processing of the two platinum antitumor compounds.⁸⁻¹¹ The differences in antitumor activity between the three isomeric forms suggest a carrier ligand specification in the processing of DNA adducts by the repair machinery or differences in cell uptake.^{7,35}

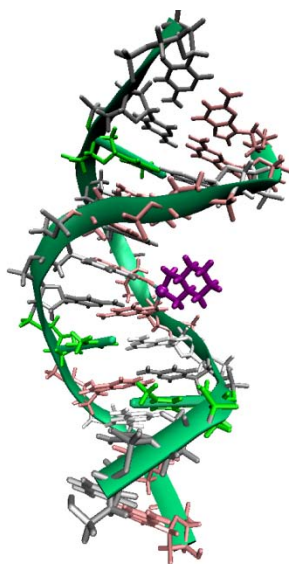


Figure 2.2: X-Ray crystal structure of double stranded DNA containing Oxaliplatin 1,2-d(GpG) intrastrand cross-link (1PG9). PDB accession code is given in parentheses.

2.3 Study Aims

The purpose of our research in this field, was to explore the chemistry of cisplatin-like anticancer derivatives in order to contribute to the elucidation of their mechanism of action. We employed advanced computational methods to study the ligand-exchange kinetics displayed by these compounds as well as the biochemical transformations of them on the way to the biological target into the cells.

The first series of studies were planned with the aim to accomplish a correct understanding of the steps preceding the DNA binding. Therefore we explored the drugs activation processes that take place as the compounds cross the cell membrane undergoing hydrolysis reactions. The final purpose was to provide insights on the active species able to efficiently bind the purine bases. **(Papers I-II)** Nevertheless, before reaching the cell, the high concentration of chloride in blood and extracellular body fluids could induce drugs degradation promoting the substitution of the O,O ligands by chloride ions. Consequently

this hypothesis was also explored, allowing us to achieve a broader understanding of the main biodegradation products in physiological conditions. **(Paper III)**

While differences in the hydrolysis rates are usually correlated to the reduced toxicity displayed from the second- and third-generation anticancer drugs in comparison with cisplatin, the steric and chemical properties of DNA lesions formed by Pt(II) complexes are thought to underlie the differences in the biological activity. However, a significant biological difference in spectrum of activity and in the ability to circumvent some cisplatin resistance mechanisms was observed only for oxaliplatin. A good understanding of the interaction of these Pt-anticancer drugs with models of binding sites present in DNA is of fundamental importance to unravel the mode of action of this class of compounds. Therefore we conducted a detailed study of the interaction of the second- and third-generation anticancer drugs Carboplatin, Nedaplatin and Oxaliplatin with Guanine (G) and Adenine (A) DNA bases in order to obtain detailed data on their binding mechanisms and on the reaction energy profiles.

(Paper IV)

2.4 Common Mechanistic details

The hydrolysis and chlorination reactions of these platinum(II) derivatives belong to the class of second-order nucleophilic substitution (S_N2) reactions. These reactions for square-planar complexes proceed via a collision between the reactant with two consecutive nucleophilic species attacking the metal center to release the ionic ligand. In such a process, a transition state in which the entering molecule, the leaving group, and the metal complex result weakly bound can be found, suggesting that the associative mechanism may be preferred and are consistent with the experimental studies on the aquation of some Pt(II) complexes with *in vivo* anticancer activities.^{36,37} The equatorial plane of the five-coordinated TS structure plays an important role in determining the hydrolysis behavior. The same features were found for the

reaction with purine bases. In that case, the overall geometry of the transition states is, in agreement with previous results for these type of associative substitution reactions, a trigonal bipyramid.³⁸

2.5 Hydrolysis Mechanisms of the Second- and Third-Generation Anticancer Drugs Nedaplatin and Oxaliplatin (Papers I and II)

As previously discussed in the section 1.1.2, hydrolysis of Pt(II) drugs is expected to play an important role in the activation of these compounds before they reach DNA. A correct understanding of the hydration mechanism of the second- and third-generation Pt(II) drugs is then essential.

In our investigation, we carried on a detailed exploration of the first and second hydrolysis step for each compound, combining density functional theory (DFT) with the conductor-like dielectric continuum model (CPCM) approach. The decomposition of nedaplatin and oxaliplatin in water proceed through a biphasic mechanism with a ring-opening process followed by the loss of the glycolate and oxalate ligands, respectively.

The reactions were studied in neutral and acidic conditions. The stationary points on the potential energy surfaces for the first and second hydrolysis steps, proceeding via a general S_N2 pathway, were fully optimized and characterized. The computed potential energy surfaces show that the rate limiting step in neutral conditions is the first hydrolysis process for both compounds. In acid conditions the trend is different, with the second hydrolysis process being the rate limiting step. On the basis of these findings, we can establish whether the mono-aquated or di-aquated complex act as alkylating species on DNA. Furthermore, our studies allow us to make a comparison with the trends previously found for the other platinum anticancer drugs currently used in the medical protocols, cisplatin³⁹ and carboplatin,⁴⁰ in order to spotlight possible common or different behavior (Figure 2.1).

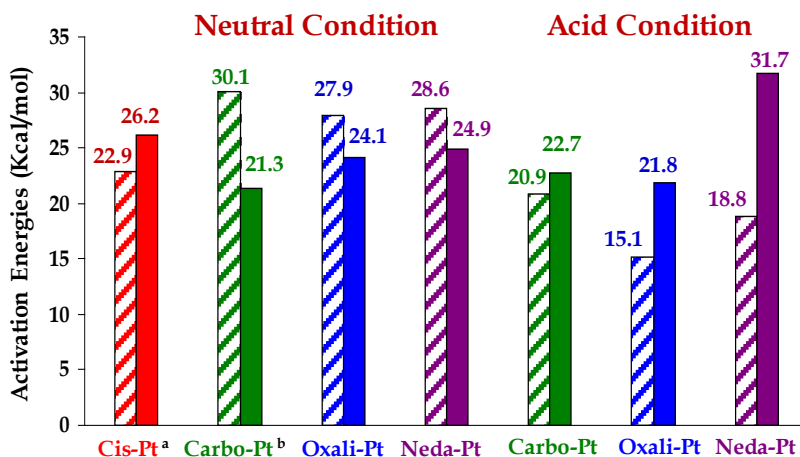


Figure 2.3: Comparison between calculated activation energies for Cisplatin, Carboplatin, Oxaliplatin, and Nedaplatin in neutral and acid conditions. Note that the striped column indicates the first aquation process, while the filled column indicates the second aquation process. ^aFrom ref 39. ^bFrom ref 40

Comparison of the neutral hydrolysis barriers for Carboplatin, Oxaliplatin and Nedaplatin, reveals that the rate limiting step is the ring opening, suggesting that the second and third generations analogues of cisplatin should reach DNA in their fully hydrolyzed forms. Moreover, the cisplatin-like compounds show all slower hydrolysis rates compared to cisplatin due to the introduction of the kinetically less labile carboxylate, oxalate and glycolate and to a presence of a large group in the NH_3 position in the case of oxaliplatin. Our data confirm that a slower hydration could be the reason of the lower side effects displayed from the second and third generation anticancer drugs. In acid condition we can observe that, again, Carboplatin follow the same trend of Oxaliplatin and Nedaplatin, becoming the loss of the ligand the rate limiting step. Nevertheless there are some differences. In the case of carboplatin, the activation barriers are similar so the possibility that the diaqua species reacts with DNA can't be excluded while for oxaliplatin and nedaplatin the gap became greater suggesting that they reach DNA monohydrated.

2.6 Chlorination Mechanism (Paper III)

The possibility that second- and third-generation Pt(II) drugs undergo O,O ligands substitution by the chloride in the plasma, has received from the early works on this area, a considerable interest. In the case of carboplatin, this eventuality was explored in several works, since carboPt has been for a long time considered as a pro-drug for cisplatin upon reaction with chloride.¹⁴ Nevertheless, the relative inertness of carboplatin to chloride substitution was demonstrated early on, leading to a suggestion that the drug crosses the cell membrane with the cyclobutanedicarboxylato group still coordinated to the platinum centre. Also the other second-generation drug nedaPt could act as a cisplatin pro-drug if reacted with chloride in the plasma hence following the same biochemical transformation into the cell. For the third-generation anticancer drugs, instead, due to the substitution of the ammine ligands with a different non-leaving spectator group, the eventual chlorination step would lead to another chemical species, different from cisplatin. For this reason, such possibility was explored in our series of studies in the case of oxaliplatin, by means of DFT/CPCM approach. We found that acidification of the chloride free solutions by which the drug is generally administered, leads to a fast substitution of the glycolate ligand by chloride ions. In these conditions, the drug could cross the cell membrane mainly in the neutral form [Pt(DACH)(H-oxalate)Cl].

2.7 Interaction of second- and third-generation anticancer drugs with DNA bases (Paper IV)

A good understanding of the interaction of the second- and third- generation Pt-anticancer drugs, with models of binding sites present in DNA is of fundamental importance to unravel the mode of action of these class of compounds. Although there is no doubt that a Pt-N7 bond forms during initial attack, the exact structure of the monofunctional adduct is not known. Herein, the reactions of platinum mono-aqua complexes with guanine (G) versus adenine (A) were explored in neutral and acidic condition and compared in the present work, then contributing to elucidate the whole mechanism employed by these compounds to reach the biological target. The guanine as a target for platination process is confirmed to be preferred over adenine for all the investigated compounds. The dominating preference for G purine base is a completely hydrogen-bonds process, confirming that H-bonds are important to impose both structural and kinetic control on the purine platination process. The lowest activation barrier for G-platination process was found for CarboPt, in both environments and seems to be a direct consequence of the more favourable network of hydrogen-bonds that take place in the transition state geometry.

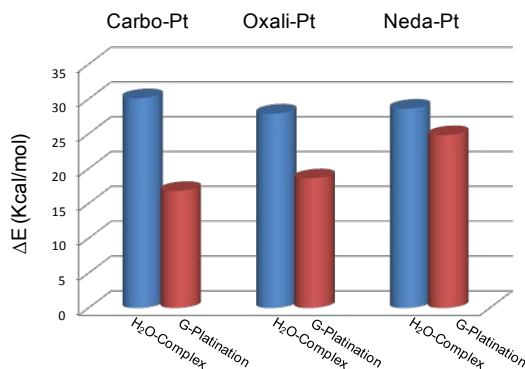


Figure 2.4. Comparison between calculated activation energies for hydrolysis and G-platination processes of Carboplatin, Oxaliplatin, and Nedaplatin in neutral condition.

It's interesting to notice that Carbo-Pt shows the slowest hydrolysis rate among the cisplatin-like compounds but, at the same time, the formation of the CarboPt-guanine adduct proceeds significantly faster than the other adducts. This chemical behavior could explicate the high activity of carboplatin compound. The investigation was performed by using Density Functional Theory (DFT) combined with the conductor-like dielectric continuum model (CPCM) approach, in order to obtain detailed data on their binding mechanisms and on the reaction energy profiles.

Bibliography

- [1] Cleare, M. J.; Hoeschele, J. D. *Bioinorg. Chem.* **1973**, 2, 187.
- [2] Cleare, M. J.; Hoeschele, J. D. *Plat. Met. Rev.* **1973**, 17, 3.
- [3] Lebwohl, D.; Canetta, R. *Eur. J. Cancer* **1998**, 34, 1522.
- [4] Fuertes, M. A.; Alonso, C.; Perez, J. M. *Chem. Rev.* **2003**, 103, 645.
- [5] Kelland, L. R.; Sharp, S. Y.; O'Neill, C. F.; Raynaud, F. I.; Beale, P. J., Judson, I. R. *J. Inorg. Biochem.* **1999**, 77, 111.
- [6] Roberts, J. J.; Knox, R.; Friedlos, D.; Lydall, D. A.; Biochemical Mechanisms of Platinum Antitumour Drugs; McBrien, D. C. H., Slater, T. F., Eds; IRL: Oxford, U.K., 1986; p 29
- [7] Di Francesco, A. M.; Ruggiero, A.; Riccardi, R., *Cellular and molecular Life sciences: CMLS* **2002**, 59, 1914.
- [8] S. Sharma, P. Gong, B. Temple, D. Bhattacharyya, N. V. Dokholyan and S. G. Chaney, *J. Mol. Biol.*, **2007**, 373, 1123.
- [9] Y. Wu, D. Bhattacharyya, C. L. King, I. Baskerville-Abraham, S.-H. Huh, G. Boysen, J. A. Swenberg, B. Temple, S. L. Campbell and S. G. Chaney, *Biochemistry*, **2007**, 46, 6477.
- [10] S. G. Chaney, S. L. Campbell, E. Bassett and Y. Wu, *Crit. Rev. Oncol. Hematol.*, **2005**, 53, 3.
- [11] Evans, B. D.; Raju, K. S.; Calvert, A. H.; Harland, S. J.; Wiltshaw, E., *Cancer Treat Rep*, **1983**, 67, 997.
- [12] Aprile, F.; Martin, D. S. *Inorg. Chem.* **1962**, 1, 551.
- [13] U. Frey, J. D. Ranford, P. J. Sadler, *Inorg. Chem.* **1993**, 32, 1333.
- [14] R. W. Hay, S. Miller, *Polyhedron*, **1998**, 17, 2337.
- [15] M. A. Allsop, G. J. Sewell, C. G. Rowland, C. M. Riley, R. L. Schowen, *Int. J. Pharm.* **1991**, 69, 197.
- [16] L. Canovesi, L. Cattalini, G. Chessa, M. L. Tobe, *J. Chem. Soc. Dalton Trans.* **1988**, 2135.
- [17] S. A. Laurie, L. L. Siu, E. Winqvist, A. Maksymiuk, E. L. Harnett, W. Walsh, D. Tu and W. R. Parkulekar, *Cancer*, **2010**, 116, 362.
- [18] R. T. Penson, D. S. Dizon, S. A. Cannistra, M. R. Roche, C. N. Krasner, S. T. Berlin, N. S. Horowitz, P. A. Di Silvestro, U. A. Matulonis, H. Lee, M. King and S. M. Campos, *J. Clin. Oncol.*, **2010**, 28, 154.
- [19] F. A. Blommaert, H. C. M. van Dijk-Knijenburg, F. J. Dijt, L. den Engelse, R. A. Baan, F. Berends and A. M. J. Fichtinger-Schepman, *Biochemistry*, **1995**, 34, 8474.
- [20] Ota, K. *Gan to Kagaku Ryoho* **1996**, 23, 379.
- [21] Inuyama, Y.; Fukuda, S.; Satoh, N. *Gan to Kagaku Ryoho* **1997**, 24, 1902.

- [22] Kameyama, Y.; Okazaki, N.; Nakagawa, M.; Koshida, H.; Nakamura, M.; Gemba, M. *Toxicol. Lett.* **1990**, 52, 15.
- [23] A. Kuwahara, M. Yamamori, K. Nishiguchi, T. Okuno, N. Chayahara, I. Miki, T. Tamura, T. Inokuma, Y. Takemoto, T. Nakamura, K. Kataoka and T. Sakaeda, *Int. J. Med. Sci.*, **2009**, 6, 305.
- [24] Y. Kawai, S. Taniuchi, S. Okahara, M. Nakamura and M. Gemba, *Biol. Pharm. Bull.*, **2005**, 28, 1385.
- [25] H. Kurita, E. Yamamoto, S. Nozaki, S. Wada, I. Furuta, M. Miyata and K. Kurashina, *Cancer Chemother. Pharmacol.*, **2010**, 65, 503.
- [26] Y. Gong, L. Ren, L. Zhou, J. Zhu, M. Huang, X. Zhou, J. Wang, Y. Lu, M. Hou and Y. Wei, *Cancer Chemother. Pharmacol.*, **2009**, 64, 327.
- [27] F. Oshita, K. Yamada, H. Saito, K. Noda, N. Hamanaka and M. Ikehara, *J. Exp. Ther. Oncol.*, **2004**, 4, 343.
- [28] H. Yamashita, H. Nakagawa, M. Tago, H. Igaka, N. Nakamura, M. Shiraiishi, N. Sasano and K. Ohtomo, *Dis. Esophagus.*, **2006**, 19, 15.
- [29] J. Zheng, G. Wang, G. Y. Yang, D. Wang, X. Luo, C. Chen, Z. Zhang, Q. Li, W. Xu, Z. Li and D. Wang, *Jpn. J. Clin. Oncol.*, **2010**, 40, 425.
- [30] F. Lordick, B. Lubber, S. Lorenzen, S. Hegewisch-Becker, G. Folprecht, E. Woll, T. Decker, E. Endlicher, N. Rothling, T. Schuster, G. Keller, F. Fend and C. Peschel, *Br. J. Cancer*, **2010**, 102, 500–505.
- [31] R. Zarate, J. Rodriguez, E. Bandres, A. Patino-Garcia, M. Ponz-Sarvisé, A. Viudez, N. Ramirez, N. Bitarte, A. Chopitea and J. Gacia-Foncillas, *Br. J. Cancer*, **2010**, 102, 987.
- [32] T. Boulikas and M. Vougiouka, *Oncol. Rep.*, **2003**, 10, 1663.
- [33] L. Kelland, *Nat. Rev. Cancer*, **2007**, 7, 573.
- [34] J. Kasparkova, M. Vojtiskova, G. Natile and V. Brabec, *Chem. Eur. J.*, **2008**, 14, 1330.
- [35] Pendyala, L.; Kidani, Y.; Perez, R.; Wilkes, J.; Bernacki, R. J.; Creaven, P. J., *Cancer Lett.* (Shannon, Irel.) **1995**, 97, 177.
- [36] Jestin, J. L.; Chottard, J. C.; Frey, U.; Layrenczy, G.; Merbach, A. E. *Inorg. Chem.* **1994**, 33, 4277.
- [37] Mikola, M.; Klika, K. D.; Hakala, A.; Arpalahti, *J. Inorg. Chem.* **1999**, 38, 571.
- [38] Baik M. H.; Friesner R. A.; Lippard, S. J. *J. Am. Chem. Soc.* **2003**, 125, 14082.
- [39] Raber, J.; Zhu, C.; Eriksson, L. A. *Mol. Phys.* **2004**, 102, 2537.
- [40] Pavelka, M.; Lucas, M. F.; Russo, N. *Chem. Eur. J.* **2007**, 13, 10108.

3

“*Non-Classical*” Anticancer Drugs

*Computational Studies on new-developed
antitumor complexes*

Introduction

In attempts to find new derivatives active toward the classical Pt(II) refractory/resistant tumors, a completely different approach to drug design has been adopted in recent years. Actually, many efforts have been directed toward the rational design of unconventional complexes that violate the original structure-activity relationships, but yet showing antitumor activities, such as *trans* compounds. Research on platinum compounds with *trans* geometry was marginalized for decades since they were supposed to be inactive. The cytotoxicities displayed recently by several *trans* Pt(II) derivatives, urges for a re-evaluation of the general structure-activity rules.

On the other hand, there is also a considerable research focused on the development of more effective non-platinum drugs that display less side effects and can be easily administered. The design of novel metal-based drugs demonstrate that biomedical inorganic chemistry is a rapidly emergent field of enormous potential for application in medicine. Within this context, besides palladium, iridium, rhodium, ruthenium, tin, copper, gallium and gold, ¹⁻¹¹ rhenium complexes have also attracted growing attention for their possible use as anticancer drugs.¹²⁻¹⁶ We believe that the development of Re compounds as promising candidates for clinical development may represent an interesting challenge in medicinal chemistry.

The following sections present some complexes that illustrate the recent strategy used in the development of new-generated antitumor agents. Together with the advances in this field, our computational studies on these novel drugs will be discussed along the text.

3.1 Trans Compounds

From the early beginning, the antitumor activity of the world’s best selling anticancer drug cisplatin (*cis*-DDP) has been related with the possibility to produce bifunctional lesions on DNA and to form 1,2-intrastrand adducts with two adjacent purine bases. It has been assumed that the clinical inactivity of the *trans*-DDP is correlated to the evidence that these kind of cross-links are stereochemically inaccessible to *trans* isomers, which on the contrary, induces monoadducts that may be repaired or undergo further rearrangements, or forms interstrand cross-links between cytosine and guanine of double-stranded DNA not able to change stability and structure of DNA markedly.¹⁷⁻²⁵ Moreover, due to the kinetic instability of *trans*-DDP, several undesired reactions on its way to the biological target take place contributing to the lack of anticancer activity. As a result, the classical structure-activity relationship of platinum drugs stressed the necessity of the *cis* geometry identifying it as critical feature, and thousands of *cis* isomers of platinum compounds have been synthesized and screened for antitumor activity. Nevertheless, in recent years several Pt(II) compounds with *trans* geometry have been shown to be endowed with antitumor activity against different tumor cells, including ones resistant to *cis*-DDP thus violating the classical *cis* geometry paradigm.^{26,27} In general, it was observed that substitution of ammine ligands in transplatin with more bulky ligands led to compounds with higher *in vitro* tumor cell growth inhibitory potency. The bulky ligands can retard substitution reactions of the two leaving chlorides, thus reducing the kinetic instability of *trans*-platinum compounds. On the other hand, DNA adducts formed by antitumor-active *trans*-platinum complexes are qualitatively different from those formed by cisplatin, thus demonstrating that cisplatin-like DNA adducts are not obligatory determinants for antitumor activity of platinum compounds.

Distinct series of trans-Pt(II) and Pt(IV) complexes with a number of different N-donor ligands have been proposed and tested in the years, maintaining the activity profiles of their parent cis-compounds.

Among these, replacement of non-leaving amines with iminoethers ligands has led to a significant increase in the cytotoxicity activity of the trans compounds.

Iminoethers are N-donor ligands which share some features with both aliphatic amines and aromatic N-donor heterocycles such as pyridine. Like aromatic N-donor heterocycles iminoether ligands are planar (*sp*² hybridization of the nitrogen atom as compared to the *sp*³ hybridization in aliphatic amines) however, like aliphatic amines, they have one hydrogen atom linked to the nitrogen and suitable for hydrogen-bond formation. Iminoethers are also nonsymmetrical having the steric hindrance concentrated on one side of the nitrogen atom (that opposite to the proton). Another characteristic of iminoethers is the possibility of isomerism within the ligand moiety. Depending upon the relative positions of the substituents with respect to the C=N double bond, they can have *E* or *Z* configurations (*E* and *Z* correspond to having the platinum and the alkoxy group *trans* and *cis* with respect to the C=N double bond, respectively).²⁸⁻³⁰

In a panel of human tumor cell lines containing examples of ovary, colon, lung, and breast cancers, *Trans*-[PtCl₂{*E*-HN=C(OCH₃)CH₃}₂] (*Trans-EE*), has showed a growth inhibitory potency comparable to that of cisplatin. Although isomer *Z* showed a lower activity compared with *E* counterpart, both overcame cisplatin resistance of ovary cancer cell lines. Interestingly, the analogues compounds containing only one molecule of iminoether, were found to be less cytotoxic than *Trans-EE*. Due to its bulky ligands, *Trans-EE* is characterized by a reduced capability to form bifunctional adducts in double helical DNA.³⁰⁻³³

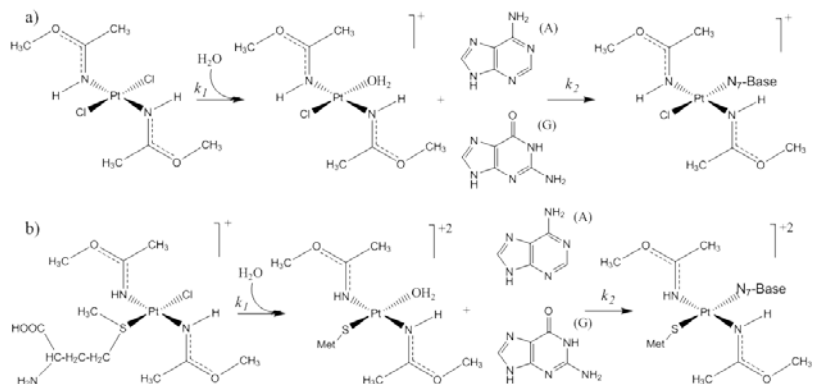
The most frequent adducts formed by cisplatin (1,2-intrastrand cross-links) are inaccessible to almost all trans compounds, and consequently they have been supposed to induce different structural perturbations in DNA compared with classical cis-compounds.

On this basis, it can be reasonably hypothesized that the general efficacy of *trans*-platinum complexes toward cisplatin resistant/refractory tumors might depend upon their specific chemical properties and type of DNA adducts. Therefore, it is important to examine the many mechanistic features of antitumor-active *trans*-platinum complexes and place them in context.

3.1.1 Computational Studies on *Trans-EE* and *Trans-EE/Met* Reaction Mechanisms (Paper V)

As introduced in the previous paragraph, *Trans*-[PtCl₂{E-HN=C(OCH₃)CH₃}₂] (*Trans-EE*), among the investigated platinum complexes with iminoethers ligands, has showed the greatest in vitro toxicity.³¹⁻³³ Moreover a recent study shows that the platination rate of both guanosine monophosphate (GMP) and DNA are significantly improved by the presence of an L-methionine (Met) ligand bound to *Trans-EE* (*Trans-EE/Met*).³⁴ Despite a limited structural modification, consisting in the substitution of one chloride with a methionine ligand, these two compounds seem to show a remarkably different chemical reactivity. Even if for *trans*-compounds the mechanism of action could be different from those with conventional *cis* geometry, also for these kind of compounds the hydrolysis process is expected to play an important role in their activation before reaching DNA. Actually, the hydrolysis steps for *Trans-EE* have been previously investigated experimentally and the relative kinetic constants are available in literature.³⁵ For *Trans-EE/Met* instead, only a global kinetic constant relative to the whole process of DNA platination was reported.³⁴ This value then does not give any indication of the specific step in which the methionine ligand promotes the reaction rate. To shed light on this aspect, the hydrolysis reaction processes as well as the reactions with DNA bases (Guanine (G) and Adenine (A)) for both *Trans-EE* and *Trans-EE/Met*, were explored separately in the framework of the DFT/CPCM approach, in order to provide a better interpretation of the experimental kinetic data available in

literature ³⁴ and provide atomistic details concerning their mechanisms of action.



Scheme 3.1: Investigated reaction paths for the formation of a) *Trans-EE*, b) *Trans-EE/Met* adducts with GN7 and AN7

From our calculations emerge that the presence of the methionine ligand enhances the hydrolysis process mostly stabilizing the penta-coordinate structure of the transition state. A detailed rationalization of the geometric and electronic factors that determine such stabilization are provided in the work. The activation barrier found for the *Trans-EE* chloride substitution is in good agreement with experimental kinetic data. ³⁵ Concerning *Trans-EE/Met*, our results clearly show that the experimental value ³⁴ is attributable to the hydrolysis process. Actually we were able to reproduce the activation barrier derived from exp. kinetic constant underestimating it by just 0.58 kcal/mol. The hydrolysis reaction, also in the case of these Pt complexes, is confirmed to be the rate determining step of the whole process. The following step is in fact the coordination to the purine base, that was found to be energetically favored in the case of Guanine. Also in this step, the methionine ligand promotes the reaction, lowering the activation barrier along the potential energy surface. The preference for the guanine platination by *Trans-EE/Met* is dominated by the possibility to establish H-bonds interactions which play then an important role in determining the hydrolysis behaviour. Interestingly, the presence of the

methionine ligand does not promote the platination of the Adenine residue, due to the lack of strong hydrogen-bonds in the structures containing that purine base and then determining the increase of both the activation energies. The indication that the adenine platination by both the Pt(II) complexes is not favored, gives evidence that the dominating preference for guanine base is a process completely hydrogen-bonds controlled. H-bonds are then confirmed to be implicated to impose both structural and kinetic control on the purine platination process, as observed in our previous works concerning cis-compounds and of course in analogy to DNA platination by cisplatin.³⁶ The results obtained in our work can well explain the published experimental observations and help to rationalize recent reports on the global effects of the amino acid methionine on DNA platination reactions of active Pt drugs having a trans geometry.

3.2 Non-platinum Compounds

In recent years, the search for new active metallodrugs has been substantially diversified by introducing various other transition metals of different clinical potential with the aims of developing alternative pharmaceuticals with high efficiency and reduced side-effects. Various metal complexes are currently tested as therapeutic agents in the treatment of malignant diseases, including several types of cancer. The major classes of metal-based anticancer drugs include ruthenium (II) and ruthenium (III), gold (I) and gold (III), metalloporphyrin, bismuth (III), rhenium (I), and copper (II) compounds.¹⁻¹¹ Octahedral **ruthenium (II) and ruthenium (III)** complexes have raised a great interest for their potential use as therapeutic anticancer agents and lower systemic toxicity than platinum(II) compounds. Tetraammine-, pentaammine-, heterocycle-, and dimethylsulfoxide-coordinated ruthenium complexes have been synthesized and exhibit significant anticancer action in vivo.³⁷⁻³⁹ Interestingly, it is now increasingly apparent that some of them do not behave

like cisplatin. Actually, a series of arene-ruthenium complexes have been designed to interact with DNA in a novel fashion compared to the platinum drugs. Compounds such as RM175 are designed to interact with DNA in a bifunctional manner by both intercalation and direct metallation.⁴⁰ Indazolium [bis-indazole-tetrachlororuthenate] (KP1019) which has promising activity against models of colorectal cancer, is redox activated and is transported by the transferring system.⁴¹ Among these, ImH[*trans*-RuCl₄(DMSO)(Im)] (NAMI-A), developed by Sava et al.,⁴² is the first ruthenium anticancer complex that has entered clinical testing and recently has finished in the clinical trials of the first phase as an antimetastatic drug.⁴³ NAMI-A is pseudooctahedral with four equatorial chloride ligands, and DMSO and imidazole as axial ligands.⁴⁴ Preclinical pharmacological studies with NAMI-A showed a selective activity against lung metastases of murine tumors⁴⁴⁻⁴⁶ and a relatively low toxicity in mice and dogs.⁴⁷⁻⁴⁹

The potential use of **gold, in particular Au(III)** complexes as anticancer drugs was also explored in the past few years. Buckley et al. first reported some organogold (III) complexes endowed with significant cytotoxic and anticancer properties.⁵⁰ The major limitation of gold (III) complexes is that few exhibit good stability under physiological conditions, due to the reduction of gold (III) to gold (I).⁵¹ Nevertheless, during the past decades, various gold (III) complexes with sufficient stability in the physiological environment have been synthesized and evaluated for in vitro anticancer properties. Some of these gold (III) complexes turned out to exhibit relevant cytotoxic effects in vitro and have been the subject of further biochemical and pharmacological investigations.⁵²⁻⁶⁵

Other transition metals have been used as anticancer drugs, including bismuth (III) labeled antibodies for systemic radioimmunotherapy^{66,67}, (MTR)₂Zn²⁺ complex that induces cancer cell death by binding to chromatin,⁶⁸ and Cu²⁺ compound chlorophyllin initiated apoptosis in human colon cancer cells through caspase-8 and apoptosis-inducing factor (AIF) activation in a cytochrome c-independent manner.⁶⁹

Within this context, **Rhenium** complexes have attracted growing attention for their possible use as anticancer drugs.¹²⁻¹⁶ Moreover, rhenium has two radioisotopes (¹⁸⁶Re and ¹⁸⁸Re) of interest for nuclear medicine, both having effectiveness for either cancer therapy (owing to the β - emission)⁷⁰⁻⁷⁴ or diagnosis⁷⁵⁻⁸² (owing to the γ emission with similar energies to that of ^{99m}Tc). To date, the studies reported in literature on the anticancer activity and the therapeutic and diagnostic applications of rhenium derivatives deal with Re(I), Re(III) or Re(V) metal complexes, while the Re(IV) oxidation state remained unexplored. Re(IV) is a 5d³ ion that usually forms octahedral complexes displaying structural similarity to those of Pt(IV), Ru(II) and Ru(III) active compounds. Moreover, they are quite inert to ligand substitution and reasonably stable against redox processes,⁸³⁻⁸⁵ this property being suitable to reduce the toxicities associated with platinum-based chemotherapies.^{86,87} Considering all these features, Re(IV) complexes seem to be promising candidates for the developments of new anticancer drugs with improved pharmacological properties. Understanding the mechanism of action of these metal-based drugs is for the design of more effective drugs.

3.2.1 Promising Rhenium(IV) complexes as anticancer drugs: an experimental and computational investigation (Paper VI)

When experimental and computational research methods are combined, improved understanding and new discoveries can result. In order to explore the still unknown rhenium chemistry and its potential role as anticancer drugs, we performed a multi-disciplinary experimental and computational study on a series of Re(IV) compounds. Mononuclear complexes of general formula ReCl₄L [ReCl₄(bpy)] **(1)**, [ReCl₄(bpym)] **(2)**, [ReCl₄(dmbpy)] **(3)** and [ReCl₄(phen)] **(4)** were prepared by means of ligand substitution reaction from [ReIVCl₆]²⁻ anion in N,N-dimethylformamide (DMF) and tested against MCF-7 breast, BG-1 ovarian, LNCaP prostate, cancer cells lines. These biomedical

studies revealed that all the synthesized compounds display *in vitro* potent antiproliferative activity, especially against the MCF-7 breast human tumor cells types. Remarkably, compounds **1-4** inhibited cell growth in a stronger manner respect to cisplatin, hence their biological activity might be relevant towards innovative anti-cancer drug discovery. It is worth noting that compounds **1** and **4** exhibited in MCF-7 cells a strong repressive effect as its lowest concentrations blocked cell growth after only one day of treatment.

Due to the presence of chloride anions as good leaving groups and the structural similarity of **1-4** to some Ru(II) and Ru(III) active complexes, for which it's accepted that the aquated species are likely to be responsible for their biological effects,^{88,89} it can be supposed that also these drugs can hydrolyze *in vivo*, forming a number of potentially active species. Computational studies were then conducted in order to explore the mechanisms of the possible hydrolysis reactions and to provide insights on the kinetic of these processes. Moreover, our hypothesis is supported by ESI MS spectra of **1-4** in DMSO/H₂O indicating the formation of mono-aquated derivatives. Also in this case, the DFT/CPCM approach was the employed tool. The results were compared with the data available in the literature on the Pt(II) anticancer drugs. From our data emerge that the formation of the **1** and **2**-aqua complexes require an amount of energy close to that demanded by the second and third Pt(II) anticancer drugs generation. In particular they show energetic profiles similar to that of carboplatin, allowing us to hypothesize that undesired reactions on the way to the DNA target could be avoided.

Bibliografia

- [1] Z. Guo, P. J. Sadler, *Angew. Chem. Int. Ed.* **1999**, 38, 1512.
- [2] N. Farrer, L. Salassa, P. J. Sadler, *Dalton Trans.* **2009**, 10690.
- [3] P. Blower, *Dalton Trans.* **2006**, 1705.
- [4] X. Wang, Z. Guo, *Dalton Trans.* **2008**, 1521.
- [5] S. P. Fricker, *Dalton Trans.* **2007**, 4903.
- [6] S. P. Fricker, *Metallomics* **2010**, 2, 366.
- [7] J. Reedijk, *Macromol. Symp.* **2008**, 270, 193.
- [8] *Metallotherapeutic Drugs and Metal-Based Diagnostic Agents: The Use of Metals in Medicine* (Eds: M. Gielen and E. R. T. Tiekink), John Wiley & Sons, **2005**.
- [9] Ying Wang and Jen-Fu Chiu, *Metal-Based Drugs*, **2008**, 1-9.
- [10] *Metal Complexes in Cancer Chemotherapy*, ed. B. K. Keppler, VCH, Weinheim, **1993**.
- [11] *Metal Compounds in Cancer Therapy*, ed. S. P. Fricker, Chapman and Hall, London, **1994**.
- [12] A. Zablotskaya, I. Segal, E. Lukevics, S. Belyakov and H. Spies *Appl. Organometal. Chem.* **2007**, 21, 288.
- [13] D.-L. Ma, C.-M. Che, F.-M. Siu, M. Yang, K.-Y. Wong, *Inorg. Chem.* **2007**, 46, 740.
- [14] N. Viola-Villegas, A. E. Rabideau, J. Cesnavicius, J. Zubieta, R. P. Doyle S. Wirth, A. U. Wallek, A. Zernickel, F. Feil, M. Sztiller-Sikorska, K. Lesiak-Mieczkowska, C. Bräuchle, I. P. Lorenz, M. Czyz, *ChemMedChem* **2008**, 3, 1387.
- [15] A. V. Shtemenko, P. Collery, N. I. Shtemenko, K. V. Domasevitch, E. D. Zabitskayac and A. A. Golichenkoa *Dalton Trans.*, **2009**, 5132.
- [16] S. Wirth, A. U. Wallek, A. Zernickel, F. Feil, M. Sztiller-Sikorska, K. Lesiak-Mieczkowska, C. Bräuchle, I.-P. Lorenz, M. Czyz, *J. Inorg. Biochem.* **2010**, 104, 774.
- [17] S. E. Sherman, S. J. Lippard, *Chem. Rev.* **1987**, 87, 1153.
- [18] W. J. Heiger-Bernays, J. M. Essigmann, S. J. Lippard, *Biochemistry* **1990**, 29, 8461.
- [19] Y. Jung, S. J. Lippard, *Chem. Rev.* **2007**, 107, 1387.
- [20] V. Brabec, M. Leng, *Proc. Natl. Acad. Sci. U.S.A.* **1993**, 90, 5345.
- [21] H. H. Zheng, Z. H. Xu, K. Wang, *Int. J. Biol. Macromol.* **1997**, 20, 107.
- [22] X. L. Zhou, Y. Yang, Z. F. Li, B. H. Wang, Y. M. Zhang, *J. Therm. Anal. Calorim.* **1999**, 58, 243.
- [23] W. H. Du, W. Han, Z. F. Li, B. H. Wang, *Thermochim. Acta* **2000**, 359, 55.
- [24] K. Wozniak, Z. Walter, *Z. Naturforsch. Teil C* **2000**, 55, 731.
- [25] O. Novakova, J. Kasparkova, J. Malina, G. Natile, V. Brabec, *Nucleic Acids Res.* **2003**, 31, 6450.
- [26] M. Coluccia, G. Natile, *Anti-Cancer Agents Med. Chem.* **2007**, 7, 111.
- [27] U. Kalinowska-Lis, J. Ochocki, K. Matlawska-Wasowska, *Coord. Chem. Rev.* **2008**, 252, 1328.
- [28] R. Cini, P. A. Caputo, F. P. Intini, G. Natile, *Inorg. Chem.*, **1995**, 34, 1130.
- [29] A. Boccarelli, M. Coluccia, F. P. Intini, G. Natile, D. Locker, M. Leng, *Anticancer Drug Design*, **1999**, 14, 253.
- [30] M. Coluccia, A. Nassi, A. Boccarelli, D. Giordano, N. Cardellicchio, D. Locker, M. Leng, M. F. Sivo, F. P. Intini, G. Natile, *J. Inorg. Biochem.*, **1999**, 77, 31.
- [31] M. Coluccia, A. Nassi, F. Loseto, A. Boccarelli, M. A. Mariggio, D. Giordano, F. P. Intini, P. Caputo, G. Natile, *J. Med. Chem.* **1993**, 36, 510.
- [32] M. Coluccia, A. Boccarelli, M. A. Mariggio, N. Cardellicchio, P. Caputo, F. P. Intini and G. Natile, *Chem. Biol. Interact.*, **1995**, 98, 251.
- [33] V. Brabec, O. Vrana, O. Novakova, V. Kleinwachter, F. P. Intini, M. Coluccia and G. Natile, *Nucleic Acids Res.*, **1996**, 24, 336.
- [34] C. Li, Z. Li, E. Sletten, F. Arnesano, M. Losacco, G. Natile, Y. Liu *Angew. Chem. Int. Ed.* **2009**, 48, 8497.

- [35] Y. Liu, F. P. Intini, G. Natile, E. Sletten *J. Chem. Soc., Dalton Trans.*, **2002**, 3489.
- [36] Baik M. H.; Friesner R. A.; Lippard, S. J. *J. Am. Chem. Soc.* **2003**, 125, 14082.
- [37] E. Reisner, V. B. Arion, M. F. C. Guedes da Silva, et al., *Inorganic Chemistry*, **2004**, 43, 7083.
- [38] M. J. Clarke, S. Bitler, D. Rennert, M. Buchbinder, and A. D. Kelman, *Journal of Inorganic Biochemistry*, **1980**, 12, 79.
- [39] L. Mishra, R. Sinha, H. Itokawa, et al., *Bioorganic & Medicinal Chemistry*, **2001**, 9, 1667.
- [40] R. E. Aird, J. Cummings, A. A. Ritchie, M. Muir, R. E. Morris, H. Chen, P. J. Sadler and D. I. Jodrell, *Br. J. Cancer*, **2002**, 86, 1652.
- [41] C. G. Hartinger, S. Zorbas-Seifried, M. A. Jakupce, B. Kynast, H. Zorbas and B. K. Keppler, *J. Inorg. Biochem.*, **2006**, 100, 891.
- [42] A. Bergamo and G. Sava, *Dalton Trans.*, **2007**, 1267.
- [43] Hotze, A. C. G.; Bacac, M.; Velders, A. H.; Jansen, B. A. J.; Kooijman, H.; Spek, A. L.; Haasnoot, J. G. and Reedijk, J. *J. Med. Chem.* **2003**, 46, 1743.
- [44] G. Sava, E. Alessio, A. Bergamo, G. Mestroni, *In Topics in Biological Inorganic Chemistry*; Clarke, M. J., Sadler, P. J., Eds.; Springer: Berlin, **1999**; p 143.
- [45] G. Sava, I. Capozzi, K. Clerici, R. Gagliardi, E. Alessio, G. Mestroni, *Clin. Exp. Metastasis* **1998**, 16, 371.
- [46] G. Sava, K. Clerici, I. Capozzi, M. Cocchietto, R. Gagliardi, E. Alessio, G. Mestroni, A. Perbellini, *Anti-Cancer Drugs* **1999**, 10, 129.
- [47] A. Bergamo, S. Zorzet, B. Gava, A. Sorc, E. Alessio, E. Iengo, G. Sava, *Anti-Cancer Drugs* **2000**, 11, 667.
- [48] M. Cocchietto, G. Sava, *Pharmacol. Toxicol.* **2000**, 87, 193.
- [49] G. Sava, M. Cocchietto, *In ViVo* **2000**, 14, 741.
- [50] R. G. Buckley, A. M. Elsome, S. P. Fricker, et al., *Journal of Medicinal Chemistry*, **1996**, 39, 5208.
- [51] C. F. Shaw, III, *Chemical Reviews*, **1999**, 99, 2589.
- [52] A. Casini, M. A. Cinellu, G. Minghetti, et al., *Journal of Medicinal Chemistry*, **2006**, 49, 5524.
- [53] M. Coronello, E. Mini, B. Caciagli, et al., *Journal of Medicinal Chemistry*, **2005**, 48, 6761.
- [54] L. Giovagnini, L. Ronconi, D. Aldinucci, D. Lorenzon, S. Sitran, and D. Fregona, *Journal of Medicinal Chemistry*, **2005**, 48, 1588.
- [55] I. Kostova, *Anti-Cancer Agents in Medicinal Chemistry*, **2006**, 6, 19.
- [56] G. Marcon, L. Messori, P. Orioli, M. A. Cinellu, and G. Minghetti, *European Journal of Biochemistry*, **2003**, 270, 4655.
- [57] G. Marcon, S. Carotti, M. Coronello, et al., *Journal of Medicinal Chemistry*, **2002**, 45, 1672.
- [58] L. Messori, F. Abbate, G. Marcon, et al., *Journal of Medicinal Chemistry*, **2000**, 43, 3541.
- [59] L. Messori, P. Orioli, C. Tempi, and G. Marcon, *Biochemical and Biophysical Research Communications*, **2001**, 281, 352.
- [60] L. Ronconi, C. Marzano, P. Zanello, et al., *Journal of Medicinal Chemistry*, **2006**, 49, 1648.
- [61] L. Ronconi, L. Giovagnini, C. Marzano, et al., *Inorganic Chemistry*, **2005**, 44, 1867.
- [62] S. Sundriyal, R. K. Sharma, and R. Jain, *Current Medicinal Chemistry*, **2006**, 13, 1321.
- [63] A. Garza-Ortiz, H. den Dulk, J. Brouwer, H. Kooijman, A. L. Spek, and J. Reedijk, *Journal of Inorganic Biochemistry*, **2007**, 101, 1922.
- [64] D. Aldinucci, D. Lorenzon, L. Stefani, L. Giovagnini, A. Colombatti, and D. Fregona, *Anti-Cancer Drugs*, **2007**, 18, 323.
- [65] F. Caruso, R. Villa, M. Rossi, et al., *Biochemical Pharmacology*, **2007**, 73, 773.
- [66] J. Kotzerke, D. Bunjes, and D. A. Scheinberg, *Bone Marrow Transplantation*, **2005**, 36, 1021.

- [67] P. L. Beaumier, P. Venkatesan, J.-L. Vanderheyden, et al., *Cancer Research*, **1991**, 51, 676.
- [68] S. Das and D. Dasgupta, *Journal of Inorganic Biochemistry*, **2005**, 99, 707.
- [69] G. D. Díaz, Q. Li, and R. H. Dashwood, *Cancer Research*, **2003**, 63, 1254.
- [70] K. Hashimoto, K. Yoshihara, *Top. Curr. Chem.* **1995**, 176, 275.
- [71] J. R. Dilworth and S. J. Parrott, *Chem. Soc. Rev.*, **1998**, 27, 43.
- [72] J. Caoa, Y. Wang, J. Yua, J. Xiaa, C. Zhanga, D. Yina, U. O. Hafelib *Journal of Magnetism and Magnetic Materials* **2004**, 277, 165.
- [73] P. Blower, *Dalton Trans.* **2006**, 1705.
- [74] B. Goins, A. Bao, W. T. Phillips, *Methods Mol Biol.* **2010**, 606, 469.
- [75] E. A. Deutsch, K. Libson, J. L. Vanderheyden, in *Technecium and Rhenium in Chemistry and Nuclear Medicine*, Raven Press, New York, **1990**;
- [76] J. F. Eary, L. Durack, D. Williams, J. L. Vanderheyden. *Clin. Nucl. Med.* **1990**, 15, 911.
- [77] W. Volkert, W. F. Goeckeler, G. J. Ehrhardt, A. R. Ketring, *J. Nucl. Med.* **1991**, 32, 174.
- [78] E. John, M. L. Thakur, J. De Fulvio, M. R. McDevitt, I. Dajanov, *J. Nucl. Med.* **1993**, 34, 260.
- [79] S. S. Jurisson, J. D. Lydon, *Chem. Rev.* **1999**, 99, 2205.
- [80] S. Liu, D. S. Edwards, *Chem. Rev.* **1999**, 99, 2235.
- [81] W. A. Volkert, T. J. Hoffman, *Chem. Rev.* **1999**, 99, 2269.
- [82] J. Sattigeri, A. L. Rodriguez, J. A. Katzenellenbogen, *Bioorg. Med. Chem.* **2002**, 10, 1381.
- [83] G. Rouschias, *Chem. Rev.* 1974, 74, 531.
- [84] K. A. Conner, R. A. Walton in *Comprehensive Coordination Chemistry*, (Eds: G. Wilkinson, R. D. Gillard, J. A. McCleverty), Pergamon Press: New York, **1987**, Vol. 4, pp. 165;
- [85] M. N. Sokolova, N. E. Fedorova, E. V. Peresykina, R. Patow, V. E. Fedorova, D. Fenske, *Inorg. Chim. Acta* **2005**, 358, 3914.
- [86] L. R. Kelland, G. Abel, M. J. McKeage, M. Jones, P. M. Goddard, M. Valenti, B. A. Murrer, K. R. Harrap, *Cancer Research* **1993**, 53, 2581.
- [87] M. D. Hall, T. W. Hambley, *Coord. Chem. Rev.* **2002**, 232, 49.
- [88] N. Bešker, C. Coletti, A. Marrone, N. Re, *J. Phys. Chem. B* **2007**, 111, 9955.
- [89] J. Chen, L. Chen, S. Liao, K. Zheng, L. Ji, *J. Phys. Chem. B* **2007**, 111, 7862.

Appendix A

Paper I

“The Second-Generation Anticancer Drug Nedaplatin:
A Theoretical Investigation on the Hydrolysis Mechanism”

Marta E. Alberto, Maria Fatima A. Lucas, Matěj Pavelka, and Nino Russo

J. Phys. Chem. B **2009**, *113*, 14473–14479

The Second-Generation Anticancer Drug Nedaplatin: A Theoretical Investigation on the Hydrolysis Mechanism

Marta E. Alberto, Maria Fatima A. Lucas, Matěj Pavelka, and Nino Russo*

Dipartimento di Chimica, Università della Calabria, Via P. Bucci, cubo 14c,
87036 Arcavacata di Rende (CS), Centro di Calcolo ad Alte Prestazioni per Elaborazioni Parallele
e Distribuite - Centro d'Eccellenza MIUR, Italy

Received: June 17, 2009; Revised Manuscript Received: August 26, 2009

The hydrolysis reaction processes of the second-generation platinum derivative Nedaplatin have been studied using density functional theory (DFT) combined with the conductor-like dielectric continuum model (CPCM) approach, in order to obtain detailed data on its mechanism of action. The first and the second hydrolysis of Nedaplatin, corresponding to the ring opening followed by the loss of the ligand, respectively, have been explored in neutral and acid conditions. The influence of an extra water molecule which could assist the degradation processes has also been considered including in our models an explicit water molecule other than the reactive one. The computed potential energy surfaces show that the rate limiting step in neutral conditions is the first hydrolysis process and, consequently, the double hydrated complex is suggested to be the species reacting with the DNA purine bases, while in acid conditions the trend is different, with the second hydrolysis process being the rate limiting step. The results obtained in this work allow us to make a comparison with the trends previously found for the other platinum anticancer drugs currently used in the medical protocols.

Introduction

The discovery of an inhibitory effect of a soluble platinum complex on the division of living cells led to the development of platinum-based drugs to treat a wide range of cancers.^{1,2}

Interaction with DNA and formation of cross-links with adjacent purine bases are considered to be the crucial steps in the antitumor activity of this class of complexes.³

Cisplatin, the first platinum and the world's best selling anticancer drug, began to be used in treatment in 1977. Testicular cancer was found to be susceptible to treatment with Cisplatin, and there were other successes with ovarian, head, bladder, cervical, and neck cancers.⁴

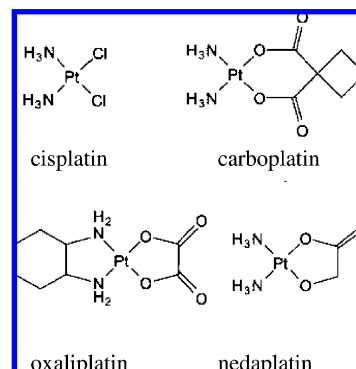
Unfortunately, its therapeutic efficacy is somewhat compromised by the occurrence of serious side effects such as nausea/vomiting and nephro-, oto-, and neurotoxicity.^{5–7}

In order to overcome these limitations, many studies have been done to find other platinum drugs with an equivalent or improved range of activity but with less toxic side effects.^{3,8–10}

Since the discovery of Cisplatin, a large number of platinum compounds (more than 3000) has been screened for antitumor activity, but only four of them are currently registered for clinical use. *cis*-Diammine(1,1-cyclobutanedicarboxylato) platinum II (Carboplatin),⁹ *trans*-L-1,2-diaminocyclohexanecarboxylato platinum II (Oxaliplatin),⁹ and *cis*-diammineglycolato platinum II (Nedaplatin)⁹ are analogues of Cisplatin and show a lowered nephrotoxicity compared with Cisplatin.^{8,10} The chemical structures of these platinum-containing drugs are shown in Scheme 1.

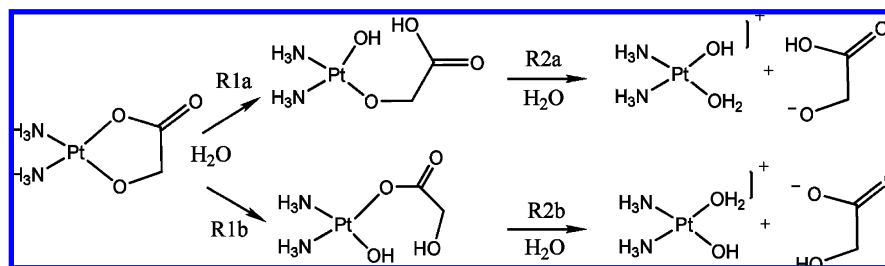
Carboplatin is effective against about the same tumor types as Cisplatin, but in contrast, it presents less side effects.¹¹ Unlike Cisplatin, that should bind to DNA monohydrated, Carboplatin has been proposed to reach DNA in its double hydrated form.¹² Nevertheless, both species are believed to exert their cytotoxicity by coordinating bifunctionally to DNA through the N7 atoms

SCHEME 1



of two adjacent guanines on the same strand (intrastrand cross-links), arresting DNA replication.^{4,13,14}

Recent research has sought to identify new platinum compounds which will treat tumors which do not respond to or which become resistant to Cisplatin and Carboplatin. The first of these drugs to reach commercialization is Oxaliplatin.¹⁵ It shows activity against some tumors that are primarily resistant to the other two platinum compounds, being the first antineoplastic agent for the treatment of metastatic colorectal cancer.^{16,17} Oxaliplatin in combination therapy has been evaluated in clinical trials against metastatic breast cancer,¹⁸ recurrent ovarian cancer,¹⁹ and pancreatic and esophagogastric cancer.^{20,21} It has been suggested that the third-generation drug Oxaliplatin acts as an alkylating agent on DNA, forming essentially three types of cross-link adducts: intrastrand, interstrand, and DNA–protein. The most commonly adduct is nevertheless the intrastrand bridging two adjacent purine bases (1,2-GG or AG) at the N7 position.^{3,13} As Carboplatin, in a previous work, it has been suggested that Oxaliplatin, would reach DNA in its fully hydrolyzed complex.²² Important differences are observed

SCHEME 2: Investigated Reaction Pathways for the Hydrolysis of Nedaplatin in Neutral Conditions

between Cisplatin and Carboplatin adducts with DNA when compared with Oxaliplatin DNA ones; these adducts are more bulky and hydrophobic than the other ones and subsequently are more effective in inhibiting DNA synthesis and usually more cytotoxic than *cis*-diammine-platinum adducts.²³ Nevertheless, Oxaliplatin shows several limitations such as a reversible peripheral neuropathy characterized by paraesthesia and dysaesthesia in hands, feet, and the oral region.^{3,8,10} The acute neurotoxic side effects have been suggested to involve voltage-gated ion channels.^{24,25} Due to the presence of the kinetically less labile carboxylate or oxalate present in Carboplatin and Oxaliplatin, these compounds are expected to be responsible for the reduced side effects observed in patients compared with those treated with Cisplatin.¹¹

Nedaplatin (*cis*-diammine-glycolate-O,O'-platinum II) is a second-generation platinum derivative, with relevant antineoplastic activity.^{26–28} It contains a novel ring structure in which glycolate is bound to the platinum by a bidentate ligand and forms reactive platinum complexes that bind to nucleophilic groups in DNA, resulting in intrastrand and interstrand DNA cross-links, apoptosis, and cell death. Nedaplatin has shown superior antitumor activity and less renal or gastrointestinal toxicity when compared to Cisplatin in several Japanese clinical studies in which the drug was used to treat head and neck, lung, and cervical cancers.^{26–28} This agent appears to be also less nephrotoxic and neurotoxic compared to both Cisplatin and Carboplatin. It has been available for use there since 1995 and shows pronounced efficacy against lung, head and neck, testicular, and gynecological cancers.^{29,30}

In this Article, we focus our attention on the degradation pathway of Nedaplatin, in both neutral and acid conditions, in order to individuate the species that probably will react with DNA.

The kinetic studies of the hydrolysis of Cisplatin and its analogues in various solution conditions have been the object of continuous interest, becoming a substantial part of contemporary medicinal inorganic chemistry. With the development of computational transition metal chemistry, the necessity to obtain an accurate picture of the hydrolysis mechanisms of anticancer drugs is increased. The employed tool (DFT-B3LYP) can be considered the state of the art of the modern theoretical methods, providing an excellent compromise between accuracy of the results and the requested computational efforts. It has been previously used in a huge number of chemical systems including the aquation processes of metal-containing anticancer drugs.^{12,31–37}

According to our results, the degradation process should take place in two consecutive steps: first, water addition with ring opening, followed by the loss of the ligand by reaction with the second water molecule.

Computational Details

All calculations were performed with the Gaussian 03³⁸ program at the density functional theory level, using the hybrid

B3LYP functional, composed of Becke's³⁹ three-parameter hybrid exchange functional (B3) and the correlation functional of Lee, Yang, and Parr (LYP).⁴⁰ Geometry optimizations without symmetry constraints and in solvent ($\epsilon = 80$) were carried out with a 6-31G(d) basis set for all atoms except the platinum atom, which was described by the quasi-relativistic Stuttgart–Dresden pseudopotentials⁴¹ with the pseudo-orbital basis set augmented by a set of diffuse functions, $\alpha_s = 0.0075$, $\alpha_p = 0.013$, and $\alpha_d = 0.025$, and polarization functions, $\alpha_f = 0.98$.⁴² In order to confirm proper convergence to equilibrium and transition state geometries, vibrational frequency analysis was done on the basis of analytical second derivatives of the Hamiltonian at this level of theory. Solvent effects were taken into account by the CPCM method.⁴³ Klamt radii were used for constructing the solute cavity.⁴⁴

More accurate energies were obtained by performing single-point calculations with the larger basis set 6-31++G(2df,2pd). Similarly, the platinum valence basis set was augmented with diffuse ($\alpha_f = 0.46$) and polarization ($\alpha_g = 1.21$) functions.⁴² Potential energy profiles were estimated from total electronic energies at the 6-31++G(2df,2pd) level adding zero point energy (ZPE) and enthalpy corrections at room temperature (298.15 K).

Results and Discussion

The hydrolysis reactions of the platinum(II) derivative anticancer drugs belong to the class of second-order nucleophilic substitution (S_N2) reactions. These reactions for square-planar complexes proceed via a collision between the reactant with two consecutive nucleophilic species attacking the metal center to release the ionic ligand. In such a process, a transition state in which the entering molecule, the leaving group, and the metal complex result weakly bound can be found, suggesting that the associative mechanism may be preferred and are consistent with the experimental studies on the aquation of some Pt(II) complexes with *in vivo* anticancer activities.⁴⁵ The equatorial plane of the five-coordinated TS structure plays an important role in determining the hydrolysis behavior. As introduced previously, the Nedaplatin degradation process should take place in two consecutive steps: first, water addition with ring opening followed by the loss of the ligand as a consequence of the second entering water molecule. We studied this kind of mechanism in both neutral and acid conditions in order to establish the most favorable energy path. A comparison between the results obtained previously^{12,22,32,34,37} on similar compounds is reported in order to spotlight possible common or different behavior. In analogy with previous studies on Cisplatin-like anticancer drugs, one of the purposes is moreover to identify which is the species that could reach DNA in each environment.

1. Energetic Profiles of Hydrolysis Reactions of Nedaplatin in Neutral Conditions. The elucidation of the degradation mechanisms, in neutral conditions, of the second anticancer drug Nedaplatin, represents the first step of our investigation. The

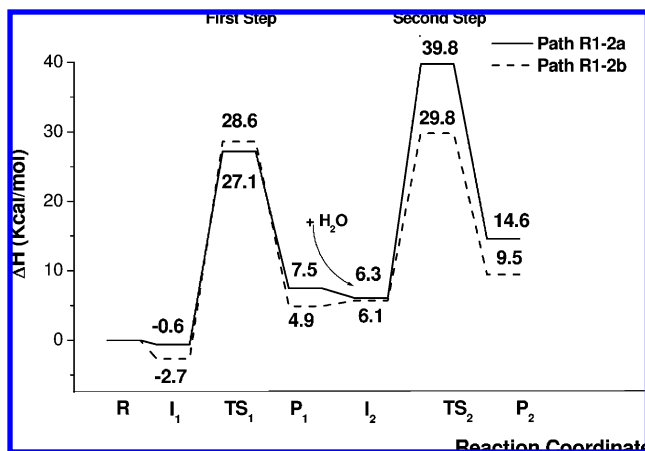


Figure 1. Activation enthalpy profiles (at 298.15 K) for the hydrolysis of Nedaplatin in neutral conditions, in the water phase.

investigated reaction paths for the hydrolysis of Nedaplatin under these conditions are depicted in Scheme 2.

The detachment of the ligand can occur in two different ways, by rupture of the bond that involves the oxygen in α to the carbonyl group (R1a) or by breaking the other Pt–O bond (R1b). The products obtained in this step show a proton transfer from the entered water molecule to the close oxygen of the ligand (O_L). Both of the products are expected to undergo a second hydrolysis process through different pathways (R2a and R2b), leading to the loss of the ligand and to the formation of *cis*-[Pt(NH₃)₂(OH)₂](OH)⁺ complexes. The hydroxo complex is accessible at physiological pH and temperature, even if in the vicinity of macromolecules the local pH could be influenced, reflecting its effect on hydrolysis rates.^{46,47}

We will discuss first the water addition and the consequent ring opening.

The potential energy surfaces are depicted in Figure 1, and the optimized structures for both reactions are depicted in Figure 2.

We considered separated reactants (R) as a reference state rather than reactant adducts (I₁) (see also Figure 2), to predict

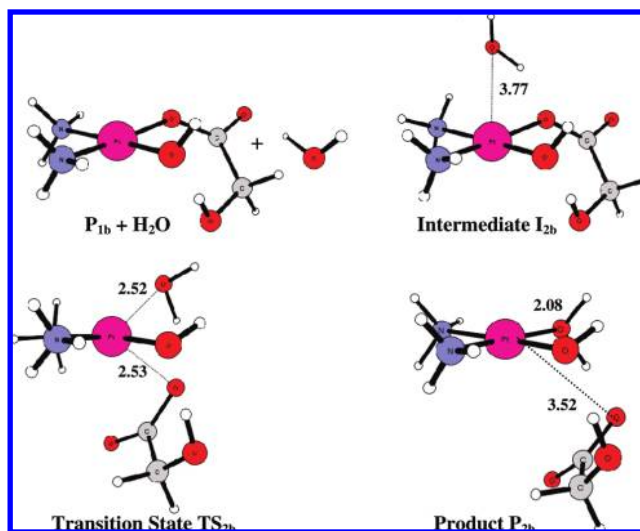


Figure 3. Optimized structures and selected structural parameters for the addition of the second water molecule to Nedaplatin (R2b) in neutral conditions, in the water phase. The distances reported are in angstroms.

the activation barriers, since it is well accepted that considering at the beginning of the reaction, the water molecule in the second coordination shell of the metal, it is acceptable only in vacuo but seems an artifact in solvent.^{34,37} The potential energy profiles, for the first step, show that both of the intermediates lie under the reactant molecules; nevertheless, the most stable is that obtained in the R1b path due to the stronger interaction of the water molecule with the oxygen of the glycolate ligand (Figure 2). The energies of the transition states for the steps R1a and R1b are very similar. The first reaction requires 27.1 kcal/mol, while step R1b shows an activation barrier of 28.6 kcal/mol and conduces to the most stable product. The imaginary frequencies observed in the transition states are about 207i cm⁻¹ for TS_{1a} and 340i cm⁻¹ for TS_{1b}, and the analysis of these vibrational modes clearly indicates the rupture of the bond between platinum and the ligand (Pt–O_L), and the simultaneous formation of the metal–water (Pt–O_W) bond.

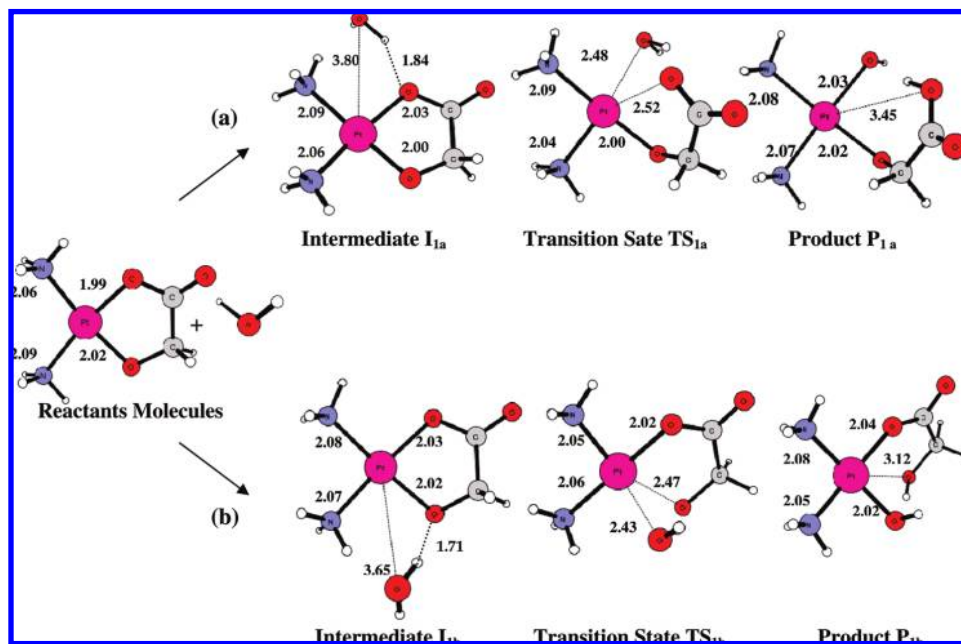


Figure 2. Optimized structures and selected structural parameters for the addition of the first water molecule to Nedaplatin in neutral conditions, in the water phase: (a) path R1a; (b) path R1b. The distances reported are in angstroms.

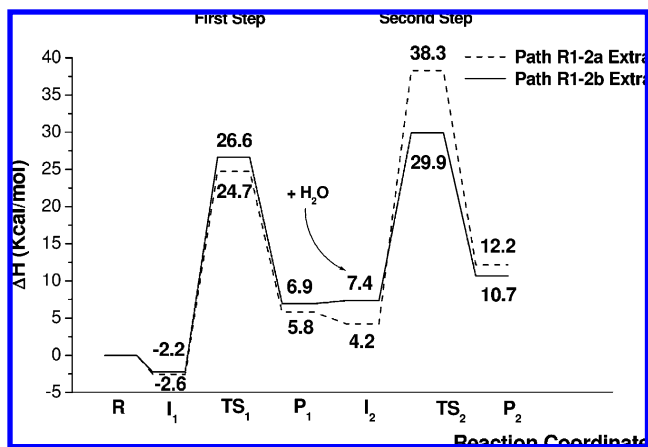


Figure 4. Activation enthalpy profiles (at 298.15 K) for the hydrolysis of Nedaplatin in neutral conditions, with an extra water molecule in the system. The energies refer to the water phase.

Both of the transition states show a penta-coordinated structure, according with an associative S_N2 reaction. The $N-Pt-O_L$ angle becomes greater than 90° in order to allow the entering of the water molecule in the opposite side of the leaving group. The final products for the first step of the reaction are obtained by overcoming similar activation barriers, and both are expected to undergo a second hydrolysis process. Moreover, it can be observed that both display a proton transfer from the water molecule to the oxygen atom O_L and the hydroxo complex re-establishes its square-planar conformation.

In the second step of the reaction, the addition of a second water molecule to both of the final products of the first step leads to the loss of the glycolate ligand. Therefore, we considered the second water molecule entering in two different orientations and following the steps R2a and R2b, as proposed in Scheme 2. As shown in Figure 1, the most energetically favorable path is R2b, with an activation barrier of 29.8 kcal/mol with respect to the initial reactant molecules, which conduces also to the most stable product. The optimized structures for the R2b reaction are displayed in Figure 3, while those relative to the R2a path are reported in Figure S1 of the Supporting Information.

In the intermediate structure, the water molecule approaches the platinum center with a distance of 3.77 Å that becomes 2.52 Å in the TS and 2.08 Å in the product. The imaginary frequency for the transition state (TS_{2b}) is $225i\text{ cm}^{-1}$ and corresponds to the $Pt-O_L$ and $Pt-O_W$ bonds being broken and formed, respectively. The activation barrier is slightly higher than the first one, being 29.8 kcal/mol, and the reaction exothermicity is 9.5 kcal/mol, considering the initial reactant molecules. Nevertheless, considering as a reference state the product obtained in the previous step and a separate water molecule, as shown in Figure 3, and according to other works on similar systems,^{34,37} we obtain an activation energy of 24.9 kcal/mol

and an exothermicity of 4.6 kcal/mol (see section 3). Thus, the reaction proceeds along path R1b in which the product P_{1b} obtained in the previous step reacts with another water molecule, leading to the loss of the ligand.

In order to verify the possible influence of an extra water molecule which could assist the hydrolysis processes, we conducted an additional study including in our systems another water molecule acting as an explicit solvent. This model incorporates the effects of hydrogen bonding and provides a more accurate description of the stabilization of the leaving group. The obtained paths for each step of reaction (R1a, R1b, R2a, and R2b) are reported in Figure 4. The results show that the main effect of considering explicitly an extra water molecule together with solvent bulk effects is observable on the energetics of the process. The activation barriers result all lowered compared with previous results, but the general trend of the reaction was not affected. Also, in this case, the ring-opening reaction (first step) requires an amount of energy very similar for the two paths (R1a and R1b); as a consequence, both of the products can be obtained and can undergo second hydrolysis. The most favorable path for the second step is again R2b.

The optimized structures of the stationary points for the ring-opening reaction as well as for the loss of the glycolate ligand are reported in Figure S2 of the Supporting Information.

It can be observed that the critical bond lengths in the transition states and in the intermediates, considering this model, do not change significantly.

2. Energetic Profiles of Hydrolysis Reactions of Nedaplatin in Acid Conditions. The degradation pathway of the second-generation drug Nedaplatin in acid conditions has also been investigated. In these conditions, the glycolate ligand results protonated. The investigated reaction paths are illustrated in Scheme 3.

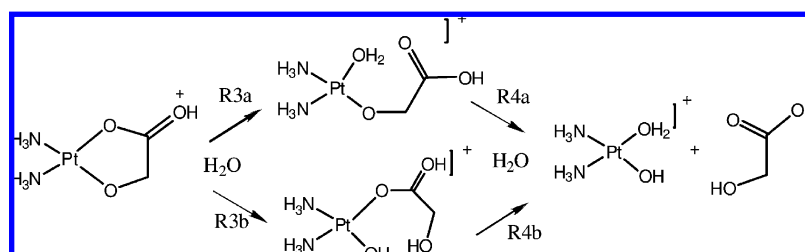
Also, in this case, the addition of the first water molecule can occur in two different ways, leading to the ring opening of the ligand. In step R3a, the detachment takes place by rupture of the bond that involves the oxygen in α to the protonated carbonyl group, while, in R3b, by breaking the other $Pt-O$ bond. The following steps conduces to the loss of the protonated glycolate and to the formation of the products by steps R4a and R4b.

It is important to notice that two orientations of the protonated carbonyl group are possible for Nedaplatin. The most stable structure of the reagent has the proton oriented toward the oxygen in α to the carbonyl, and in our calculations, we considered this one.

The potential energy profiles for the hydrolysis processes in acid conditions are depicted in Figure 5.

The activation barriers for the first aquation processes are substantially different in acid conditions and the ring-opening caused by a water molecule entering on the same side of the protonated carbonyl group (R3a) results favored. Therefore, in acid condition, the rupture of the bond that involves the oxygen

SCHEME 3: Investigated Reaction Pathways for the Hydrolysis of Nedaplatin in Acid Conditions



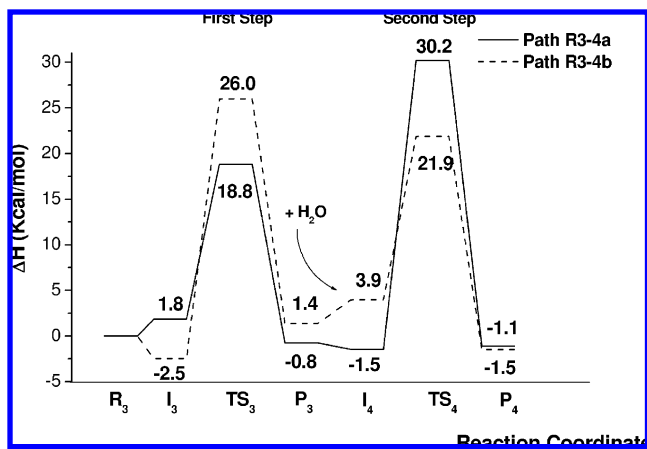


Figure 5. Activation enthalpy profiles (at 298.15 K), for the hydrolysis of Nedaplatin in acid conditions, in the water phase.

in α to the protonated carbonyl group seems to be unequivocally favored, requiring 18.8 kcal/mol instead of 26.0 kcal/mol, which is necessary for the other path.

The optimized structures of the stationary points along R3a are reported in Figure S3a of the Supporting Information, while those relative to the R3b path are reported in Figure S3b.

It can be observed that when the reacting water molecule approaches the platinum center, the protonated carbonyl group changes its orientation to minimize the repulsion, adopting the other diastereoisomeric form. The distance of the water molecule from the metallic center in the intermediate structure is 3.85 Å and becomes 2.50 Å in the transition state. Also, in this case, the transition state results in a penta-coordinated-like structure with the entering and leaving group equidistant from platinum. The imaginary frequency for this transition state is 170i cm^{-1} . The activation barrier is lower than the neutral one, by 8.3 kcal/mol.

The next step leads to the release of the fully protonated glycolate ligand that takes place as the second water molecule approaches the metal. Our results show that, since the most stable path for the first step in acid condition is R3a, the product obtained in that step reacts with the second water molecule, leading to the loss of the ligand following path R4a. As can be seen from Figure 5, the second hydrolysis process is highly unfavorable, being the rate limiting step of the reaction. The optimized structures along path R4a are shown in Figure S4a of the Supporting Information, while stationary points along the R4b path are reported in Figure S4b.

In the intermediate structure, the water molecule approaches the platinum center with a distance of 3.62 Å interacting also with the oxygen bonded to the metal (1.77 Å). In the transition state, that distance become shorter, reaching 2.42 Å and the analysis of the obtained vibrational frequency (250 cm^{-1}) clearly indicates the rupture of the Pt–O_L bond and the formation of the new Pt–O_W one. The final product is obtained with the release of the ligand, and a proton transfer from the water molecule to the leaving group is observed. These results indicate that the rate limiting step under acid conditions is the loss of the ligand and suggest that probably Nedaplatin reaches DNA in its monohydrated form.

Also, in this case, we considered the influence of an explicit extra water molecule included in the considered reactions. The obtained results (Figure 6), for the first and the second hydrolysis processes, demonstrate that the main effect is observable, again, in the energetics of the process, lowering the activation barriers, while no significant changes are appreciable in the optimized

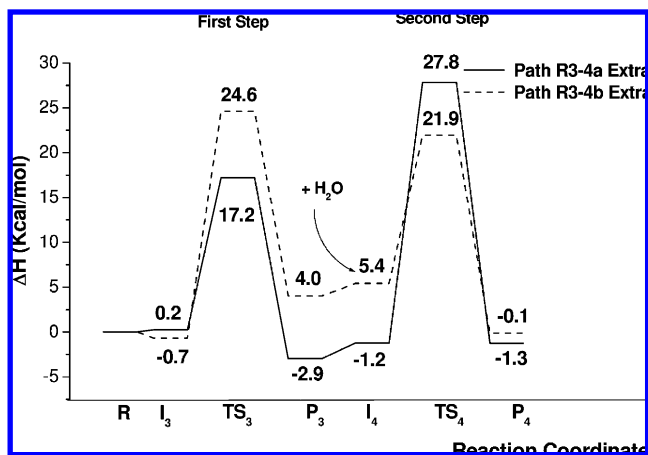


Figure 6. Activation enthalpy profiles (at 298.15 K) for the hydrolysis of Nedaplatin in acid conditions, with an extra water molecule in the system. The energies refer to the water phase.

geometries and, above all, in the trend of the reaction. In particular, the barriers for the preferred path are now 17.2 and 21.9 kcal/mol for the first and second hydrolysis processes, respectively.

The optimized structures of the stationary points for the ring-opening reaction as well as for the loss of the ligand are reported in Figure S5 of the Supporting Information section.

3. Comparison with Other Pt-Containing Anticancer Drugs. Previous studies on Pt(II)-containing anticancer drugs^{12,22,32,34,37} reported that these kinds of complexes degrade, as Nedaplatin, according to a biphasic process and the mono- or diaquated form could reach DNA. Therefore, we can make a direct comparison between the results presented in this work and the other ones. To do this, we need to consider the activation barriers computed as the difference from the reactant molecules, for the first hydrolysis process, and, for the second one, from the product obtained in the previous step and the nucleophilic water molecule. In this way, we can report consistent values, that are collected in Figure 7. Moreover, this way to proceed is well accepted and several works concord with this way to reproduce activation energies.^{34,37}

Note that, although several computational studies have been done with the aim of contributing to the common effort of deriving a better understanding of how Cisplatin reaches DNA, it is still not established whether the monoaquated or diaquated complex acts as an alkylating species on DNA. In Figure 7, we report the data obtained in a similar computational work in order to make a direct comparison, but other studies arrived at different conclusions predicting a similar activation barrier for both the hydrolysis step of Cisplatin and suggesting the diaqua complex as an active species.^{34,37} Comparison of the neutral hydrolysis barriers for Carboplatin, Oxaliplatin, and Nedaplatin reveals that the rate limiting step is the ring opening, suggesting that the second- and third-generation analogues of Cisplatin should reach DNA in their fully hydrolyzed forms. Moreover, the Cisplatin-like compounds show all slower hydrolysis rates compared to Cisplatin due to the introduction of the kinetically less labile carboxylate, oxalate, and glycolate and to the presence of a large group in the NH₃ position in the case of Oxaliplatin. Therefore, a slower hydration could be the reason for the lower side effects displayed from the second- and third-generation anticancer drugs. It is important to note that this consideration can be done according to all of the activation energies proposed for the hydrolysis of Cisplatin and not only to the values reported in Figure 7.^{34,37}

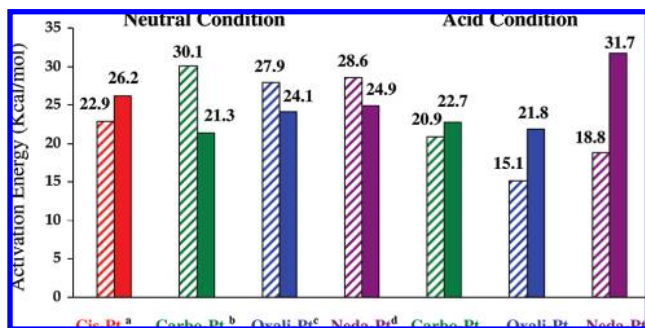


Figure 7. Comparison between calculated activation energies for Cisplatin, Carboplatin, Oxaliplatin, and Nedaplatin in neutral and acid conditions. Note that the striped column indicates the first aquation process, while the filled column indicates the second aquation process. ^aFrom ref 32. ^bFrom ref 12. ^cFrom ref 22. ^dFrom this work.

In acid condition we can observe that, again, Carboplatin and Oxaliplatin follow the same trend of Nedaplatin, with the loss of the ligand becoming the rate limiting step. Nevertheless, there are some differences; in the case of Carboplatin, the activation barriers are similar, so the possibility that the diaqua species reacts with DNA cannot be excluded, while for Oxaliplatin and Nedaplatin the gap became greater, suggesting that they reach DNA monohydrated.

Conclusions

In this work, we have performed a detailed mechanistic study of the hydrolysis reactions of the second-generation anticancer drug Nedaplatin by means of density functional theory and employing the CPCM approach in order to take into account the bulk solvent effect. Both neutral and acid conditions have been studied in order to establish the most favorable energy path. The degradation mechanism of Nedaplatin proceeds via a collision between the reactant with two consecutive nucleophilic species attacking the metal center to release the ionic ligand, by a classical second-order nucleophilic substitution (S_N2) reaction. The transition states found for each step of the reaction show a pentacoordinated structure, suggesting that the associative mechanism may be preferred.

In the first step of the reaction, the detachment of the ligand can occur in two different ways, by rupture of the bond that involves the oxygen in α to the carbonyl group or by breaking the other Pt–O bond. The latest one, in neutral conditions, should be the preferable path with an activation barrier of 28.6 kcal/mol and the product obtained in this step reacting with another water molecule, leading to the formation of the *cis*-[Pt(NH₃)₂(OH)₂(OH)]⁺ complex. In acid condition, we were able to ascertain that the reaction begins with the rupture of the ligand between the metal center and the oxygen in α to the carbonyl group and proceed with the loss of the ligand. In those conditions, the second hydrolysis process is the rate limiting step with an activation barrier of 31.7 kcal/mol.

In order to verify the possible influence of an extra water molecule which could assist the hydrolysis processes, we conducted an additional study including in our systems another water molecule acting as explicit solvent, obtaining for the reactions the same trends. That model incorporates the effects of hydrogen bonding and provides a more accurate description of the stabilization of the leaving group.

A comparison between Nedaplatin and the other Pt(II)-containing anticancer drugs currently used in the medical protocols reveals some common trends. In neutral condition, in analogy with the other second-generation anticancer drug

Carboplatin and with the third-generation drug Oxaliplatin, the rate limiting step is the first aquation process. We can therefore hypothesize that the fully hydrolyzed complexes should be the main products reacting with DNA. In acid condition, again, Carboplatin, Oxaliplatin, and Nedaplatin reveal the same behavior, and in these conditions, they are supposed to reach DNA in their mono-aquated form.

Supporting Information Available: Figures showing optimized structures of the stationary points along various reaction pathways. This material is available free of charge via the Internet at <http://pubs.acs.org>.

References and Notes

- (1) Rosenberg, B.; Camp, L.; Krigas, T. *Nature* **1965**, *205*, 698.
- (2) Rosenberg, B.; Camp, L.; Trosko, J.; Mansour, V. H. *Nature* **1969**, *222*, 385.
- (3) Jamieson, E. R.; Lippard, S. J. *Chem. Rev.* **1999**, *99*, 2467.
- (4) Sherman, S. E.; Lippard, S. J. *Chem. Rev.* **1987**, *87*, 1153.
- (5) Bokemeyer, C.; Berger, C.; Kynast, B.; Schmoll, H.-J.; Poliwooda, H. *Eur. J. Cancer* **1993**, *29*, S241.
- (6) Bokemeyer, C.; Frank, B.; Rhee, J.; Berger, C.; Schmoll, H.-J. *Tumordiagn. u. Ther.* **1993**, *14*, 232.
- (7) Cornelison, T. L.; Reed, E. *Gynecol. Oncol.* **1993**, *50*, 147.
- (8) (a) Reedijk, J. *Proc. Natl. Acad. Sci. U.S.A.* **2003**, *100*, 3611. (b) Wang, D.; Lippard, S. J. *Nat. Rev. Drug Discovery* **2005**, *4*, 307.
- (9) Lebwohl, D.; Canetta, R. *Eur. J. Cancer* **1998**, *34*, 1522.
- (10) Jakupec, M. A.; Galaski, M.; Keppler, B. K. *Rev. Physiol. Biochem. Pharmacol.* **2003**, *146*, 1.
- (11) Roberts, J. J.; Knox, R.; Friedlos, D.; Lydall, D. A.; *Biochemical Mechanisms of Platinum Antitumor Drugs*; McBrien, D. C. H., Slater, T. F., Eds; IRL: Oxford, U.K., 1986; p 29.
- (12) Pavelka, M.; Lucas, M. F.; Russo, N. *Chem.—Eur. J.* **2007**, *13*, 10108.
- (13) Reedijk, J. *Pure Appl. Chem* **1987**, *59*, 181.
- (14) Fuertes, M. A. A.; Pérez, J. M. *Chem. Rev* **2003**, *103*, 645.
- (15) Kidani, Y.; Noji, M.; Tashiro, T. *Gann.* **1980**, *71*, 637.
- (16) Brienza, S.; Bignound, J.; Itzhaki, M.; Krikorian, A. *Eur. J. Cancer* **1995**, *31A*, S194.
- (17) Dunn, T. A.; Schmoll, H. J.; Grunwald, V.; Bokemeyer, C.; Casper, J. *Invest. New Drugs* **1997**, *15*, 109.
- (18) Airoidi, M.; Cattel, L.; Passera, R.; Pedani, F.; Delprino, L.; Micari, C. *Am. J. Clin. Oncol.* **2006**, *29*, 490.
- (19) Ferrandina, G.; Ludovisi, M.; De Vincenzo, R.; Salutati, V.; Lorusso, D.; Colangelo, M.; Prantera, T.; Valerio, M. R.; Scambia, G. *Ann. Oncol.* **2007**, *18*, 1348.
- (20) Desai, S. P.; Ben-Josef, E.; Normolle, D. P.; Francis, I. R.; Greenson, J. K.; Simeone, D. M.; Chang, A. E.; Colletti, L. M.; Lawrence, T. S.; Zalupski, M. M. *J. Clin. Oncol.* **2007**, *25*, 4587.
- (21) Cunningham, D.; Starling, N.; Rao, S.; Iveson, T.; Nicolson, M.; Coxon, F.; Middleton, G.; Daniel, F.; Oates, J.; Norman, A. R. *N. Engl. J. Med.* **2008**, *358*, 36.
- (22) Lucas, M. F.; Pavelka, M.; Alberto, M. E.; Russo, N. *J. Phys. Chem. B* **2009**, *113*, 831.
- (23) Schmidt, W.; Chaney, S. G. *Cancer Res.* **1993**, *53*, 799.
- (24) Adelsberger, H.; Quasthoff, S.; Grosskreutz, J.; Lepier, A.; Eckel, F.; Lersch, C. *Eur. J. Pharmacol.* **2000**, *406*, 25.
- (25) Benoit, E.; Brienza, S.; Dubois, J. M. *Gen. Physiol. Biophys.* **2006**, *25*, 263.
- (26) Ota, K. *Gan to Kagaku Ryoho* **1996**, *23*, 379.
- (27) Inuyama, Y.; Fukuda, S.; Satoh, N. *Gan to Kagaku Ryoho* **1997**, *24*, 1902.
- (28) Kameyama, Y.; Okazaki, N.; Nakagawa, M.; Koshida, H.; Nakamura, M.; Gemba, M. *Toxicol. Lett.* **1990**, *52*, 15.
- (29) Akaza, H.; Togashi, M.; Nishio, Y.; Miki, T.; Kotake, T.; Matsumura, Y.; Yoshida, O.; Aso, Y. *Cancer Chemother. Pharmacol.* **1992**, *31*, 187.
- (30) Fukuda, M.; Shinkai, H.; Eguchi, K.; Sasaki, Y.; Tamura, T.; Ohe, Y.; Kojima, A.; Oshita, F.; Hara, K.; Saijo, N. *Cancer Chemother. Pharmacol.* **1990**, *26*, 393.
- (31) Chen, J.; Chen, L.; Liao, S.; Zheng, K.; Ji, L. *J. Phys. Chem. B* **2007**, *111*, 7862.
- (32) Raber, J.; Zhu, C.; Eriksson, L. A. *Mol. Phys.* **2004**, *102*, 2537.

- (33) Zhang, Y.; Guo, Z.; You, X. Z. *J. Am. Chem. Soc.* **2001**, *123*, 9378.
- (34) Deubel, D. V. *J. Am. Chem. Soc.* **2006**, *128*, 1654.
- (35) Sarmah, P.; Deka, R. C. *Int. J. Quantum Chem.* **2008**, *108*, 1400.
- (36) Alberto, M. E.; Lucas, M. F.; Pavelka, M.; Russo, N. *J. Phys. Chem. B* **2008**, *112*, 10765.
- (37) Lau, J.K.-C.; Deubel, D. V. *J. Chem. Theory Comput.* **2006**, *2*, 103.
- (38) Frisch, M. J.; Trucks, G. W.; Schlegel, H. B.; Scuseria, G. E.; Robb, M. A.; Cheeseman, J. R.; Montgomery, J. A., Jr.; Vreven, T.; Kudin, K. N.; Burant, J. C.; Millam, J. M.; Iyengar, S. S.; Tomasi, J.; Barone, V.; Mennucci, B.; Cossi, M.; Scalmani, G.; Rega, N.; Petersson, G. A.; Nakatsuji, H.; Hada, M.; Ehara, M.; Toyota, K.; Fukuda, R.; Hasegawa, J.; Ishida, M.; Nakajima, T.; Honda, Y.; Kitao, O.; Nakai, H.; Klene, M.; Li, X.; Knox, J. E.; Hratchian, H. P.; Cross, J. B.; Bakken, V.; Adamo, C.; Jaramillo, J.; Gomperts, R.; Stratmann, R. E.; Yazyev, O.; Austin, A. J.; Cammi, R.; Pomelli, C.; Ochterski, J. W.; Ayala, P. Y.; Morokuma, K.; Voth, G. A.; Salvador, P.; Dannenberg, J. J.; Zakrzewski, V. G.; Dapprich, S.; Daniels, A. D.; Strain, M. C.; Farkas, O.; Malick, D. K.; Rabuck, A. D.; Raghavachari, K.; Foresman, J. B.; Ortiz, J. V.; Cui, Q.; Baboul, A. G.; Clifford, S.; Cioslowski, J.; Stefanov, B. B.; Liu, G.; Liashenko, A.; Piskorz, P.; Komaromi, I.; Martin, R. L.; Fox, D. J.; Keith, T.; Al-Laham, M. A.; Peng, C. Y.; Nanayakkara, A.; Challacombe, M.; Gill, P. M. W.; Johnson, B.; Chen, W.; Wong, M. W.; Gonzalez, C.; Pople, J. A. *Gaussian 03*, revision A.1; Gaussian, Inc.: Pittsburgh, PA, 2003.
- (39) Becke, A. D. *J. Chem. Phys.* **1993**, *98*, 5648.
- (40) Lee, C. T.; Yang, W. T.; Parr, R. G. *Phys. Rev. B* **1988**, *37*, 785.
- (41) Andrae, D.; Haussermann, U.; Dolg, M.; Stoll, H.; Preuss, H. *Theor. Chim. Acta* **1990**, *77*, 123.
- (42) Burda, J. V.; Zeizinger, M.; Sponer, J.; Leszczynski, J. *J. Chem. Phys.* **2000**, *113*, 2224.
- (43) (a) Klamt, A.; Schüürmann, G. *J. Chem. Soc., Perkin Trans. 2* **1993**, 799. (b) Andzelm, J.; Kölmel, C.; Klamt, A. *J. Chem. Phys.* **1995**, *103*, 9312. (c) Barone, V.; Cossi, M. *J. Phys. Chem. A* **1998**, *102*, 1995. (d) Cossi, M.; Rega, N.; Scalmani, G.; Barone, V. *J. Comput. Chem.* **2003**, *24*, 669.
- (44) Klamt, A.; Jonas, V.; Burger, T.; Lohrenz, J. C.W. *J. Phys. Chem. A* **1998**, *102*, 5074.
- (45) (a) Jestin, J. L.; Chottard, J. C.; Frey, U.; Layrenczy, G.; Merbach, A. E. *Inorg. Chem.* **1994**, *33*, 4277. (b) Mikola, M.; Klika, K. D.; Hakala, A.; Arpalahti, J. *Inorg. Chem.* **1999**, *38*, 571.
- (46) Lamm, G.; Pack, G. R. *Proc. Natl. Acad. Sci. U.S.A.* **1990**, *87*, 9033.
- (47) Vinje, J.; Sletten, E.; Kozelka, J. *Chem.—Eur. J.* **2005**, *11*, 3863.

JP9056835

The second generation anticancer drug Nedaplatin: A theoretical investigation on the hydrolysis mechanism

*Marta E. Alberto, Maria Fatima A. Lucas, Matěj Pavelka and Nino Russo**

Dipartimento di Chimica Università della Calabria, Via P. Bucci, cubo 14c, 87036 Arcavacata di Rende (CS), Centro di Calcolo ad Alte Prestazioni per Elaborazioni Parallele e Distribuite – Centro d'Eccellenza MIUR, Italy

Supporting Information

Table of Contents:

Figure S1: Optimized structures of the stationary points along the path R2a, in neutral conditions

Figure S2: Optimized structures of the stationary points along the paths R1a, R2a, R1b, R2b with an extra water molecule in the system, in neutral conditions

Figure S3a: Optimized structures of the stationary points along the path R3a, in acid conditions

Figure S3b: Optimized structures of the stationary points along the path R3b, in acid conditions

Figure S4a: Optimized structures of the stationary points along the path R4a, in acid conditions

Figure S4b: Optimized structures of the stationary points along the path R4b, in acid conditions

Figure S5: Optimized structures of the stationary points along the paths R3a, R4a, R3b, R4b with an extra water molecule in the system, in acid conditions

Figure S1: Optimized structures of the stationary points along the path R2a, in neutral conditions

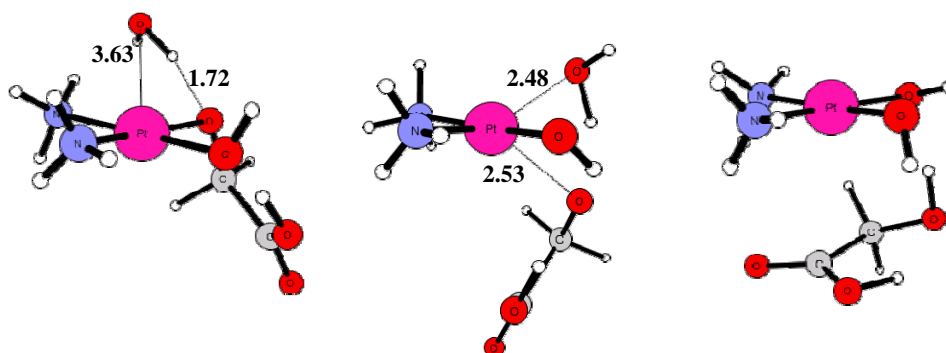
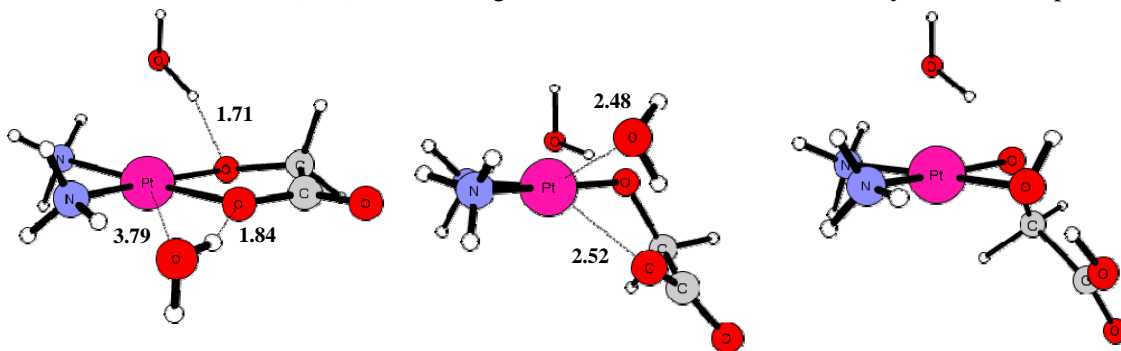
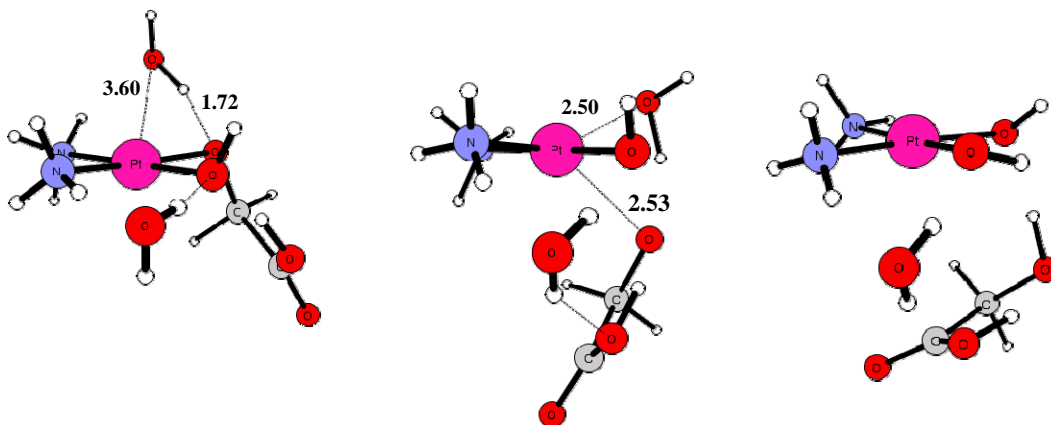


Figure S2: Optimized structures of the stationary points along the paths R1a, R2a, R1b, R2b with an extra water molecule in the system, in neutral conditions

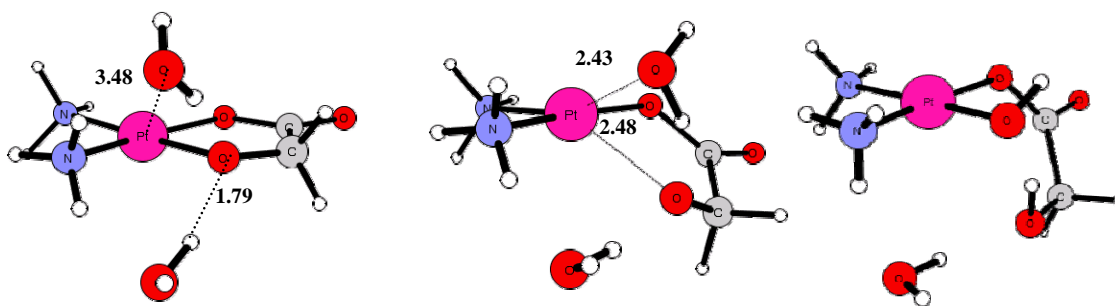
a) Optimized structures and selected structural parameters for the addition of the first water molecule to nedaplatin in neutral condition (R1a), considering an extra-water molecule in the system. Water phase.



b) Optimized structures and selected structural parameters for the addition of the second water molecule to nedaplatin in neutral condition (R2a), considering an extra-water molecule in the system. Water phase.



c) Optimized structures and selected structural parameters for the addition of the first water molecule to nedaplatin in neutral condition (R1b), considering an extra-water molecule in the system. Water phase.



d) Optimized structures and selected structural parameters for the addition of the second water molecule to nedaplatin in neutral condition (R2b), considering an extra-water molecule in the system. Water phase.

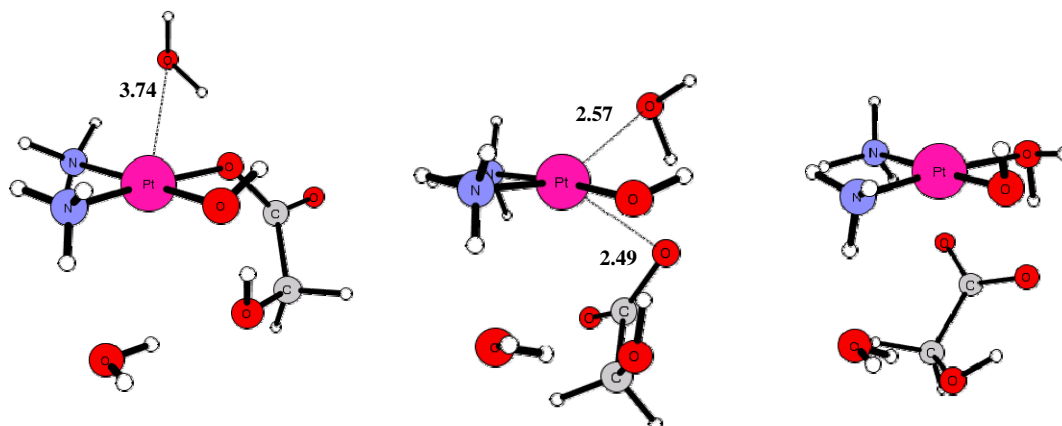


Figure S3a: Optimized structures of the stationary points along the path R3a, in acid conditions

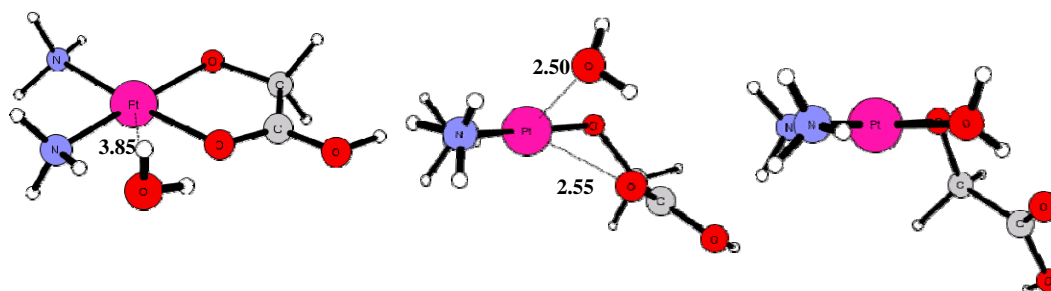


Figure S3b: Optimized structures of the stationary points along the path R3b, in acid conditions

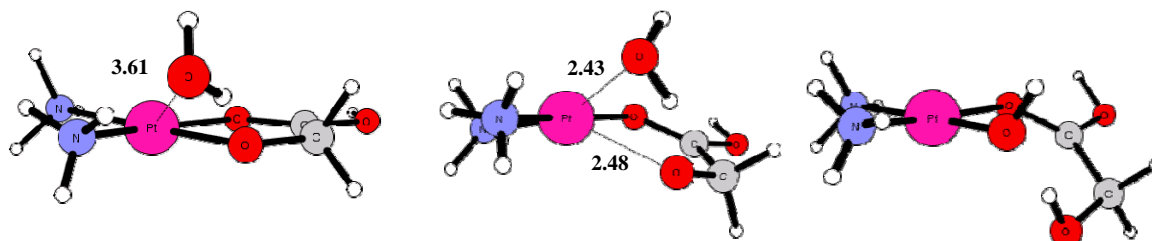


Figure S4a: Optimized structures of the stationary points along the path R4a, in acid conditions

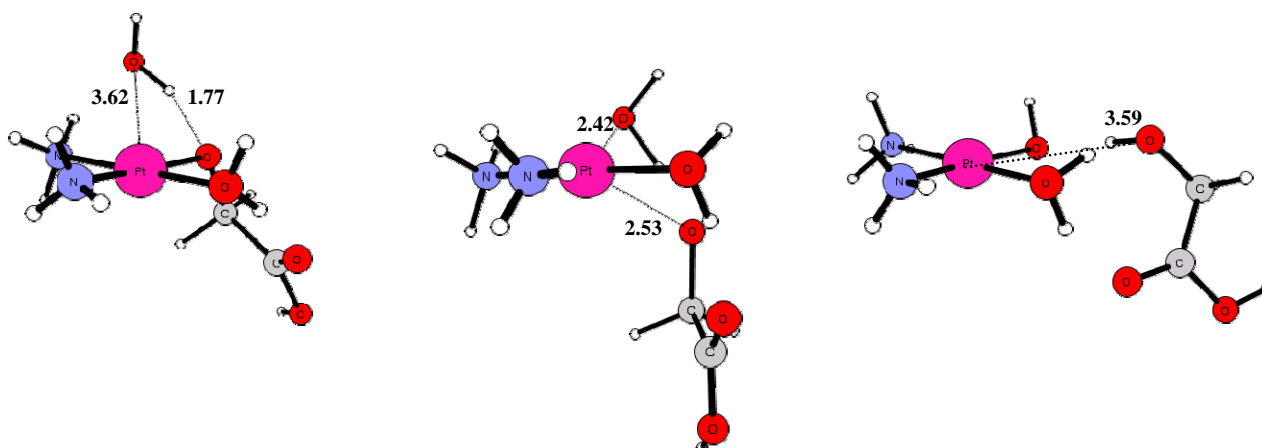


Figure S4b: Optimized structures of the stationary points along the path R4b, in acid conditions

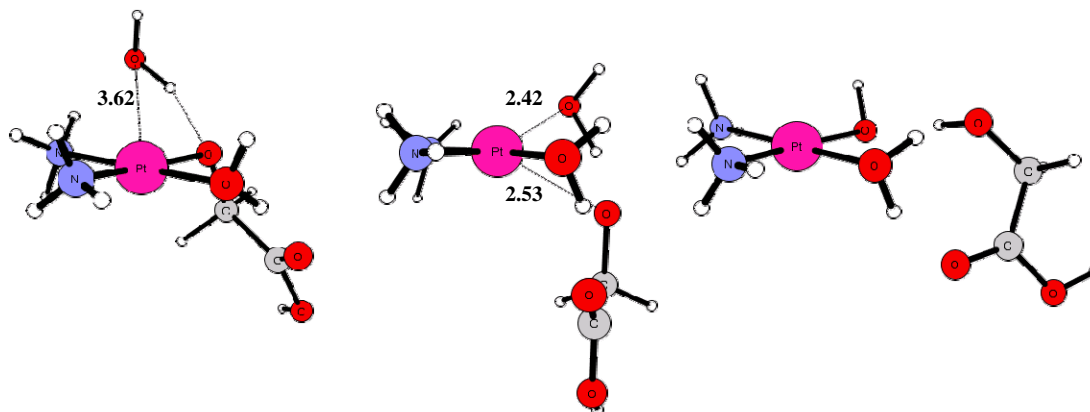
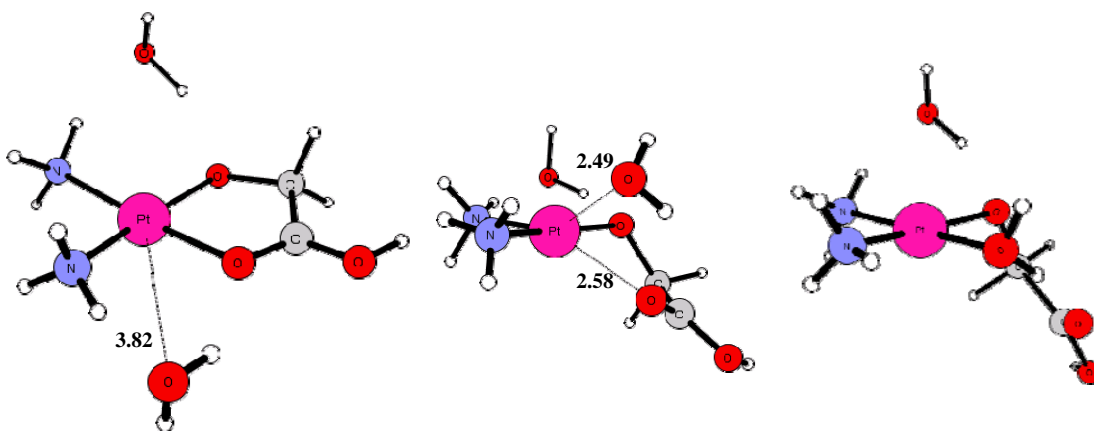
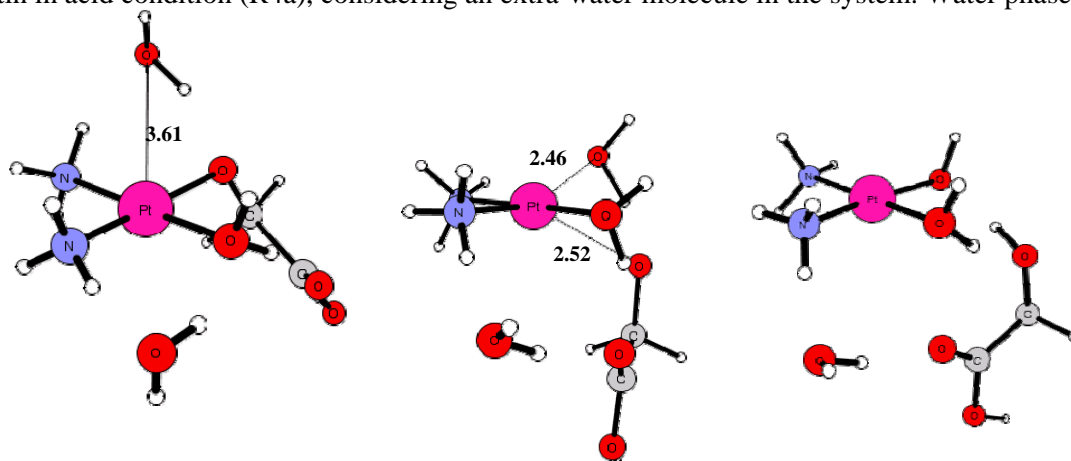


Figure S5: Optimized structures of the stationary points along the paths R3a, R4a, R3b, R4b with an extra water molecule in the system, in acid conditions

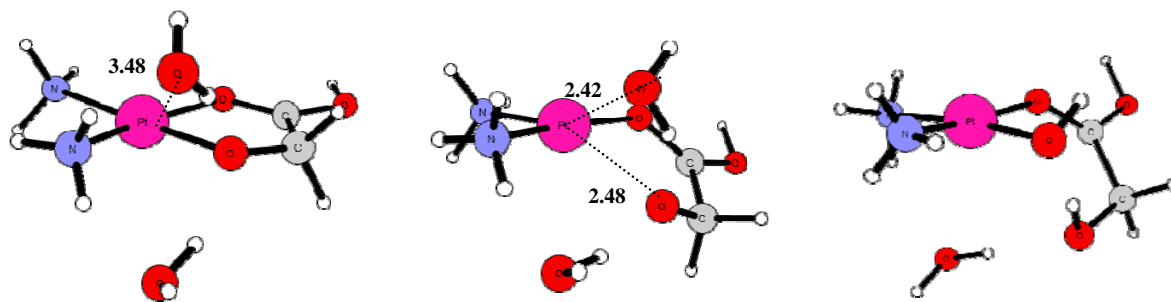
a) Optimized structures and selected structural parameters for the addition of the first water molecule to nedaplatin in acid condition (R3a), considering an extra-water molecule in the system. Water phase.



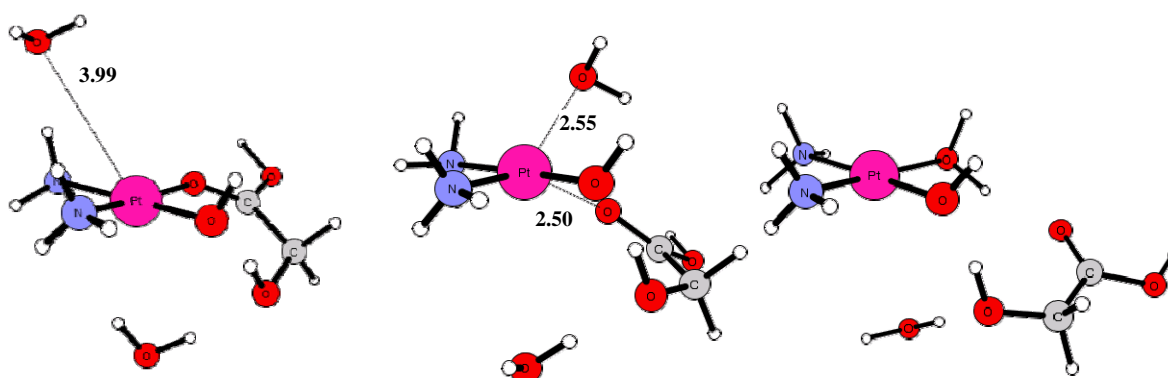
b) Optimized structures and selected structural parameters for the addition of the second water molecule to nedaplatin in acid condition (R4a), considering an extra-water molecule in the system. Water phase.



c) Optimized structures and selected structural parameters for the addition of the first water molecule to nedaplatin in acid condition (R3b), considering an extra-water molecule in the system. Water phase.



d) Optimized structures and selected structural parameters for the addition of the second water molecule to nedaplatin in acid condition (R4b), considering an extra-water molecule in the system. Water phase.



Paper II

“Neutral and Acidic Hydrolysis Reactions of the Third
Generation Anticancer Drug Oxaliplatin”

Maria F. Lucas, Marta E. Alberto, Matěj Pavelka and Nino Russo

J. Phys. Chem. B **2009**, *113*, 831-838

Neutral and Acidic Hydrolysis Reactions of the Third Generation Anticancer Drug Oxaliplatin

Maria Fatima A. Lucas, Matěj Pavelka, Marta E. Alberto, and Nino Russo*

Dipartimento di Chimica Università della Calabria, Via P. Bucci, cubo 14c, 87036 Arcavacata di Rende (CS), Centro di Calcolo ad Alte Prestazioni per Elaborazioni Parallele e Distribuite - Centro d'Eccellenza MIUR, Rende 87036, Italy

Received: September 30, 2008; Revised Manuscript Received: November 14, 2008

The hydrolysis of oxaliplatin, a third generation anticancer drug, is expected to play an important role in the activation of this compound before it reaches DNA. The first and second hydrolysis corresponding to the addition of the first water molecule concomitant with the ring-opening, followed by addition of a second water and loss of the monodentate oxalato ligand, respectively, were studied combining density functional theory (DFT) with the conductor-like dielectric continuum model (CPCM) approach. The reaction was studied in neutral and acidic conditions, and all stationary points have been identified. The computed potential energy surfaces show that, for the neutral hydrolysis, the ring-opening reaction is the rate-limiting process, with an activation barrier of about 28 kcal/mol. For the acid degradation in water, according to experimental data, the reaction is expected to proceed in a faster biphasic process, and the rate-limiting process is the ligand detachment that occurs with a barriers of about 22 kcal/mol. According to the calculated results, we expect that the reaction is favored in acidic conditions and that the monoaquated complex should be the species reacting with DNA.

Introduction

In 1965, Rosenberg unexpectedly found that *cis*-diamminedichloroplatinum, commonly known as cisplatin, was able to inhibit cell division.¹ This discovery led to the investigation on the antitumor properties of platinum compounds.² Cisplatin-based chemotherapy has become a fundamental treatment in some types of tumors that were essentially fatal before the introduction of this drug. Cisplatin exhibits high efficiency in the treatment of ovarian, bladder, head, and neck as well as non-small lung and cervical cancers.³ However, in spite of the impressive antitumor activity, this drug presents several limitations. Side effects such as nausea/vomiting, nephrotoxicity, and ototoxicity have been registered for cisplatin. In addition, it has poor activity (intrinsic resistance) against some of the most common types of cancer, such as colorectal and pancreatic. Acquired resistance has also been observed with the inability to confer lasting remissions. These limitations have promoted the search for new drugs that are able to circumvent cisplatin's resistance and reduce its toxicity.

Carboplatin (*cis*-diamminecyclobutane-1,1-dicarboxylateplatinum) was the first drug to follow cisplatin in cancer treatment; however, in spite of the reduction of some side effects, when compared to cisplatin, this drug still exhibits limitations.⁴

Through the years many platinum-based compounds have been synthesized and investigated. Compounds containing 1,2-diaminocyclohexane (DACH) carrier ligands were identified in the early 1970s as non-cross-resistant with cisplatin, and for this reason they have received special attention.^{5,6} These DACH compounds were considered promising given their reduced nephrotoxic activity toward acquired cisplatin resistance and appeared to be clinically effective in intrinsically resistant tumor cells.

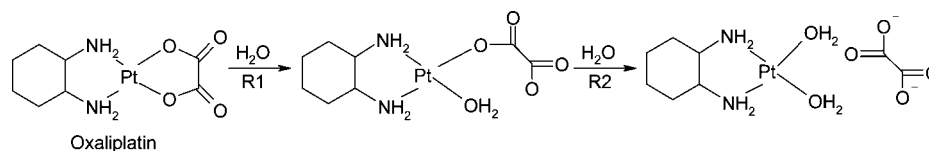
Oxaliplatin (1,2-diaminocyclohexaneoxalateplatinum) developed by Kidani et al.,⁷ in 1980, while testing several new platinum compounds, was accepted as a third generation platinum drug.⁸ Oxaliplatin was initially approved in France in 1998, followed by the rest of Europe and finally, in 2002, in the United States. It is active against some tumors that are primarily resistant to cisplatin and carboplatin being the first antineoplastic agent to exhibit activity against metastatic colorectal cancer.^{9–11} It is normally used in combination with 5-fluorocil and leucovorin^{12,13} in the treatment of this type of tumor which is the second leading cause of cancer death in developed countries. It has also been reported that oxaliplatin is active in platinum-pretreated advanced ovarian cancer.^{14,15}

Much research has been done in this area, and platinum compounds are expected to interact with DNA following several steps: aquation of the platinum complex, preassociation with the DNA, monofunctional adduct formation, closure of the bifunctional adduct, distortion of the DNA, and recognition of this distortion.^{16,17}

A large amount of experimental evidence shows that the success of platinum complexes, in killing tumor cells, mainly results from their ability to form various types of adducts with DNA.¹⁸ Oxaliplatin acts as an alkylating agent on DNA, forming essentially three types of cross-link adducts: intrastrand, interstrand, and DNA–protein. In spite of the different binding modes, it has been suggested that only the kinetically preferred binding modes are important in biological systems.¹⁹ The most common adduct is the intrastrand that bridges two adjacent purine bases (1,2-GG or AG) at the N7 position.^{20,21} Guanine N7 is the most easily oxidized site on DNA, and the major adducts of platinum drugs with DNA are 1,2-GpG and 1,2 ApG intrastrand cross-links. The properties of these adducts have been extensively characterized.^{5,22,23}

Comparison of the crystal structure of oxaliplatin adduct of a DNA duplex reveals that it is identical to the cisplatin

* Corresponding author. E-mail: nrusso@unical.it.

SCHEME 1: Investigated Reaction Path for Oxaliplatin Ring-Opening (R1) and the Loss of the Ligand (R2) in Neutral Conditions


adduct.^{24–27} However, important differences are observed between cisplatin and carboplatin adducts when compared with oxaliplatin DNA adducts. The presence of the cyclohexane ring in oxaliplatin induces a strong nonpolar region in the DNA, leading to differences in cellular recognition. The DACH–platinum DNA adducts resulting from oxaliplatin are more bulky and hydrophobic than the ones formed from cisplatin and carboplatin. As a consequence, these adducts are more effective in inhibiting DNA synthesis and usually more cytotoxic than *cis*-diamineplatinum adducts.²⁸

Structure–activity relationships for platinum compounds have been formulated, and most drugs reported possess two amines in the *cis* position.^{29,30} For the antitumor activity of platinum compounds it is significant that they possess two labile groups in *cis* geometry. Chloride found in cisplatin is a good leaving group, but the kinetically less labile carboxylate, glycolate or oxalate, present in second and third generations drugs such as carboplatin, nedaplatin, and oxaliplatin are expected to be responsible for the reduced side effects observed on patients treated with these drugs in comparison with cisplatin.

The higher lipophilicity observed in oxaliplatin should be responsible for the more efficient removal from the blood through enhanced tissue penetration. For this reason, substitutions at the nonleaving group should influence the tumor inhibiting activity of oxaliplatin.³¹

The proposed hydration process for cisplatin is consistent with the fact that water is a better leaving group than the chloro ligand,³² and several theoretical studies exposing the most likely path for cisplatin hydrolysis prior to DNA binding can be found in the literature.^{33–38} A correct understanding of the hydration mechanism of these drugs is essential. It is expected that the difference between cisplatin and oxaliplatin results from the resistance mechanisms rather than from any fundamental difference in their modes of action.^{39,40} However, it is still essential to have a correct understanding on all steps preceding the DNA binding.

The rapid development of computational chemistry has allowed the theoretical modeling of a large variety of chemical reactions. DFT methods have been successfully applied in the study of reactions such as oxidative/reductive eliminations, nucleophilic additions, and substitutions involving transition metals as well as catalytic processes.^{41–43} Many platinum anticancer drugs have been subject of theoretical study,^{44–48} and in this work we present the first computational approach to the hydrolysis mechanisms of oxaliplatin in water and acid conditions. According to experimental results, oxaliplatin degradation in water should take place in two consecutive steps: first, water addition with ring-opening followed by loss of the ligand with the reaction of the second water molecule.^{49,50}

Computational Details

All structures were optimized using density functional theory (DFT) with the B3LYP functional which includes the Becke's hybrid⁵¹ exchange and correlation functional of Lee, Yang, and Parr⁵² as implemented in the Gaussian 03 quantum chemical

program package.⁵³ For all structure optimizations, we have used the 6-31G(d) basis set for all atoms except the platinum atom, which was described by the quasi-relativistic Stuttgart–Dresden pseudopotentials⁵⁴ with pseudo-orbital basis set augmented by a set of diffuse functions— $\alpha_s = 0.0075$, $\alpha_p = 0.013$, and $\alpha_d = 0.025$ —and polarization functions— $\alpha_f = 0.98$.³⁷ In order to confirm proper convergence to equilibrium and transition state geometries, vibrational frequency analysis were done based on analytical second derivatives of Hamiltonian at this level of theory.

Geometry optimizations were then redone in water environment performing a PCM calculation using the CPCM⁵⁵ polarizable conductor calculation model. In these methods, dominating electrostatic interaction with a continuum is provided by polarization charges appearing on the boundary surface of studied molecule.⁵⁶ In here, this solvent-accessible surface was constructed using Klamt's radii⁵⁷ with explicit hydrogens.

On the optimized structures, single-point (SP) energy calculations were also carried out with the larger basis set 6-31++G-(2df,2pd). Similarly, platinum valence basis set was augmented with diffuse ($\alpha_f = 0.46$) and polarization ($\alpha_g = 1.21$) functions.³⁷ Potential energy profiles were estimated from total electronic energies at the 6-31++G(2df,2pd) level adding zero point energy (ZPE) and enthalpy corrections at room temperature (298.15 K).

Results

1. Oxaliplatin Hydrolysis in Neutral Conditions. As previously exposed, oxaliplatin is expected to undergo water degradation in a biphasic process: addition of the first water molecule connected to the ring-opening process followed by the release of the oxalato ligand upon reaction with a second water molecule.

The first reaction studied was the degradation of oxaliplatin in water. The proposed hydrolysis mechanism, in neutral conditions, is presented in Scheme 1.

The potential energy profile for reaction R1 (Scheme 1) and the optimized structures for the stationary points along R1 are

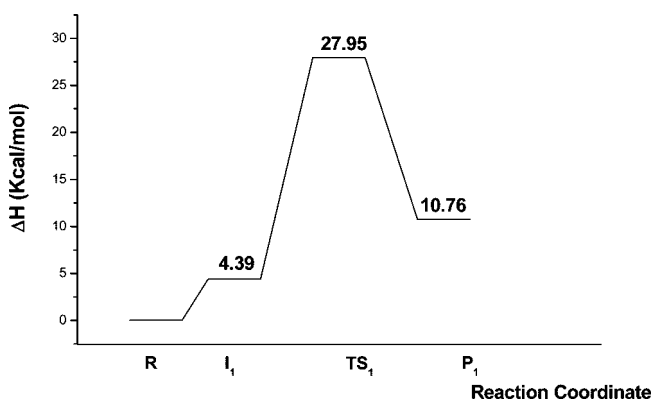


Figure 1. Activation enthalpy (at 298.15 K) and reaction heat for the addition of the first water molecule to oxaliplatin (R1), in neutral conditions, in water phase.

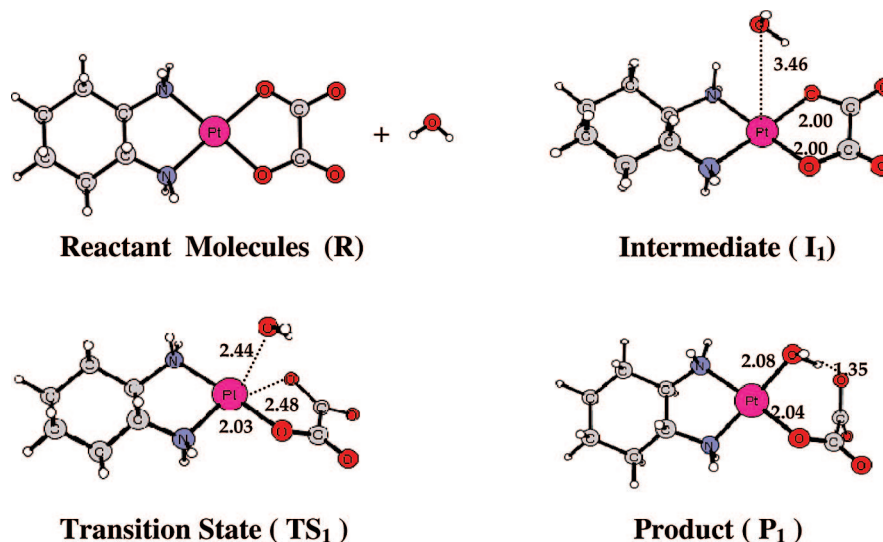


Figure 2. Optimized structures and selected structural parameters for the addition of the first water molecule to oxaliplatin (R1), in neutral conditions, in water phase. The distances reported are in angstroms.

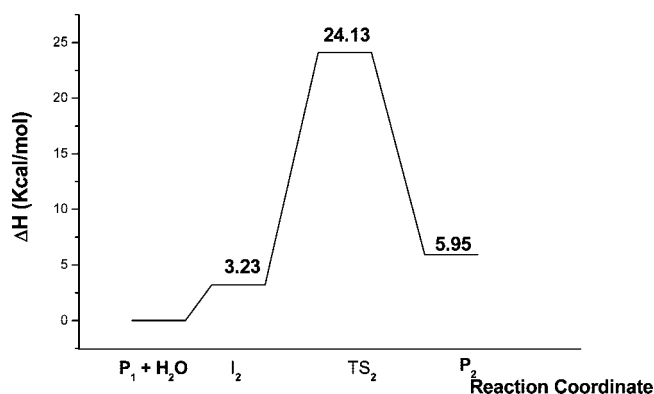


Figure 3. Activation enthalpy (at 298.15 K) and reaction heat for the addition of the second water molecule to oxaliplatin in the opposite plane of the exiting ligand (R2), in neutral conditions, in water phase.

are always essentially 2.0 Å in the reactants as well as the products. As the water molecule approaches the Pt center, the platinum–oxygen (of the ligand) bond distance starts to increase until the transition state geometry is reached. The distances of the bonds being broken and formed in the transition state (TS₁) geometry do not change significantly upon optimization of the structures in gas phase or including solvent effects (2.45 and 2.48 Å, respectively). The platinum–oxygen bond distance between the entering water molecule (Pt–OW) in gas phase is 2.34 Å while in solvent it is 2.44 Å. The imaginary frequency observed in the transition state is about 200i cm⁻¹ in gas phase and 183i cm⁻¹ in solvent, and the analysis of this vibrational mode clearly indicates the rupture of the Pt–OL bond and the simultaneous formation of the Pt–OW bond. The activation barrier is 27.95 kcal/mol in solvent. The reaction is endothermic by 10.76 kcal/mol in water. The final product of this reaction in gas phase displays a proton transfer from the water molecule bonded to platinum to the carboxylate group of the ligand. On the contrary in solvent, the final product does not exhibit proton transfer.

displayed in Figures 1 and 2. The reacting water molecule lies at 3.46 Å away from the platinum atom. The distances between the oxygen atoms in the oxalato ligand and the platinum atom

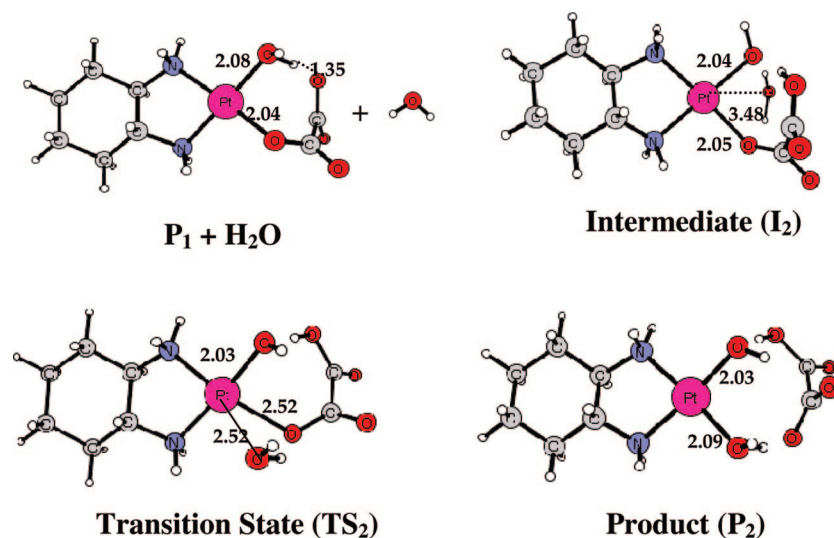
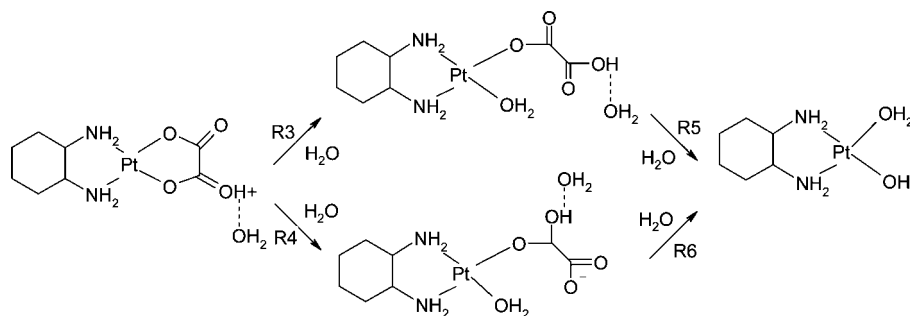


Figure 4. Optimized structures and selected structural parameters for the addition of the second water molecule to oxaliplatin (R2), in neutral conditions, in water phase. The distances reported are in angstroms.

SCHEME 2: Investigated Reaction Path for Oxaliplatin Ring-Opening (R3, R4) in Acid Conditions as Well as the Loss of the Ligand (R5, R6)^a


^a The protonated ligand has the extra proton in a cis position relative to the entering water molecule in reactions R3 and R5 and in a trans position in reactions R4 and R6.

In the next step of the reaction, leading to the loss of the oxalate ligand (R2), the addition of the second water molecule can occur in two different ways. In the first, we consider addition on the same plane of the monodentate ligand while in the second one the addition occurs on the opposite plane. This last water attack result to be the lowest energy path, and the results are shown in Figures 3 and 4. In the intermediate structure the water molecule approaches the platinum center with a distance of 3.48 Å which becomes 2.52 Å in the TS and 2.09 Å in the product. Similar results are obtained in the gas phase. The imaginary frequencies for the transition state corresponding to the Pt–OL and Pt–OW bonds being broken and formed, respectively, are 190i cm⁻¹ in solvent. The activation barrier is found to be 24.13 kcal/mol, and the reaction endothermicity is 5.95 kcal/mol.

It is interesting to notice that although the final product of reaction R1 is different, depending on the medium it has been optimized, the reactants for this step are identical. In fact, starting from the reactant containing or not a proton transferred to the oxalate monodentate ligand, the obtained structure of the intermediate is identical.

From Figures 1 and 3 it is evident that, in neutral solution, the rate-limiting process is the ring-opening. The computed activation barriers (27.95 kcal/mol) agree with that extracted from the experimental reaction rate (26.50 kcal/mol).⁵⁰

2. Oxaliplatin Hydrolysis in Acid Conditions. Oxaliplatin degradation in acid conditions has also been investigated. We have initiated the study by introducing a H₃O⁺ molecule to the system and observed a proton transfer to oxaliplatin. Once the proton is transferred, the water molecule remains hydrogen bonded to this proton throughout the hydrolysis process. The addition of the first water molecule with consequent ring-opening has been explored following two possibilities: Pt–OL cleavage with proton in the neighboring carboxylate oxygen or in the trans position considering the Pt–OL bond. In Scheme 2 both situations are illustrated as well as the proposed reaction path for acid degradation of oxaliplatin water.

In Figure 5 the potential energy profile for reaction R3 (Scheme 2) and the relative optimized structures for the stationary points along this reaction liquid phase are depicted in Figure 6. Also in this case, for both the considered media, the optimized structures of the species located along the path are very similar (e.g., for the transition state the Pt–OW distance is 2.47 Å in gas phase and 2.50 Å in water). The final product for this reaction displays cleavage of the Pt–OL bond and the formation of the monodentate ligand. On the contrary to what took place in neutral conditions, no proton transfer is observed. Imaginary frequencies for the transition state corresponds to the Pt–OL and Pt–OW bonds being broken and formed are about

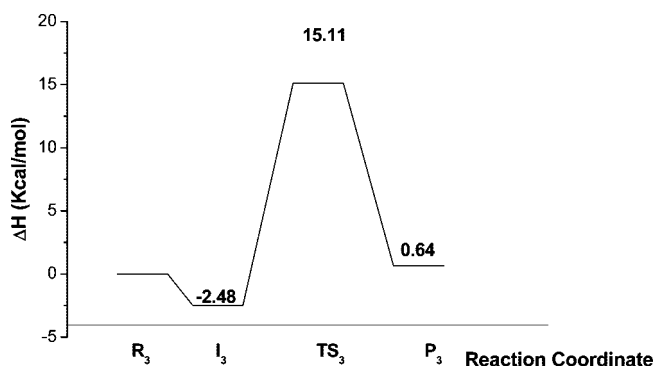


Figure 5. Activation enthalpy (at 298.15 K) and reaction heat for the addition of the first water molecule to oxaliplatin in acidic conditions (R3), in water phase.

150i cm⁻¹ in gas phase and solvent. The reaction presents a similar potential energy profile in gas and in solution with an activation barrier of 15.11 kcal/mol (optimizations in water) and is essentially thermoneutral.

In addition to the protonated system on the carboxylate group in the vicinity of the Pt–OL breaking bond, we have investigated the acidic hydrolysis of oxaliplatin with an extra proton in a trans position (R4) relatively to the bond that is being broken. Also in this case, the activation energy is not significantly affected by the inclusion of solvent effects on the calculations. In fact, in the identical reaction R3 (addition of the water molecule in a cis position to the proton), the activation barrier is essentially the same in both mediums. In this case, however, the energy to be surmounted is higher, 18.26 kcal/mol opposed to 15.11 kcal/mol. The distance separating the water molecule from the Pt center is about 0.10 Å shorter than in the R3 reaction, and also the TS critical distances are slightly smaller. As in the R3 reaction, two products are expected depending on the conditions of the optimizations. For gas phase the product is formed by simultaneous Pt–OL cleavage and proton transfer from the water molecule to the neighboring carboxylate group. When solvent effects are included, this proton shift does not take place, and the final product contains a water molecule bonded to the Pt atom. The reaction is endothermic in both mediums with a calculated energy gain of 3.15 kcal/mol in water. Imaginary frequencies are somewhat larger than in R3 with about 170i cm⁻¹ instead of 150i cm⁻¹.

The reaction should then proceed with the addition of a second water molecule (R5). Like in the case of the neutral solution, in acid conditions we must consider the possibility of addition of the second attacking water molecule in the same plane of the exiting ligand or on the opposite plane. Reaction

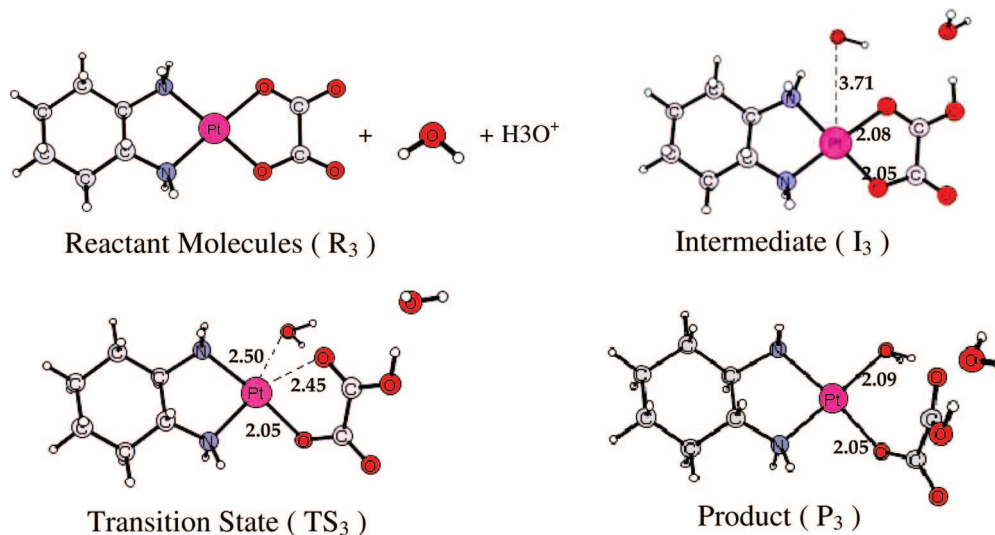


Figure 6. Optimized structures and selected structural parameters for the addition of the first water molecule to oxaliplatin in acidic conditions (R₃), in water phase. The distances reported are in angstroms.

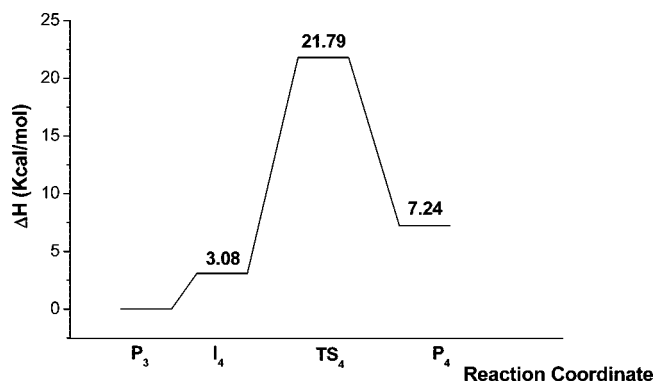


Figure 7. Activation enthalpy (at 298.15 K) and reaction heat for the addition of the second water molecule to oxaliplatin (R₅), in the same plane of the ligand, in acid conditions, in water phase.

on the same plane of the ligand for the system with an extra proton on the cis position (following reaction R₃) lies at lower energy than on the opposite plane. The potential energy profile

for this reaction is depicted in Figure 7 while the corresponding optimized structures are reported in Figure 8. In gas phase, the reacting water molecule in the intermediate lies 3.55 Å away from the platinum center. This water molecule then approaches the metal, and the transition state geometry is reached with a Pt–OW distance of 2.39 Å in gas phase and the Pt–OL distance is 2.36 Å. When solvent effects are included, the distances are somewhat longer with 2.49 Å for the Pt–OW and 2.42 Å for the Pt–OL bond. The final product for this reaction consists of a double aqua complex for the water optimization and a proton transfer from the water molecule to the oxalate ligand in gas phase.

According to the results here obtained, reaction on the same plane requires an activation barrier of 21.79 kcal/mol. The imaginary frequencies for the transition state are 180i cm⁻¹ in gas and 170i cm⁻¹ in solvent.

Considering the addition of the second water molecule in the system with an extra proton on the trans position (following reaction R₄), we must analyze, just as in R₅, the possibility of

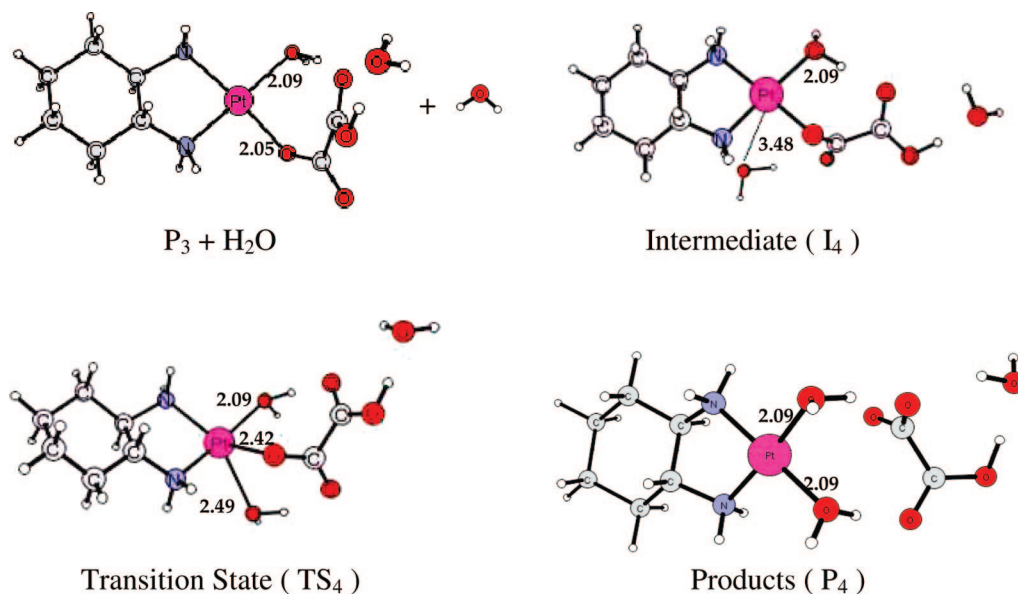


Figure 8. Optimized structures and selected structural parameters for the addition of the second water molecule to oxaliplatin (R₅), in the same plane of the ligand, in acidic conditions, in water phase. The distances reported are in angstroms.

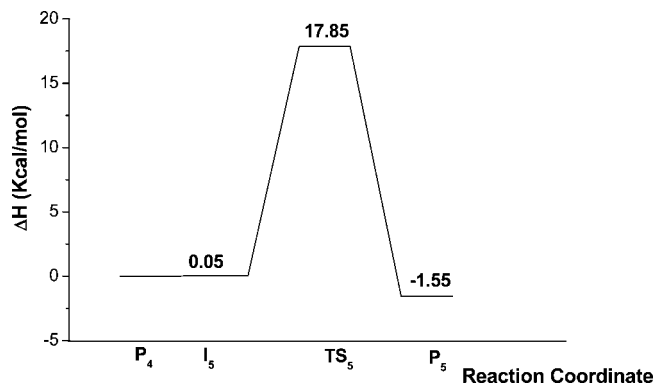


Figure 9. Activation enthalpy (at 298.15 K) and reaction heat for the addition of the second water molecule to oxaliplatin with an extra proton on the trans position, in the opposite plane of the ligand, in acid conditions, in water phase.

addition in the same or opposite plane of the exiting ligand (R6). Results show that addition on the opposite plane exhibits a lower energy path which is reported in Figure 9. The optimized structures are shown in Figure 10. The reacting water molecule is 3.84 Å away from the platinum atom in the intermediate system. The critical distances in the transition state are identical in water and gas phase, with a Pt–OW distance of about 2.50 Å and the Pt–OL distance about 2.45 Å in both phases. Concerning the addition of the second water molecule in the opposite plane of the ligand, and in spite of the fact that the product from the previous step shifted a proton from the water molecule to the ligand (in gas phase), we have observed that the optimization of the reactant for next step (extra water molecule) retrieves the proton back to the water ligand. However, in the remaining stationary points (TS and products in gas phase) the proton is located on the exiting ligand. In case of reaction proceeding in solvent, the proton always stays with the attacking water molecule during the whole reaction. The calculated activation energy in water phase is 17.85 kcal/mol, and the process is slightly exothermic (−1.55 kcal/mol). As previously observed, also here, the final product is different depending on the medium. The final product is a double aqua complex for the system optimized with solvent effects included

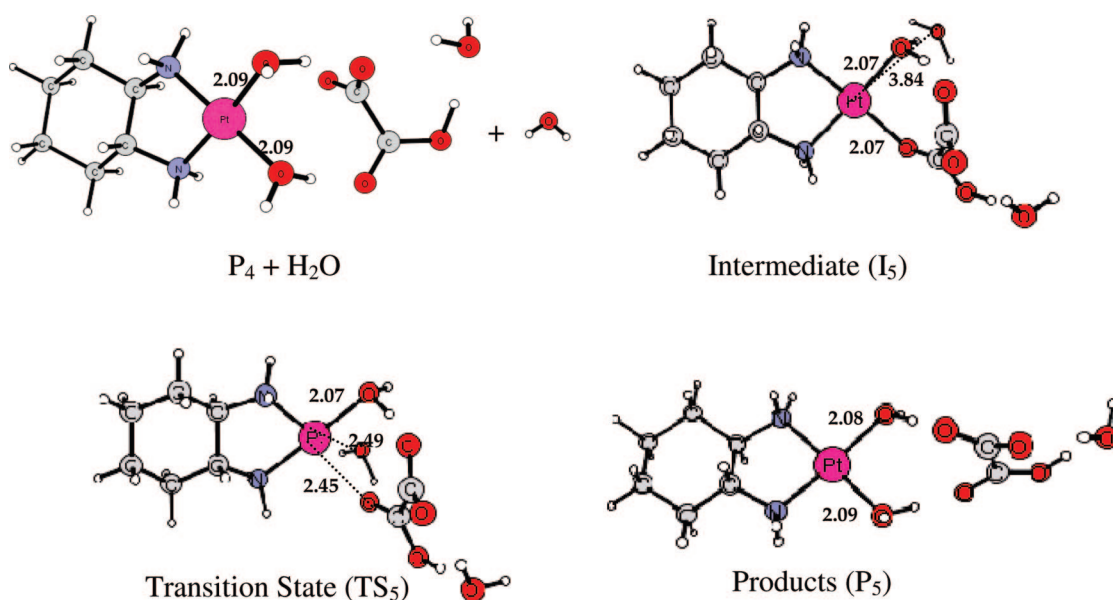


Figure 10. Optimized structures and structural parameters for the addition of the second water molecule to oxaliplatin with an extra proton on the trans position, in the opposite plane of the ligand, in acid conditions, in water phase. The distances reported are in angstroms.

one water molecule, while in gas phase we observed a proton transfer from the water molecule to the oxalate ligand. The transition states have an imaginary frequencies of about 200i cm^{-1} .

Discussion

From the results obtained we can see that the relative position of the proton on the oxalate ligand has an important influence on the energetics of the system. A cis position leads to a faster reaction with an activation barrier of 15.11 kcal/mol (R3) opposed to 18.26 observed for the trans configuration (R4). We have also established that the most favorable position for the second entering water molecule is in the case of neutral conditions, in the same plane of the exiting ligand, while in the acidic conditions the entering water molecule prefers the opposite side.

In acid conditions according to our calculations this reaction should overcome a 21.79 kcal/mol activation barrier corresponding to the second water attack.

As previously reported, oxaliplatin has proven to be an important drug in cancer treatment. It is active in some cisplatin intrinsic and acquired resistant tumors, and a correct description of the aqueous degradation products is essential. Just as its predecessor, cisplatin, we can expect that in solution oxaliplatin should degrade according to a biphasic process. Cisplatin can undergo two hydrolysis reactions; however, the second process is much slower, and for this reason, it has been suggested that cisplatin should bind to DNA monohydrated.³⁸ Oxaliplatin exhibits a different behavior depending on the medium. In neutral conditions, the rate-limiting process is the ring-opening reaction with the ligand release occurring quickly, and for this reason oxaliplatin is more likely to bind to DNA in its completely hydrolyzed form. In acid conditions, the first step is faster than the second, and the activation barriers for the first and second hydrolysis are $R3 = 15.11$ kcal/mol and $R5 = 21.79$ kcal/mol. In addition, the presence of the large monodentate oxalate group can promote stereochemical hindrance in reaction with DNA.

Comparison of the neutral hydrolysis barriers (Table 1), between oxaliplatin, carboplatin, and cisplatin, reveals that

TABLE 1: Comparison between Calculated Activation Energies for Cisplatin, Carboplatin, and Oxaliplatin in Neutral and Acid Conditions

compound	neutral			acid		
	first aquation	second aquation	rate-limiting step	first aquation	second aquation	rate-limiting step
cisplatin ^a	22.9	26.2	second			
carboplatin ^b	30.1	21.3	first	20.9	22.7	second
oxaliplatin ^c	27.9	24.1	first	15.1	21.8	second

^a From ref 38. ^b From ref 46. ^c From this work.

the oxaliplatin and carboplatin exhibit a common behavior with the rate-limiting step in the first aquation process and have values higher than the corresponding barrier in cisplatin. It has been reported that cisplatin-like compounds with one or two large groups in the NH₃ position have slower hydrolysis rates compared to that of cisplatin.⁵⁸ Computational studies, in good agreement with experimental data, have confirmed this for drugs such as JM118⁵⁹ and carboplatin.⁴⁶

This aspect is important since a slower hydration may allow the drug to reach its cellular targets in its original form, which in turn can be one of the reasons of the lower side effects displayed by oxaliplatin. For oxaliplatin, the second hydrolysis reaction, in neutral conditions, is much faster than the first reaction just as carboplatin. This behavior is dissimilar to cisplatin's where the displacement of the second chloride ion is slower than the first. If we compare carboplatin and oxaliplatin, it is clear that their behaviors are quite different. Carboplatin is very stable in neutral conditions with an activation barrier of 30.1 kcal/mol while oxaliplatin degrades much faster. On the other hand, it is known that these two drugs exhibit lesser side effects when compared to cisplatin. The differences in toxicity can be related to their binding to DNA; however, it can also be a consequence of the different behavior in water and/or dissimilar hydrated forms that react with DNA.

In acid solution both drugs show, again, similar behavior being the second aquation reaction the rate-limiting step.

Conclusions

In this work, we have investigated the hydrolysis reactions of the third generation anticancer drug oxaliplatin by means of density functional theory and employing the CPCM approach in order to take into account the bulk solvent effect. We were able to establish all pertinent stationary points of the aqueous degradation in neutral and acid conditions. In agreement with experimental data, the neutral hydrolysis is much slower than the acid counterpart with a calculated activation barrier of 23.6 kcal/mol opposed to 27.95 kcal/mol. We have also established that for the neutral degradation the limiting process is the first step, the ring-opening reaction, while in acid conditions the slowest process is the ligand detachment. For the reaction in acid conditions, the presence of the extra proton in the carboxylate group has an effect on the activation barriers observed. It is clear that the most favored position is a cis arrangement regarding the bond being broken.

From the results, we can see that oxaliplatin exhibits a different behavior from cisplatin. The degradation in water is slower, and the rate-limiting process is expected to be the first substitution. Cisplatin has been proposed to reach DNA in its monohydrated form, in neutral conditions, while we expect that if oxaliplatin undergoes hydration processes

before reacting with DNA, the fully hydrolyzed complex should be the main product.

On the contrary, in acid condition, [Pt(1,2-diaminocyclohexaneoxalateplatinum)(H₂O)(HO)] should reach DNA in its mono-aquated forms.

Acknowledgment. Financial support from the Università della Calabria and Regione Calabria (POR Calabria 2000/2006 misura 3.16 progetto PROSICA) is gratefully acknowledged.

References and Notes

- (1) Rosenberg, B.; Camp, L.; Krigas, T. *Nature (London)* **1965**, *205*, 698.
- (2) Rosenberg, B.; Camp, L.; Trosko, J.; Mansour, V. H. *Nature (London)* **1969**, *222*, 385.
- (3) Sherman, S. E.; Lippard, S. J. *Chem. Rev.* **1987**, *99*, 1153.
- (4) Neidle, S.; Ismail, I. M.; Sadler, P. J. *J. Inorg. Chem.* **1980**, *13*, 205.
- (5) Hambley, T. W. *Coord. Chem. Rev.* **1997**, *166*, 181.
- (6) Ziegler, C. J.; Silverman, A. P.; Lippard, S. J. *J. Biol. Inorg. Chem.* **2000**, *5*, 774.
- (7) Kidani, Y.; Noji, M.; Tashiro, T. *Gann* **1980**, *71*, 637.
- (8) Lim, K. H.; Huang, M. J.; Lin, H. C.; Su, Y. W.; Chang, Y. F.; Lin, J.; Chang, M. C.; Hsieh, R. K. *Anti-Cancer Drugs* **2004**, *15*, 605–7.
- (9) Balzer, K. M. *Cancer Pract.* **2000**, *8*, 201.
- (10) Lokich, J. *Cancer Invest.* **2001**, *19*, 756.
- (11) Wiseman, L. R.; Adkins, J. C.; Plosker, G. L.; Goa, K. L. *Drugs Aging* **1999**, *14*, 459.
- (12) Cvitkovic, E.; Bekradda, M. *Semin. Oncol.* **1999**, *26*, 647.
- (13) O'Dwyer, P. J.; Johnson, S. W. *Semin. Oncol.* **2003**, *30*, 78.
- (14) Chollet, P.; Bensmain, A.; Brienza, S.; Deloche, C.; Curé, H.; Caillet, H.; Cvitkovic, E. *Ann. Oncol.* **1996**, *7*, 1065.
- (15) Soulie, P.; Bensmaine, A.; Garrino, C.; Chollet, P.; Brain, E.; Fereres, M.; Jasmin, C.; Musset, M.; Misset, J. L.; Cvitkovic, E. *Eur. J. Cancer* **1997**, *33*, 1400.
- (16) Hambley, T. W. *J. Chem. Soc., Dalton Trans.* **2001**, 2711.
- (17) Jung, Y.; Lippard, S. J. *Chem. Rev.* **2007**, *107*, 1387.
- (18) Jamieson, E. R.; Lippard, S. J. *Chem. Rev.* **1999**, *99*, 2467.
- (19) Reedijk, J. *Pure Appl. Chem.* **1987**, *59*, 181.
- (20) Fichtinger-Schepman, A. M. J.; Veer, J. L.; Hartog, J. H. J.; Lohman, P. H. M.; Reedijk, J. *Biochemistry* **1985**, *24*, 707.
- (21) Eastman, A. *Pharmacol. Ther.* **1987**, *34*, 155.
- (22) Reedijk, J. *Chem. Commun.* **1996**, 801.
- (23) Yang, D.; Wang, A. H.-J. *Prog. Biophys. Mol. Biol.* **1996**, *66*, 81.
- (24) Takahara, P. M.; Rosenzweig, A. C.; Frederick, C. A.; Lippard, S. J. *Nature (London)* **1995**, *377*, 649.
- (25) Spingler, B.; Whittington, D. A.; Lippard, S. J. *Inorg. Chem.* **2001**, *40*, 5596.
- (26) Jennerwein, M. M.; Eastman, A.; Khokhar, A. *Chem. Biol. Interact.* **1989**, *70*, 39.
- (27) Woynarowski, J. M.; Faivre, S.; Herzig, M. C.; Arnett, B.; Chapman, W. G.; Trevino, A. V.; Raymond, E.; Chaney, S. G.; Vaisman, A.; Varchenko, M.; Juniewicz, P. E. *Mol. Pharmacol.* **2000**, *58*, 920.
- (28) Schmidt, W.; Chaney, S. G. *Cancer Res.* **1993**, *53*, 799.
- (29) Reedijk, J. *Inorg. Chim. Acta* **1992**, *198–200*, 873.
- (30) Bloemink, M. J.; Heetebrij, R. J.; Inagaki, K.; Kidani, Y.; Reedijk, J. *Inorg. Chem.* **1992**, *31*, 4656.
- (31) Galanski, M.; Yasemi, A.; Jakupec, M. A.; Graf, v; Keyserlingk, N.; Keppler, B. K. *Monatsh. Chem.* **2005**, *136*, 693.
- (32) Arpalahiti, J.; Mikola, M.; Mauristo, S. *Inorg. Chem.* **1993**, *32*, 3327.
- (33) Chval, Z.; Sip, M. *J. Mol. Struct.: THEOCHEM* **2000**, *532*, 59.
- (34) Zang, Y.; Guo, Z.; You, X.-Z. *J. Am. Chem. Soc.* **2001**, *123*, 9378.
- (35) Burda, J. V.; Zeizinger, M.; Leszczynski, J. *J. Chem. Phys.* **2004**, *120*, 1253.
- (36) Lau, J. K.-C.; Deubel, D. V. *J. Chem. Theory Comput.* **2006**, *2*, 103.

- (37) Burda, J. V.; Zeizinger, M.; Šponer, J.; Leszczynski, J. *J. Chem. Phys.* **2000**, *113*, 2224.
- (38) Raber, J.; Zhu, C.; Eriksson, L. A. *Mol. Phys.* **2004**, *102*, 2537.
- (39) Misset, J. L.; Bleiberg, H.; Sutherland, W.; Bekradda, M.; Cvitkovic, E. *Crit. Rev. Oncol./Hem.* **2000**, *35*, 75.
- (40) Brabec, V.; Kasparkova, J. *Drug Resist. Updates* **2002**, *5*, 147.
- (41) Chiodo, S.; Kondakova, O.; Michelini, M. C.; Russo, N.; Sicilia, E.; Irigoras, A.; Ugalde, J. M. *J. Phys. Chem. A* **2004**, *108*, 1069.
- (42) Leopoldini, M.; Pitarch, I. P.; Russo, N.; Toscano, M. *J. Phys. Chem. A* **2004**, *108*, 92.
- (43) Lucas, M. F.; Ramos, M. J. *J. Am. Chem. Soc.* **2005**, *127*, 6902.
- (44) Deubel, D. V. *J. Am. Chem. Soc.* **2006**, *128*, 1654.
- (45) Magistrato, A.; Ruggerone, P.; Spiegel, K.; Carloni, P.; Reedijk, J. *J. Phys. Chem. B* **2006**, *110*, 3604.
- (46) Pavelka, M.; Lucas, M. F.; Russo, N. *Chem.—Eur. J.* **2007**, *13*, 10108.
- (47) Spiegler, K.; Magistrato, A. *Org. Biomol. Chem.* **2006**, *4*, 2507.
- (48) Sarmah, P.; Deka, R. C. *Int. J. Quantum Chem.* **2008**, *108*, 1400.
- (49) Jerremalm, E.; Eksborg, S.; Ehrsson, H. *J. Pharm. Sci.* **2003**, *92*, 436.
- (50) Jerremalm, E.; Videhult, P.; Alvelius, G.; Griffiths, W. J.; Bergman, T.; Eksborg, S.; Ehrsson, H. *J. Pharm. Sci.* **2002**, *91*, 10–2116.
- (51) Becke, A. D. *J. Chem. Phys.* **1993**, *98*, 5648.
- (52) Lee, C. T.; Yang, W. T.; Parr, R. G. *Phys. Rev. B* **1988**, *37*, 785.
- (53) Frisch, M. J.; et al. *Gaussian 03*; Gaussian, Inc.: Pittsburgh, PA, 2003.
- (54) Andrae, D.; Haussermann, U.; Dolg, M.; Stoll, H.; Preuss, H. *Theor. Chim. Acta* **1990**, *77*, 123.
- (55) (a) Klamt, A.; Schüürmann, G. *J. Chem. Soc., Perkin Trans. 2* **1993**, 799. (b) Andzelm, J.; Kölmel, C.; Klamt, A. *J. Chem. Phys.* **1995**, *103*, 9312–9320. (c) Barone, V.; Cossi, M. *J. Phys. Chem. A* **1998**, *102*, 1995–2001. (d) Cossi, M.; Rega, N.; Scalmani, G.; Barone, V. *J. Comput. Chem.* **2003**, *24*, 669–681.
- (56) Tomasi, J.; Cammi, R.; Mennucci, B.; Cappelli, C.; Corni, S. *Phys. Chem. Chem. Phys.* **2002**, *4*, 5697.
- (57) Klamt, A.; Jonas, V.; Burger, T.; Lohrenz, J. C. W. *J. Phys. Chem. A* **1998**, *102*, 5074.
- (58) Chen, Y.; Guo, Z.; Parsons, S.; Sadler, P. *Chem.—Eur. J.* **1998**, *4*, 672.
- (59) Zhu, C.; Raber, J.; Eriksson, L. A. *J. Phys. Chem. B* **2005**, *109*, 12195.

JP8086539

Paper III

“The Degradation Pathways in Chloride Medium of the
Third Generation Anticancer Drug Oxaliplatin”

Marta E. Alberto, Maria F. Lucas, Matěj Pavelka and Nino Russo

J. Phys. Chem. B **2008**, *112*, 10765–10768

The Degradation Pathways in Chloride Medium of the Third Generation Anticancer Drug Oxaliplatin

Marta E. Alberto, Maria F. Lucas, Matěj Pavelka, and Nino Russo*

Dipartimento di Chimica, Università della Calabria - Via P. Bucci, cubo 14c,
87036 Arcavacata di Rende (CS), Centro di Calcolo ad Alte Prestazioni per Elaborazioni Parallele e
Distribuite – Centro d'Eccellenza MIUR, Italy

Received: January 17, 2008; Revised Manuscript Received: July 18, 2008

We have investigated the degradation reactions, in chloride medium, of the third generation drug oxaliplatin using density functional theory. Our calculations confirm that this drug should be administered in chloride free solutions, and we have ascertained the main biodegradation products upon chloride binding, which are essential to establish the active compounds reacting with DNA. In addition, detailed knowledge of these platinum complexes is fundamental for correct elimination procedures in wastewater treatments.

Introduction

Cisplatin (*cis*-diamminedichloroplatinum(II)) is a successful anticancer drug,^{1,2} yet it was nearly discarded in the early 1970s because of its gastrointestinal and renal toxicities. When it was established that these side effects could be alleviated by antiemetic drugs and intense hydration of the patient, cisplatin became a fundamental drug in testicular, ovarian, bladder, lung, head, neck, and cervical cancers.³ Most patients with metastatic testicular cancer will be long-term survivors thanks to cisplatin-based chemotherapy. However, cisplatin exhibits two severe limitations: potentially long-term side effects such as oto-,⁴ neuro-,⁵ and nephrotoxicity⁶ and drug resistance which prevents some of the patients from achieving long-term remissions. In order to overcome these limitations, many structural analogues have been investigated.^{7–10} Oxaliplatin¹¹ (1,2-diaminocyclohexaneoxalate–platinum) is active against some tumors that are primarily resistant to cisplatin and carboplatin (a second generation platinum drug) being the first antineoplastic agent to exhibit activity against metastatic colorectal cancer.^{12,13}

It is thought that platinum complexes exert their cytotoxic action in a similar manner to alkylating agents by causing inter- and intrastrand cross-links with DNA, inhibiting its synthesis and inducing apoptotic cell death.^{14–16} Much research has been done in this area, and it has been proposed that these drugs interact with DNA following several steps: aquation of the platinum complex, preassociation with the DNA, monofunctional adduct formation, closure of the bifunctional adduct, and distortion of the DNA and recognition of this distortion.¹⁷ Oxaliplatin is normally administered by intravenous infusion, and it is biotransformed essentially by water and nucleophiles such as Cl[−] and HCO₃[−].¹⁸ It has been established that oxaliplatin's degradation in aqueous media depends on chloride concentration as well as the pH. However, in contrast to cisplatin, the decay of oxaliplatin is promoted by increasing the concentration of chloride with [Pt(DACH)Cl₂] (DACH stands for 1,2-diaminocyclohexyl) being the major product.^{18–20} Some

studies account that oxaliplatin undergoes extensive biotransformation (17 products have been reported) leading to the degradation of the parent drug into a variety of platinum containing products.^{21,22} [Pt(DACH)OxCl][−], a transformation product from oxaliplatin, upon chloride binding, has been identified, and in the presence of chloride, oxaliplatin rapidly degrades initially to this compound. It supports the recommendations that oxaliplatin should not be mixed with solutions containing chloride. On the other hand, the slower degradation seen subsequently must be due to the fact that the [Pt(DACH)OxCl][−] is converted back to oxaliplatin by an intramolecular reaction. At pH 7.4 and 37°, this takes place within an hour;¹⁸ moreover, the rate of formation of [Pt(DACH)Cl₂] is slow.

Given that oxaliplatin is administered by infusion solutions, it is very important to ascertain its degradation reaction in the presence of chloride ions. In addition, analysis of patient urine suggests that oxaliplatin is present in wastewater as a variety of biotransformed products.²² The investigation of the ecotoxicity of oxaliplatin and the development of elimination procedures during sewage treatment requires a complete knowledge of all degradation products of this drug.

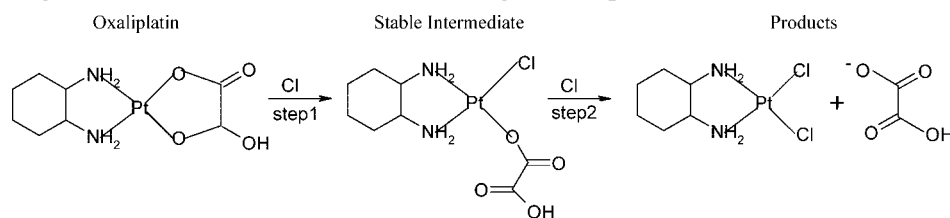
Although different theoretical studies already exist on the aquation reactions of platinum anticancer compounds,^{23–27} no investigation has been carried on the chloride binding processes. In this communication, we present, for the first time, the acid and neutral degradation reactions for oxaliplatin reactions with chloride. The reaction is expected to take place in a two-step process, as illustrated in Scheme 1.

Methods

The considered reactions were investigated using density functional theory (DFT), with the B3LYP²⁸ functional, as implemented in Gaussian 03.²⁹ Gas phase optimizations were carried out under neutral conditions as well as in acid (one oxygen atom on oxaliplatin's carboxylate group protonated) and in strong acid (both carboxylate oxygen atoms protonated). All structures were optimized with the 6-31G(d) basis set on all atoms except the platinum atom, which was described by the

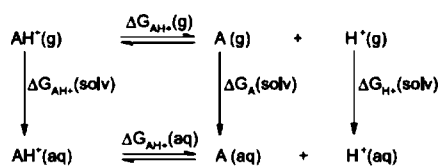
* To whom correspondence should be addressed. E-mail: nrusso@unical.it.

SCHEME 1: Investigated Reaction Paths for Chloride Binding to Oxaliplatin under Acid Conditions



quasi-relativistic Stuttgart–Dresden pseudopotential³⁰ with pseudo-orbital basis set augmented by a set of diffuse functions— $\alpha_s = 0.0075$, $\alpha_p = 0.013$, and $\alpha_d = 0.025$ —and polarization functions— $\alpha_f = 0.98$. In order to confirm proper convergence to equilibrium and transition state geometries, vibrational frequency analysis was done based on analytical second derivatives of Hamiltonian at this level of theory. For all transition states, intrinsic reaction coordinate (IRC) calculations were used to verify corresponding reactant and product structures. The final energies were obtained with single point energy calculations on optimized structures using the 6-31++G(2df,2pd) basis set, and the water environment modeled using the conductor-like polarized continuum model (CPCM).³¹ Klamt radii were used for constructing the solute cavity.³² Similarly, the platinum valence basis set was augmented with diffuse ($\alpha_f = 0.46$) and polarization ($\alpha_g = 1.21$) functions. Potential energy profiles were estimated from total electronic energies at the 6-31++G(2df,2pd) level (with solvent effects included) adding zero point energy (ZPE), enthalpy, and Gibbs corrections at room temperature (298.15 K). Previous studies on platinum-based compounds²⁷ have shown an excellent agreement between experimental and calculated data, and for this reason, the present level of theory has been considered appropriate.

For the calculation of the absolute pK_a , the following thermodynamic cycle was used:



The $G_{H^+}(g)$ and $\Delta G_{H^+}(solv)$ terms are -6.28^{33} and -263.98 kcal/mol,³⁴ respectively, and a term $-RT \ln(24.46)$ was added to take into account the transformation of concentration units in the aqueous phase (atm to mol dm⁻³).

Results

As a first step of our investigation, we considered the neutral process. The reaction should begin with the addition of a chloride ion and the consequent ring-opening process. We tried to locate the transition state for step 1 under neutral conditions, but in spite of the many attempts performed, it was not possible to find this structure. In addition to DFT, the Hartree–Fock level of theory using the 6-31G(d) basis set was also employed in the search of this saddle point. However, also in this case, it was not found on the potential energy surface (PES). This situation is not new, and theoretical calculations done on cisplatin from Mu-Hyun Baik et al. reveal that not all structures can be located on the PES.³⁵ Thus, we have considered an alternative path in which the attack of a chloride ion on the platinum center leads to the opening of the DACH ring. We were able to locate the pertinent stationary points on the potential

energy surface and observed that this step requires 30.93 kcal·mol⁻¹ activation energy and presents an endothermic reaction heat of 10.95 kcal·mol⁻¹. Since it is well-known that the *N,N*-chelates of Pt(II) are thermodynamically more stable than *O,O*-chelates, we think that the barrier to open the Pt–O bond under chlorine attack should be lower than that found for the Pt–N bond breaking.

For the step 2 reaction, we have located all the stationary points on the PES. The initial complex and the transition states lie at 5.98 and 36.24 kcal·mol⁻¹, respectively, above the reactant energies. The reaction is found to be endothermic by 15.45 kcal·mol⁻¹. On the basis of our results, we can reasonably hypothesize that the second chlorination step should have a barrier greater than the first ones.

In order to establish the conditions in which oxaliplatin can be administered as well as the degradation products, it is essential to investigate these reactions also under acidic conditions. For this, we have assumed that the oxaliplatin's oxalato group will be protonated (under physiological conditions, to some extent, it can exist in protonated form and will be present in normal urine). In order to have information on pK_a values

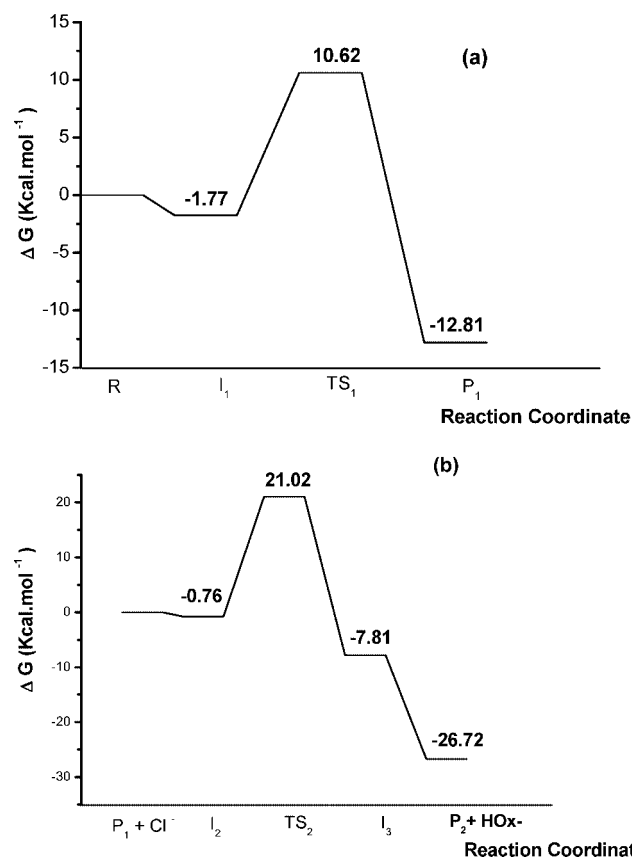


Figure 1. Potential energy surface for (a) the addition of the first chloride ion to oxaliplatin (step 1) and for (b) the addition of chloride ion to the [Pt(DACH)(HOx)Cl]⁻ (step 2), under acidic conditions.

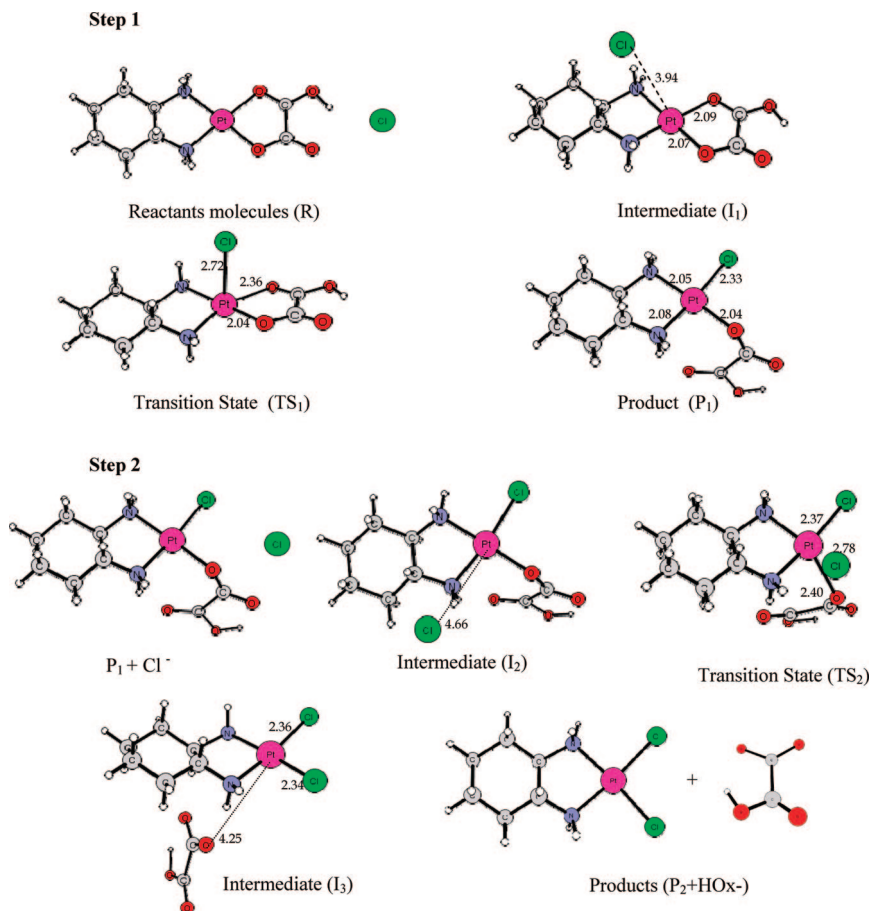


Figure 2. Optimized structures of the stationary points along the PES of step 1 and step 2 reactions. The indicated values are bond distances in angstroms.

and on the reliability of the method in predicting this parameter, we have computed these values for the oxalic acid and oxalate (for which the experimental values are known) and for the corresponding oxaliplatin complex. The theoretical values for oxalic acid (H_2Ox) and H-oxalate (HOx^-) are found to be 0.98 and 4.81, respectively. The experimental counterparts are 1.23 and 4.27, respectively. The agreement is quite satisfactory, and the experimental trend is well reproduced. In analogy, for $[\text{Pt}(\text{DACH})\text{H}_2\text{Ox}]^{+2}$ and $[\text{Pt}(\text{DACH})\text{HOx}]^+$ complexes, the calculated $\text{p}K_a$ is -1.52 and 6.37 , respectively. The increase of the $\text{p}K_a$ value of HOx^- upon binding the platinum(II) moiety is essentially due to the greater O–H bond polarization in the HOx system, as evidenced by the computed atomic net charges. Furthermore, we note a decrease of the C–OH bond distance in going from the HOx^- to $[\text{Pt}(\text{DACH})\text{HOx}]^+$ complex.

The potential energy surfaces for the first and second chlorination reactions (steps 1 and 2 reported in Scheme 1) under acid conditions are reported in parts a and b of Figure 1, respectively. The optimized geometrical structure for the reactants, transition states, and products are depicted in Figure 2.

The reaction starts with the attack of the chloride ion on the platinum center and the consequent formation of a weak complex (I_1) that lies at $1.77 \text{ kcal}\cdot\text{mol}^{-1}$ below the reactant energies. The Pt–Cl bond distance is 3.94 \AA , and the geometrical parameters of the initial oxaliplatin are essentially unchanged. In the transition state, located at $10.62 \text{ kcal}\cdot\text{mol}^{-1}$, the platinum H-oxalate bond (Pt–HOx) is stretched to 2.36 \AA , while the chloride platinum bond (Pt–Cl) is 2.72 \AA . The reaction proceeds with the scission of the Pt–Ox bond from

the transition state TS_1 and by the formation of the product (P_1) that lies at $12.81 \text{ kcal}\cdot\text{mol}^{-1}$ below the reactants (R).

The product from step 1 is the $[\text{Pt}(\text{DACH})(\text{HOx})\text{Cl}]$ with oxalate ligand bonded by only one oxygen atom.

The second chloride addition begins with the approach of the Cl^- ion that is found further away from the platinum center than in the previous reaction. The attack of the chloride ion gives rise to the intermediate (I_2) which is found at $0.76 \text{ kcal}\cdot\text{mol}^{-1}$ below the reactants and is characterized, as in the corresponding complex of step 1, by a long Pt–Cl bond distance (4.66 \AA). In the transition state structure (TS_2), the Pt–Cl bond is 2.78 \AA and the Pt–O bond is 2.40 \AA . The computed imaginary frequency for the transition state is $124i \text{ cm}^{-1}$, and the following IRC optimization clearly shows the formation of the Pt–Cl bond and the scission of the Pt–O one. For such reaction, the activation barrier is $21.02 \text{ kcal}\cdot\text{mol}^{-1}$.

An intermediate complex is then observed (I_3) at $7.81 \text{ kcal}\cdot\text{mol}^{-1}$ below the reactants which proceed without any barrier, to the separated products ($\text{P}_2 + \text{HOx}$). The exothermicity is $26.72 \text{ kcal}\cdot\text{mol}^{-1}$.

In addition, we have considered the possibility that the chlorine attack could break the Pt–N bond. For the first chlorination, we have located the intermediate complex and the transition state at -0.80 and $23.97 \text{ kcal}\cdot\text{mol}^{-1}$ with respect to the reactants, respectively. The reaction is endothermic by $9.93 \text{ kcal}\cdot\text{mol}^{-1}$. As expected from much experimental evidence, the Pt–N bond breaking requires a higher energy than that demanded for the Pt–O bond scission.

Considering the lowest energy path, it is clear that the formation of the [Pt(DACH)(HOx)Cl] (step 1) is strongly favored over the formation of [Pt(DACH)Cl₂] (step 2).

Finally, we have also considered the strong acid condition with both carboxylate groups protonated. The results indicate that, under these conditions, the decomposition of oxaliplatin into [Pt(DACH)Cl₂] takes place with a calculated activation barrier of 15.53 kcal·mol⁻¹ for step 1 and 17.19 kcal·mol⁻¹ for step 2. Step 1 is exothermic by 15.53 kcal·mol⁻¹ and step 2 by 15.01 kcal·mol⁻¹.

Conclusions

In summary, we have explored the decomposition of oxaliplatin in the presence of chloride using density functional theory with the B3LYP functional. Under neutral conditions, we have seen that reaction, according to step 1, is not observed on the potential energy surface due to the lack of the localization of the transition state for the Pt—O bond breaking. On the other hand, under acidic conditions, the presence of chloride ion leads to the decomposition of oxaliplatin. We were also able to establish that the most favorable reaction leads to the decomposition of oxaliplatin following steps 1 and 2 with the formation of [Pt(DACH)Cl₂]. The first step for this reaction is the ring-opening process with a calculated activation barrier of 10.62 kcal·mol⁻¹ accompanied by a 12.81 kcal·mol⁻¹ energy release. The final product is obtained by overcoming a 21.02 kcal·mol⁻¹ activation barrier, which makes it the rate limiting process, and is exothermic by 7.81 kcal·mol⁻¹. In addition, as expected, both processes leading to the detachment of the DACH ligand require a big amount of energy and are endothermic. For this reason, the formation of [PtOxCl₂]²⁻ and [Pt(HOx)Cl₂]⁻ is not favored both kinetically and thermodynamically.

This study is of importance for the clinical use of oxaliplatin, since it is essential to identify the active form of the drug reacting with DNA. It also concurs with the previous experimental findings that oxaliplatin should be administered in chloride free solutions and that acidification leads to fast chloride reaction with this drug. In addition, we were able to ascertain the most likely products that can be found in wastewaters. Urine is normally acidic (pH ≈ 6),³⁶ and we have established that, under these conditions, oxaliplatin is degraded into a variety of products.

Acknowledgment. Financial support from the Università della Calabria and Regione Calabria (POR Calabria 2000/2006 misura 3.16 progetto PROSICA) is gratefully acknowledged.

References and Notes

- (1) Rosenberg, B.; Camp, L.; Krigas, T. *Nature* **1965**, *205*, 698.
- (2) Rosenberg, B.; Camp, L.; Trosko, J.; Mansour, V. H. *Nature* **1969**, *222*, 385.
- (3) Sherman, S. E.; Lippard, S. J. *Chem. Rev.* **1987**, *87*, 1153.
- (4) Bokemeyer, C.; Berger, C.; Kynast, B.; Schmoll, H.-J.; Poliwođa, H. *Eur. J. Cancer* **1993**, *29*, S241.
- (5) Bokemeyer, C.; Frank, B.; Rhee, J.; Berger, C.; Schmoll, H.-J. *Tumordiagn. u. Ther.* **1993**, *14*, 232.
- (6) Cornelison, T. L.; Reed, E. *Gynecol. Oncol.* **1993**, *50*, 147.
- (7) Farrell, N. *Cancer Invest.* **1993**, *11*, 578.
- (8) Wong, E.; Giandomenico, C. M. *Chem. Rev.* **1999**, *99*, 2451.
- (9) Jung, Y.; Lippard, S. J. *Chem. Rev.* **2007**, *107*, 1387.
- (10) Zhang, C. X.; Lippard, S. J. *Curr. Opin. Chem. Biol.* **2003**, *7*, 481.
- (11) Kidani, Y.; Noji, M.; Tashiro, T. *Gann.* **1980**, *71*, 637.
- (12) Brienza, S.; Bignound, J.; Itzhaki, M.; Krikorian, A. *Eur. J. Cancer* **1995**, *31A*, S194.
- (13) Dunn, T. A.; Schmoll, H. J.; Grunwald, V.; Bokemeyer, C.; Casper, J. *Invest. New Drugs* **1997**, *15*, 109.
- (14) Jamieson, E. R.; Lippard, S. J. *Chem. Rev.* **1999**, *99*, 2467.
- (15) Reedijk, J. P. A. C. **1987**, *59*, 181.
- (16) Fuertes, M. A. A. C.; Pérez, J. M. *Chem. Rev.* **2003**, *103*, 645.
- (17) Hambley, T. W. *J. Chem. Soc., Dalton Trans.* **2001**, 2711.
- (18) Jerremalm, E.; Hedeland, M.; Wallin, I.; Bondesson, U.; Ehrsson, H. *Pharm. Res.* **2004**, *21*, 891.
- (19) Bouvet, D.; Michalowicz, A.; Crauste-Manciet, S.; Curis, E.; Nicolis, I.; Olivi, L.; Vlaic, G.; Brossard, D.; Provost, K. *J. Synchrotron Radiat.* **2006**, *13*, 477.
- (20) Curis, E.; Provost, K.; Bouvet, D.; Nicolis, I.; Crauste-Manciet, S. D. B.; Bénazeth, S. *J. Synchrotron Radiat.* **2001**, *8*, 716.
- (21) Graham, M. A.; Lockwood, G. F.; Greenslade, D.; Brienza, S.; Bayssas, M. E. G. *Clin. Cancer Res.* **2000**, *6*, 1205.
- (22) Hann, S.; Stefanka, Z.; Lenz, K.; Stingeder, G. *Anal. Bioanal. Chem.* **2005**, *381*, 405.
- (23) Zhang, Y.; Guo, Z.; You, X.-Z. *J. Am. Chem. Soc.* **2001**, *123*, 9378.
- (24) Lau, J.; Deubel, D. V. *J. Chem. Theory Comput.* **2006**, *2*, 103.
- (25) Raber, J.; Zhu, C.; Eriksson, L. A. *Mol. Phys.* **2004**, *102*, 2537.
- (26) Burda, J. V.; Zeizinger, M.; Leszczynski, J. *J. Comput. Chem.* **2005**, *26*, 907.
- (27) Pavelka, M.; Lucas, M. F.; Russo, N. *Chem.—Eur. J.* **2007**, *13*, 10108.
- (28) (a) Becke, A. D. *J. Chem. Phys.* **1993**, *98*, 1372. (b) Becke, A. D. *J. Chem. Phys.* **1993**, *98*, 5648. (c) Lee, C.; Yang, W.; Parr, R. G. *Phys. Rev. B* **1988**, *37*, 785.
- (29) Frisch, M. J.; Trucks, G. W.; Schlegel, H. B.; Scuseria, G. E.; Robb, M. A.; Cheeseman, J. R.; Montgomery, J. A.; Vreven, J. T.; Kudin, K. N.; Burant, J. C.; Millam, J. M.; Iyengar, S. S.; Tomasi, J.; Barone, V.; Mennucci, B.; Cossi, M.; Scalmani, G.; Rega, N.; Petersson, G. A.; Nakatsuji, H.; Hada, M.; Ehara, M.; Toyota, K.; Fukuda, R.; Hasegawa, J.; Ishida, M.; Nakajima, T.; Honda, Y.; Kitao, O.; Nakai, H.; Klene, M.; Knox, X. L. J. E.; Hratchian, H. P.; Cross, J. B.; Adamo, C.; Jaramillo, J.; Gomperts, R.; Stratmann, R. E.; Yazyev, O.; Austin, A. J.; Cammi, R.; Pomelli, C.; Ochterski, J. W.; Ayala, P. Y.; Morokuma, K.; Voth, G. A.; Salvador, P.; Dannenberg, J. J.; Zakrzewski, V. G.; Dapprich, S.; Daniels, A. D.; Strain, M. C.; Farkas, O.; Malick, D. K.; Rabuck, A. D.; Raghavachari, K.; Foresman, J. B.; Ortiz, J. V.; Cui, Q.; Baboul, A. G.; Clifford, S.; Cioslowski, J.; Stefanov, B. B.; Liu, H.; Liashenko, A.; Piskorz, P.; Komaromi, I.; Martin, R. L.; Fox, D. J.; Keith, T.; Al-Laham, M. A.; Peng, C. Y.; Nanayakkara, A.; Challacombe, M.; Gill, P. M. W.; Johnson, B.; Chen, W.; Wong, M. W.; Gonzalez, C.; Pople, J. A. *Gaussian 03*, revision A.1; Gaussian, Inc.: Pittsburgh, PA, 2003.
- (30) Schwerdtfeger, P.; Dolg, M.; Schwarz, W. H. E.; Bowmaker, G. A.; Boyd, P. D. W. *J. Chem. Phys.* **1989**, *91*, 1762.
- (31) (a) Klamt, A.; Schüürmann, G. *J. Chem. Soc., Perkin Trans. 2* **1993**, 799. (b) Andzelm, J.; Kölmel, C.; Klamt, A. *J. Chem. Phys.* **1995**, *103*, 9312–9320. (c) Barone, V.; Cossi, M. *J. Phys. Chem. A* **1998**, *102*, 1995–2001. (d) Cossi, M.; Rega, N.; Scalmani, G.; Barone, V. *J. Comput. Chem.* **2003**, *24*, 669–681.
- (32) Klamt, A.; Schüürmann, G. *J. Chem. Soc., Perkin Trans. 2* **1993**, 799.
- (33) Topol, I. A.; Tawa, G. J.; Burt, S. K.; Rashin, A. A. *J. Chem. Phys.* **1999**, *111*, 10998.
- (34) Tissandier, M. D.; Cowen, K. A.; Feng, W. Y.; Gundluach, E.; Cohen, M. H.; Earhart, A. D.; Coe, J. V.; Tuttle, T. R. *J. Phys. Chem. A* **1998**, *102*, 7787.
- (35) Baik, M.-H.; Richard, A. F.; Lippard, S. J. *J. Am. Chem. Soc.* **2003**, *125*, 14082.
- (36) Guyton, A. C. *Textbook of Medical Physiology*, 8th ed.; Harcourt College Pub: New York, 1990.

Paper IV

“Which one among the Pt-containing anticancer drugs forms
more easily monoadducts with **G** and **A** DNA bases?
A comparative study between oxaliplatin, nedaplatin and carboplatin”

Marta E. Alberto, Valeria Butera and Nino Russo

manuscript

Which one among the Pt-containing anticancer drugs forms more easily monoadducts with G and A DNA bases? A comparative study between oxaliplatin, nedaplatin and carboplatin

Marta E. Alberto^a, Valeria Butera^a and Nino Russo^a

Received (in XXX, XXX) Xth XXXXXXXXXX 200X, Accepted Xth XXXXXXXXXX 200X

First published on the web Xth XXXXXXXXXX 200X

DOI: 10.1039/b000000x

A detailed study of the interaction of second- and third-generation anticancer drugs with Guanine (G) and Adenine (A) DNA bases, has been performed by using DFT/CPCM approach, in order to obtain detailed data on their binding mechanisms and on the reaction energy profiles.

The antineoplastic activity of Cisplatin, the first platinum-based drug to enter clinical use, was unexpectedly discovered in the late 1960s.^{1,2} Although the wide spectrum of anticancer activity showed by this Pt compound (primarily administered for testicular tumors³ but also for ovarian, cervical, head and neck, esophageal, and non-small-cell lung cancers³⁻⁵), its therapeutic efficacy is somewhat compromised by the occurrence of serious side effects such as nausea/vomiting and nephro-, oto-, and neurotoxicity^{3,6-7} and development of resistance.⁸

Much progress has been made in elucidating the cisplatin mode of action and many details of the mechanism by which platinum-based drugs kill cancer are now well established. It's generally accepted that these compounds induce apoptosis in tumor cells, first being non-enzymatically converted to active derivatives by hydrolysis, and then by binding to nuclear DNA predominantly to the N7 position of Guanine bases. The so generated monofunctional adducts, subsequently closes by coordination to the N7 position of an adjacent purine to afford an intrastrand cross-link (mainly 1,2-d(GpG) and 1,2-d(ApG)).^{14,15}

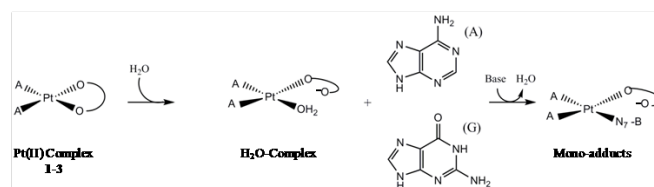
The induced structural distortions are key for the antitumor activity of cisplatin suppressing DNA transcription efficiently and ultimately leading to cell death.¹⁶

Significant efforts have been devoted to design new platinum antitumor agents in an attempt to overcome cisplatin resistance or enhance its antitumor activity. Nevertheless only four of them are currently registered for clinical use, namely oxaliplatin,^{9,10} carboplatin,^{11,12} and nedaplatin¹³. Due to the introduction of the kinetically less labile cyclobutane dicarboxylate, oxalate, and glycolate and to the presence of a large group in the NH₃ position in the case of Oxaliplatin (DACH), the Cisplatin-like compounds show a reduced rate of replacement of the O,O ligands. The reduced toxicity displayed from these second- and third-generation anticancer drugs in comparison with cisplatin is usually correlated to the slower hydrolysis processes. The hydration mechanisms were previously studied in order to have a correct understanding on all steps preceding the DNA binding and to provide insights on the active species that probably will react with the purine bases.¹⁷⁻²⁰

On the other hand, the steric and chemical properties of DNA lesions formed by cisplatin and its analogues are thought to underlie the differences in their biological activity, even if significant improvements in the ability to circumvent some cisplatin resistance mechanisms was observed only for oxaliplatin. A good understanding of the interaction of the second- and third- generation Pt-anticancer drugs, with models of binding sites present in DNA is of fundamental importance to unravel the mode of action of this class of compounds. Although there is no doubt that a Pt-N7 bond forms during initial attack, the energetic profiles for the formation of the monofunctional adducts are not known. Herein, the reactions of platinum mono-aqua complexes with Guanine (G) versus Adenine (A) were explored in neutral and acidic condition and compared in the present work, then contributing to elucidate the whole mechanism employed by these compounds to reach the biological target.

The reaction path for the formation of the mono-aquated Pt(II) complexes and the consequent monofunctional binding to DNA bases G and A is reported in the Scheme 1.

Scheme 1



It should be noticed that two mono-aqua complexes can be obtained in the hydrolysis process for NedaPt, due to the asymmetric nature of the glycolate ligand. As reported in our previous study,¹⁷ the detachment of the ligand can occur in two different ways, by rupture of the bond that involves the oxygen in α to the carbonyl group or by breaking the other Pt-O bond forming two different H₂O-complexes. Herein, we considered the reactions of both the nedaplatin mono-hydrated complexes with G and A purine bases determining a significant difference in the energetic profiles considering the 2 possible reactants. Only the most favourable paths concerning the mentioned reactions are reported along the text. The energetic profiles for the monofunctional binding of mono-hydrated CarboPt, NedaPt, OxaliPt compounds to Guanine and Adenine purine bases are reported in Fig.1, while the optimized structures of the stationary

points and key geometrical parameters are showed in the SI section.

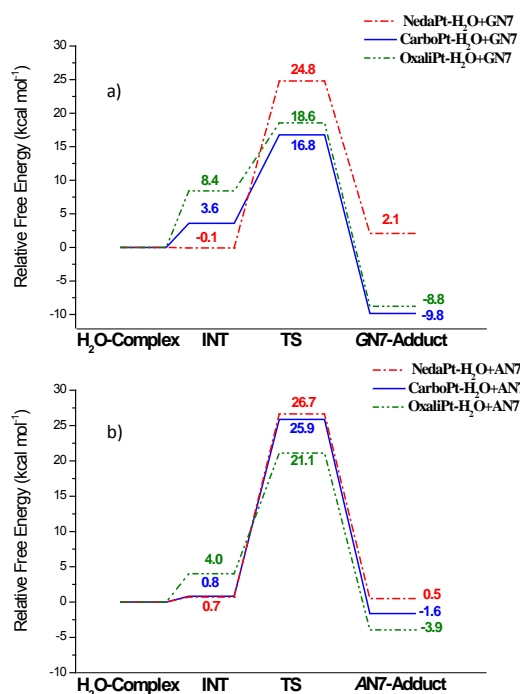


Figure 1. Overposition of the computed relative free energies profiles (at 298.15 K), for the reactions of mono-hydrated NedaPt, OxaliPt, CarboPt with a) N7-Guanine and b) N7-Adenine purine bases, in neutral conditions.

Concerning the Guanine platination processes, no significant differences were found in the geometries of the stationary points considering the three Pt(II) complexes. According to previous findings,^{17,19-20} the mono-aqua complexes show all a proton transfer from the entered water molecule to the close oxygen of the ligand (O_L). Actually, the hydroxo complexes are accessible at physiological pH and temperature, even if in the vicinity of macromolecules the local pH could be influenced, reflecting its effect on hydrolysis rates.^{28,29} In the intermediate structures, for all the compounds, the Guanine ring is oriented such as to allow the ammine ligand to act as hydrogen-bond donors to oxo group at C6 position and with the N7 atom of the ring interacting with the hydroxo ligand. The overall geometry of the transition states for the reaction with the purine bases is, in agreement with previous results for these type of associative substitution reactions, a trigonal bipyramid.^{17-20,30} A proton transfer between the O ligand and the hydroxo group is observed in each transition state geometry, allowing the release of the water molecule, better leaving group than the hydroxo one. In the penta-coordinated transition states, the Pt-N7 bond has started to form at distances of 2.592, 2.606 and 2.527 Å and the Pt-OH₂ bond is halfway broken at a distance of 2.370, 2.322 and 2.398 Å, for NedaPt, OxaliPt and CarboPt, respectively. All the TS structures are largely characterized by a hydrogen bond between the ammine ligands and the C6-oxo groups as well as by interactions between the leaving water molecules and the carboxylate groups of the Pt-coordinated O ligands. (Fig.2) As a result, a similar network of intermolecular bonds governs the energetic of these reactions.

Nevertheless, it is possible to observe that such interactions are stronger in the CarboPt transition state, as observable by the shorter distances between the G-C6 oxo group and the ammine as well as between the leaving water molecule and the O ligand. Therefore, the lower activation barrier found for the G-platination process by CarboPt (Fig.1a) is a direct consequence of the more favourable network of hydrogen-bonds that takes place in the transition state geometry. The intermolecular forces are then implicated to impose a kinetic control on the platination processes. The adducts are then obtained with the complete loss of the water molecule and with the coordinated Guanine still interacting by its C6-oxo group with the ammine ligand.

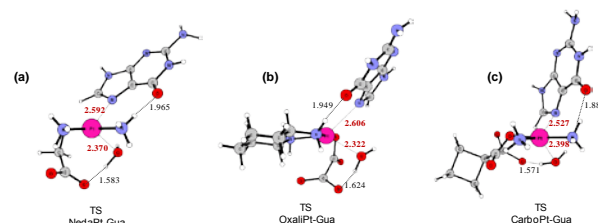


Figure 2. Transition states structures for the Guanine platination process using mono-aqua complexes.

Common mechanistic details were found in the reactions of the Pt(II) complexes with Adenine base. Actually, given the similarity of the N7 binding site in both bases, it is difficult to imagine a fundamentally different Pt-binding mechanism. The platination of Adenine proceeds through the formation of the classical pentacoordinated transition state in which the entering purine base and the leaving water molecule show from the metal centre, similar distances found in the case of G-platination process. Only slightly differences in the intermolecular forces governing the interactions between the Pt moiety with the nucleobases were observed. The weaker interactions have been previously suggested to be the reason of the observed preference of Guanine over Adenine as a target for platination.³⁰ Actually, in the case of Adenine, due to the less hydrogen-bond acceptor nature of the amino group at the C6 position of the Adenine ring compared to the C6-oxo-group of the Guanine, we found that the interactions with the ammine ligand are significantly weaker as reflected in a pronounced longer distances between them (SI). Nevertheless, a concurrent H-bond between the amino group at the C6 position with the water molecule is observed in those structures. The NH₂ group of the Adenine has then the possibility to act also as weak hydrogen-bond donor, as already suggested.³⁰ As it can be deduced from the potential energy profiles in Fig.1, we observed that the monofunctional binding of the second and third generation anticancer drugs to Guanine is privileged in a competitive reaction with Adenine site. Nevertheless, a significant difference in the activation energy barriers between G and A platination processes takes place only in the case of CarboPt, while for the other compounds the reaction with Adenine is also feasible.

The comparison between the kinetic barriers for the platination of both the purine bases obtained in this work and those previously found concerning the formation of the mono-aquated

Carboplatin,²⁰ Oxaliplatin,¹⁹ and Nedaplatin¹⁷ complexes, allow us to provide insight into the kinetics governing the whole process employed by these Pt(II) drugs to reach their final target. It should be noticed that the activation barrier is defined as the difference between the energy of the transition state (TS) and the energy of separated reactants, since it is generally accepted that second-shell adducts (INT) could be correctly considered as reference state of the intrinsic reaction coordinate in vacuo but it is artifacts in aqueous solution.^{31,32} From our data emerge that both *G* and *A* purine bases coordination processes are faster than the hydrolysis reactions, in neutral condition. This finding confirms the general trend observed for the other platinum containing anticancer drugs, for which the formation of the aqua-complex is the rate limiting step of the process. (Fig.3)

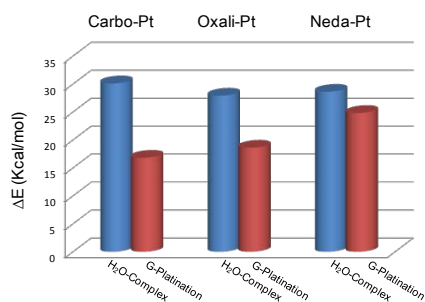


Figure 3. Comparison between calculated activation energies for hydrolysis and G-platination processes of Carboplatin, Oxaliplatin, and Nedaplatin in neutral condition.

It's interesting to notice that Carbo-Pt shows the slowest hydrolysis rate among the cisplatin-like compounds but, at the same time, the formation of the CarboPt-Guanine adduct proceeds significantly faster than the other adducts. This chemical behavior could explicate the high activity of carboplatin compound.

The monofunctional binding to Guanine and Adenine by mono-hydrated complexes in acid solution was also investigated in this work. In such condition, the cyclobutane dicarboxylate, oxalate, and glycolate groups results protonated. Our previously results concerning the hydrolysis processes showed that acidification of the solution increases the rate of the reactions.¹⁷⁻²⁰ In analogy to that findings, also *G* and *A* platination processes were found to proceed faster at lower pH. From geometric point of view (See Figure S3 and S4), in acid condition we observe a stronger network of H-bonds between the Pt moiety and the purine bases, probably responsible of the lower activation barriers (Fig.4). The dominating preference for *G* purine base is observable also in such conditions, and again it seems to be a completely hydrogen-bonds process. The rate of Guanine-platination processes is confirmed to be improved in the case of Carbo-Pt.

The possibility that the diaqua complex acts as platination agent was also explored in our investigation. Nevertheless, it should be noticed that the fully hydrolyzed complexes in the case of NedaPt and CarboPt are equivalent to the diaquated form of cisplatin, previously investigated from both experimentally³³ and theoretical point of view.³⁰

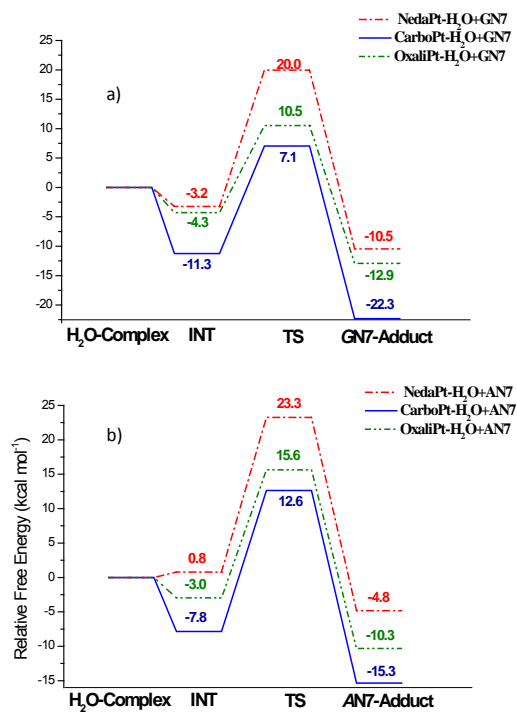


Figure 4. Overposition of the computed relative free energies profiles (at 298.15 K), for the reactions of mono-hydrated NedaPt, OxaliPt, CarboPt with a) N7-Guanine and b) N7-Adenine purine bases, in acid conditions.

It is evident that for these complexes only the hydrolysis process could be involved to explicate the differences in the biological activity, since in their hydrolyzed forms CarboPt, NedaPt and CisPt complexes give rise to the same active species. On the contrary, in the case of oxaliplatin, the structure of the diaquated complex is different due to the presence of the diaminocyclohexane as carrier ligand in place of ammonia ones. Actually, oxaliplatin is the only cisplatin analogue showing significant biological difference in spectrum of activity. This phenomenon could then be a consequence of steric and chemical different properties of DNA lesions. The potential energy profiles for the monofunctional binding to Guanine and Adenine base using oxaliPt diaqua complex as reactant, are reported in Fig.5. The optimized structures of the stationary points along the paths and key geometrical parameters are reported in the SI section. As it can be observed from the energetic profiles, (Fig. 5) the platination of both purine bases is favoured in the case of fully hydrated complex, confirming our previous indications on the active species able to reach DNA target.^{17,19-20} Moreover, according to our calculation, a higher selectivity for Guanine base is observed in such case, in analogy with previous findings on cisplatin drug.³⁰ Actually, the comparison between the energetic profiles reported in Fig.5, reveals that the Guanine coordination process proceed significantly faster than the Adenine binding. In addition, there is also a thermodynamic preference for Guanine platination when the diaqua Pt-complex is the active agent. Nevertheless, from our data concerning the fully hydrolyzed form of oxaliplatin, emerge that the binding to Adenine site, although not preferred over Guanine and considerably slower, could also be observable at standard conditions if the diaqua complex is the

only active reagent. Therefore, oxaliplatin seems to have a different behaviour compared with the $[\text{Pt}(\text{NH}_3)_2(\text{H}_2\text{O})_2]^{2+}$ active species, for which it was found that the Adenine binding is highly disfavored.³⁰

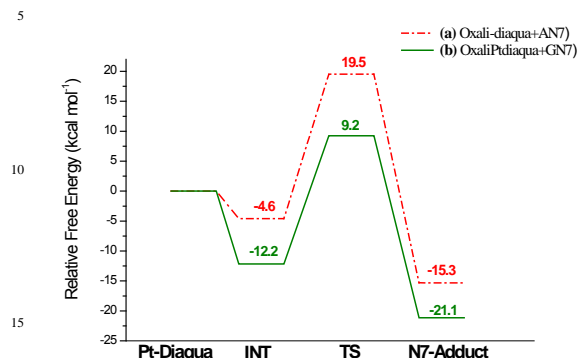


Figure 4. Overposition of the computed relative free energies profiles (at 298.15 K), for the reactions of fully-hydrated OxaliPt with (a) N7-Guanine and (b) N7-Adenine purine bases.

From geometric point of view, the intermolecular forces governing the energetics are not equivalent to those for the mono-aqua species. In these cases, there is a preference for the water ligand on Pt to act as the H-bond donor toward both the oxo and amino groups at the C6 position. Moreover, the short distances between the hydrogen-donors and hydrogen-acceptor groups in the molecules, indicate strong interactions between them, leading to a greater stabilization of all the stationary points (See Figure S5). The other possible hydrogen-bond patterns involving the ammine-hydrogen of diaqua complexes and the O=C6 as well as H₂N=C6 moieties of Guanine and Adenine respectively, were also considered. In such cases we found that the transition states lie at higher energy values, confirming previous indications on cisplatin.³⁰ (See Figure S6).

In summary, the binding mechanism of second- and third-generation anticancer drugs with Guanine (G) and Adenine (A) DNA bases, in both neutral and acidic conditions has been investigated by using Density Functional Theory (DFT) combined with the conductor-like dielectric continuum model (CPCM) approach. This work allowed us to make a direct comparison between the rate of formation of the mono-functional adducts of these compounds and spotlight common or different behaviour. The Guanine as a target for platination process is confirmed to be preferred over Adenine for all the investigated compounds. The dominating preference for G purine base is a completely hydrogen-bonds process, confirming that H-bonds are important to impose both structural and kinetic control on the purine platination processes. The lowest activation barrier for G-platination process was found for CarboPt, in both environments and seems to be a direct consequence of the more favourable network of hydrogen-bonds that takes place in the transition state geometry.

From our data concerning G- and A- platination by the double-hydrated form of oxaliplatin, result that the binding to Adenine site, although considerably slower, could also be observable at standard conditions, in contrast to previous findings on $[\text{Pt}(\text{NH}_3)_2(\text{H}_2\text{O})_2]^{2+}$ active species.

The Università della Calabria and the MIUR PRIN 2008 are gratefully acknowledged.

Notes and references

^a Dipartimento di Chimica, Università della Calabria, 87036 Arcavacata di Rende (CS), Italy. Email: nrusso@unical.it

† Electronic Supplementary Information (ESI) available: Computational details, Optimized structures, NBO analysis, Homo-Lumo MOs plots.

- Rosenberg, B.; Camp, L.; Trosko, J.; Mansour, V. H. *Nature* 1969, 222, 385.
- Rosenberg, B.; Camp, L.; Krigas, T. *Nature* 1965, 205, 698.
- P. J. Loehrer and L. H. Einhorn, *Ann. Intern. Med.*, 1984, 100, 704.
- H. M. Keys, B. N. Bundy, F. B. Stehman, L. I. Muderspach, W. E. Chafe, C. L. Suggs III, J. L. Walker and D. Gersell, *N. Engl. J. Med.*, 1999, 340, 1154.
- M. Morris, P. J. Eifel, J. Lu, P. W. Grigsby, C. Levenback, R. E. Stevens, M. Rotman, D. M. Gershenson and D. G. Mutch, *N. Engl. J. Med.*, 1999, 340, 1137.
- Bokemeyer, C.; Berger, C.; Kynast, B.; Schmoll, H.-J.; Poliwooda, H. *Eur. J. Cancer* 1993, 29, S241
- Cornelison, T. L.; Reed, E. *Gynecol. Oncol.* 1993, 50, 147.
- M. Kartalou and J. M. Essigmann, *Mutat. Res.*, 2001, 478, 23.
- Raymond, E.; Chaney, S. G.; Taamma, A.; Cvitkovic, E. *Ann. Oncol.* 1998, 9, 1053.
- Spingler, B.; Whittington, D. A.; Lippard, S. J. *Inorg. Chem.* 2001, 40, 5596.
- Wagstaff, A. J.; Ward, A.; Benfield, P.; Heel, R. C. *Drugs* 1989, 37, 162.
- Teuben, J. M.; Bauer, C.; Wang, A. H. J.; Reedijk, J. *Biochemistry* 1999, 38, 12305.
- Piccart, M. J.; Lamb, H.; Vermorken, J. B. *Ann. Oncol.* 2001, 12, 1195.
- Bancroft, D. P.; Lepre, C. A.; Lippard, S. J. *J. Am. Chem. Soc.* 1990, 112, 6860.
- Sherman, S. E.; Lippard, S. J. *Chem. Rev.* 1987, 87, 1153.
- [16] Mello, J. A.; Lippard, S. J.; Essigmann, J. M. *Biochemistry* 1995, 34, 14783.
- Alberto, M.E., Lucas, M.F., Pavelka, M., Russo, N. *J. Phys. Chem. B*, 2009, 113, 14473.
- Alberto, M.E., Lucas, M.F., Pavelka, M., Russo, N. *J. Phys. Chem. B*, 2008, 112, 10765.
- Lucas, M.F., Pavelka, M., Alberto, M.E.; Russo, N. *J. Phys. Chem. B*, 2009, 113, 831.
- Pavelka, M., Lucas, M.F., Russo, N. *Chem. Eur. J.* 2007, 13, 10108.
- Frisch, M. J.; Trucks, G. W.; Schlegel, H. B.; Scuseria, G. E.; Robb, M. A.; Cheeseman, J. R.; Montgomery, J. A.; Vreven, J., T.; Kudin, K. N.; Burant, J. C.; Millam, J. M.; Iyengar, S. S.; Tomasi, J.; Barone, V.; Mennucci, B.; Cossi, M.; Scalmani, G.; Rega, N.; Petersson, G. A.; Nakatsuji, H.; Hada, M.; Ehara, M.; Toyota, K.; Fukuda, R.; Hasegawa, J.; Ishida, M.; Nakajima, T.; Honda, Y.; Kitao, O.; Nakai, H.; Klene, M.; Knox, X. L., J. E.; Hratchian, H. P.; Cross, J. B.; Adamo, C.; Jaramillo, J.; Gomperts, R.; Stratmann, R. E.; Yazyev, O.; Austin, A. J.; Cammi, R.; Pomelli, C.; Ochterski, J. W.; Ayala, P. Y.; Morokuma, K.; Voth, G. A.; Salvador, P.; Dannenberg, J. J.; Zakrzewski, V. G.; Dapprich, S.; Daniels, A. D.; Strain, M. C.; Farkas, O.; Malick, D. K.; Rabuck, A. D.; Raghavachari, K.; Foresman, J. B.; Ortiz, J. V.; Cui, Q.; Baboul, A. G.; Clifford, S.; Cioslowski, J.; Stefanov, B. B.; Liu, H.; Liashenko, A.; Piskorz, P.; Komaromi, I.; Martin, R. L.; Fox, D. J.; Keith, T.; Al-Laham, M. A.; Peng, C. Y.; Nanayakkara, A.; Challacombe, M.; Gill, P. M. W.; Johnson, B.; Chen, W.; Wong, M. W.; Gonzalez, C.; Pople, J. A. *Gaussian 03, Revision A.1*; Gaussian, Inc.: Pittsburgh PA, 2003.
- Becke, A. D.; *J. Chem. Phys.* 1993, 98, 5648.
- Lee, C. T.; Yang, W. T.; Parr, R. G. *Phys. Rev. B* 1988, 37, 785.

-
- 24 Andrae, D.; Haussermann, U.; Dolg, M.; Stoll, H.; Preuss, H. *Theor. Chim. Acta* 1990, 77, 123.
- 25 Burda, J. V.; Zeizinger, M.; Sponer, J.; Leszczynski, J. *J. Chem. Phys.* 2000, 113, 2224.
- 5 26 (a) Klamt, A.; Schüürmann, G. *J. Chem. Soc., Perkin Trans. 2* 1993, 799. (b) Andzelm, J.; Kölmel, C.; Klamt, A. *J. Chem. Phys.* 1995, 103, 9312. (c) Barone, V.; Cossi, M. *J. Phys. Chem. A* 1998, 102, 1995-2001. (d) Cossi, M.; Rega, N.; Scalmani, G.; Barone, V.; *J. Comput. Chem.* 2003, 24, 669.
- 10 27 Klamt, A.; Jonas, V.; Burger, T.; Lohrenz, J. C.W. *J. Phys. Chem. A*, 1998, 102, 5074.
- 28 Lamm, G.; Pack, G. R. *Proc. Natl. Acad. Sci. U.S.A.* 1990, 87, 9033.
- 29 Vinje, J.; Sletten, E.; Kozelka, J. *Chem. Eur. J.* 2005, 11, 3863.
- 15 30 Baik M. H.; Friesner R. A.; Lippard, S. J. *J. Am. Chem. Soc.* 2003, 125, 14082.
- 31 Deubel, D. V.; *J. Am. Chem. Soc.*, 2006, 128, 1654.
- 32 Lau, J.K.-C.; Deubel, D. V.; *J. Chem. Theory Comput.*, 2006, 2, 103.
- 20 33 Arpalahiti, J.; Lippert, B. *Inorg. Chem.* 1990, 29, 104.

Supporting Information

Which one among the Pt-containing anticancer drugs forms more easily monoadducts with G and A DNA bases? A comparative study between oxaliplatin, nedaplatin and carboplatin

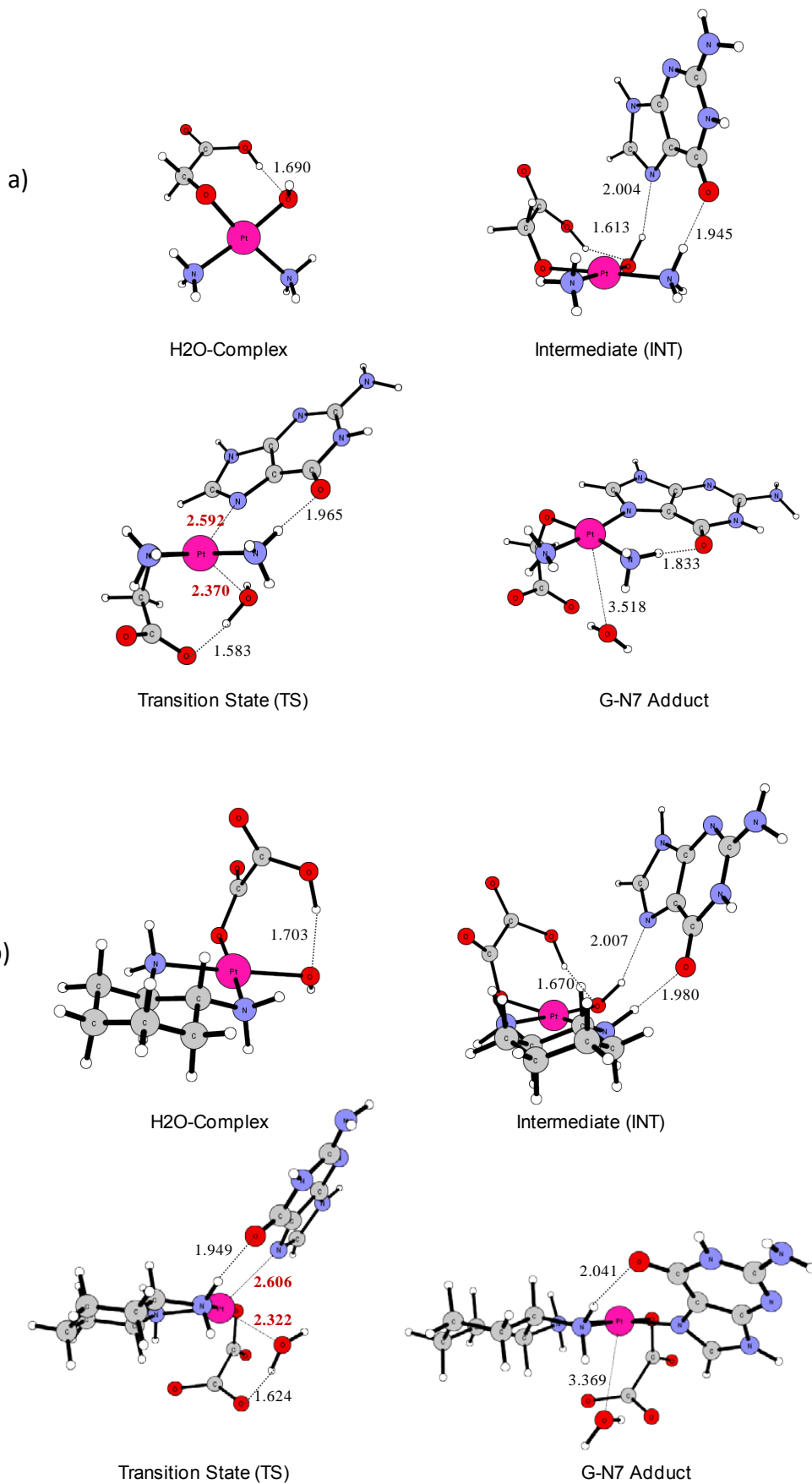
*Marta E. Alberto, Valeria Butera and Nino Russo **

Dipartimento di Chimica, Università della Calabria, 87036 Arcavacata di Rende (CS), Italy

- Optimized structures and selected geometric parameters of the stationary points for the binding of Guanine base to a) NedaPt, b) OxaliPt, c) CarboPt mono-hydrated complexes in neutral condition; **-S1-**
- Optimized structures and selected geometric parameters of the stationary points for the binding of Adenine base to a) NedaPt, b) OxaliPt, c) CarboPt mono-hydrated complexes in neutral condition; **-S2-**
- Optimized structures and selected geometric parameters of the stationary points for the binding of Guanine base to a) NedaPt, b) OxaliPt, c) CarboPt mono-hydrated complexes in acid condition; **-S3-**
- Optimized structures and selected geometric parameters of the stationary points for the binding of Adenine base to a) NedaPt, b) OxaliPt, c) CarboPt mono-hydrated complexes in acid condition; **-S4-**
- Optimized structures and selected geometric parameters of the stationary points for the binding of a) Guanine, b) Adenine bases to OxaliPt diaqua complex; **-S5-**
- Optimized structures and potential energy profiles for the platination of a) Guanine, b) Adenine by OxaliPt diaqua complex considering the other possible H-bond patterns. **-S6-**

Figure -S1-

Optimized structures and selected geometric parameters of the stationary points for the binding of Guanine base to a) NedaPt, b) OxaliPt, c) CarboPt mono-hydrated complexes in neutral condition



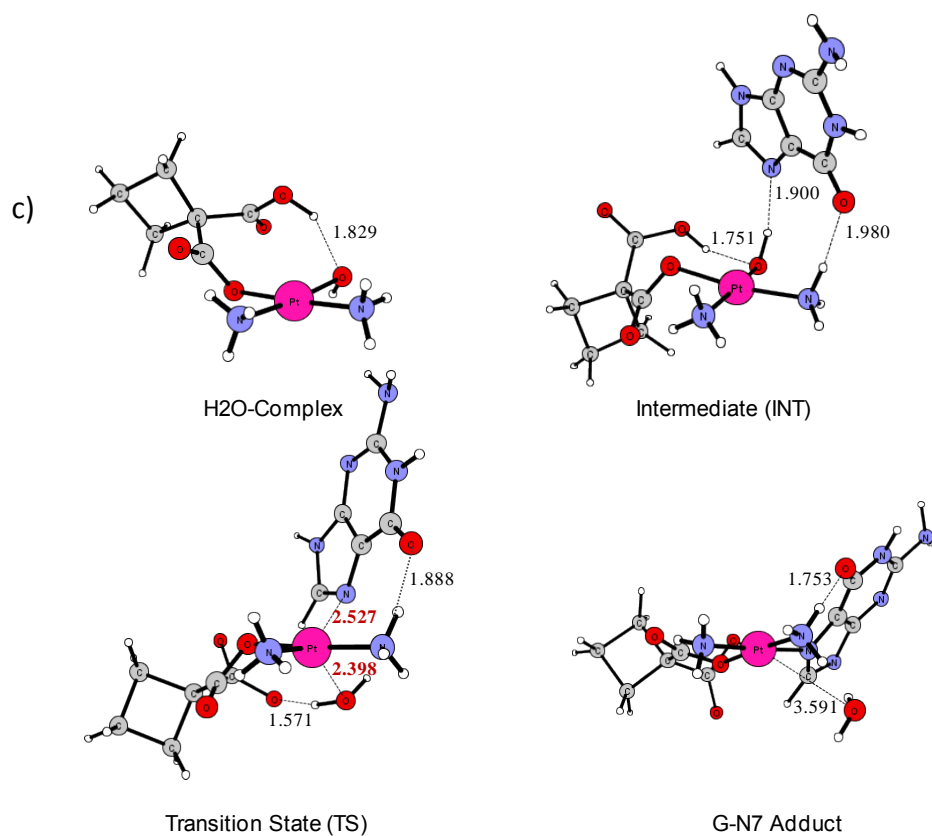
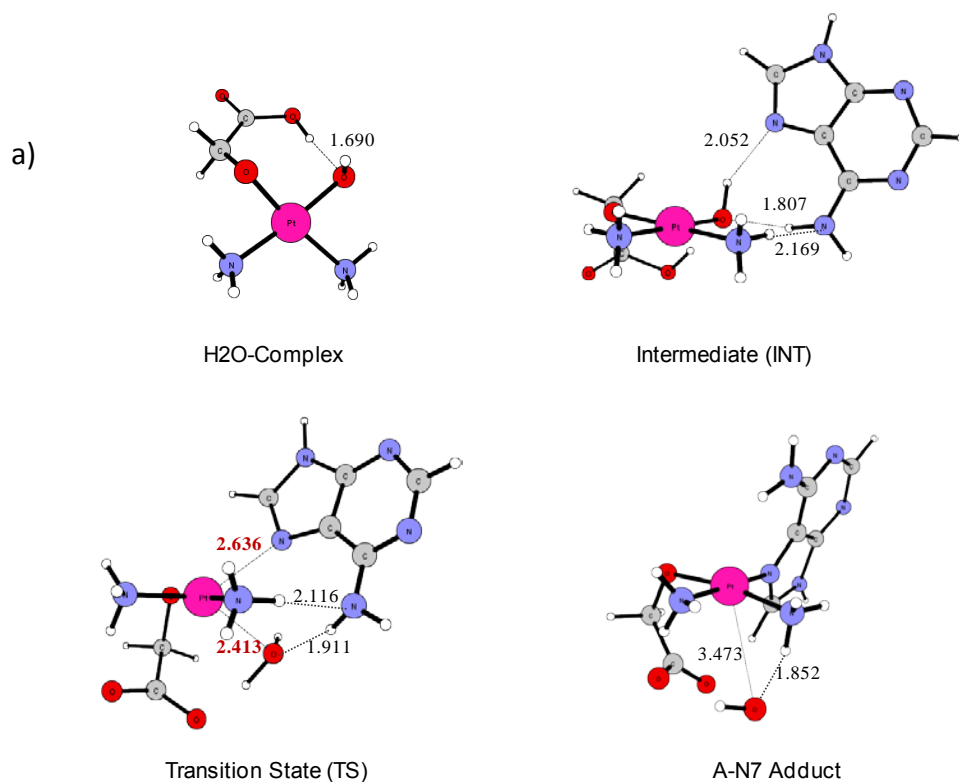
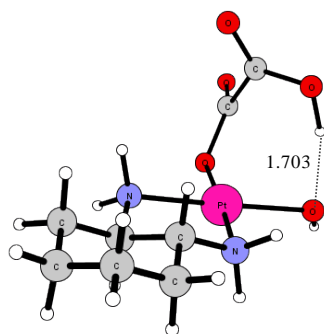


Figure -S2-

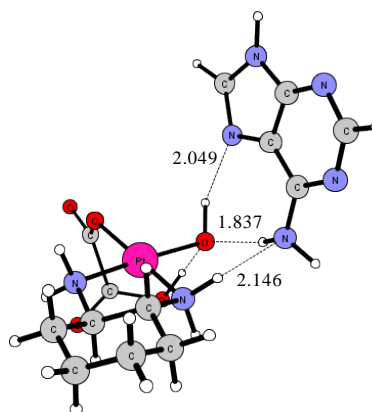
Optimized structures and selected geometric parameters of the stationary points for the binding of Adenine base to a) NedaPt, b) OxaliPt, c) CarboPt mono-hydrated complexes in neutral condition;



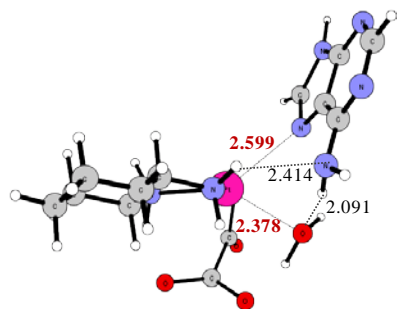
b)



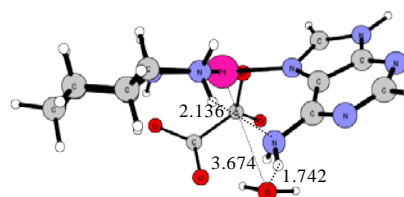
H2O-Complex



Intermediate (INT)

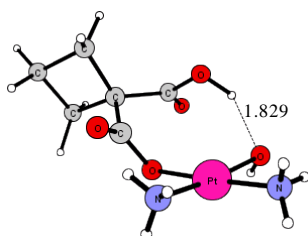


Transition State (TS)

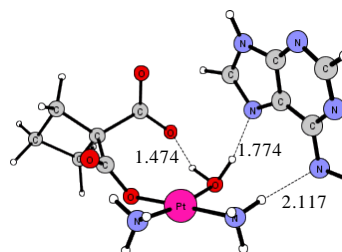


A-N7 Adduct

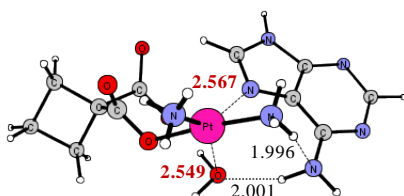
c)



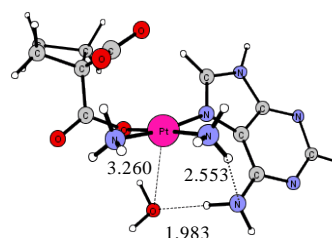
H2O-Complex



Intermediate (INT)



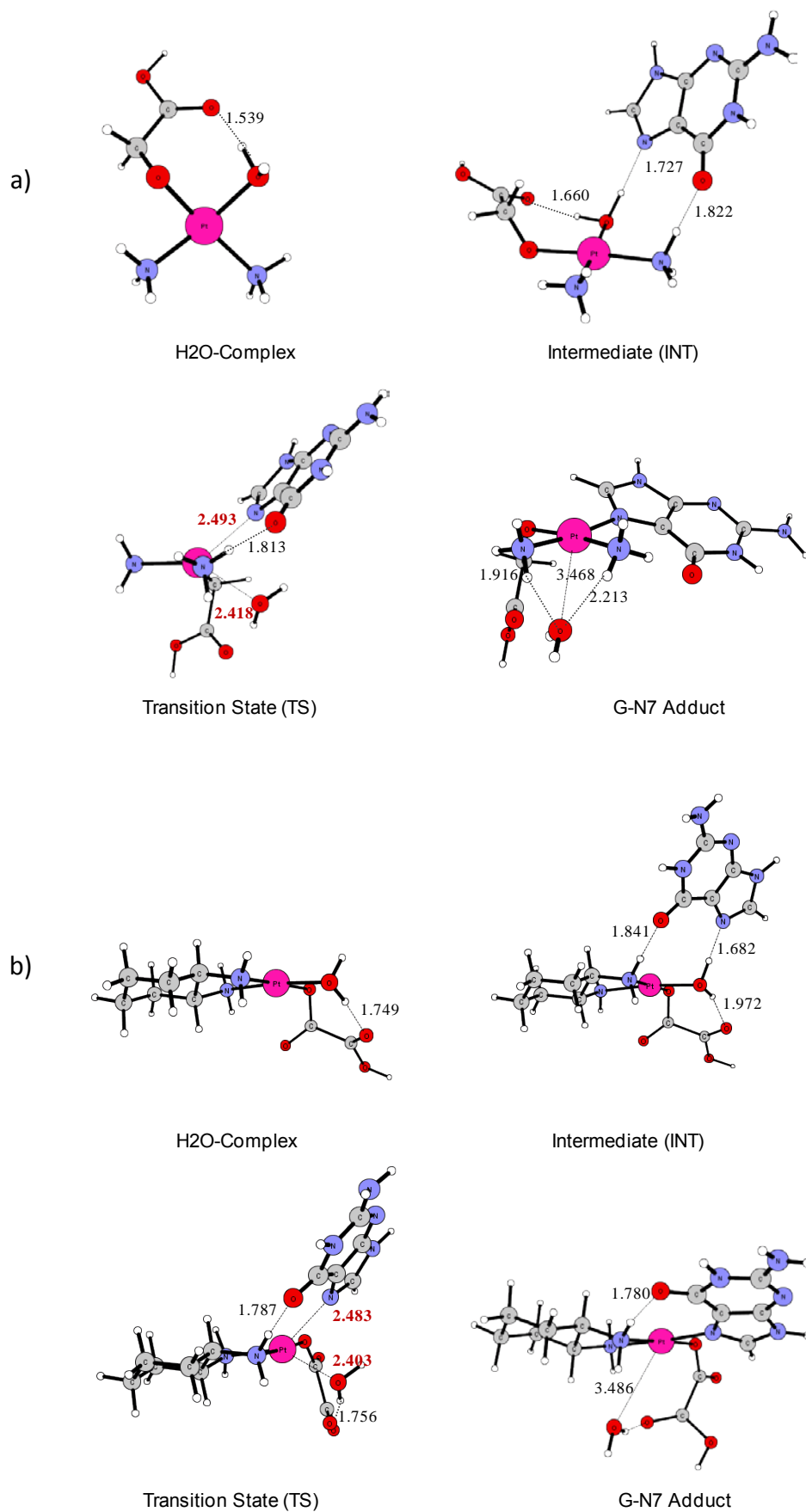
Transition State (TS)



A-N7 Adduct

Figure -S3-

Optimized structures and selected geometric parameters of the stationary points for the binding of Guanine base to a) NedaPt, b) OxaliPt, c) CarboPt mono-hydrated complexes in acid condition;



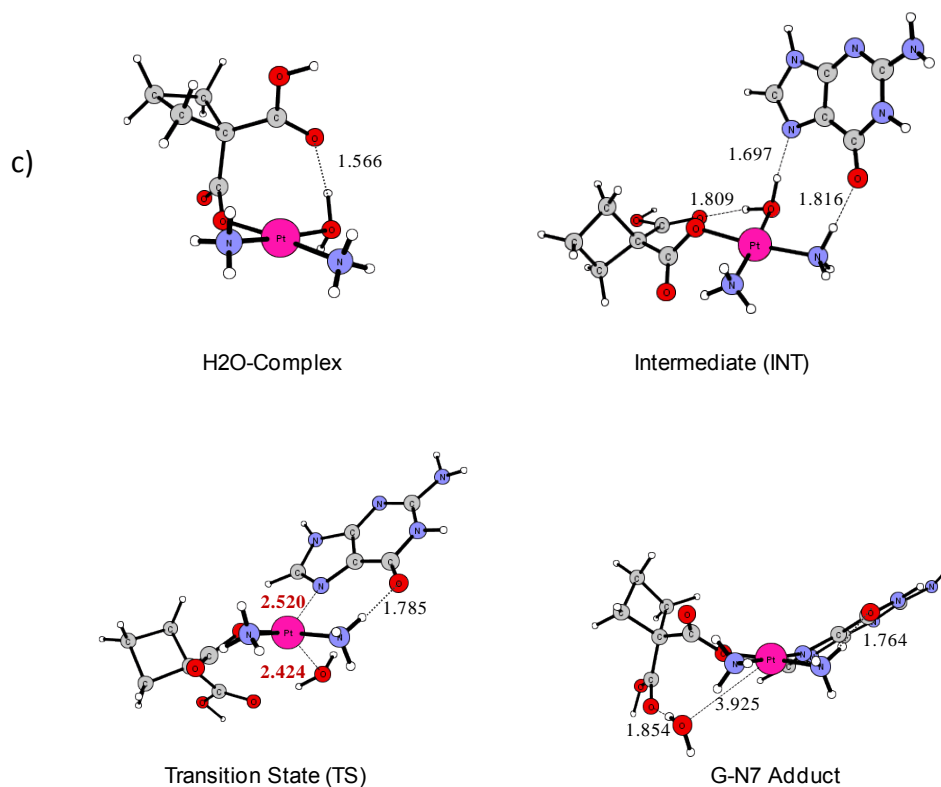
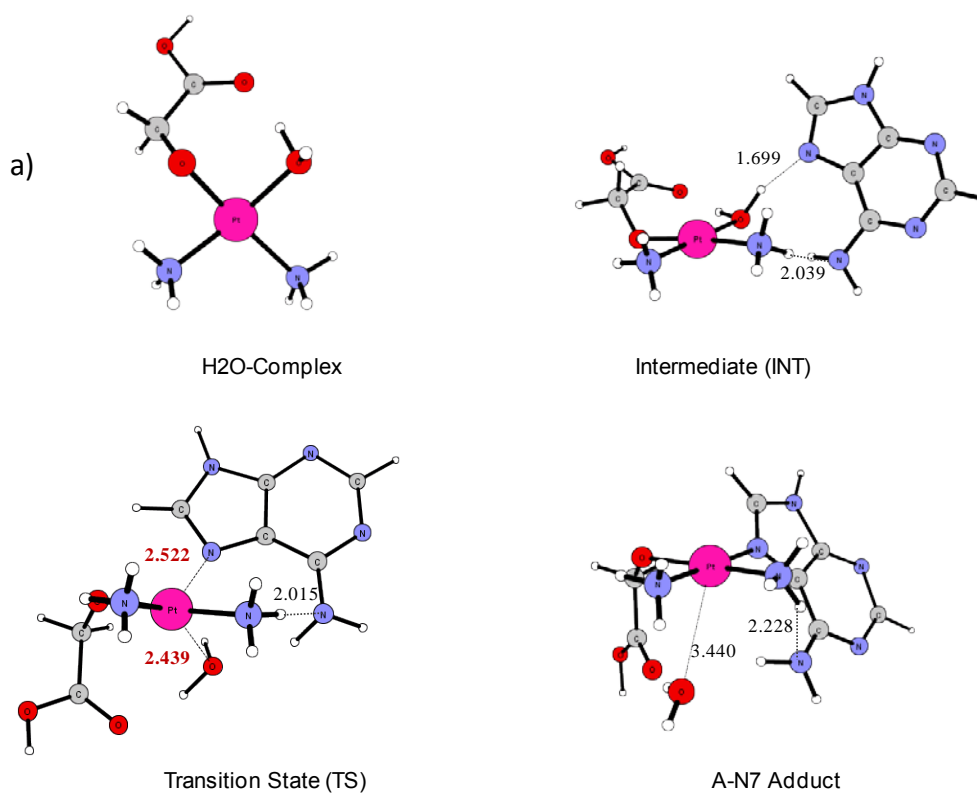
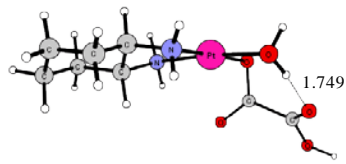


Figure -S4-

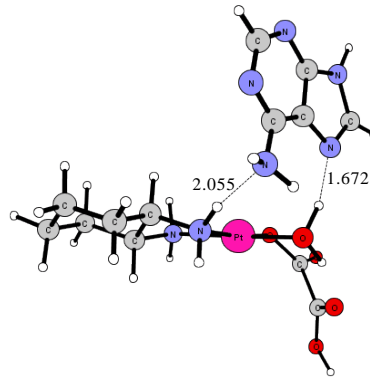
Optimized structures and selected geometric parameters of the stationary points for the binding of Adenine base to a) NedaPt, b) OxaliPt, c) CarboPt mono-hydrated complexes in acid condition;



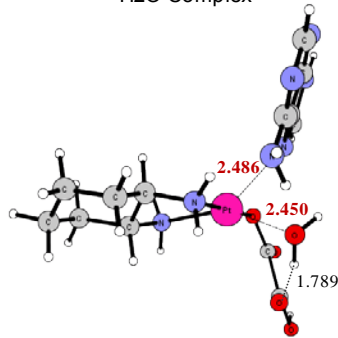
b)



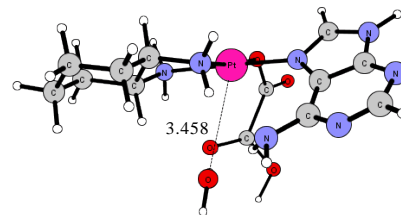
H2O-Complex



Intermediate (INT)

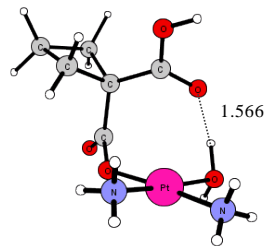


Transition State (TS)

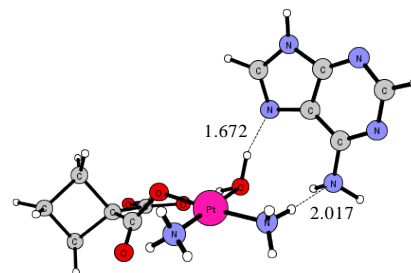


A-N7 Adduct

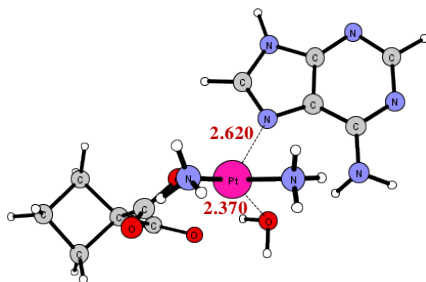
c)



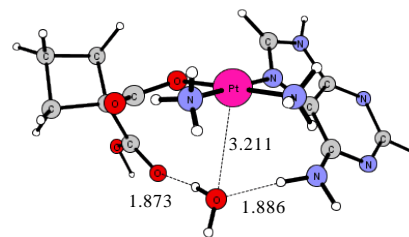
H2O-Complex



Intermediate (INT)



Transition State (TS)



A-N7 Adduct

Figure -S5-

Optimized structures and selected geometric parameters of the stationary points for the binding of
a) Guanine, b) Adenine bases OxaliPt diaqua complex

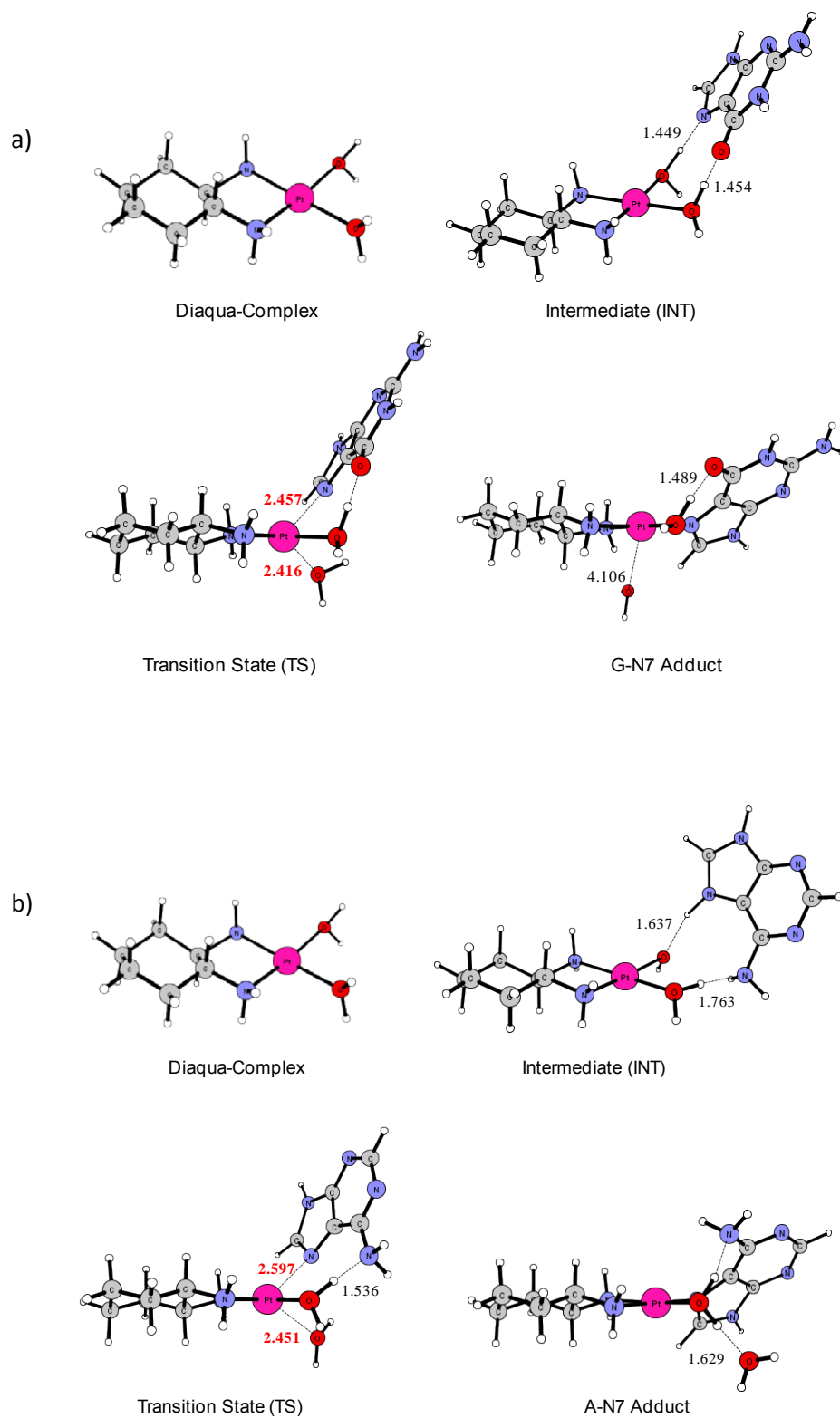
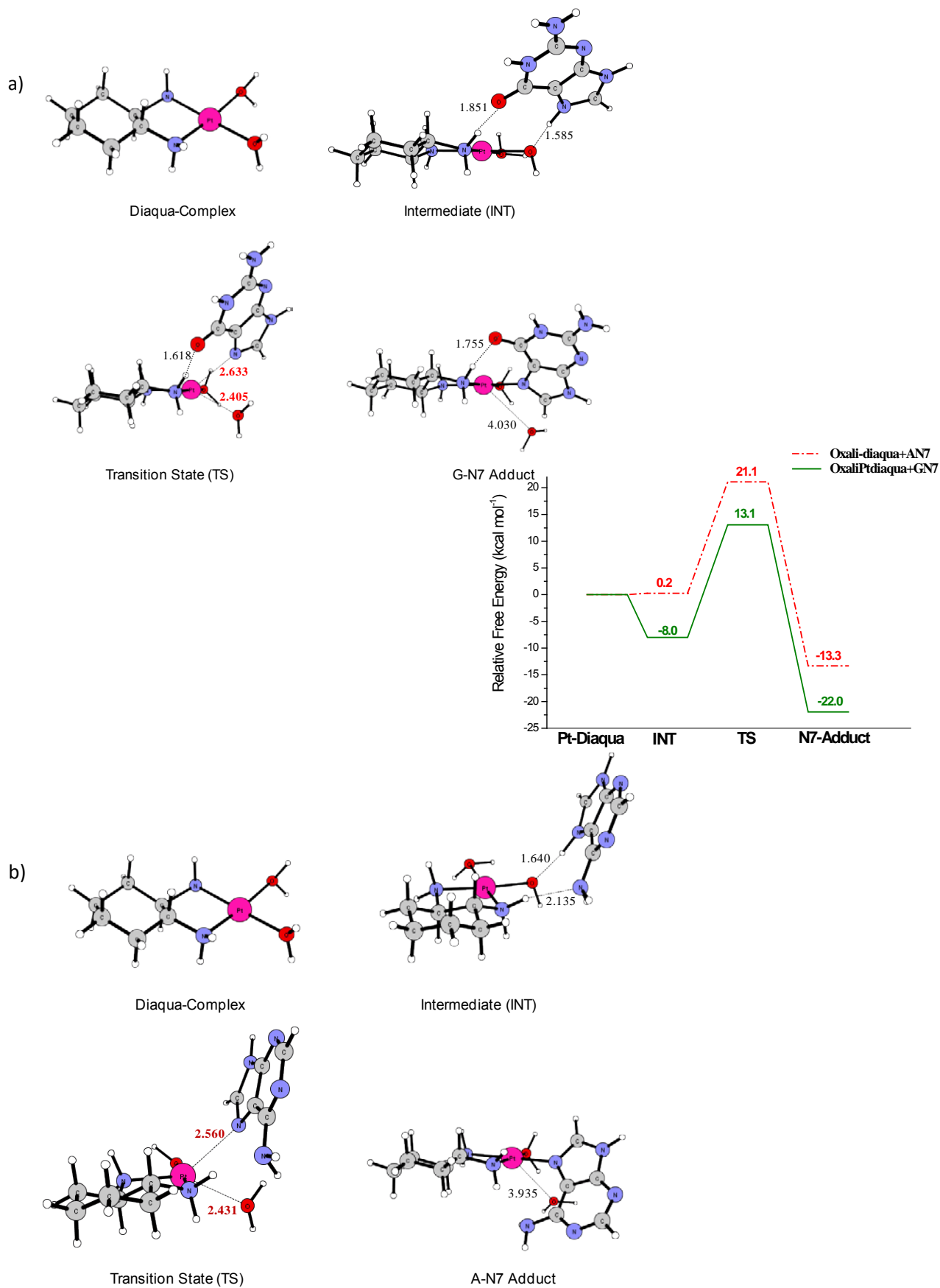


Figure –S6-

Optimized structures and potential energy profiles for the platination of a) Guanine, b) Adenine by OxaliPt diaqua complex considering the other possible H-bond patterns.;



Paper V

“Methionine ligand selectively promotes monofunctional adducts between *Trans-EE* platinum anticancer drug and guanine DNA base”

Marta E. Alberto and Nino Russo

Chem. Commun. 2010 DOI: 10.1039/c0cc03605f

Methionine ligand selectively promotes monofunctional adducts between *trans-EE* platinum anticancer drug and guanine DNA base†

Marta E. Alberto* and Nino Russo

Received 1st September 2010, Accepted 20th October 2010

DOI: 10.1039/c0cc03605f

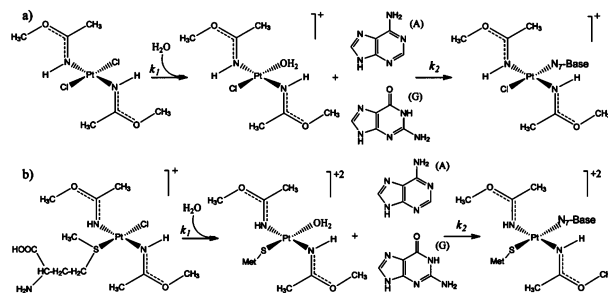
A detailed study on the reaction mechanism of *trans-EE* and *trans-EE*/Met Pt-containing anticancer drugs was carried out in order to rationalize the experimental kinetic data concerning the whole process leading to DNA platination.

From the early beginning, the antitumor activity of the world's best selling anticancer drug cisplatin (*cis*-DDP)¹ has been related with the possibility to produce bifunctional lesions on DNA and to form 1,2-intrastrand adducts with two adjacent purine bases.² It has been assumed that the clinical inactivity of the *trans*-DDP is correlated to the evidence that these kind of cross-links are stereochemically inaccessible to *trans* isomers, which on the contrary induces monoadducts that may be repaired or undergo further rearrangements, or forms interstrand cross-links between cytosine and guanine of double-stranded DNA not able to change the stability and structure of DNA markedly.³ Moreover, since *trans*-DDP is kinetically more reactive than the corresponding *cis* isomer, several undesired reactions on its way to the biological target take place contributing to the lack of pharmacological activity. As a result, the classical structure–activity relationship of platinum drugs stressed the necessity of the *cis* geometry identifying it as critical for activity. Nevertheless, in recent years several Pt(II) compounds with *trans* geometry have been shown to be endowed with antitumor activity against different tumor cells, including those resistant to *cis*-DDP thus violating the classical *cis* geometry paradigm.^{4,5} *trans*-[PtCl₂{*E*-HN=C(OCH₃)CH₃}₂] (*trans-EE*), among the investigated platinum complexes with iminoethers ligands, has shown the greatest *in vitro* toxicity. Due to its bulky ligands, *trans-EE* has been suggested to form monofunctional adducts at guanine residues, in contrast with those formed by cisplatin.⁶ Moreover a recent study shows that the platination rate of both guanosine monophosphate (GMP) and DNA are significantly improved by the presence of an *L*-methionine (Met) ligand bound to *trans-EE* (*trans-EE*/Met).⁷ Even if for *trans*-compounds the mechanism of action could be different from those with conventional *cis* geometry, also for these kinds of compounds the hydrolysis process is expected to play an important role in their activation before reaching DNA. Despite a limited structural modification, consisting in the substitution of one chloride with a methionine ligand, these two compounds seem to show a remarkably different chemical reactivity. Herein, the hydrolysis reaction processes as well as

the reactions with DNA bases (guanine (G) and adenine (A)) for both *trans-EE* and *trans-EE*/Met were investigated theoretically in the framework of the DFT/CPCM approach, in order to provide a better interpretation of the experimental kinetic data available in literature.⁷ Additional computational details are reported in ESI.† The latter values refer to the whole process of DNA platination by these compounds but don't give any indication of the specific step in which the methionine ligand promotes the reaction rate. To shed light on this aspect, the hydrolysis and bases platination processes were explored separately with the aim to characterize the step in which the methionine ligand plays its predominant role enhancing the velocity of the whole process and providing atomistic details concerning their mechanisms of action (Scheme 1).

It is widely accepted that the Pt(II) anticancer drugs undergo a hydrolysis process through second-order nucleophilic substitution (S_N2) reactions.^{8,9} In such a process, the equatorial plane of the five-coordinated TS structure plays an important role in determining the hydrolysis behaviour.⁸ As well as the other platinum(II) compounds,⁸ *trans-EE* and its derivative *trans-EE*/Met are believed to react with water molecules according to the same reaction mechanism. The computed relative free energy profiles for the hydrolysis reactions of *trans-EE* and *trans-EE*/Met are reported in Fig. 1, while the optimized structures for the stationary points located along the paths are illustrated in the ESI.†

The presence of the Met ligand enhances the hydrolysis rate of the *trans-EE* as it can be deduced from the activation barrier values reported in Fig. 1. The greater stabilization of the *trans-EE*/Met transition state arises from geometric and electronic factors. In the latter, the entering water molecule and the leaving chloride both lie at shorter distances from the metallic centre (2.330 and 2.792 Å, respectively) compared with the *trans-EE* TS₁ ones (2.474 and 2.870 Å). These geometric features promote a more compact transition state in the case of *trans-EE*/Met and allow the entering group to be better orientated to perform its attack (see ESI†).



Scheme 1 Investigated reaction paths for the formation of (a) *trans-EE* and (b) *trans-EE*/Met adducts with N7-guanine and N7-adenine.

Dipartimento di Chimica, Università della Calabria, 87036 Arcavacata di Rende (CS), Italy. E-mail: nrusso@unical.it

† Electronic supplementary information (ESI) available: Computational details, optimized structures, NBO analysis, HOMO–LUMO MOs plots. See DOI: 10.1039/c0cc03605f

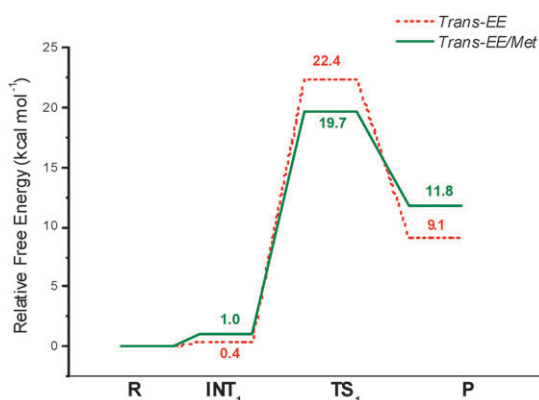


Fig. 1 Overposition of the computed relative free energy profiles (at 298.15 K), for the hydrolysis of *trans-EE* and *trans-EE*/Met in water phase.

The NBO charge on the oxygen atom and the Wiberg bond index with the Pt one (see ESI[†]) reveal that a sort of donor–acceptor interaction may take place in the *trans-EE*/Met transition state compared with the *trans-EE* one, in which a more negative NBO charge on the water-O atom and a smaller value of the Wiberg bond index between it and Pt metal were found. These effects may contribute to the overall stabilization. Furthermore, the NBO charge on the leaving chloride ion and the MO bond order between it and Pt show that the chloride ion still interacts with the metallic centre in *trans-EE*/Met TS₁, as observable also from HOMO molecular orbital plots reported in the ESI.[†] Such interaction could be involved in the stabilization of the pentacoordinated structure of the *trans-EE*/Met transition state determining the decrease of the activation energy. Interestingly, according to our calculations, the formation of the *trans-EE* aqua complex requires an amount of energy close to that demanded by *cis*-DDP,¹⁰ in agreement with experimental evidence proposed in previous studies.¹¹ This evidence, together with the high cytotoxicity showed by this *trans*-compound against several tumor cells, supports the strategy of the introduction of sterically demanding carrier ligands to reduce the rate of replacement of the chloro ligands leading to the suggestion that the difference in antitumor activity between *cis* and *trans* isomers is due to kinetic effects.¹² The calculated activation energy barrier corresponding to the first solvolysis step of *trans-EE* compound found in our work (22.44 kcal mol⁻¹) is in good agreement with that obtained from the experimental rate constant given in the previous work ($2.103 \times 10^{-4} \text{ s}^{-1}$). By using the conventional transition-state theory (TST)^{13–15} according to the Eyring equation, it's possible to connect the kinetic data (*k*) with the free energy of reaction obtaining for the mentioned process a value of 22.49 kcal mol⁻¹, very close to our result. No direct measurement of the rate constant for the hydrolysis process has been given in literature for *trans-EE*/Met, nevertheless a recent study⁷ provided kinetic data relative to the whole process that leads to GMP platination by *trans-EE*/AcMet ($8.1 \times 10^{-3} \text{ s}^{-1}$). That value should be attributable to the rate limiting step of the process, but the knowledge of which one of the steps is the RDS of the reaction is still lacking. By using the same procedure adopted in the case of *trans-EE*, we can convert the kinetic constant value to the free energy of

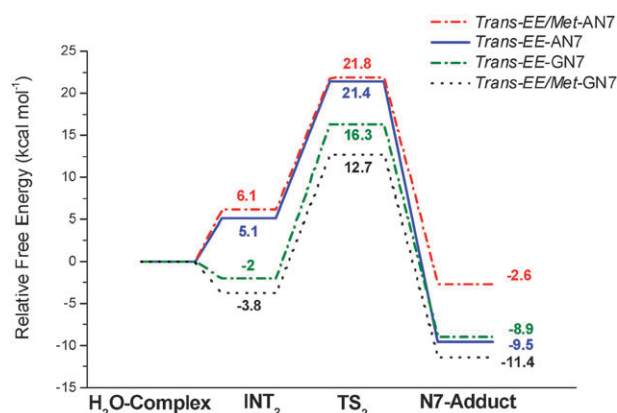


Fig. 2 Overposition of the computed relative free energy profiles (at 298.15 K), for the reaction of *trans-EE* and *trans-EE*/Met with N7-guanine (GN7) and N7-adenine (AN7).

reaction obtaining 20.33 kcal mol⁻¹. From our calculation, emerges that the hydrolysis process requires 19.7 kcal mol⁻¹ to occur. Our data are close to the experimental result, underestimating it by just 0.58 kcal mol⁻¹. We can hypothesize that the experimental value refers to the solvolysis process.

In order to provide further mechanistic insight into the whole process leading to the formation of adducts, the reactions of the mono-hydrated *trans-EE* and *trans-EE*/Met with G and A purine bases were investigated. From our data emerges that the platination rate of guanine residue through N7 binding site is significantly enhanced by the presence of the methionine ligand (Fig. 2). In addition, the formation of the adduct with that purine base is obtained exothermically with an energy gain of 11.4 kcal mol⁻¹. For both the reactants, the guanine coordination process is faster than the hydrolysis reaction, confirming the general trend observed for the other platinum containing anticancer drugs, for which the formation of the aqua-complex is the rate limiting step of the process.

The optimized structures of the stationary points for the binding of guanine base to *trans-EE* and *trans-EE*/Met compound are reported in the ESI.[†] The *trans-EE*/Met structures are characterized by stronger interactions with the purine base, leading to a significant stabilization of all the stationary points located along the reaction energy paths. The lower activation barrier observed in the case of *trans-EE*/Met–GN7 reaction arises from a significant H-bond between the hydrogen of the leaving water ligand and the C6-oxo group of the G fragment (1.651 Å) as well as with the methionine moiety (2.098 Å). In the *trans-EE* transition state structure (see ESI[†]), the latter interaction is obviously lacking and the H-bond between water and the C6-oxo group, although still conserved, is found at a longer distance. The *trans-EE*/Met–Gua adduct is then obtained exothermically and its structural stabilization is promoted also in this case by H-bonds between the water molecule and both G–C6-oxo and methionine amino groups. Then, our calculation suggests that the hydrogen bonds are implicated to impose both structural and kinetic control on the purine platination process. From the electronic point of view, NBO analysis shows that in the *trans-EE*/Met TS₁, the energy of the lone-pair at N7 position of the purine ring is lower compared with the *trans-EE* one suggesting that a stronger donor–acceptor

interaction between guanine and the S-containing Pt-complex may be involved in the stabilization of such a transition state. Moreover, the isosurface plots reveal that in the *trans-EE*/Met pentacoordinated TS structure, the guanine N7 lone pair character is the dominating feature of this MO while in *trans-EE* one the N7 lone-pair, although present, is a minor component. The probable lower donor ability may be responsible for the higher energy of the *trans-EE* transition state. Further details are given in the ESI.† Interestingly, the presence of the methionine ligand does not promote the platination of the adenine residue, as observable from the energetic profiles reported in Fig. 2. In that case, the activation barriers for *trans-EE* and *trans-EE*/Met are comparable, suggesting that the substitution of one chloride with Met does not affect the rate of the process, leaving it almost unchanged. Such a result is interesting since it not only shows that the G-N7 is the favourite coordination site for both compounds but also that the S-containing ligand enhances the platination rate only in the case of the specific DNA purine base. Actually our calculation clearly suggests that the A platination by these compounds is not privileged in a competitive reaction with G sites although the reaction with it is also feasible. This effect can be rationalized from the geometric point of view. The lack of strong hydrogen-bonds in the structures containing adenine is responsible for the higher activation barriers. The optimized structures of the stationary points for the binding of adenine base to *trans-EE* and *trans-EE*/Met compounds are reported in the ESI.† When adenine approaches the platinum centre of both *trans-EE* and *trans-EE*/Met, only a weak hydrogen bond forms between the water ligand and the H₂N-C6 group of adenine. As expected, the amino group is much less a hydrogen-bond acceptor than the oxo-group of the guanine ring, and the formation of the intermediate complexes is then energetically not favorable. Both the INT₁ complexes lie above the separated reactants at 5.1 kcal mol⁻¹ and 6.1 kcal mol⁻¹ for *trans-EE* and *trans-EE*/Met, respectively (Fig. 2). The transition states are characterized by the familiar trigonal-bipyramidal structural motif but no significant hydrogen bonds have been formed in such a case, determining the increase of the activation energies compared with those obtained in the case of the guanine ring. Moreover, the indication that the adenine platination process is not favored gives evidence that the dominating preference for the guanine base is controlled by hydrogen-bonds.

In summary, from our calculations it emerges that the presence of the methionine ligand enhances the hydrolysis process mostly by stabilizing the pentacoordinated structure of the transition state. Such stabilization arises from geometric and electronic factors. The activation barrier found for the *trans-EE* chloride substitution is in good agreement with experimental kinetic data. Concerning *trans-EE*/Met, only a global rate constant is available in the literature and does not give any indication about the step that it is referred to. Our results clearly show that the experimental value is attributable to the hydrolysis process underestimating the activation

barrier derived from the exp. kinetic constant by just 0.58 kcal mol⁻¹. The hydrolysis reaction is confirmed to be the rate determining step of the whole process. The preference for the GN7 platination by *trans-EE*/Met is dominated by the possibility to establish H-bond interactions which play then an important role in determining the hydrolysis behaviour. On the contrary, the presence of the methionine ligand does not promote the platination of the A residue. The indication that the A platination by both the Pt(II) complexes is not favored gives evidence that the dominating preference for guanine base is a process completely hydrogen-bonds controlled. H-bonds are then confirmed to be implicated to impose both structural and kinetic control on the purine platination process.

The Università della Calabria and the MIUR PRIN 2008 are gratefully acknowledged.

Notes and references

- (a) B. Rosenberg, L. Camp and T. Krigas, *Nature*, 1965, **205**, 698; (b) B. Rosenberg, L. Camp, J. Trosko and V. H. Mansour, *Nature*, 1969, **222**, 385.
- Y. Jung and S. J. Lippard, *Chem. Rev.*, 2007, **107**, 1387 and references therein.
- (a) V. Brabec and M. Leng, *Proc. Natl. Acad. Sci. U. S. A.*, 1993, **90**, 5345; (b) H. H. Zheng, Z. H. Xu and K. Wang, *Int. J. Biol. Macromol.*, 1997, **20**, 107; (c) W. H. Du, W. Han, Z. F. Li and B. H. Wang, *Thermochim. Acta*, 2000, **359**, 55; (d) O. Novakova, J. Kasparkova, J. Malina, G. Natile and V. Brabec, *Nucleic Acids Res.*, 2003, **31**, 6450.
- M. Coluccia and G. Natile, *Anti-Cancer Agents Med. Chem.*, 2007, **7**, 111.
- U. Kalinowska-Lis, J. Ochocki and K. Matlawska-Wasowska, *Coord. Chem. Rev.*, 2008, **252**, 1328.
- (a) M. Coluccia, A. Nassi, F. Loseto, A. Boccarelli, M. A. Mariggio, D. Giordano, F. P. Intini, P. Caputo and G. Natile, *J. Med. Chem.*, 1993, **36**, 510; (b) M. Coluccia, A. Nassi, A. Boccarelli, D. Giordano, N. Cardellicchio, D. Locker, M. Leng, M. Sivo, F. P. Intini and G. Natile, *J. Inorg. Biochem.*, 1999, **77**, 31; (c) M. Coluccia, A. Boccarelli, M. A. Mariggio, N. Cardellicchio, P. Caputo, F. P. Intini and G. Natile, *Chem.-Biol. Interact.*, 1995, **98**, 251; (d) V. Brabec, O. Vrana, O. Novakova, V. Kleinwachter, F. P. Intini, M. Coluccia and G. Natile, *Nucleic Acids Res.*, 1996, **24**, 336.
- C. Li, Z. Li, E. Sletten, F. Arnesano, M. Losacco, G. Natile and Y. Liu, *Angew. Chem., Int. Ed.*, 2009, **48**, 8497.
- (a) M. E. Alberto, M. F. Lucas, M. Pavelka and N. Russo, *J. Phys. Chem. B*, 2009, **113**, 14473; (b) M. E. Alberto, M. F. Lucas, M. Pavelka and N. Russo, *J. Phys. Chem. B*, 2008, **112**, 10765; (c) M. Pavelka, M. F. Lucas and N. Russo, *Chem.-Eur. J.*, 2007, **13**, 10108; (d) M. F. Lucas, M. Pavelka, M. E. Alberto and N. Russo, *J. Phys. Chem. B*, 2009, **113**, 831.
- (a) J. L. Jestin, J. C. Chottard, U. Frey, G. Layrenczy and A. E. Merbach, *Inorg. Chem.*, 1994, **33**, 4277; (b) M. Mikola, K. D. Klika, A. Hakala and J. Arpalahti, *Inorg. Chem.*, 1999, **38**, 571.
- J. Raber, C. Zhu and L. A. Eriksson, *Mol. Phys.*, 2004, **102**, 2537 and reference therein.
- Y. Liu, F. P. Intini, G. Natile and E. Sletten, *J. Chem. Soc., Dalton Trans.*, 2002, 3489.
- N. Farrell, T. T. B. Ha, J. P. Souchard, F. L. Wimmer, S. Cros and N. P. Johnson, *J. Med. Chem.*, 1989, **32**, 2240.
- H. Eyring, *J. Chem. Phys.*, 1935, **3**, 107.
- M. G. Evans and M. Polanyi, *Trans. Faraday Soc.*, 1935, **31**, 875.
- D. G. Truhlar, W. L. Hase and J. T. Hynes, *J. Phys. Chem.*, 1983, **87**, 2664.

Supplementary Information

Methionine Ligand selectively promotes monofunctional adducts between *Trans-EE* platinum anticancer drug and Guanine DNA base

Marta E. Alberto, Nino Russo *

Dipartimento di Chimica, Università della Calabria, 87036 Arcavacata di Rende (CS), Italy

- **Computation Details;** -S1-
- **Optimized structures and selected geometric parameters of the stationary points along the hydrolysis reaction paths; a) *Trans-EE* and b) *Trans-EE/Met*;** -S2-
- **Natural Bond charges of the stationary points located along the hydrolysis paths for a) *Trans-EE* and b) *Trans-EE/Met* complexes;** -S3-
- **Selected calculated Wiberg bond index for Pt-Cl leaving group and Pt-O water during the hydrolysis reactions for a) *Trans-EE* and b) *Trans-EE/Met* complexes;** -S4-
- **Homo-Lumo molecular orbital plots for the stationary points along the hydrolysis reaction path for *Trans-EE* compound;** -S5-
- **Homo-Lumo molecular orbital plots for the stationary points along the hydrolysis reaction path for *Trans-EE/Met* compound;** -S6-
- **Optimized structures and selected geometric parameters of the stationary points for the binding of Guanine base to a) *Trans-EE* and b) *Trans-EE/Met*;** -S7-
- **Homo-Lumo molecular orbital plots and G-N7 lone-pairs energies for *Trans-EE* and *Trans-EE/Met* transition state structures;** -S8-
- **Optimized structures and selected geometric parameters of the stationary points for the binding of Adenine base to a) *Trans-EE* and b) *Trans-EE/Met*;** -S9-
- **Natural Bond charges of the stationary points of the reaction with Guanine base a) *Trans-EE* and b) *Trans-EE/Met* complexes;** -S10-
- **References;** -S11-

Computational Details

All calculations were performed with the Gaussian 03^[1] program at the density functional theory level, using the hybrid B3LYP functional, composed of Becke's^[2] three-parameter hybrid exchange functional (B3) and the correlation functional of Lee, Yang, and Parr (LYP).^[3] Geometry optimizations without symmetry constraints were carried out with a 6-31G(d) basis set for all atoms except the platinum atom, which was described by the quasi-relativistic Stuttgart-Dresden pseudopotentials^[4] with the pseudo-orbital basis set augmented by a set of diffuse functions, $\alpha_s=0.0075$, $\alpha_p=0.013$, and $\alpha_d=0.025$, and polarization functions, $\alpha_f=0.98$.^[5] In order to confirm proper convergence to equilibrium and transition state geometries, vibrational frequency analysis was done on the basis of analytical second derivatives of the Hamiltonian at this level of theory. Solvent effects ($\epsilon = 80$) were taken into account by the CPCM method^[6] and using Klamt radii for constructing the solute cavity.^[7] More accurate energies were obtained in gas phase and in solvent by performing single point calculations with the larger basis set 6-31++G(2df,2pd).

Figure -S2-

Optimized structures and selected structural parameters of the stationary points along the hydrolysis reaction paths; a) *Trans-EE* and b) *Trans-EE/Met*;

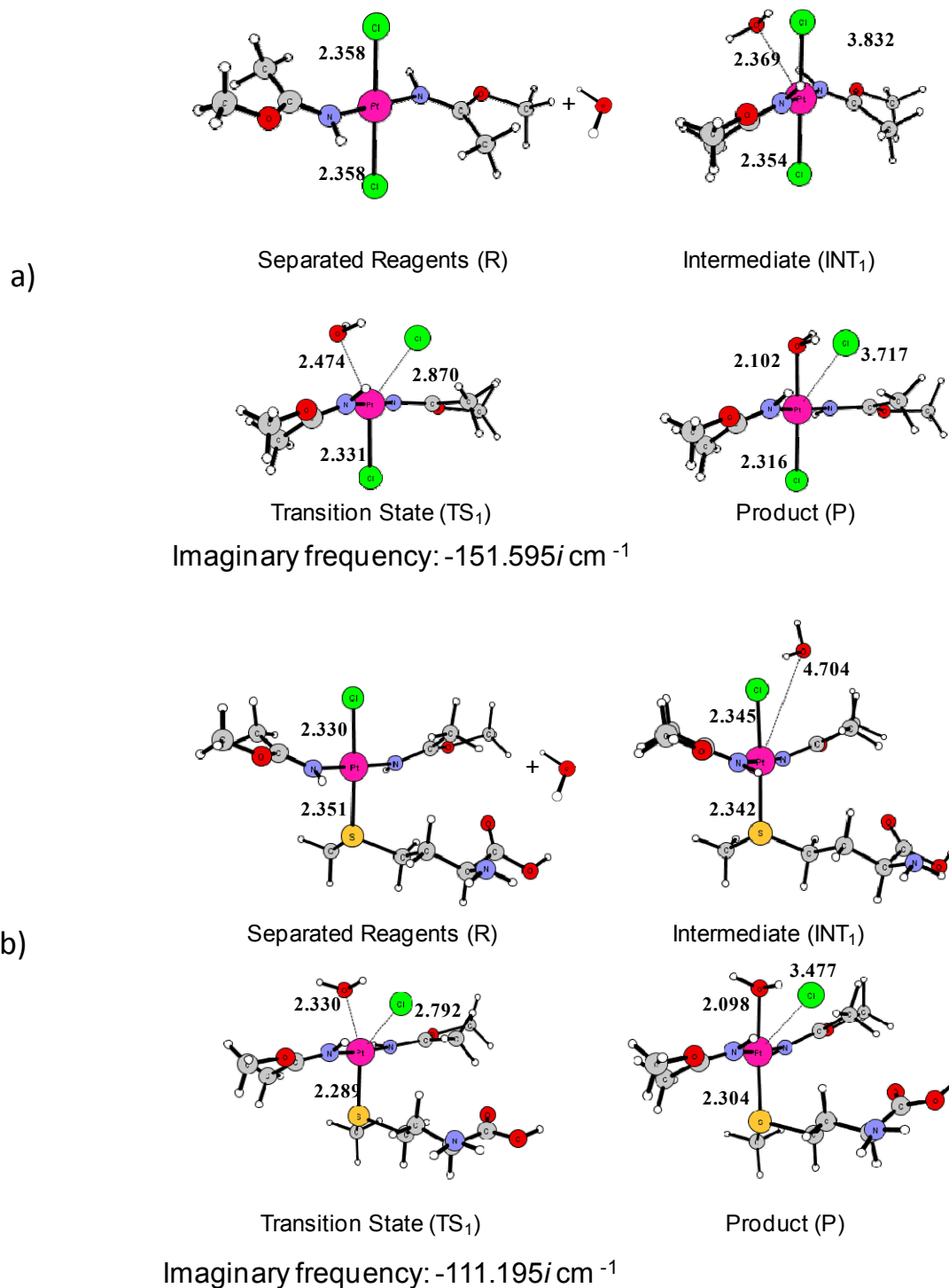


Figure -S3-

Natural Bond charges of the stationary points located along the hydrolysis paths for

a) *Trans-EE* and b) *Trans-EE/Met* complexes;

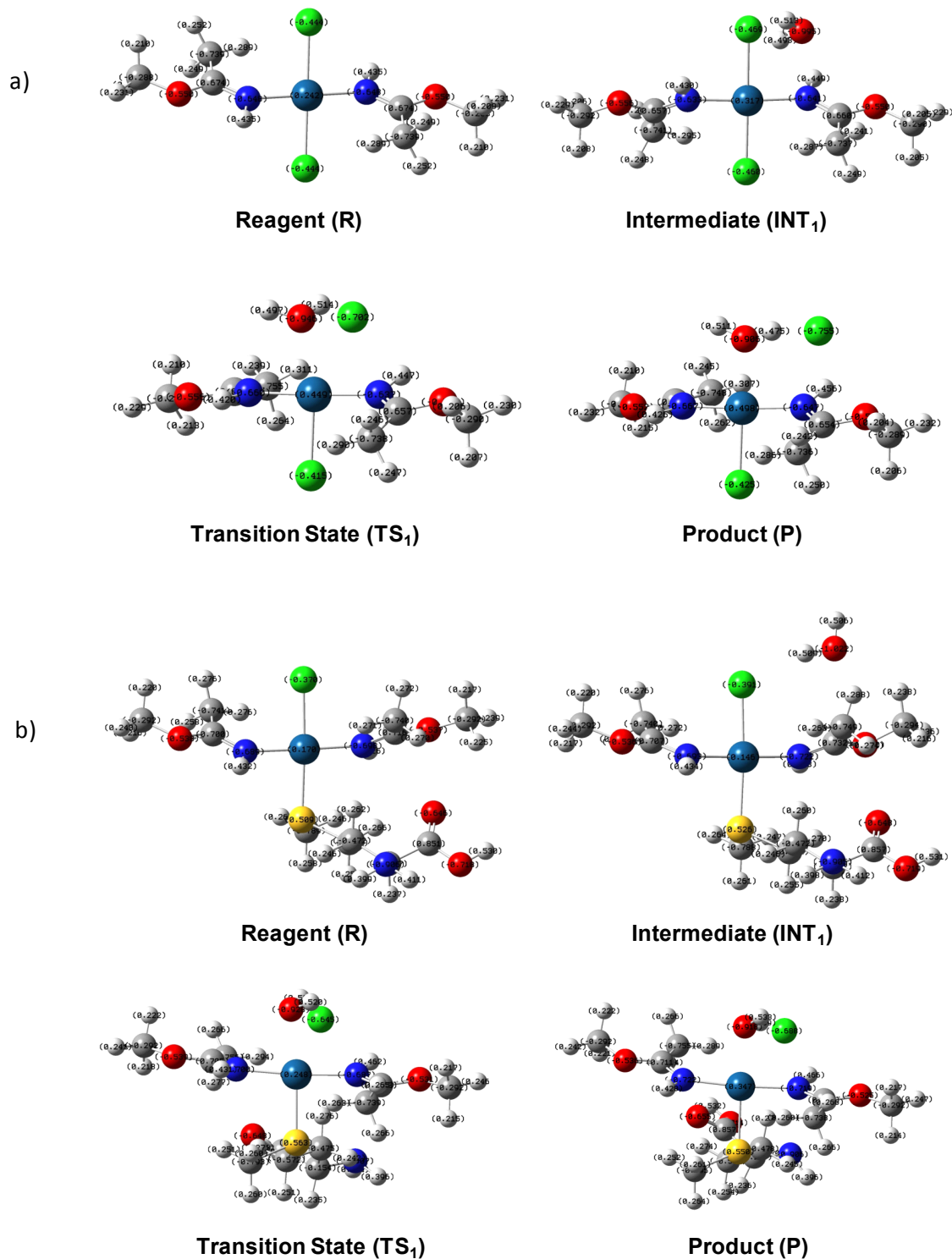


Figure -S4-

Selected calculated Wiberg bond index for Pt-Cl_{leaving group} and Pt-O_{water} during the hydrolysis reactions for a) *Trans-EE* and b) *Trans-EE/Met* complexes;

	<i>Pt-Cl(leaving)</i>			<i>Pt-O(water)</i>		
	<i>INT₁</i>	<i>TS₁</i>	P	<i>INT₁</i>	<i>TS₁</i>	P
<i>Trans-EE</i>	0.6798	0.3227	0.0333	0.0089	0.2037	0.3981
<i>Trans-EE/Met</i>	0.7265	0.3934	0.0772	0.0022	0.2677	0.3934

Figure -S5-

**Homo-Lumo molecular orbital plots for the stationary points along the hydrolysis reaction path
for *Trans-EE* compound. a) Reactant b) Transition state c) Product**

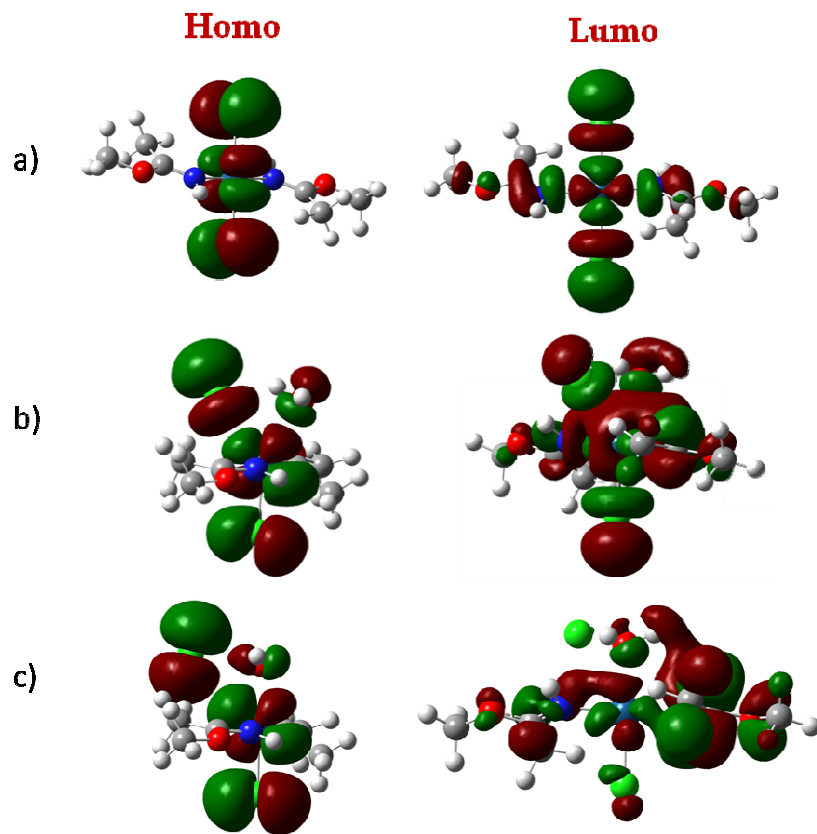


Figure -S6-

Homo-Lumo Molecular orbital plots for the stationary points along the hydrolysis path for *Trans-EE/Met* compound. a) Reactant b) Transition state c) Product

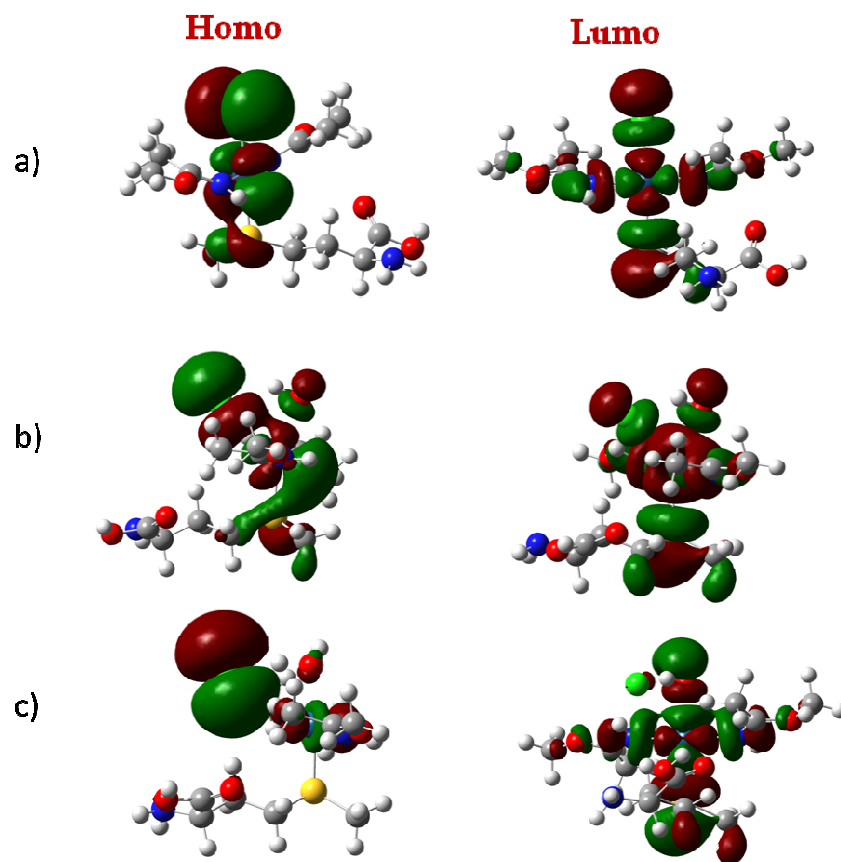


Figure -S8-

Homo-Lumo molecular orbital plots and G-N7 lone-pairs energies for a) *Trans-EE* and b) *Trans-EE/Met* transition state structures;

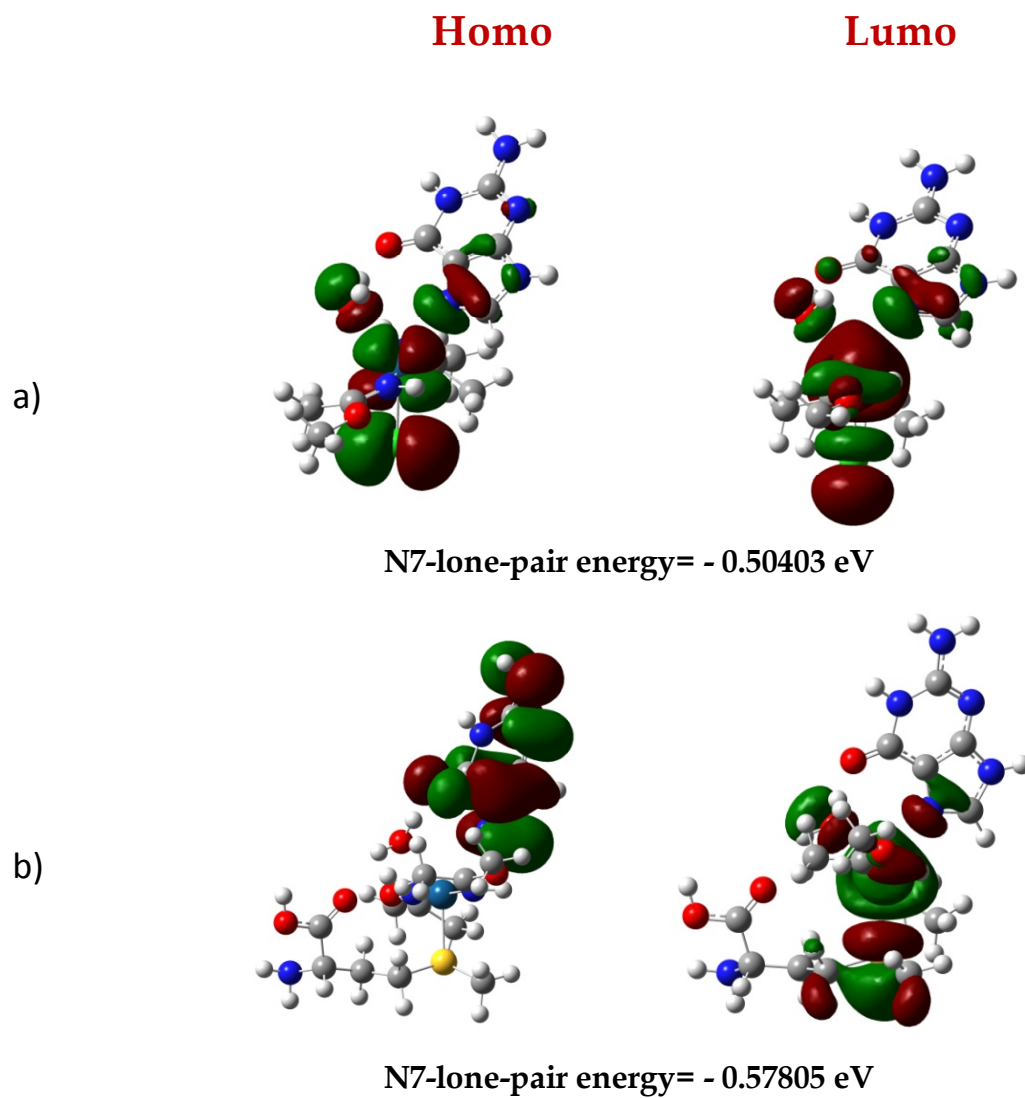


Figure -S9-

Optimized structures and selected geometric parameters of the stationary points for the binding of Adenine base to a) *Trans-EE* and b) *Trans-EE/Met*;

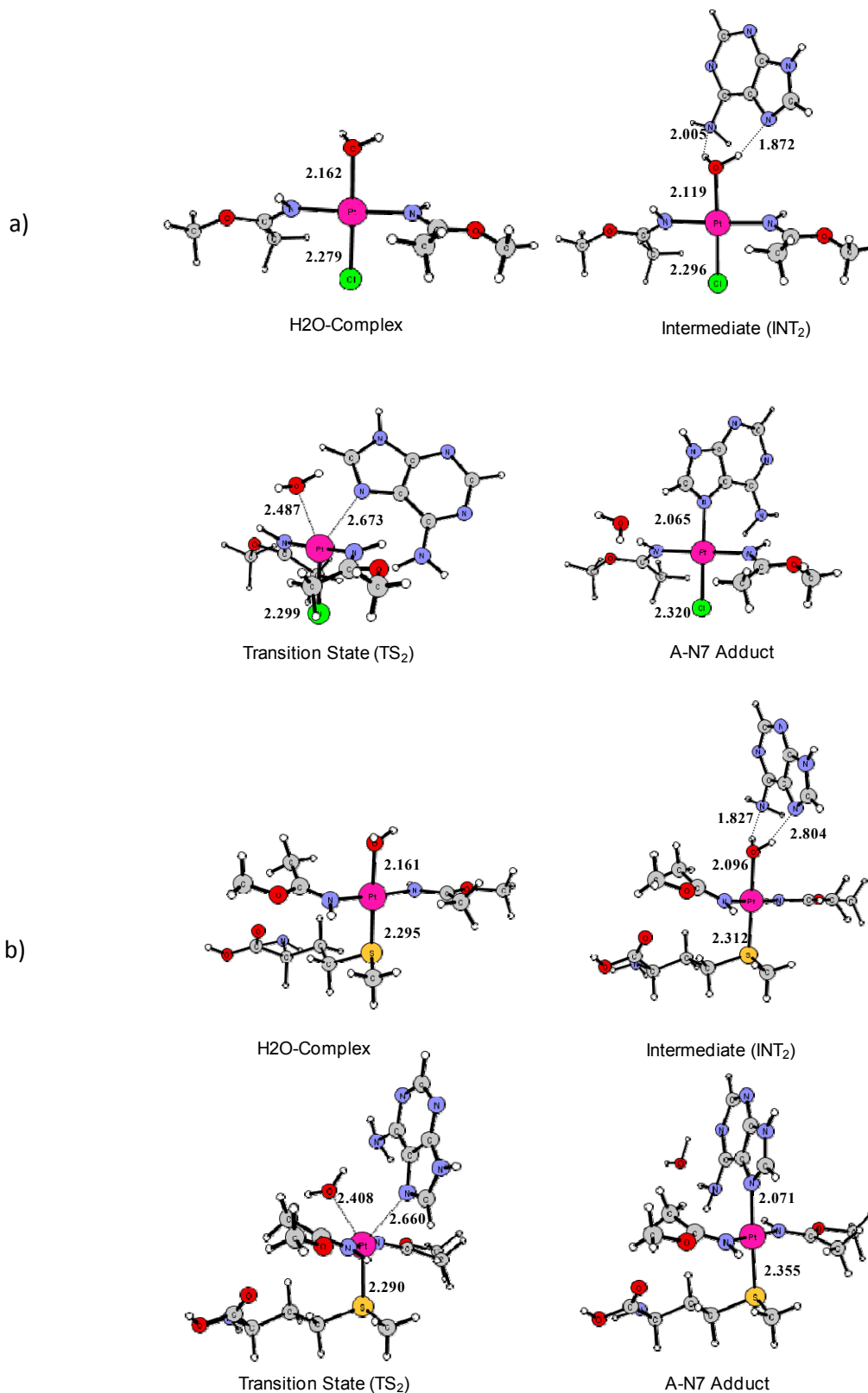
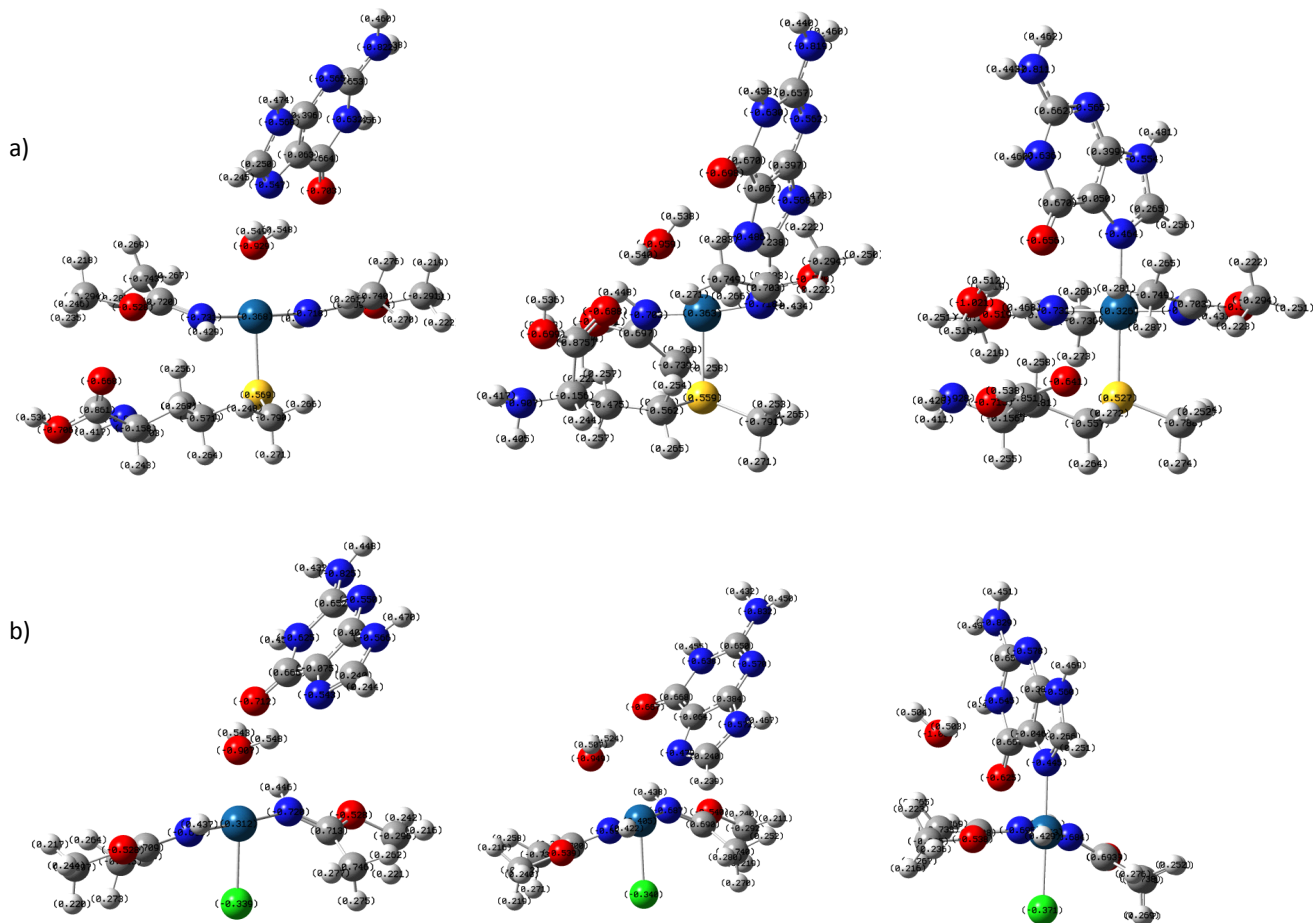


Figure -S10-

Natural Bond charges of the stationary points of the reaction with Guanine base

a) *Trans-EE* and b) *Trans-EE/Met* complexes;



References

- [1] Frisch, M. J.; Trucks, G. W.; Schlegel, H. B.; Scuseria, G. E.; Robb, M. A.; Cheeseman, J. R.; Montgomery, J. A., Jr.; Vreven, T.; Kudin, K. N.; Burant, J. C.; Millam, J. M.; Iyengar, S. S.; Tomasi, J.; Barone, V.; Mennucci, B.; Cossi, M.; Scalmani, G.; Rega, N.; Petersson, G. A.; Nakatsuji, H.; Hada, M.; Ehara, M.; Toyota, K.; Fukuda, R.; Hasegawa, J.; Ishida, M.; Nakajima, T.; Honda, Y.; Kitao, O.; Nakai, H.; Klene, M.; Li, X.; Knox, J. E.; Hratchian, H. P.; Cross, J. B.; Bakken, V.; Adamo, C.; Jaramillo, J.; Gomperts, R.; Stratmann, R. E.; Yazyev, O.; Austin, A. J.; Cammi, R.; Pomelli, C.; Ochterski, J. W.; Ayala, P. Y.; Morokuma, K.; Voth, G. A.; Salvador, P.; Dannenberg, J. J.; Zakrzewski, V. G.; Dapprich, S.; Daniels, A. D.; Strain, M. C.; Farkas, O.; Malick, D. K.; Rabuck, A. D.; Raghavachari, K.; Foresman, J. B.; Ortiz, J. V.; Cui, Q.; Baboul, A. G.; Clifford, S.; Cioslowski, J.; Stefanov, B. B.; Liu, G.; Liashenko, A.; Piskorz, P.; Komaromi, I.; Martin, R. L.; Fox, D. J.; Keith, T.; Al-Laham, M. A.; Peng, C. Y.; Nanayakkara, A.; Challacombe, M.; Gill, P. M. W.; Johnson, B.; Chen, W.; Wong, M. W.; Gonzalez, C.; Pople, J. A. Gaussian 03, revision A.1; Gaussian, Inc.: Pittsburgh, PA, 2003.
- [2] Becke, A. D. *J. Chem. Phys.* **1993**, *98*, 5648.
- [3] Lee, C. T.; Yang, W. T.; Parr, R. G. *Phys. Rev. B* **1988**, *37*, 785.
- [4] Andrae, D.; Haussermann, U.; Dolg, M.; Stoll, H.; Preuss, H. *Theor. Chim. Acta* **1990**, *77*, 123.
- [5] Burda, J. V.; Zeizinger, M.; Sponer, J.; Leszczynski, J. *J. Chem. Phys.* **2000**, *113*, 2224.
- [6] (a) Klamt, A.; Schüürmann, G. *J. Chem. Soc., Perkin Trans. 2* **1993**, 799. (b) Andzelm, J.; Kölmel, C.; Klamt, A. *J. Chem. Phys.* **1995**, *103*, 9312. (c) Barone, V.; Cossi, M. *J. Phys. Chem. A* **1998**, *102*, 1995. (d) Cossi, M.; Rega, N.; Scalmani, G.; Barone, V. *J. Comput. Chem.* **2003**, *24*, 669.
- [7] Klamt, A.; Jonas, V.; Burger, T.; Lohrenz, J. C. W. *J. Phys. Chem. A* **1998**, *102*, 5074.

Paper VI

“Rhenium(IV) Compounds act as Anticancer Agents”

J. Martínez-Lillo, T. F. Mastropietro, R. Lappano, A. Madeo, Marta E. Alberto,
N. Russo, M. Maggiolini and G. De Munno

submitted

Rhenium(IV) Compounds act as Anticancer Agents**

José Martínez-Lillo, Teresa F. Mastropietro, Rosamaria Lappano, Antonio Madeo, Marta E. Alberto, Nino Russo, Marcello Maggiolini, and Giovanni De Munno*

Recent advances both in therapeutic and diagnostic medicine are strictly related to the design of novel metal-based drugs, demonstrating that biomedical inorganic chemistry is a rapidly emergent field of enormous potential for application in medicine.¹ Since the discovery of cisplatin, platinum derivatives have been widely investigated because of their high impact on cancer chemotherapy.² Three such agents (cisplatin, carboplatin, and oxaliplatin) in particular gained widespread clinical distribution for the treatment of malignancy diseases. They are hypothesised to act by forming DNA adducts and to have similar molecular-level mechanism of actions.³ The chemotherapeutic treatment efficacy, however, has been overlapped by acquired and intrinsic drug resistance along with important side effects, especially nephrotoxicity, neurotoxicity, ototoxicity and emetogenesis.⁴ Moreover, the poor water solubility of cisplatin and its derivatives makes difficult their use in clinical practice.⁵ To overcome such limitations, the search for new active metallodrugs has been substantially diversified by introducing various other transition metals of different clinical potential with the aims of developing alternative pharmaceuticals with high efficiency and reduced side-effects.^{1,6}

Within this context, rhenium complexes have attracted growing attention for their possible use as anticancer drugs.⁷ Moreover,

rhenium has two radioisotopes (¹⁸⁶Re and ¹⁸⁸Re) of interest for nuclear medicine, both having effectiveness for either cancer therapy (owing to the β - emission)⁸ or diagnosis⁹ (owing to the γ emission with similar energies to that of ^{99m}Tc). To date, the studies reported in literature on the anticancer activity and the therapeutic and diagnostic applications of rhenium derivatives deal with Re(I), Re(III) or Re(V) metal complexes, while the Re(IV) oxidation state remained unexplored. Re(IV) is a 5d³ ion that usually forms octahedral complexes displaying structural similarity to those of Pt(IV), Ru(II) and Ru(III) active compounds. Moreover, they are quite inert to ligand substitution and reasonably stable against redox processes,¹⁰ this property being suitable to reduce the toxicities associated with platinum-based chemotherapies.¹¹ All these features, together with the lacking of any previously reported study on this topic, encouraged us to explore the potential of Re(IV) complexes for the development of new anticancer drugs, this choice being also motivated by the gained experience of some of us in Re(IV) chemistry,¹²

To this end, we synthesized a series of mononuclear Re(IV) compounds (Figure 1) of general formula ReCl₄L (where L is a chelating ligand such as bpy, bpym, dmpy and phen [bpy = 2,2'-bipyridine; bpym = 2,2'-bipyrimidine; dmbpy = 4,4'-dimethyl-2,2'-bipyridine; phen = 1,10-phenanthroline]) for testing their biological activity in MCF-7 (breast), BG-1 (ovarian) and LNCaP (prostate) cancer cells.

[*] Dr. J. Martínez-Lillo, Dr. T. F. Mastropietro, Prof. G. De Munno
Centro di Eccellenza CEMIF.CAL,
Dipartimento di Chimica
Università della Calabria
via P. Bucci 14/c, 87030 Arcavacata di Rende, Cosenza (Italy)
E-mail: demunno@unical.it

Dr. R. Lappano, Dr. A. Madeo, Prof. M. Maggiolini
Dipartimento Farmaco-Biologico
Università della Calabria
via P. Bucci, 87030 Arcavacata di Rende, Cosenza (Italy)

Dr. M. E. Alberto, Prof. Nino Russo
Dipartimento di Chimica
Università della Calabria
via P. Bucci 14/c, 87030 Arcavacata di Rende, Cosenza (Italy)

[**] Acknowledgements Financial support was received from the Ministero dell'Istruzione, dell'Università e della Ricerca Scientifica (MiUR) through the Centro di Eccellenza CEMIF.CAL (CLAB01TYEF). The authors wish to thank Dr. Leonardo Di Donna for the HRESI-ToF mass spectra.



Supporting information for this article is available on the WWW under <http://www.angewandte.org> or from the author. ((Please delete if not appropriate))

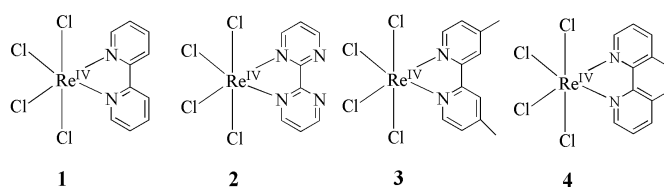


Figure 1. Structure of complexes 1-4

All compounds synthesized displayed potent antiproliferative activity. In particular, the inhibitory activity exerted by the bpy-containing compound was considerably stronger than that of cisplatin in MCF-7 breast tumor cells. Theoretical studies were also conducted in order to explore the mechanisms of the possible hydrolysis reactions and to provide insights on the kinetic of these processes, and the results were compared with the data available in the literature on the Pt(II) anticancer drugs.¹³ Although the mechanisms of action of this novel class of compounds could be different from that exhibited by the conventional platinum drugs, the hydrolysis process is expected to play an important role in their activation before reaching DNA, one of the most suitable biological target.

The attainments of the present investigation indicate that these Re(IV) complexes should represent novel potentially active metallo-drugs, displaying apoptotic activity in selected cell lines.

The Re(IV) compounds $\text{ReCl}_4(\text{bpy})$ (**1**), $\text{ReCl}_4(\text{bpym})$ (**2**), $\text{ReCl}_4(\text{dmbpy})$ (**3**) and $\text{ReCl}_4(\text{phen})$ (**4**) were prepared by ligand substitution reaction from $[\text{Re}^{\text{IV}}\text{Cl}_6]^{2-}$ anion in *N,N*-dimethylformamide (DMF). The synthesis and crystal structure of **1** and **2**, together with their magnetism (**1**, **2**) and electrochemical (**2**) studies, were previously reported.^{14, 15} The compounds **3** and **4** have been synthesized and characterized for the purpose of the biomedical studies carried out in this work (See Supporting Information, S1 for the Experimental Information and S2 for Crystallographic Details). The crystal structures of **1-4** consist of discrete $\text{ReCl}_4(\text{L})$ (L = bpy (**1**), bpym (**2**), dmbpy (**3**) and phen(**4**)) molecules held together by means of van der Waals interactions. Each $\text{ReCl}_4(\text{L})$ contains a Re(IV) atom in a somewhat distorted octahedral environment, being bonded to a bidentate N-heterocyclic ligand and four chloride anions. The main distortion of the ideal octahedral geometry is due to the reduced bite angle of the chelating ligands [77.2(1)° (**1**), 76.3(3)° (**2**), 76.9(1)° (**3**) and 76.8(3)° (**4**)].

The values of the Re-Cl and Re-N bond distances are in agreement with those reported for other similar Re(IV) compounds in literature.^{14,15} The Re-Cl bond lengths in *trans* position to the nitrogen donors are slightly shorter than those in *cis* positions, this effect being more evident in compounds **2** and **3**.

The nitrogen atoms of the chelating ligands and the *trans* chlorides constitute the best equatorial plane around the metal centre, the largest deviation from planarity being 0.012(1) Å for N(1) and N(2) in **1**, 0.009(3) Å for N(1) in **2**, 0.038(1) Å for N(1) in **3** and 0.006(4) Å for N(1) in **4**, respectively. The Re atom is practically placed in this plane. The N-heterocyclic ligands are almost planar in **1** and **3**, the means deviations correspondingly being 0.013(2) Å (**1**) and 0.016(2) Å (**3**). On the contrary, the bpym and the phen ligands in **2** and **4**, respectively, show evident deviation from planarity, the largest deviations from the mean planes being 0.183(8) Å in **2** and -0.08 Å in **4**. The metal atom is -0.246(9) Å (**2**) and 0.15 Å (**4**) out of the mean plane of the ligands.

All compounds are stable in the solid state and their stability in DMSO/H₂O solution was also confirmed by ESI MS spectra. (see Supporting Information, S3).

In order to investigate the potential anticancer properties of **1-4** rhenium complexes, MCF-7 breast, BG1 ovarian and LnCaP prostate cancer cells were used as model systems (see Supporting Information, S4). In addition, cells were exposed to cisplatin in order to compare the anticancer effects of chemicals used. Compounds **1** and **2** inhibited cell proliferation in a dose and time-dependent manner, as shown in Figure 2 and S5.

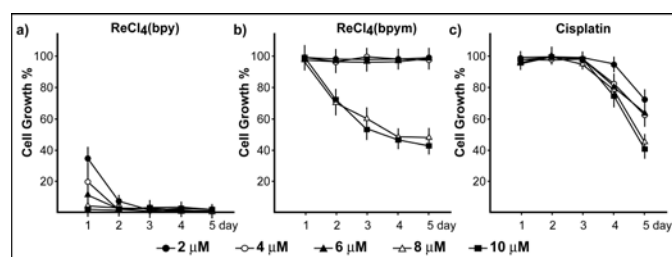


Figure 2. a-c, evaluation of cell growth by compounds **1**, **2** and cisplatin in MCF-7 breast cancer cells, as determined using the MTT assay.

Compounds **3** and **4** also showed antiproliferative effects, as shown in Figure S6. Remarkably, compounds **1-4** inhibited cell growth in a stronger manner respect to cisplatin, hence their biological activity might be relevant towards innovative anti-cancer drug discovery. It is worth noting that compounds **1** and **4** exhibited in MCF-7 cells stronger repressive effects respect to those observed in the remaining used tumor cells, as the lowest concentration (2 μM) blocked cell growth after only one day of treatment (Figure 2, S5 and S6) and in a stronger manner respect to the highest concentration used for cisplatin throughout the treatment.

In order to provide mechanistic insights into the antiproliferative activity elicited by compounds **1** and **2**, we first evaluated DNA fragmentation by TUNEL assay. MCF-7 cells exposed to 10 μM of both chemicals for 24 h were positive for TUNEL staining (Figure 3).

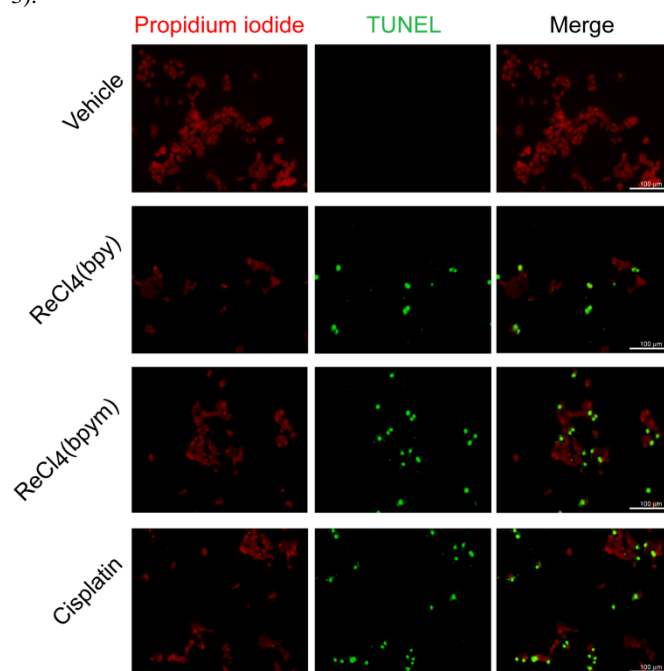


Figure 3. Representative images of TUNEL staining for apoptosis evaluation in MCF-7 cells treated for 24 h with 10 μM of **1**, **2** or cisplatin. In left panels, propidium iodide staining of nuclei; in middle panels, TUNEL staining and in right panels merged images. Magnification is indicated by the bars (100 μm). Each experiment shown is representative of 20 random fields observed.

Next, the treatment for 2 h with 10 μM of **1** and **2** induced c-Jun N-terminal phosphorylation at serine 73 (S73) (Figure 4), which correlates with a pro-apoptotic activity.¹⁶

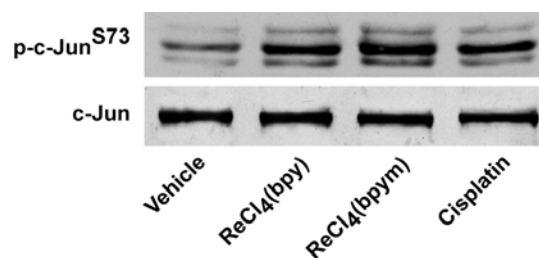


Figure 4. c-Jun S73 phosphorylation and total c-Jun were evaluated in MCF-7 cells treated for 2 h with vehicle or compounds **1**, **2** or cisplatin.

Taken together, these results indicate that the apoptosis of MCF-7 cells induced by compounds **1** and **2** is associated to c-Jun phosphorylation, according to previous data obtained using well known anticancer molecules.¹⁶

Due to the presence of chloride anions as good leaving groups and the structural similarity of **1-4** to some Ru(II) and Ru(III) active complexes, for which it is accepted that the aquated species are likely to be responsible for their biological effects,¹⁷ it can be supposed that also these drugs can hydrolyze *in vivo*, forming a number of potentially active species. At this purpose, the ESI MS spectra of **1-4** in DMSO/H₂O indicate the formation of mono-aquated derivatives (see Supporting Information, S3).

This experimental evidence was also supported by the results of the theoretical studies, carried out to explore the hydrolysis reactions of compounds **1** and **2** (see also Supporting Information, S5). The degradation reaction pathways of ReCl₄(bpy) (**1**) and ReCl₄(bpym) (**2**) were investigated in the framework of DFT/CPCM approach in order to elucidate the basic step of the hydrolysis process. At this purpose, we employed the DFT-B3LYP tool, which has been previously used in a huge number of chemical systems including the aquation processes of metal containing anticancer drugs.¹⁷⁻¹⁸

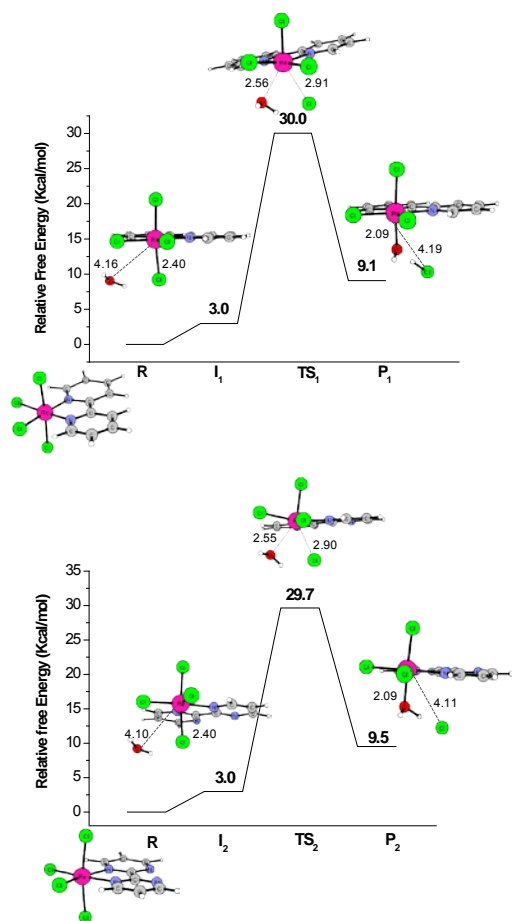


Figure 5. Computed relative free energies profiles (at 298.15 K) and optimized structures of the stationary points for the hydrolysis process of **1** and **2**, in water phase.

The substitution reactions of chloride ion by water can occur, in principle, from axial or equatorial position. We ascertain that for both compounds **1** and **2**, the release of the axial chloride is favoured. An associative mechanism, characterized by a transition state with the entering molecule, the leaving group and the metal complex resulting weakly bound, was found for this process. A

similar behaviour has been proposed for cisplatin and its analogues, and for some octahedral Ru(III) complexes with *in vivo* anticancer activities.¹⁷⁻¹⁸ The potential energy profiles for axial Cl⁻ substitution, as well as the optimized structures for the stationary points along these reactions for compounds **1** and **2** are reported in Figure 5, while those relative to the equatorial Cl⁻ substitution are reported in the Supporting Information section, S8. It is interesting to notice that the formation of the **1** and **2**-aqua complexes require an amount of energy close to that demanded by the second and third Pt(II) anticancer drugs generation. In particular, they show energetic profiles similar to that of carboplatin for which the first activation barrier was found to be 30.1 kcal/mol⁻¹,¹⁸ in good agreement with experimental data.¹⁹ The cisplatin-like compounds show all slower hydrolysis rates compared to cisplatin due to the introduction of sterically demanding carrier ligands. The reduced velocity of this process has been related with the lower side effects displayed by the second and third generation anticancer drugs in therapy.²⁰ From this point of view, the results obtained in this work for compounds **1** and **2**, indicate a reasonable hydrolysis rate and allow us to hypothesize that undesired reactions on the way to the DNA target could be avoided. An alternative path, in which the attack of the water molecule on rhenium centre leads to ring opening processes with formation of monodentate bpy or bpym ligands was also considered. The results indicate that the release of bpy or bpym ligands followed by the addition of a second water molecule is an unfavourable process. (See Supporting Information, S9).

In summary, selected Re(IV)-based complexes of the type [ReCl₄(L)] (**1-4**) have been for the first time tested toward their anticancer activity and they have been found to exhibit potent *in vitro* antiproliferative effects against MCF-7, BG1 and LnCaP cancer cell lines. In particular, compounds **1** and **4** exert a significant inhibitory activity in MCF-7 cells even at the lowest micromolar concentrations, their cytotoxic effect being considerably stronger than that exhibited by cisplatin under the same experimental conditions. The mode of action of compounds **1** and **2** has been associated with c-Jun S73 phosphorylation, which represents a hallmark of chemical-induced apoptosis

In conclusion, the satisfactory results of this investigation suggest that the strategic combination of Re(IV) with suitable ligands in the same molecular species may provide a new class of rhenium(IV) complexes exhibiting enhanced antitumor properties. The appropriate modification of the coordinating ligands could be crucial in enhancing the chemotherapeutic properties of this class of compounds, as the fine-tune of their supramolecular functions could be effective in modifying their reactivity and lipophilicity on one hand and to reduce adverse effects of the metal ion on the other. In this regard, studies on Re(IV) complexes containing other ligands as well as experiments using other cancer cell types are in progress. Moreover, our current aim is the identification of the molecular and cellular mechanism(s) involved in the anticancer properties elicited by each Re(IV) derivative in the diverse cancer cell types, in order to provide exciting insights into their potential chemotherapeutic action.

Received: ((will be filled in by the editorial staff))
Published online on ((will be filled in by the editorial staff))

Keywords: antitumor agents • bioinorganic chemistry • rhenium complexes • theoretical studies

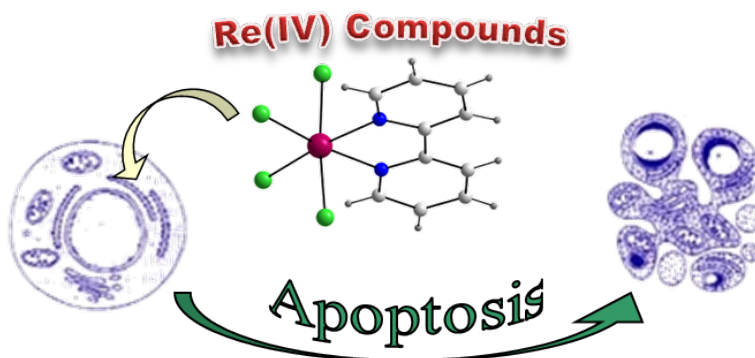
- [1] a) Z. Guo, P. J. Sadler, *Angew. Chem. Int. Ed.* **1999**, *38*, 1512-1531; b) *Metallotherapeutic Drugs and Metal-Based Diagnostic Agents: The Use of Metals in Medicine* (Eds: M. Gielen and E. R. T. Tiekink), John Wiley & Sons, **2005**; c) P. Blower, *Dalton Trans.* **2006**, 1705-1711; d) S. P. Fricker, *Dalton Trans.* **2007**, 4903-4917; e) X. Wang, Z. Guo, *Dalton Trans.* **2008**, 1521-1532; f) J. Reedijk *Macromol. Symp.* **2008**, *270*, 193-201; g) N. Farrer, L. Salassa, P. J. Sadler, *Dalton Trans.* **2009**, 10690-10701; h) S. P. Fricker, *Metallomics* **2010**, *2*, 366-377.
- [2] a) E. R. Jamieson, S. J. Lippard, *Chem. Rev.* **1999**, *99*, 2467-2498; b) E. Wong, C. M. Giandomenico, *Chem. Rev.* **1999**, *99*, 2451-2466; c) M. A. Fuertes, C. Alonzo; J. M. Perez, *Chem. Rev.* **2003**, *103*, 645-662; d) L. Kelland, *Nat. Rev. Cancer* **2007**, *7*, 573-584; e) Y. Yung, S. J. Lippard, *Chem. Rev.* **2007**, *107*, 1387-1407; f) J. Reedijk, in *Platinum Met. Rev.* **2008**, Vol. 52, (Eds. B. W. Copping), Johnson Matthey Public Limited Company, Royston, **2008**, 2-11.
- [3] a) S. J. Lippard, J. M. Berg in *Principles of Bioinorganic Chemistry*, University Science Books, Mill Valley, CA, **1994**; b) J. Reedijk, *Chem. Commun.* **1996**, 801 - 806; c) A. Eastman, in *Cisplatin: Chemistry and Biochemistry of a Leading Anticancer Drug* (Ed. B. Lippert), VCH & Wiley-VCH, Zurich & Germany, **1999**, pp. 111-134; d) B. Lippert in *Cisplatin, Chemistry and Biochemistry of a Leading Anticancer Drug*, Wiley-VCH, Weinheim, **1999**; e) J. D. Roberts, J. Peroutka, N. Farrell, *J. Inorg. Biochem.* **1999**, *77*, 51 - 57; f) Z. J. Guo, P. J. Sadler, *Adv. Inorg. Chem.* **2000**, *49*, 183 - 306; g) T. W. Hambley, *J. Chem. Soc., Dalton Trans.* **2001**, *40*, 307-16; h) C. Li, Z. Li, E. Sletten, F. Arnesano, M. Losacco, G. Natile, Y. Liu, *Angew. Chem. Int. Ed.* **2009**, *48*, 8497-8500.
- [4] a) W. Dempke, W. Voigt, A. Grothey, B. T. Hill, H. J. Schmoll, *Anti-Cancer Drugs* **2000**, *11*, 225-236; b) S. M. Cohen, S. J. Lippard, *Prog. Nucleic Acid Res. Mol. Biol.* **2001**, *67*, 93-130.
- [5] a) S. J. Lippard, *Progress in Inorganic Chemistry: Bioinorganic Chemistry*; Wiley: Sydney, **1995**; Vol. 48; b) M. Galanski, M. A. Jakupec, B. K. Keppler, *Curr. Med. Chem.* **2005**, *12*, 2075-2094.
- [6] a) *Metal Complexes in Cancer Chemotherapy*, (Eds: B. K. Keppler), VCH, Weinheim, **1993**; b) *Metal Compounds in Cancer Therapy*, (Eds: S. P. Fricker), Chapman and Hall, London, **1994**; c) C. H. A. Goss, W. Henderson, A. L. Wilkins, C. J. Evans, *Organomet. Chem.* **2003**, *679*, 194-201; d) A. G. Quiroga, C. N. Ranninger, *Coord. Chem. Rev.* **2004**, *248*, 119-133; e) S. Ray, R. Mohan, J. K. Singh, M. K. Samantaray, M. M. Shaikh, D. Panda, P. Ghosh, *J. Am. Chem. Soc.* **2007**, *129*, 15042-15053.
- [7] a) A. Zablotskaya, I. Segal, E. Lukevics, S. Belyakov and H. Spies *Appl. Organometal. Chem.* **2007**, *21*, 288-293; b) D.-L. Ma, C.-M. Che, F.-M. Siu, M. Yang, K.-Y. Wong, *Inorg. Chem.* **2007**, *46*, 740-749; c) N. Viola-Villegas, A. E. Rabideau, J. Cesnavicious, J. Zubieta, R. P. Doyle, S. Wirth, A. U. Wallek, A. Zernickel, F. Feil, M. Sztiller-Sikorska, K. Lesiak-Mieczkowska, C. Bräuchle, I. P. Lorenz, M. Czyn ChemMedChem **2008**, *3*, 1387-1394; d) A. V. Shtemenko, P. Collery, N. I. Shtemenko, K. V. Domasevitch, E. D. Zabitskayac, A. A. Golichenkoa *Dalton Trans.*, **2009**, 5132-5136; e) S. Wirth, A. U. Wallek, A. Zernickel, F. Feil, M. Sztiller-Sikorska, K. Lesiak-Mieczkowska, C. Bräuchle, *J. Inorg. Biochem.* **2010**, *104*(7), 774-789.
- [8] a) K. Hashimoto, K. Yoshihara, *Top. Curr. Chem.* **1995**, *176*, 275-291; b) J. R. Dilworth and S. J. Parrott, *Chem. Soc. Rev.*, **1998**, *27*, 43-55; c) J. Cao, Y. Wang, J. Yua, J. Xiaa, C. Zhanga, D. Yina, U. O. Hafelib *Journal of Magnetism and Magnetic Materials* **2004**, *277*, 165-174; d) P. Blower, *Dalton Trans.* **2006**, 1705-1711; e) B. Goins, A. Bao, W. T. Phillips, *Methods Mol Biol.* **2010**, *606*, 469-491.
- [9] a) E. A. Deutsch, K. Libson, J. L. Vanderheyden, in *Technecium and Rhenium in Chemistry and Nuclear Medicine*, Raven Press, New York, **1990**; b) J. F. Eary, L. Durack, D. Williams, J. L. Vanderheyden. *Clin. Nucl. Med.* **1990**, *15*, 911-916 c) W. Volkert, W. F. Goeckeler, G. J. Ehrhardt, A. R. Ketring, *J. Nucl. Med.* **1991**, *32*, 174-185; d) E. John, M. L. Thakur, J. De Fulvio, M. R. McDevitt, I. Dajanov, *J. Nucl. Med.* **1993**, *34*, 260-267; e) S. S. Jurisson, J. D. Lydon, *Chem. Rev.* **1999**, *99*, 2205-2218; f) S. Liu, D. S. Edwards, *Chem. Rev.* **1999**, *99*, 2235-2268; g) W. A. Volkert, T. J. Hoffman, *Chem. Rev.* **1999**, *99*, 2269-2292; h) J. Sattigeri, A. L. Rodriguez, J. A. Katzenellenbogen, *Bioorg. Med. Chem.* **2002**, *10*, 1381.
- [10] a) G. Rouschias, *Chem. Rev.* **1974**, *74*, 531-566; b) K. A. Conner, R. A. Walton in *Comprehensive Coordination Chemistry*, (Eds: G. Wilkinson, R. D. Gillard, J. A. McCleverty), Pergamon Press: New York, **1987**, Vol. 4, pp. 165; c) M. N. Sokolova, N. E. Fedorova, E. V. Peresypkina, R. Patow, V. E. Fedorova, D. Fenske, *Inorg. Chim. Acta* **2005**, *358*, 3914.
- [11] a) L. R. Kelland, G. Abel, M. J. McKeage, M. Jones, P. M. Goddard, M. Valenti, B. A. Murrer, K. R. Harrap, *Cancer Research* **1993**, *53*, 2581; b) M. D. Hall, T. W. Hambley, *Coord. Chem. Rev.* **2002**, *232*, 49-67.
- [12] J. Martínez-Lillo, D. Armentano, G. De Munno, F. Lloret, M. Julve, J. Faus, *Dalton Trans.* **2008**, 40 and references therein.
- [13] D. P. Bancroft, C. A. Lepre, S. J. Lippard, *J. Am. Chem. Soc.* **1990**, *112*, 6860-6871.
- [14] J. Martínez-Lillo, D. Armentano, G. De Munno, J. Faus, *Polyhedron* **2008**, *27*, 1447-1454.
- [15] R. Chiozzone, R. González, C. Kremer, M. F. Cerdá, D. Armentano, G. De Munno, J. Martínez-Lillo, J. Faus, *Dalton Trans.* **2007**, 653-660.
- [16] M. Vinciguerra, I. Esposito, S. Salzano, A. Madeo, G. Nagel, M. Maggiolini, A. Gallo, A. M. Musti, *Int. J. Biochem. Cell. Biol.* **2008**, *40*, 307-316 and references therein.
- [17] a) N. Bešker, C. Coletti, A. Marrone, N. Re, *J. Phys. Chem. B* **2007**, *111*, 9955-9964; b) J. Chen, L. Chen, S. Liao, K. Zheng, L. Ji, *J. Phys. Chem. B* **2007**, *111*, 7862-7869.
- [18] a) J. Raber, C. Zhu, L. A. Eriksson, *Mol. Phys.*, **2004**, *102*, 2537-2544; b) D. V. Deubel, *J. Am. Chem. Soc.*, **2006**, *128*, 1654-1663; c) M. E. Alberto, M. F. Lucas, M. Pavelka, N. Russo, *J. Phys. Chem. B*, **2009**, *112*, 10765-10768; d) M. F. Lucas, M. Pavelka, M. E. Alberto, N. Russo, *J. Phys. Chem. B*, **2009**, *113*, 831-838; e) M. E. Alberto, M. F. Lucas, M. Pavelka, N. Russo, *J. Phys. Chem. B*, **2009**, *113*, 14473-14479.
- [19] R. W. Hay, S. Miller, *Polyhedron*, **1998**, *17*, 2337-2343.
- [20] M. Galanski, B. K. Keppler, *Anticancer Agents Med Chem*, **2007**, *7*, 55-73 and references therein.

Rhenium(IV) Anticancer Agents

José Martínez-Lillo, Teresa F. Mastropietro, Rosamaria Lappano, Antonio Madeo, Marta E. Alberto, Nino Russo, Marcello Maggolini, and Giovanni De Munno

_____ Page – Page

Rhenium(IV) Compounds act as Anticancer Agents



Opening new perspectives in anticancer drug discovery: first study on the biological activity of Rhenium(IV)-based complexes.

Supporting Informations.

Anticancer Agents Based on Rhenium(IV) Compounds

José Martínez-Lillo, Teresa F. Mastropietro, Rosamaria Lappano, Antonio Madeo, Marta E. Alberto, Nino Russo, Marcello Maggiolini, and Giovanni De Munno.

S1. Experimental Section

S2. Crystallography

S3. Biological characterization

S4. HRESIMS

S5. Evaluation of cell growth by compounds 1, 2 and cisplatin in BG-1 ovarian (a-c) and LNCaP prostate (d-f) cancer cells, as determined using the MTT assay

S6. Evaluation of cell growth by compounds 3 and 4 in MCF-7 (a-b), BG-1 (c-d) and LNCaP (e-f) cancer cells, as determined using the MTT assay

S7. Additional Computational Details

S8. Computed relative free energies profiles (at 298.15 K) and optimized structures of the stationary points for the equatorial Cl⁻ substitution; a) complex 1, b) complex 2, in water phase

S9. Computed relative free energies profiles (at 298.15 K) and optimized structures of the stationary points for the release of ligand a) ReCl₄(bpy) and b) ReCl₄(bpym), in water phase

-S1-

Experimental Section

Materials. All chemicals and solvents used in the synthesis were of reagent grade and employed without further purification. Compounds [ReCl₄(bpy)] (**1**) and [ReCl₄(bpym)] (**2**) as well as ammonium hexachlororhenate(IV), (NH₄)₂[ReCl₆], were prepared according to literature procedures.

Physical Measurements. Elemental analyses (C, H, N) were performed by a CE Instruments EA 1110 CHNS analyzer and the Re/Cl molar ratio of 1:4 was determined for **1-4** by means of a Philips XL-30 scanning electron microscope (SEM) equipped with an X-ray microanalysis system. Infrared spectra were recorded with a Perkin-Elmer 1750 FTIR spectrophotometer as KBr pellets in the 4000-400 cm⁻¹ region. High resolution ESI MS spectra of compound **1-4** were acquired on a hybrid Q-Star Pulsar-i (MSD Sciex, Applied Biosystem, Toronto, Canada) mass spectrometer equipped with an ion spray ionization source. The instrument was calibrated using two standard flavonoids compound to achieve a mass accuracy less than 5 ppm. Analytes, dissolved in a solution of DMSO/H₂O 5:95 at a concentration of 25 mg/L, were introduced by direct infusion (3 μL/min) at the optimum ion spray (IS) voltage of 4800 V. The source

nitrogen (GS1) and the curtain gas (CUR) flows were set at pressures of 20 and 25 psi, respectively, whereas the first declustering potential (DP1), the focusing potential (FP), and the second declustering potential (DP2) were kept at 50, 220, and 10 V relative to ground, respectively

Synthesis of [ReCl₄(dmbpy)] (3) and [ReCl₄(phen)] (4). Compounds **3** and **4** were obtained by following a very similar procedure to that described for [ReCl₄(bpy)] (**1**). A mixture of ammonium hexachlororhenate(IV) (1.38 mmol) and dmbpy (**3**) or phen (**4**) (3.20 mmol) in 5 mL of DMF was refluxed under argon atmosphere during 2–3 h leading to a dark green solution. After cooling at room temperature, the solution was filtered and heated at 60 °C to eliminate fully the solvent. 50 mL of acetone were added to the residue thus obtained stirring for 20 min. Then, the insoluble solid was removed by filtration and discarded. Finally, 4–5 drops from a 0.5M HCl solution were added and by slow evaporation at room temperature brown-yellowish needles were formed in two weeks. Yield: ca. 35–40%. Anal. Calc. for C₁₂H₈N₂Cl₄Re (**3**): C, 28.36; H, 1.59; N, 5.51. Found: C, 28.30; H, 1.60; N, 5.53%. Anal. Calc. for C₁₂H₁₂N₂Cl₄Re (**4**): C, 28.14; H, 2.36; N, 5.47. Found: C, 28.50; H, 2.38; N, 5.12%. IR peaks associated to dmbpy ligand (**3**) appear at (cm⁻¹) 3080m, 1602s, 1550m, 1465s, 1440s, 952m, 770s, 720m and 651m; and those assigned to phen ligand (**4**) at (cm⁻¹) 3084m, 3056m, 1577m, 1516m, 1427s, 854s, 717s and 653w cm⁻¹.

-S2-

Crystallography.

Crystallographic Data Collection and Structure Determination. X-ray diffraction data were collected using a Bruker-Nonius X8APEXII CCD area detector diffractometer. Graphite-monochromated Mo-K α radiation ($\lambda = 0.71073 \text{ \AA}$) was used in all cases. The data were processed through the SAINT [1] reduction and SADABS [2] absorption software. The unit cell parameters, which are listed in Table 1 together with a summary of the structure refinement data, were based upon least-squares refinement of 5343 (**1**), 9318 (**3**) and 7277 (**4**) reflections. The structures were solved by direct methods and subsequently completed by Fourier recycling using the SHELXTL software package.[3]

Non-hydrogen atoms were refined anisotropically. Hydrogen atoms were set in calculated positions and refined as riding atoms. Full-matrix least-squares refinements on F², carried out by minimizing the function $R_w(|F_o| - |F_c|)^2$, reached convergence with values of the discrepancy indices given in Table 1. The graphical manipulations were performed using the XP utility of the SHELXTL system. Testing the two enantiomeric models of the crystal **1** with a final refined Flack parameter of 0.019(4) shows that the handedness was uniquely determined. CCDC reference numbers are 797402, 797403 and 797404 for complexes **1**, **3** and **4**, respectively.

[1] *SAINT-Ver. 6.45 Copyright (c)*, BrukerAnalyticalX-ray Systems, Inc., Madison, WI, USA, 2003.

[2] G. M. Sheldrick, *SADABS Program for Absorption Correction, Version 2.10*, Analytical X-ray Systems, Madison, WI, USA, 2003.

[3] *SHELXTL, Bruker Analytical X-ray Instruments*, Madison, WI, USA, 1998.

Figure 1. Perspective drawings of the structure of compounds **1**, **3** and **4** showing the atomic numbering scheme.

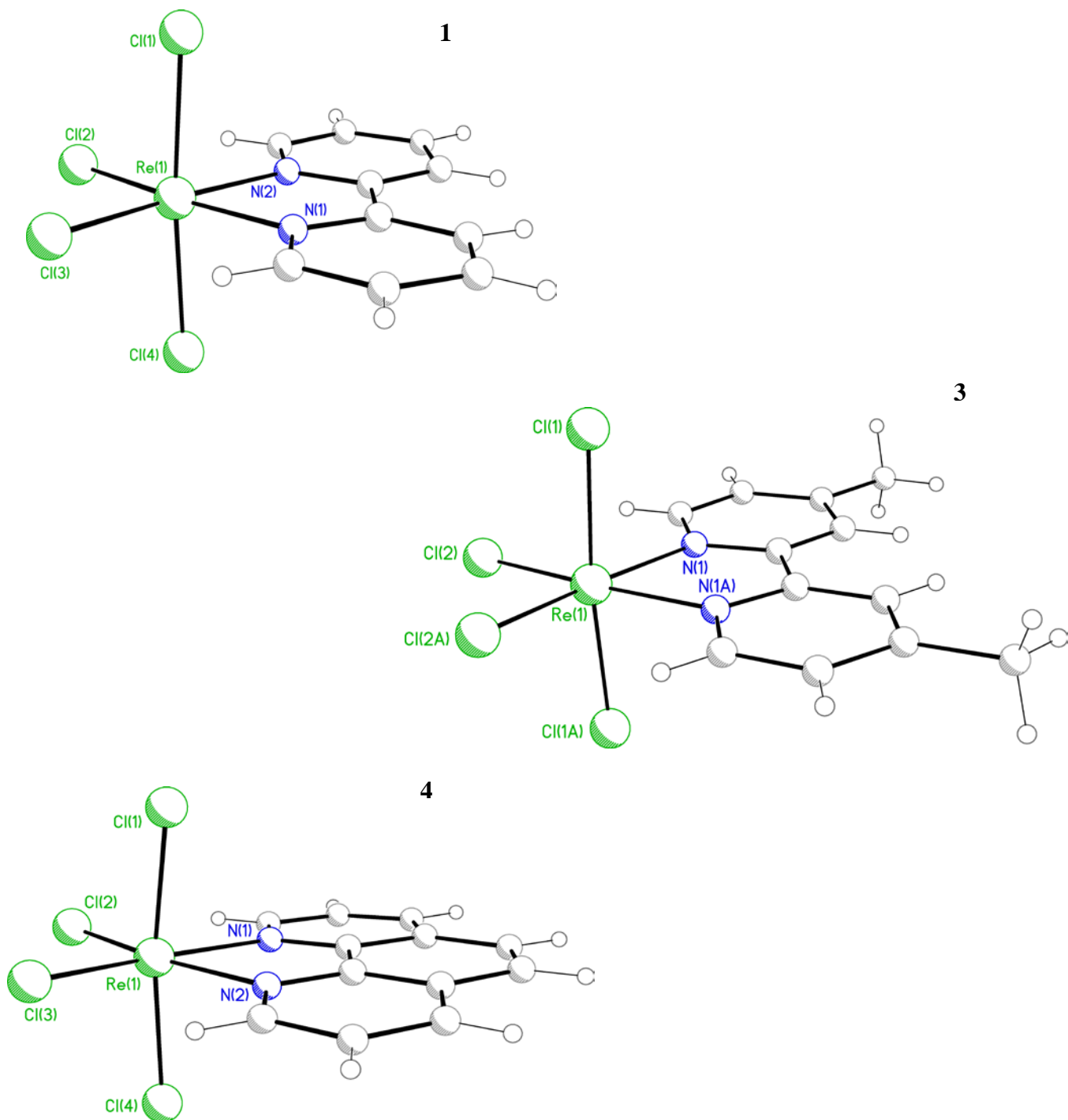


Table 1. Crystal data and structure refinement for compound **1**, **3** and **4**.

Compound	1	3	4
Empirical formula	C10H8Cl4N2Re	C12H12Cl4N2Re	C12H8Cl4N2Re
Formula weight	484.18	512.24	508.20
Crystal system	Monoclinic	Orthorombic	Monoclinic
Space group	Pn	Pccn	P2 ₁ /c
a/ Å	8.195(1)	6.9640(2)	7.5973(2)
b/ Å	6.737(1)	13.4511(4)	18.9753(6)
c/ Å	12.397(2)	17.4989(5)	10.3352(3)
β/°	104.45(1)		108.249(1)
V/ Å ³	662.73(16)	1639.18(8)	1415.00(7)
Z	2	4	4
D _c /g cm ⁻³	2.426	2.076	2.386
Absorption coefficient/mm ⁻¹	9.950	8.052	9.327
F(000)	450	964	948
Reflections collected	14857	32431	22670
Independent reflections	4276 [R(int) = 0.0242]	2674 [R(int) = 0.0257]	4255 [R(int) =
Data / restraints / parameters	4276 / 2 / 154	2674 / 0 / 88	0.0290]
Goodness-of-fit on F ²	0.767	1.180	4255 / 0 / 172
R ₁ [I>2σ(I)]	0.0158	0.0192	1.090
wR2	0.0278	0.0482	0.0721
Absolute structure parameter	0.019(4)		0.1809
Largest diff. peak and hole/ e.Å ⁻³	0.510 and -0.519	0.367 and -1.276	4.758 and -5.374

^aR1 = $\sum |F_o| - |F_c| / \sum |F_o|$; ^bwR2 = $\{ \sum [w(F_o^2 - F_c^2)^2] / [\sum (w(F_o^2)^2)] \}^{1/2}$; ^cw = $1 / [\sigma^2(F_o^2) + (aP)^2 + bP]$; with $P = [F_o^2 + 2F_c^2] / 3$, a = 0 (1), 0.0205 (3), 0.0623 (4);
b = 0 (1), 1.22 (3), 28.10 (4).

Table 2. Bond lengths [\AA] and angles [$^\circ$] for **1**.

Re(1)-N(2)	2.118(2)	N(1)-Re(1)-Cl(2)	171.44(6)
Re(1)-N(1)	2.120(2)	Cl(3)-Re(1)-Cl(2)	94.00(3)
Re(1)-Cl(3)	2.3148(7)	N(2)-Re(1)-Cl(4)	87.94(6)
Re(1)-Cl(2)	2.3164(7)	N(1)-Re(1)-Cl(4)	87.92(6)
Re(1)-Cl(4)	2.3278(7)	Cl(3)-Re(1)-Cl(4)	92.32(3)
Re(1)-Cl(1)	2.3312(7)	Cl(2)-Re(1)-Cl(4)	91.11(3)
		N(2)-Re(1)-Cl(1)	87.56(6)
N(2)-Re(1)-N(1)	77.15(8)	N(1)-Re(1)-Cl(1)	88.28(6)
N(2)-Re(1)-Cl(3)	171.67(6)	Cl(3)-Re(1)-Cl(1)	91.72(3)
N(1)-Re(1)-Cl(3)	94.54(6)	Cl(2)-Re(1)-Cl(1)	92.09(3)
N(2)-Re(1)-Cl(2)	94.31(6)	Cl(4)-Re(1)-Cl(1)	174.65(3)

Table 3. Bond lengths [\AA] and angles [$^\circ$] for **3**.

Re(1)-N(1)	2.114(2)	Cl(2A)-Re(1)-Cl(2)	93.24(4)
Re(1)-Cl(2)	2.3174(6)	N(1)-Re(1)-Cl(1a)	88.99(6)
Re(1)-Cl(1)	2.3290(7)	N(1)-Re(1)-Cl(1)	86.42(6)
		Cl(2A)1-Re(1)-Cl(1)	91.60(3)
N(1A)-Re(1)-N(1)	76.91(10)	Cl(2)-Re(1)-Cl(1)	92.43(3)
N(1)-Re(1)-Cl(2a)	171.64(5)	Cl(1)-Re(1)-Cl(1a)	174.14(4)
N(1)-Re(1)-Cl(2)	94.95(5)		

Symmetry transformations used to generate equivalent atoms: a) $-x+5/2, -y+3/2, z$

Table 4. Bond lengths [Å] and angles [°] for **4**.

Re(1)-N(1)	2.143(8)	N(2)-Re(1)-Cl(3)	93.8(2)
Re(1)-N(2)	2.164(8)	Cl(2)-Re(1)-Cl(3)	95.7(2)
Re(1)-Cl(2)	2.166(4)	N(1)-Re(1)-Cl(1)	87.6(3)
Re(1)-Cl(3)	2.289(3)	N(2)-Re(1)-Cl(1)	86.3(2)
Re(1)-Cl(1)	2.331(3)	Cl(2)-Re(1)-Cl(1)	92.6(2)
Re(1)-Cl(4)	2.344(3)	Cl(3)-Re(1)-Cl(1)	90.6(1)
		N(1)-Re(1)-Cl(4)	88.2(2)
N(1)-Re(1)-N(2)	76.8(3)	N(2)-Re(1)-Cl(4)	86.0(2)
N(1)-Re(1)-Cl(2)	93.7(3)	Cl(2)-Re(1)-Cl(4)	94.6(2)
N(2)-Re(1)-Cl(2)	170.5(2)	Cl(3)-Re(1)-Cl(4)	92.5(1)
N(1)-Re(1)-Cl(3)	170.5(3)	Cl(1)-Re(1)-Cl(4)	171.9(1)

-S3-

HRESIMS

compound **1** m/z 447.9296 [M-Cl]⁺ (calculated m/z 447.9305), m/z 465.9416
[M-Cl+H₂O]⁺ (calculated m/z 465.9410).

compound **2** m/z 449.9223 [M-Cl]⁺ (calculated m/z 449.9210), m/z 467.9321
[M-Cl+H₂O]⁺ (calculated m/z 467.9315).

compound **3** m/z 475.9625 [M-Cl]⁺ (calculated m/z 475.9618), m/z 493.9740
[M-Cl+H₂O]⁺ (calculated m/z 493.9723).

compound **4** m/z 472.9389 [M-Cl]⁺ (calculated m/z 472.9383), m/z 490.9475
[M-Cl+H₂O]⁺ (calculated m/z 490.9483).

Biological characterization.

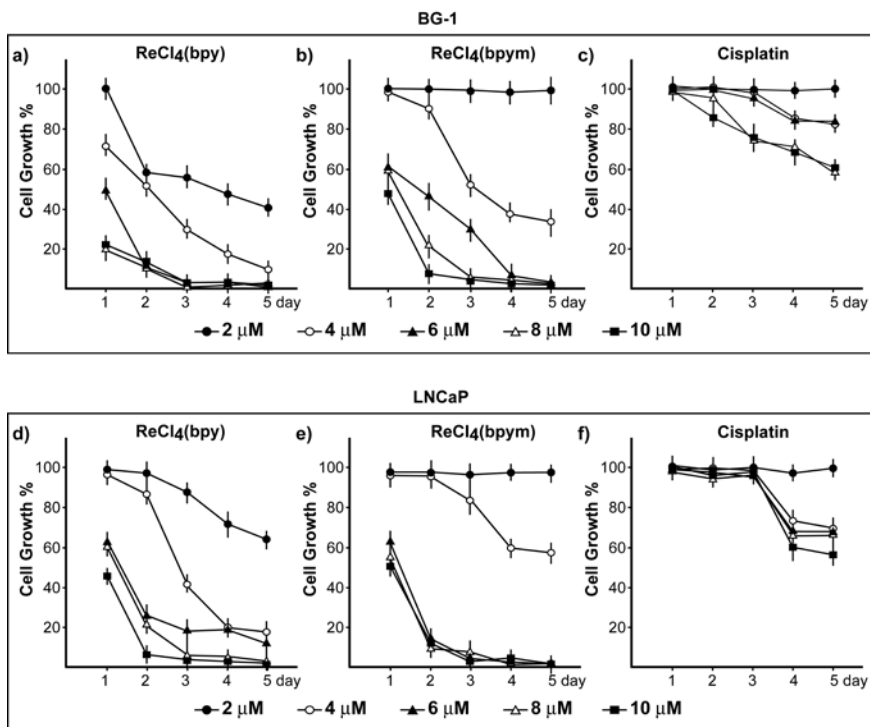
Cell culture. MCF-7 breast and LNCaP prostate cancer cells were cultured in DMEM and RPMI 1640, respectively, with phenol red supplemented with 10% fetal bovine serum (FBS). BG-1 ovarian cancer cells were maintained in DMEM without phenol red supplemented with 10% FBS. Cells were switched to medium without serum the day before experiments for immunoblots.

Growth assay. The effects of each compound on cultured cells were measured using the MTT [3-(4,5-dimethylthiazol-2-yl)-2,5-diphenyltetrazolium bromide] assay, which is based on the conversion of MTT to MTT-formazan by mitochondrial enzyme. Cells were seeded in regular growth medium and grown until 70-80% confluence. Cells were washed once they had attached and then treated with different concentrations of agents (2-10 μ M) for the indicated time (for one day up to 5 days). Relative cell viability was monitored/determined by MTT assay according to the manufacturer's protocol (SigmaAldrich, Milan, Italy).

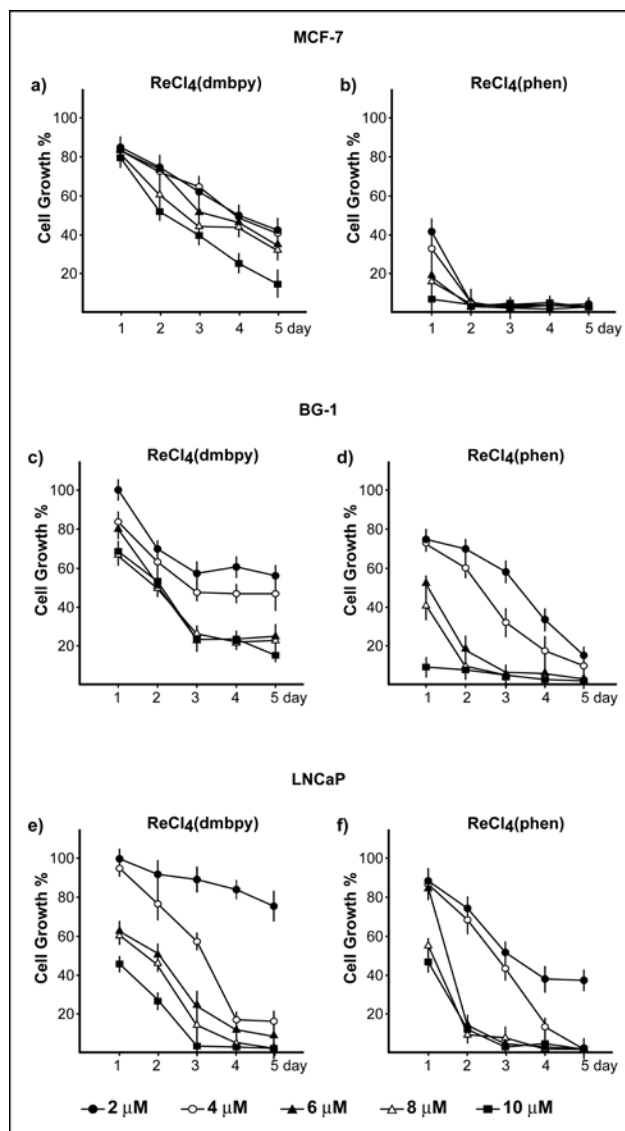
Immunoblotting. Cells were grown in 10-cm dishes, exposed to treatments and then lysed in 50 mM HEPES (pH 7.5), 150 mM NaCl, 1.5 mM MgCl₂, 1 mM EGTA, 10% glycerol, 1% Triton X-100, 0.1% SDS, and a mixture of protease inhibitors (Boeringher). Equal amounts of whole protein extract were resolved on a 10% PAGE, transferred to a nitrocellulose membrane (Amersham Biosciences, Arlington Heights, IL), probed overnight at 4°C with the antibodies against p-c-JunS73 and c-Jun, (from Santa Cruz Biotechnology) and then revealed using the enhanced chemiluminescence system (Amersham Biosciences).

TUNEL assays. Cells were seeded in 2-well Lab-TekII chamber slides at a density of 1×10^5 /well and incubated for 24 h in the corresponding maintenance media. Cells were then switched to medium without serum and treated with vehicle (DMSO), compound **1**, compound **2** and cisplatin. For the detection of DNA fragmentation at the cellular level, cells were stained using DeadEnd™ Fluorometric TUNEL System (Promega Milan, Italy) following the manufacturer's instructions. Nuclei of cells were stained with propidium iodide (1:1000) (Sigma-Aldrich Milan, Italy). Leica AF6000 Advanced Fluorescence Imaging System supported by image processing software Leica Application Suite Advanced Fluorescence (Leica Microsystems CMS, GbH Mannheim, Germany) were used for experiment evaluation.

Evaluation of cell growth by compounds 1, 2 and cisplatin in BG-1 ovarian (a-c) and LNCaP prostate (d-f) cancer cells, as determined using the MTT assay.



Evaluation of cell growth by compounds 3 and 4 in MCF-7 (a-b), BG-1 (c-d) and LNCaP (e-f) cancer cells, as determined using the MTT assay.

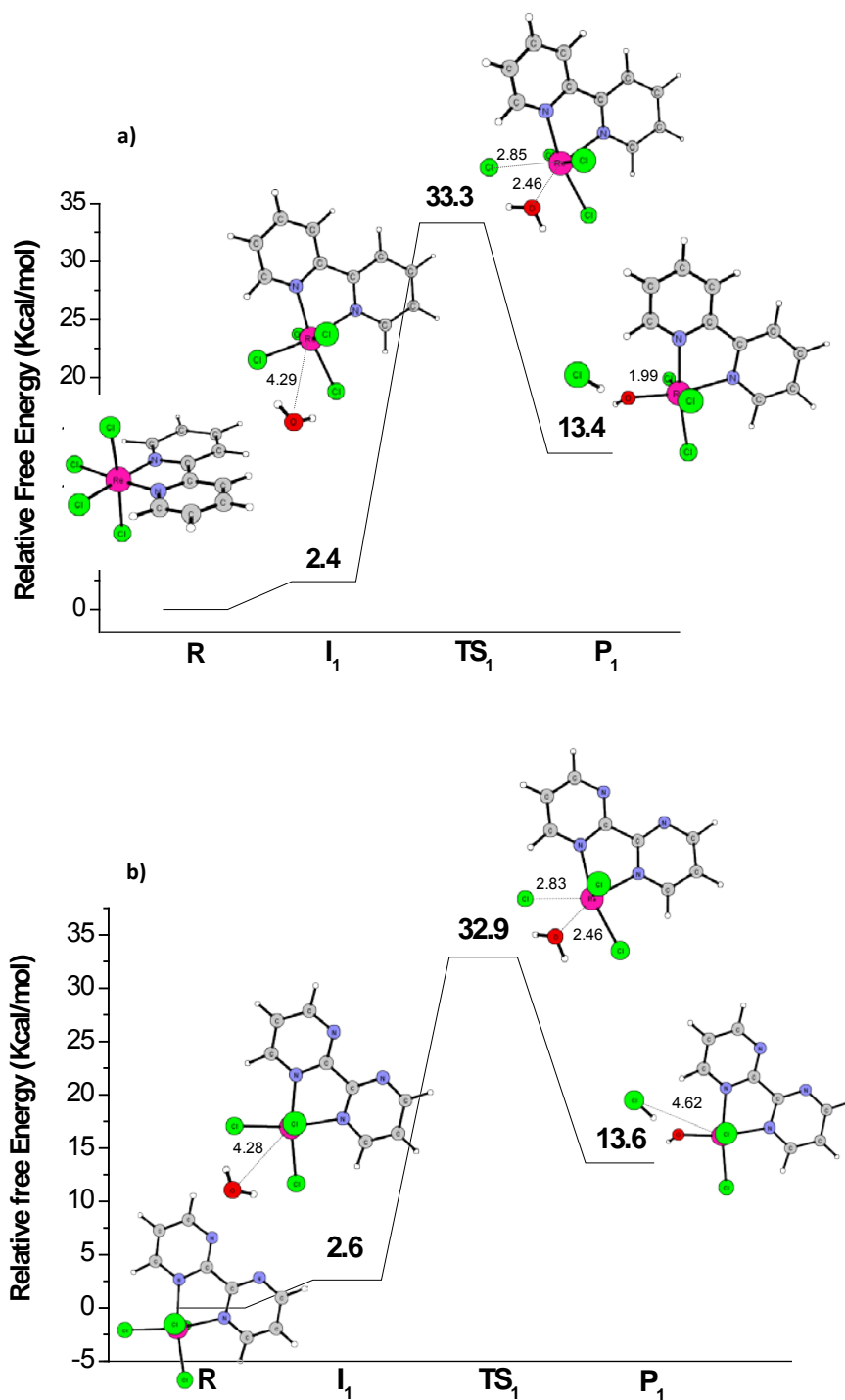


Additional Computational Details

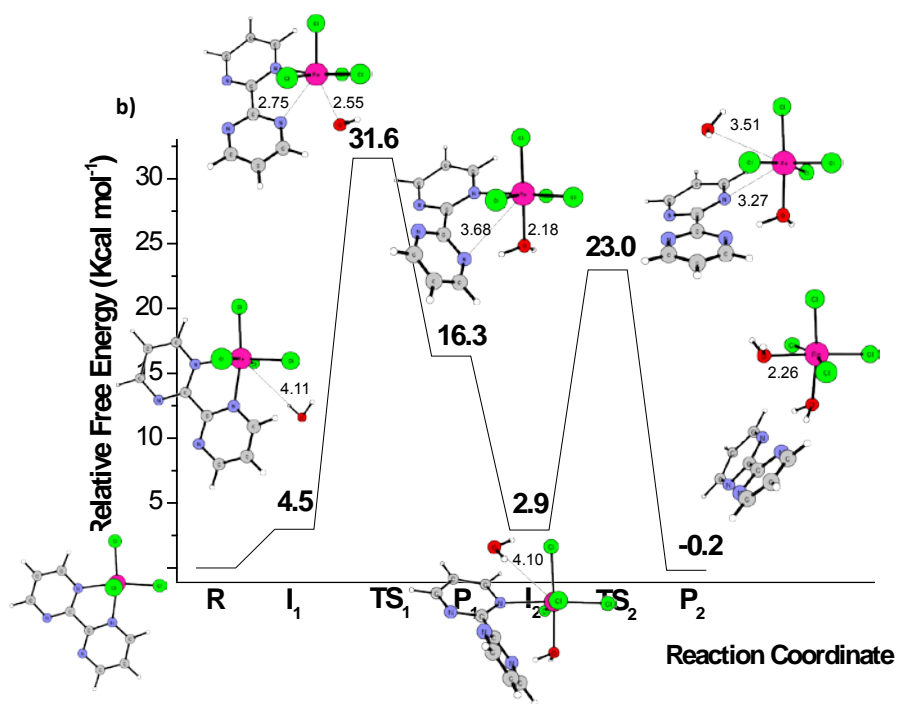
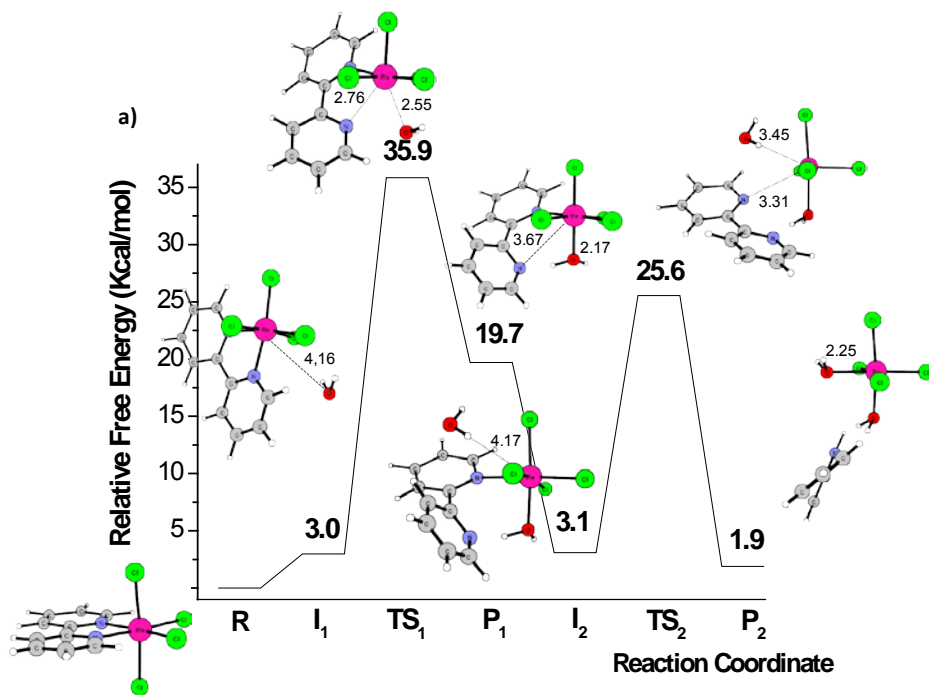
All calculations were performed with GAUSSIAN 03 [1] program at Density Functional Theory level, using the hybrid B3LYP functional, composed by Becke's [2] three-parameter hybrid exchange functional (B3) and the correlation functional of Lee, Yang and Parr (LYP) [3]. Geometry optimizations without symmetry constraints were carried out with a 6-31G(d) basis sets for all atoms except the Rhenium atom, which was described by the quasi-relativistic Stuttgart-Dresden pseudopotentials [4]. In order to confirm proper convergence to equilibrium and transition state geometries, vibrational frequency analysis were done based on analytical second derivatives of Hamiltonian at this level of theory. Solvent effects were taken into account performing single point calculations (SP) by the CPCM method employing a dielectric constant of $\epsilon = 80$ [5]. Klamt radii were used for constructing the solute cavity [6]. On the optimized structures, SP energy calculations were also carried out with the larger basis set 6-31++G(2df,2pd) in gas phase and in water.

- [1] Frisch, M. J.; Trucks, G. W.; Schlegel, H. B.; Scuseria, G. E.; Robb, M. A.; Cheeseman, J. R.; Montgomery, J. A.; Vreven, J., T.; Kudin, K. N.; Burant, J. C.; Millam, J. M.; Iyengar, S. S.; Tomasi, J.; Barone, V.; Mennucci, B.; Cossi, M.; Scalmani, G.; Rega, N.; Petersson, G. A.; Nakatsuji, H.; Hada, M.; Ehara, M.; Toyota, K.; Fukuda, R.; Hasegawa, J.; Ishida, M.; Nakajima, T.; Honda, Y.; Kitao, O.; Nakai, H.; Klene, M.; Knox, X. L., J. E.; Hratchian, H. P.; Cross, J. B.; Adamo, C.; Jaramillo, J.; Gomperts, R.; Stratmann, R. E.; Yazyev, O.; Austin, A. J.; Cammi, R.; Pomelli, C.; Ochterski, J. W.; Ayala, P. Y.; Morokuma, K.; Voth, G. A.; Salvador, P.; Dannenberg, J. J.; Zakrzewski, V. G.; Dapprich, S.; Daniels, A. D.; Strain, M. C.; Farkas, O.; Malick, D. K.; Rabuck, A. D.; Raghavachari, K.; Foresman, J. B.; Ortiz, J. V.; Cui, Q.; Baboul, A. G.; Clifford, S.; Cioslowski, J.; Stefanov, B. B.; Liu, H.; Liashenko, A.; Piskorz, P.; Komaromi, I.; Martin, R. L.; Fox, D. J.; Keith, T.; Al-Laham, M. A.; Peng, C. Y.; Nanayakkara, A.; Challacombe, M.; Gill, P. M. W.; Johnson, B.; Chen, W.; Wong, M. W.; Gonzalez, C.; Pople, J. A. Gaussian 03, Revision A.1; Gaussian, Inc.: Pittsburgh PA, 2003.
- [2] Becke, A. D. *J. Chem. Phys.* 1993, 98, 5648.
- [3] Lee, C. T.; Yang, W. T.; Parr, R. G. *Phys. Rev. B* 1988, 37, 785.
- [4] Andrae, D.; Haussermann, U.; Dolg, M.; Stoll, H.; Preuss, H. *Theor. Chim. Acta* 1990, 77, 123.
- [5] (a) Klamt, A.; Schüürmann, G. *J. Chem. Soc., Perkin Trans. 2* 1993, 799. (b) Andzelm, J.; Kölmel, C.; Klamt, A. *J. Chem. Phys.* 1995, 103, 9312. (c) Barone, V.; Cossi, M. *J. Phys. Chem. A* 1998, 102, 1995. (d) Cossi, M.; Rega, N.; Scalmani, G.; Barone, V. *J. Comput. Chem.* 2003, 24, 669.
- [6] Klamt, A.; Jonas, V.; Burger, T.; Lohrenz, J. C.W.; *J. Phys. Chem. A*, 1998, 102, 5074.

Computed relative free energies profiles (at 298.15 K) and optimized structures of the stationary points for the equatorial Cl⁻ substitution in water phase. a) compound 1, b) compound 2.



Computed relative free energies profiles (at 298.15 K) and optimized structures of the stationary points for the release of ligand in water phase. a) compound 1, b) compound 2.





Part 2

A common structural feature found in approximately one-third of all enzymes purified is the presence in the active site of one or more metal ions, optimally conditioned by protein structure and environment, in order to accomplish a specific biological function. Understanding why some enzymes employ a different number of metal ions to work is one of the most intellectually attractive and experimentally demanding frontiers in modern bioinorganic chemistry. Our understanding of enzymatic catalysis has evolved slowly, in parallel with the development of experimental tools to probe chemical and kinetic mechanisms. The relatively recent explosion of computational power, made it possible to model enzyme active sites and reaction mechanisms in a quite realistic way. Several studies have been done in order to give better insights on how metal ions and their scaffolds can promote biochemical reactions. Many mechanistic problems have then been addressed and solved and it is increasingly clear that computational contribution in the field of Bioinorganic Enzymology is crucial in order to provide a full understanding of catalysis.

4

Metallohydrolases

*On the functional roles of binuclear metal
center in enzyme's active site*

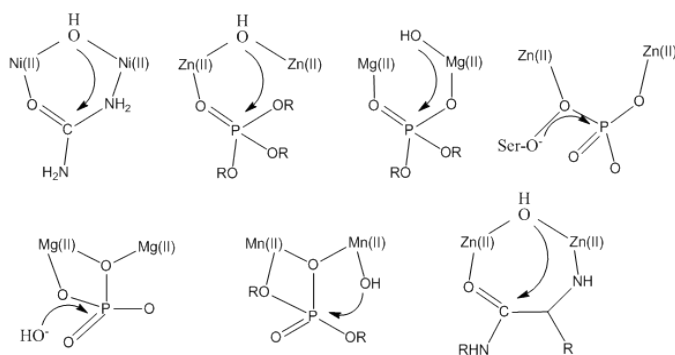
Introduction

Metalloenzymes are widespread proteins, ubiquitous in all life kingdoms, being involved in various biosynthetic processes. They require one or more metal ions for full activity and represent approximately one-third of the known enzymes.¹ The metal ions promote a variety of reactions in these enzymes, including bond cleavage and formation, electron transfer, atom transfer, and radical chemistry. Among these, binuclear metalloenzymes have received in the last years a special attention.²⁻⁷ Binuclear sites and their scaffold in enzymes appear to have several potentially useful properties not found in mononuclear centers. In the context of a metalloenzyme, a scaffold can be defined as a framework of atoms and bonds that supports the activity of the metal ions. The precise role of the protein scaffold, catalytic or structural, is still not well defined, being it subject of a heated debate. The two metals can work more or less independently, being required for distinct functions either structural or catalytic, or alternatively, catalyzing different steps in a multistep sequence. The individual metal ions in a bimetallic center can exhibit independent physicochemical properties in cases where the metal ions are decoupled by larger polyatomic bridging ligands which also electrostatically screen the metals (i.e., μ -carboxylate, μ -imidazolate). By contrast, in many cases the distinct functions are not completely independent. An interaction between the sites is generally observed in many bimetallic enzymes when they share a monoatomic or conjugated bridging ligand (i.e., μ -aqua, μ -hydroxo, μ -oxo) and particularly when they possess uncompensated (net) charges.⁸ In these conditions, the metal ions exhibit strongly correlated physicochemical properties appearing essential for catalysis. Possible examples being hydrolytic metalloenzymes.

4.1 Binuclear Metallohydrolases

Metallohydrolases use binuclear metal ion centers to catalyze the hydrolysis of amides and esters of carboxylic and phosphoric acids. ⁹Each metal ion seems to be employed for different functions although they are connected by bridging ligands, leading in some cases to a coupled binuclear center in the active site. Binuclear Metallohydrolases is an interesting family of enzymes whose members have been recognized as potential targets for the development of chemotherapeutics and for drug design against a wide variety of human disorders, including osteoporosis, cancer, cystic fibrosis, and depression. Moreover they represent also a promising candidates in bioremediation since they can be modified to degrade pesticides or organophosphorus nerve gases. Similarities in the first coordination shell can be found across the entire family of Binuclear Metallohydrolases and, although the identity of the nucleophiles and the nature of the metals are different, they are suggested to employ variants of similar basic mechanism to work. ² Some examples of this family are collected in Scheme1.

Scheme 4.1: Schematic illustration of some proposed mechanisms for binuclear metallohydrolases



The focus here is on the elucidation of the catalytic mechanisms of binuclear metallohydrolases by examining two related enzymes, purple acid phosphatases (PAPs) and prolidase.

Each description of the metallohydrolases under investigation is followed by a section regarding our work in which the purposes of the computations, the various models proposed for the hydrolytic reaction mechanism and the roles of each metal ions in catalysis are discussed.

4.2 Modeling enzymatic reactions: Cluster Models

One clear trend in the computational modeling of enzymatic reactions in recent year has been to use relatively small cluster models of enzyme active sites and apply accurate quantum chemical methods to study their reaction mechanisms.¹⁰⁻¹⁴ The advances made in hybrid density functional theory (DFT) methods and the tremendous and continuous growth of computer power made it possible to model enzyme active sites large enough to reproduce the reaction mechanisms in a quite realistic way. With such a model (≈ 120 atoms), it is generally possible to identify all structural changes in the model during a reaction and make certain that these changes are not artifacts of the model. A quantum chemical study of a reaction mechanism implies the determination of all intermediates and transition states along the reaction path. The approach of modelling small clusters has proved particularly fruitful in the modelling of the catalytic reaction mechanisms of metalloenzymes, since all the important chemical steps take place at the metal ions and their immediate environment.^{11,16} Actually, a large portion of the catalysis is dictated by the electronic structure of the metal ions. A correct model of a metal active site should hence represent the electronic structure of the metal correctly.

Typically, the available X-ray structures of the enzyme is used to devise a cluster model, by cut out a relatively small portion of it where the reaction is supposed to take place. The primary coordination sphere of ligating atoms that are directly attached to the metal ions must be included in the model. The secondary coordination sphere, which includes residues that are near but not directly attached to the bimetallic center, in some extent can be considered as

part of the scaffold, since the properties of some of them can strongly influence the reactivity of the metal ions. Only the side chains of the residues included in the active site were kept in cluster model hence making use of small molecules to represent important functional groups. To keep the model reasonably close to the X-ray structure and in order to mimic the steric effects produced by the surrounding protein, the carbon atoms where truncation is done are kept fixed to their crystallographic positions¹⁷ during the optimizations. This approach ensures structural integrity of the model yet allowing some flexibility of the various groups. Again, the error made by this approximation becomes smaller as the freezing points move further away from the active site, i.e., as the size of the quantum model increases.

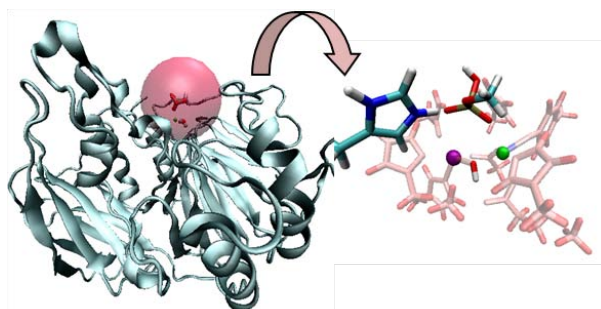


Figure 4.1: Active site cluster model extracted from the X-Ray structure of an enzyme

To account for the polarization effects caused by the part of the surrounding enzyme that is not explicitly included in the quantum model, cavity techniques can be used. This approximation assumes that the surrounding is a homogenous polarizable medium with some dielectric constant, usually chosen to be $\epsilon = 4$ for protein environment. Nevertheless, when a large model of the active site is used, most of the polarization effects are already explicitly included in the quantum calculations. This, in addition to the fact that the solvation effect saturates very quickly as a function of ϵ , makes the particular choice of the dielectric constant less critical. The solvation energies are usually

calculated as single points on top of the gas-phase optimized geometries by means of DFT/CPCM approach.

The following applications will illustrate some of the points concerned with the modeling of metal active sites as well as the reliability of such approach in exploring the reaction mechanism of metalloenzymes.

4.3 Purple acid phosphatases

Purple acid phosphatases¹⁸⁻²⁰ (E.C. 3.1.3.2) are the only binuclear metallohydrolases that use an heterovalent active site Fe(III)-M(II) to catalyze the hydrolysis of monophosphates at acidic to neutral pH.¹⁸⁻²⁵ The identity of the divalent metal ion varies with the source of the enzyme. Mammalian PAPs contain an antiferromagnetically coupled binuclear iron center Fe(III)-Fe(II)²⁶⁻³² in the active site, while plant PAPs most typically have Fe(III)-Zn(II)^{25, 33-35} centers although an interesting example of an enzymatically active binuclear Fe(III)-Mn(II) center was found in the case of PAP from sweet potato.^{23,24,36} Purple acid phosphatase from the red kidney bean (*rkbPAP*) object of our investigation, was the first member of this family for which a crystal structure became available and is by far the most explored in the years.^{37,38}

In spite of the scarce similarity in the primary sequences of mammalian and plant PAPs, the active site structure and the residues coordinating the metal ions are identical. Consequently they display similar enzymatic and spectroscopic properties.³⁹ The identity of their active sites has been demonstrated in several studies by using the metal ion replacement and by spectroscopic⁴⁰⁻⁴⁸ and magnetochemical measurements,⁴⁹⁻⁵⁰ giving evidence that they employ similar mechanism to work. For this reason, the full understanding of *rkbPAP* behavior can contribute to major advancement of our current understanding of the catalytic mechanisms that operate in PAPs enzymes. Moreover sequence alignment of *rkbPAP* with porcine TRAP suggested that *rkbPAP* is a good model also for the structure and mechanism of other acid phosphatase.⁵¹

4.3.1 Computational Investigation on the Catalytic Mechanism of Fe(III)-Zn(II)PAP (Paper VII)

Despite the accumulation of structural spectroscopic and kinetic data, the individual steps of the PAPs-catalyzed hydrolysis reaction remain a matter of controversy. The general mechanism proposed in literature for PAP-catalyzed reactions involves a nucleophilic attack performed by the bridging hydroxide to the phosphorus center leading to hydrolytic cleavage of the phosphate-ester bond and to the release of the leaving group activated by a proton-shift from an histidine residue. Several crucial aspects are still uncertain such as the binding mode of the substrate in the active site prior the hydrolysis. The crystal structure of red kidney bean PAP determined in the presence of the inhibitor phosphate, is likely to illustrate the phase of catalysis in which the reaction product phosphate is still bound to the active site. That structure reveal that both the metal ions are involved in that step but doesn't give any indication about the effective role of each one and also, about the coordination of the substrate in the pre-catalytic complex.

In order to better characterize the several steps of the catalytic mechanism of the Fe(III)-Zn(II)-PAP (from *rkb*PAP), we performed for the first time an extensive theoretical exploration of the hydrolysis process, providing characterization of the transition states and intermediates involved, and presenting the potential energy profiles for the reaction in different environment (gas phase, protein environment and water). Moreover our computations can contribute to give important insights into some interesting aspects concerning the pre-catalytic complex and the substrate coordination mode into the active site prior to hydrolysis.

4.3.1.1 *rkbPAP* Active Site and Cluster Model

The crystal structure of red kidney bean PAP, determined in the presence of phosphate acting as inhibitor (PDB code 4kbp, chain A),³⁸ was used to devise a model of the active site of the enzyme. The latter contains the metal ions Fe(III) and Zn(II) and the seven amino acids of their first shell ligands: three histidines, two aspartates, a tyrosine and an asparagine residues. Although ENDOR measurements supported the presence of a water molecule terminally coordinated to the divalent metal ion, it was not included in our model since the formation of the pre-catalytic complex has been suggested to cause the expulsion of this labile terminal water ligand.⁵²

In addition, the crystal structures of PAPs determined in the presence of phosphate, both product and competitive inhibitor of the reaction, show a network of hydrogen bonds with uncoordinated histidine residues of the second shell of the ligands (His 202 and His 296 for *rkbPAP*), which could play therefore essential roles in catalysis. Although the importance of these conserved histidine has been demonstrated by site-directed mutagenesis studies,^{41,53} it's still not clear the effective role of each one in the stabilization of the substrate in the catalytic cavity. For this reason His 296 and His 202 of the second shell of the ligands were also included into the model, in order to elucidate their roles in the catalytic cycle. Only the side chains of the residues were kept in our model. Moreover the carbon atoms where truncation was done were kept fixed to their X-ray crystal positions during the optimizations to avoid an unrealistic expansion of the cluster during the calculations. This procedure gives rise to smaller imaginary frequencies but the latter does not significantly contribute to the ZPE and can thus be tolerated.

In the absence of crystallographic data for the enzyme-substrate complex (ES), the chosen methyl-phosphate was modelled in the active site after an accurate evaluation of several crucial aspects such as the substrate's orientation into the active site, its protonation state and the coordination binding mode to the dimetallic centre. The cluster model was completed including a bridging

hydroxide as nucleophile, whose presence was sustained by electron density maps and EXAFS studies.^{54,57} The resulting cluster contains 114 atoms. In order to establish the most stable spin multiplicity of the system, preliminary calculations on the ES complex with different values of spin multiplicity ($2S+1=2,4,6,8$) were performed. The lowest energy was obtained with a value of 6, which arises from a high spin configuration of the Fe(III) centre, in agreement with EPR measurements that support our result²⁴.

4.3.1.2 Function of the binuclear metal center in the catalytic process

In the ES structure the substrate binds in a monodentate-like manner the Fe(III) site resulting in an ideal near-attack configuration⁵⁸ and with the leaving group optimally oriented along the axis of the access channel to easily leave the active site after the hydrolysis process.

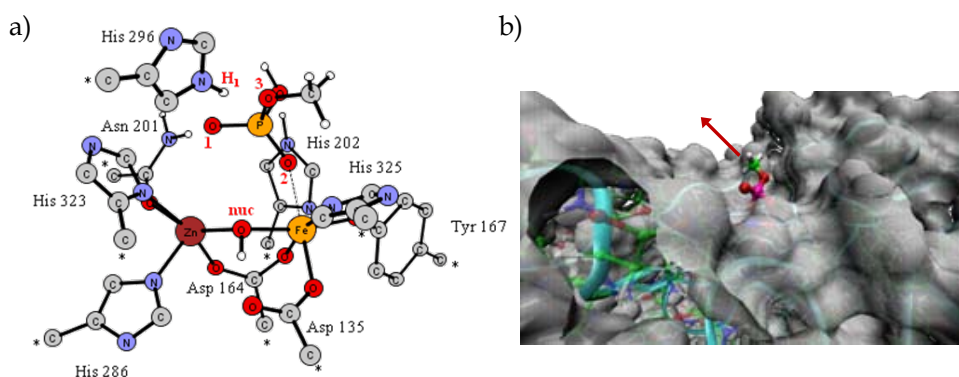


Figure 4.2: a) Optimized structure of the enzyme-substrate complex. Only the most significant hydrogen atoms are reported. Stars indicate the atoms kept fixed to their crystallographic positions during optimizations; b) Orientation of the methyl phosphate group into the enzymatic channel. B3LYP optimized coordinates of the active site introduced in the crystallographic file of the *rkbPAP* (pdb code 4KBP).

According to our calculation, the first step of the reaction involve a nucleophilic attack of the bridging hydroxide to the substrate-phosphorus atom (TS_1) leading to the first enzyme-intermediate complex (INT_1). (Figure 4.3).

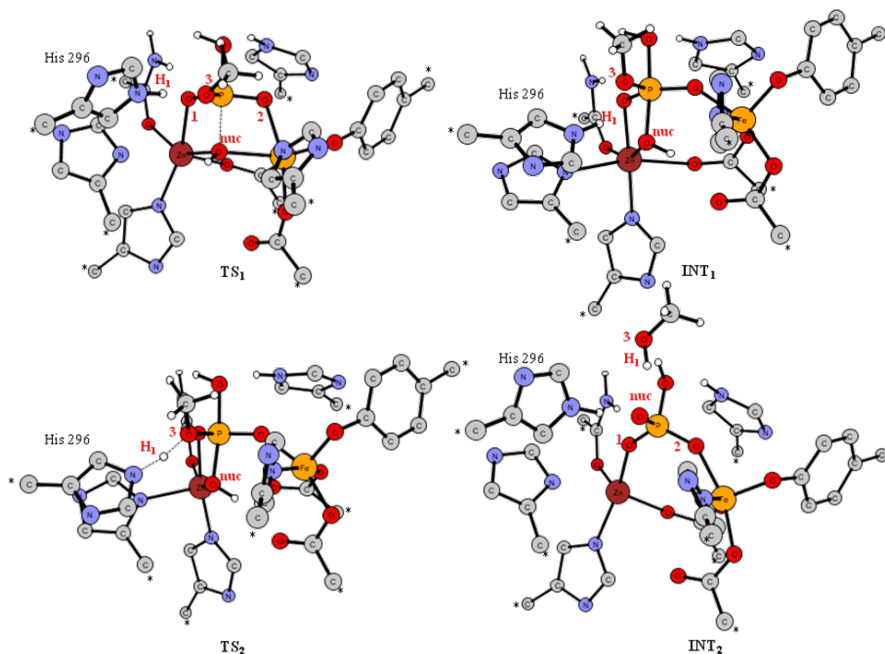


Figure 4.3: Optimized structures of the stationary points TS_1 , INT_1 , TS_2 and EP for the hydrolysis of the methyl-phosphate promoted by *rkb*-PAP enzyme. Stars indicate the atoms kept fixed to their crystallographic positions during optimizations. Only the most significant hydrogen atoms are reported in the figure.

The first transition state (TS_1) induces a cascade of geometric changes in the substrate coordination mode to the active site. The methyl-phosphate group binds now in a bidentate manner the dimetallic center. The bridging coordination geometry adopted led to an elongation of the Zn-Fe distance consenting to increase the nucleophilicity of the metals-bound hydroxide. Therefore the second metal ion seems to be required to allow a larger charge delocalization binding the substrate. A trigonal bipyramidal geometry was found for the phosphorus atom in the intermediate complex (INT_1) in which the P-O_{nuc} bond is completely formed. This mode of coordination has been

observed in the crystal structures of sweet potato PAP⁵⁹ and di-Ni(II) urease⁶⁰, both with bound phosphate, and di-Mn(II) λPP⁶¹, with bound sulfate. Although the substrate remains still bicoordinated to the dimetallic centre, the distance between the Zn and Fe ions increases significantly and the bridging hydroxide is completely shifted away from the trivalent metal ion toward the divalent one. The lengthening of the metal-metal distance was already suggested in a previous work, in which the binding of the substrate has been shown to decrease the coupling interaction between the two metal centers, as indicated by a decrease in J from 20 to 6 cm⁻¹.⁵⁴ To get the final product, a proton shift from the His 296 to the substrate's methylated oxygen atom was observed in the second transition state TS₂. Subsequent structural rearrangements culminate in the INT₂ structure and in the complete loss of the protonated leaving group. The product of the reaction results still bicoordinated to the dimetallic centre.

4.3.1.3 Energetic of the reaction

Different exchange-correlation functionals were used to estimate the energies of the stationary points located on the paths in gas phase and in different environment (water and proteic). This benchmark could be interesting since a large number of density functionals at different levels of sophistication has become available and a well-established computation protocol for the enzymatic reaction is still lacking. A detailed analysis of the performance of the popular B3LYP functional in the reproduction of a large variety of chemical properties and system types was performed in a recent study.⁶² The latter shows that the B3LYP performance in the prediction of geometrical structures including closed-and open -shell structures is satisfactory and is able to compete in accuracy with the other proposed XC functional, as well as with other ab-initio methods.

On the contrary, for some properties several new density functionals significantly outperform this popular hybrid functional. Many studies have

demonstrated that the Hybrid-meta GGA methods give more reliable results in the reproduction of the reaction kinetics showing great ability in the calculation of barrier heights with high accuracy.⁶² Taking these aspects under consideration, in our investigation we chose the B3LYP functional for the optimizations of all the stationary points along the reaction path and, to obtain energetic values, we performed single point calculation with a larger basis set testing the hybrids B3LYP, PBE0PBE and the meta-hybrids BB1K, MPWB1K, MW1B95.

The energy barriers calculated using meta-hybrids functional, better agree with those extracted from the k_{cat} experimentally obtained for reactions catalyzed by PAPs enzymes (13-15 Kcal/mol depending from the substrate),^{23,59,63} confirming their ability in the reproduction of the reaction kinetics. On the contrary, the profiles obtained at B3LYP and PBE0PBE levels of theory show higher energy results.

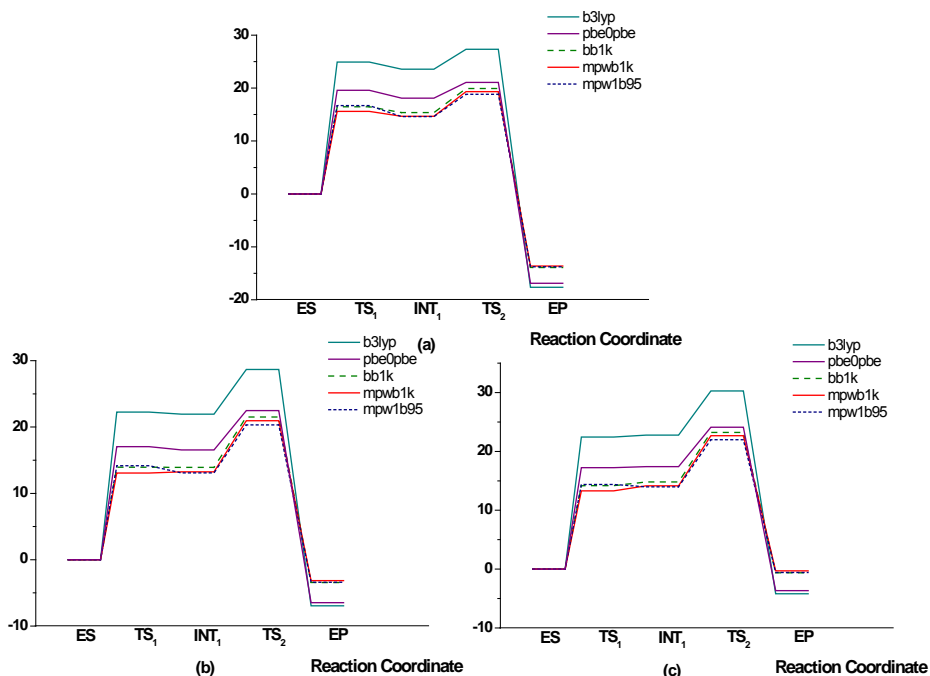


Figure 4.4: Potential Energy Profiles for the Reaction (a) in gas phase, (b) $\epsilon=4$, (c) $\epsilon=80$

4.4 Prolidases

Prolidases (EC 3.4.13.9) are the only metalloenzymes, among the peptidases, able to catalyze the hydrolysis of the imide bond between an α -carboxyl group and proline or hydroxyproline residue at the C-terminal end. This kind of bonds are not susceptible to generic peptidase cleavage, having proline its side chain cycling back to the backbone amino group and generating a pyrrolidine ring not easy to be hydrolysed.⁶⁴ Only a limited number of mammalian peptidases are known to be able to hydrolyse proline adjacent bonds and their activity is influenced by the isomeric state (cis-trans) as well as by the position of proline in the peptide chain. All the known proline-specific peptidases cleave only when the peptide bond preceding proline has trans conformation.^{65,66} Due to its peculiarity, the presence of this aminoacid strongly influences the conformation, properties and biological functions of several molecules such as peptides involved in immunomodulation and coagulation, cytokines, growth factors, neuro- and vasoactive peptides.⁶⁶ Members of this class have been isolated from different mammalian tissues⁶⁷ as well as from bacteria^{68,69} and an archeon (*Pyrococcus furious*).⁷⁰

While the physiological role of prolidase in bacteria and archaea is unclear, in humans it is relevant in the latest stage of protein catabolism particularly of those molecules rich in imino acids such as collagens, thus being involved in matrix remodelling. A deficiency of this enzyme in humans causes a recessive connective tissue disorder (prolidase deficiency) characterized by abnormalities of the skin, mental retardation and respiratory tract infections.^{71,72}

Their main activity is Gly-Pro dipeptides hydrolysis,^{68,73,74} although the enzyme is also active against Ala-Pro, Met-Pro, Phe-Pro, Leu-Pro and Val-Pro. To date, the majority of prolidases that have been studied exhibit metal-dependent activity, requiring divalent cations such as Zn^{2+} , Mn^{2+} , or Co^{2+} for maximal activity.^{9,75} They have been purified either as monomers or as dimers

depending on the enzyme.⁷⁶⁻⁷⁸ The best characterized prolidase in terms of structure and catalytic site composition is the one isolated from the archaeon *Pyrococcus furiosus* (Pfprol) for which the complete structure and active site organization were described in details by crystallographic and site directed mutagenesis studies, both in native and *E. Coli* recombinant enzyme.⁷⁹ Pfprol is a homodimer with two subunits. Each monomer has a dinuclear metal cluster requiring **Co(II)** for full activity.⁸⁰

The enzyme activity could also be supported by the presence of **Mn(II)** as demonstrated by the results concerning the human prolidase synthesized in prokaryotic and eukaryotic hosts. The recombinant enzyme was found to require Mn(II) for full activity identical to the endogenous human fibroblasts prolidase.⁸¹

The influence of the **Zn(II)** ion was also evaluated experimentally and it was observed ^{67,79,80} that its presence in the active site significantly reduces prolidase activity. Actually, there are also indirect evidences that the binding site is not highly selective against the nature of the bonded divalent ion. A typical case in this respect is represented by prolidase in *Pyrococcus furiosus* (Pfprol) for which, during the crystallization process, it was observed that Zn(II) substituted native Co(II) ions,⁸⁰ supposedly necessary for full enzymatic activity. In addition, it was recently reported the first experimental evidence for the coexistence of two different metal ions in the active site of human prolidase (Zn(II) and Mn(II)) with the protein remaining partially active. ⁸² So the Zn(II) cation in the active site seems to lead toward a decreasing of activity although the enzyme preserves a significant activity.

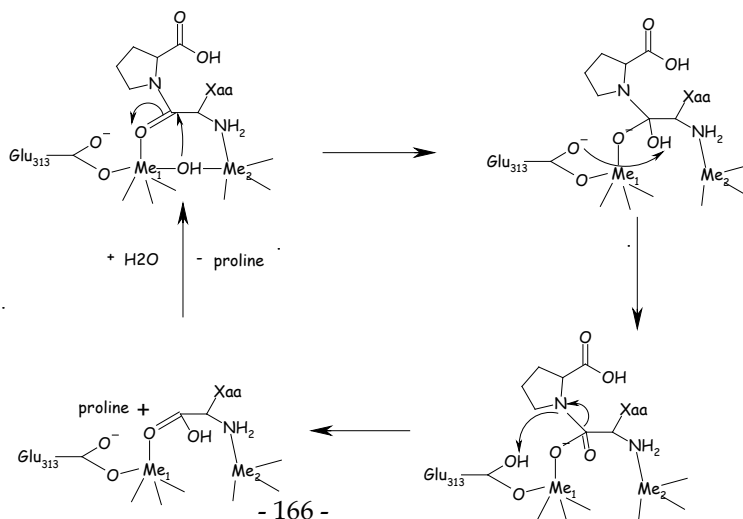
4.4.1 Computational Investigation of human prolidase: can it use different metals for full catalytic activity? (Paper VIII)

The mechanism of prolidase catalysis is still largely unknown. Nevertheless, due to strong structural homologies among prolidase and other proteins such

as methionine aminopeptidases⁸³ and proline aminopeptidase,⁸⁴ prolidase becomes a member of a group of enzymes whose most distinctive shared feature is a “pita-bread” fold of the C-terminal catalytic domain. Since the dinuclear metal clusters in these enzymes are coordinated by identical sets of residues,⁷⁵ they are suggested to share a common reaction mechanism in which the metals coordinated hydroxide group performs a nucleophilic attack on the carbonyl carbon of the scissile peptide bond.⁸⁰ The cleavage of the amide bond is provided by a proton shift played by a conserved Glu residue which acts as a proton shuttle, first abstracting an H⁺ from the bridging nucleophile water molecule and then transferring it to the nitrogen atom of the substrate (see Scheme 4.2).⁷⁵ Such a role as proton carrier is similar to that proposed for Glu133 in peptide deformylase,⁸⁵ Glu270 in carboxypeptidase A,^{86,87} Asp120 in β -lactamase,⁸⁸ and Glu106 in carbonic anhydrase.⁸⁹

With the purpose of identifying which is the most efficient dimetallic centre for the Prolidase catalyzed reaction, Zn(II), Co(II) and Mn(II) were examined as the potential catalytic metals of this enzyme. Furthermore, in order to better elucidate the exact roles played by the metals occupying the site 1 and site 2 positions, the heterobimetallic active site having Zn and Mn cations was also investigated, considering the two derivatives Mn1-Zn2 and Zn1-Mn2.

Scheme 4.2: Schematic illustration of some proposed mechanisms for binuclear metallohydrolases



4.4.1.1 Prolidase Active Site and Cluster model

The active site model cluster was built from the X-ray structure of the recombinant human prolidase produced in *E. Coli* (PDB code = 2OKN).⁹⁰ The cluster is made up by two metallic cations (Zn, Co, Mn) and their first coordination sphere including five amino acids that function as metal-binding residues in this enzyme: Histidine-371 and glutamate-413 solely bind to the first metal center (Me1), aspartate-277 to the second metal center (Me2), and aspartate-288 and glutamate-453 are ligands to both metal cations. Some residues of the second shell were also included in the cluster (Phe227, His256, His378 and Arg451). Only the side chains were kept in our model. Pro-Gly substrate was located in the active site according to the binding mode of the substrate in other enzymes of the same family.⁹¹

Electronic ground states were singlet for Zn-, septet for Co-, and undecaplet for Mn-homodimetallic clusters, and sextet for the mixed Zn-Mn ones.

4.4.1.2 Function of the binuclear metal center in the catalytic process

According to our calculation, and independently of the particular divalent metal ion considered, the reaction proceeds following the same steps. The metals-bridging hydroxide ion performs a nucleophilic attack on the peptide carbonyl carbon atom, leading to a tetrahedral intermediate. The cleavage of the amide bond is provided by a proton shift played by Glu413 residue which acts as a proton shuttle, first abstracting an H⁺ from the bridging nucleophile and then transferring it to the nitrogen atom of the substrate, entailing the release of the two products, glycine and proline.

The investigation of the catalytic mechanism of prolidase allowed us to better explore the role, either structural or catalytic, played by the binuclear metallic center in the active site of this enzyme. In the ES complex, the substrate interacts only with Me2 centre through the glycine amide NH₂ lone pair. Such coordination to the active site, changes when the nucleophilic attack by the bridging OH on the substrate carbon atom (TS₁) occurs. Actually, in the first

transition state, the incoming negative charge of the oxygen of the C=O bond is stabilized by its coordination to the Me1 site. The substrate results bicoordinated to the dimetallic centre hence contributing to the stabilization of the first transition state, in analogy to what observed in PAP hydrolysis reaction. Such coordination mode is then retained along the reaction path. TS₁ evolves into the tetrahedral intermediate INT₁, in which the C-OH bond is completely formed and, through a TS₂, the proton moves from the OH to the oxygen of Glu413 residue leading to a second intermediate. Protonation of the proline nitrogen by Glu413 occurs through the transition state TS₃, leading to the cleavage of the C-N bond. (Figure 4.5)

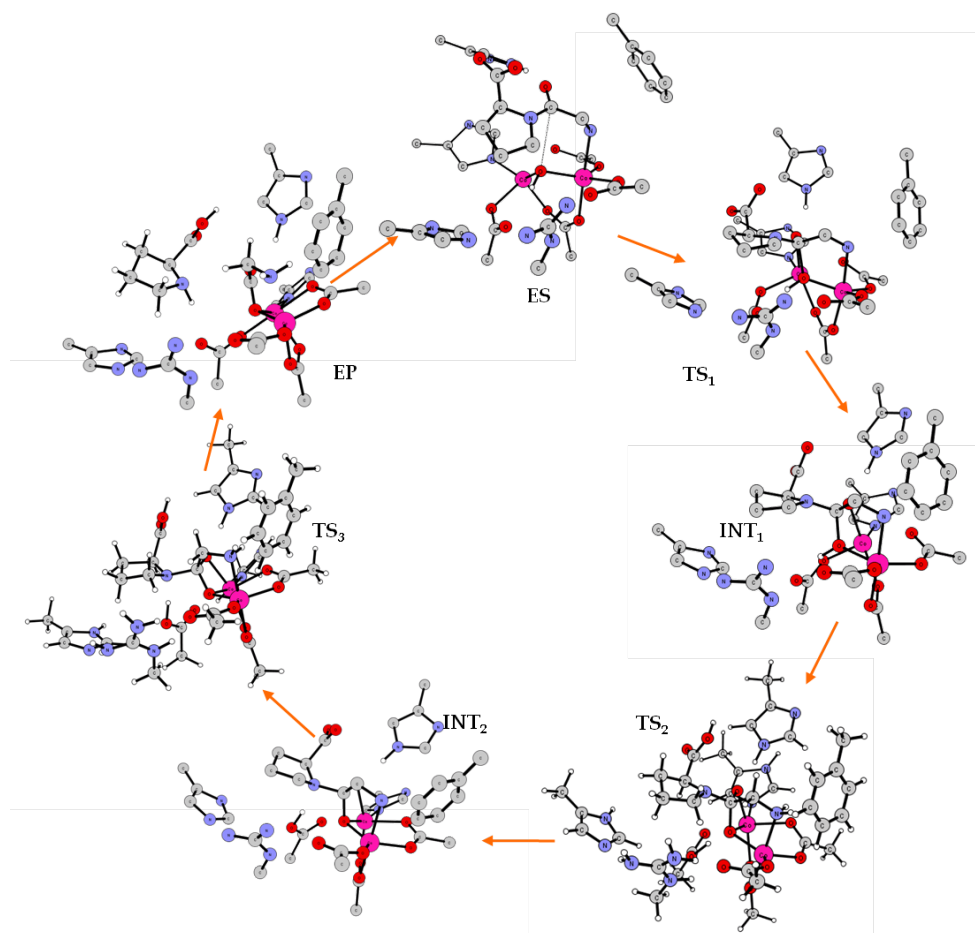


Figure 4.5: Optimized structures of the stationary points for the hydrolysis of the Gly-Pro peptide promoted by prolidase enzyme. Only the most significant hydrogen atoms are reported in the figure.

Investigating the influence of different binuclear metal center on the prolidase catalytic efficiency, a slightly better performance of the cobalt containing cluster was observed over the Zn- and Mn-homodimetallic active sites. According to our calculation, this trend appears to be associated to the occurrence of a charge transfer from ligands to metals, not observed for zinc and manganese divalent metals. Nevertheless, we found that Mn better catalyze the first step of the reaction. Such evidence was supported also by our data obtained considering the two derivatives Mn1-Zn2 and Zn1-Mn2. Such study reveal that manganese in position 1 entails a slight decrease in the first energy barrier compared to what occur when Mn \rightarrow Zn substitution at that position take place. On the contrary, site 2 is implicated in the collapse of the tetrahedral intermediate into the products. Interestingly, Mn metal ion at site 2 does not catalyze well that step in the homodimetallic cluster. In analogy, considering the mixed derivatives Mn1-Zn2, Zn \rightarrow Mn replacement entails slightly higher energies in this step of the reaction.

However, the obtained potential energy profiles for both homodimetallic and heterobimetallic clusters, seem to be very feasible in all considered cases, with very small differences in energetics. Results obtained in this study reveal that prolidase catalytic activity seem to be not highly selective against the nature of the bonded divalent ion. A clear dependence of the catalytic activity on a particular transition metal is then not revealed, suggesting that prolidase can efficiently perform the hydrolysis of Xaa-Pro substrates with Zn(II), Co(II) and Mn(II) as a cofactor.

Bibliography

- [1] Stephen W. Ragsdale, *Chem. Rev.* **2006**, *106*, 3317-3337, and references therein
- [2] Mitić, N.; Smith, S. J.; Neves, A.; Guddat, L. W.; Gahan, L. R.; Schenk, G.; *Chem. Rev.* **2006**, *106*, 3338.
- [3] Sträter, N.; Lipscomb, W. N.; Klabunde, T.; Krebs, B. *Angew. Chem., Int. Ed. Engl.* **1996**, *35*, 2024.
- [4] Barford, D.; Das, A. K.; Egloff, M.P. *Annu. Rev. Biophys. Biomol. Struct.* **1998**, *27*, 133.
- [5] Rusnak, F.; Mertz, P. *Physiol. Rev.* **2000**, *80*, 1483.
- [6] Jackson, M. D.; Denu, J. M. *Chem. Rev.* **2001**, *101*, 2313.
- [7] Lowther, W. T.; Matthews, B. W. *Biochim. Biophys. Acta* **2000**, *1477*, 157.
- [8] Dismukes, G. C. *Chem. Rev.* **1996**, *96*, 2909.
- [9] Wilcox, D. E. *Chem. Rev.* **1996**, *96*, 2435.
- [10] Ramos, M. J.; Fernandes, P. A. *Acc Chem Res.*, **2008**, *41*, 689;
- [11] Georgieva, P.; Himo, F.; *J. Comput. Chem.*, **2010**, *31*, 1707-1714
- [12] Siegbahn, P. E. M.; Himo, F. *J Biol Inorg Chem* **2009**, *14*, 643.
- [13] Siegbahn, P. E. M.; Borowski, T. *Acc Chem Res* **2006**, *39*, 729;
- [14] Himo, F.; Siegbahn, P. E. M. *Chem Rev* **2003**, *103*, 2421;
- [15] Leopoldini, M.; Russo, N.; Toscano, M. *J. Am. Chem. Soc.* **2007**, *129*, 7776-7784.
- [16] Leopoldini M.; Marino, T.; Toscano, M. *Theor. Chem. Acc.*, **2008**, *120*, 459-466.
- [17] Siegbahn, P. E. M.; Blomberg, M. R. A. *Chem. Rev.* **2000**, *100*, 421-437.
- [18] Twitchett, M. B.; Sykes, A. G. *Eur. J. Inorg. Chem.* **1999**, 2105.
- [19] Klabunde, T.; Krebs, B. *Struct. Bonding* **1997**, *89*, 177.
- [20] Oddie, G. W.; Schenk, G.; Angel, N. Z.; Walsh, N.; Guddat, L. W.; De Jersey, J.; Cassidy, A. I.; Hamilton, S. E.; Hume, D. A. *Bone* **2000**, *27*, 575.
- [21] Antanaitis, B. C.; Aisen, P. *J. Biol. Chem.* **1982**, *257*, 5330.
- [22] Doi, K.; Bradley, C.; Aisen, P. *Struct. Bonding* **1988**, *70*, 1.
- [23] Schenk, G.; Ge, Y.; Carrington, L. E.; Wynne, C. J.; Searle, I. R.; Carroll, B. J.; Hamilton, S.; de Jersey, J. *Arch. Biochem. Biophys.* **1999**, *370*, 183.
- [24] Durmus, A.; Eicken, C.; Sift, B. H.; Kratel, A.; Kappi, R.; Hütterman, J.; Krebs, B. *Eur. J. Biochem.* **1999**, *260*, 709.
- [25] Merckx, M.; Averill, B. A. *Biochemistry* **1998**, *37*, 8490.
- [26] Chen, T. T.; Bazer, F. W.; Cetorelli, J. J.; Pollard, W. E.; Roberts, R. M. *J. Biol. Chem.* **1973**, *248*, 8560.
- [27] Campbell, H. D.; Zerner, B. *Biochem. Biophys. Res. Commun.* **1973**, *54*, 1493.
- [28] Campbell, H. D.; Dionysius, D. A.; Keough, D. T.; Wilson, B. E.; de Jersey, J.; Zerner, B. *Biochem. Biophys. Res. Commun.* **1978**, *82*, 615.
- [29] Robinson, D. B.; Glew, R. H. *J. Biol. Chem.* **1980**, *255*, 5864.
- [30] Hayman, A. R.; Warburton, M. J.; Pringle, J. A.; Coles, B.; Chambers, T. J. *Biochem. J.* **1989**, *261*, 601.
- [31] Allen, S. H.; Nuttleman, P. R.; Ketcham, C. M.; Roberts, R. M. *J. Bone Miner. Res.* **1989**, *4*, 47.
- [32] Janckila, A. J.; Woodford, T. A.; Lam, K. W.; Li, C. Y.; Yam, L. T. *Leukemia* **1992**, *6*, 199.
- [33] Beck, J. L.; McConachie, L. A.; Summors, A. C.; Arnold, W. N.; de Jersey, J.; Zerner, B. *Biochim. Biophys. Acta* **1986**, *869*, 61.
- [34] Bozzo, G. G.; Raghothama, K. G.; Plaxton, W. C. *Biochem. J.* **2004**, *377*, 419.
- [35] Bozzo, G. G.; Raghothama, K. G.; Plaxton, W. C. *Eur. J. Biochem.* **2002**, *269*, 6278.
- [36] Schenk, G.; Bouchard, C. L.; Carrington, L. E.; Noble, C. J.; Moubaraki, B.; Murray, K. S.; de Jersey, J.; Hanson, G. R.; Hamilton, S. *J. Biol. Chem.* **2001**, *276*, 19084.
- [37] Sträter, N.; Klabunde, T.; Tucker, P.; Witzel, H.; Krebs, B. *Science* **1995**, *268*, 1489.

- [38] Klabunde, T.; Sträter, N.; Fröhlich, R.; Witzel, H.; Krebs, B. *J. Mol. Biol.* **1996**, *259*, 737.
- [39] Schenk, G.; Guddat, L. W.; Ge, Y.; Carrington, L. E.; Hume, D. A.; Hamilton, S.; de Jersey, J. *Gene* **2000**, *250*, 117.
- [40] Beck, J. L.; Keough, D. T.; de Jersey, J.; Zerner, B. *Biochim. Biophys. Acta* **1984**, *791*, 357.
- [41] Funhoff, E. G.; Ljusberg, J.; Wang, Y.; Andersson, G.; Averill, B. A. *Biochemistry* **2001**, *40*, 11614.
- [42] Funhoff, E. G.; Klaassen, C. H. W.; Samyn, B.; Van Beeumen, J.; Averill, B. A. *ChemBioChem* **2001**, *2*, 355.
- [43] Merckx, M.; Averill, B. A. *Biochemistry* **1998**, *37*, 11223.
- [44] Merckx, M.; Pinkse, M. W. H.; Averill, B. A. *Biochemistry* **1999**, *38*, 9914.
- [45] Pinkse, M. W. H.; Merckx, M.; Averill, B. A. *Biochemistry* **1999**, *38*, 9926.
- [46] Funhoff, E. G.; Bollen, M.; Averill, B. A. *J. Inorg. Biochem.* **2005**, *99*, 521.
- [47] Beck, J. L.; McArthur, M. J.; de Jersey, J.; Zerner, B. *Inorg. Chim. Acta* **1988**, *153*, 39.
- [48] Beck, J. L.; de Jersey, J.; Zerner, B. *J. Am. Chem. Soc.* **1988**, *110*, 3317.
- [49] Gehring, S.; Fleischhauer, P.; Behlendorf, M.; Huber, M.; Lorösch, J.; Haase, W.; Dietrich, M.; Witzel, H.; Locke, R.; Krebs, B. *Inorg. Chim. Acta* **1996**, *252*, 13.
- [50] Battistuzzi, G.; Dietrich, M.; Locke, R.; Witzel, H. *Biochem. J.* **1997**, *323*, 593.
- [51] Klabunde, T.; Sträter, N.; Krebs, B., and Witzel, H. *FEBS Lett.* **1995**, *367*, 56.
- [52] Schenk, G.; Elliott, T. W.; Leung, L.; Carrington, L. E.; Mitić, N.; Gahan, L. R.; Guddat, L. W.; *BMC Struct. Biol.*, **2008**, *8*, 6.
- [53] Kaija, H.; Alatalo, S. L.; Halleen, J. M.; Lindqvist, Y.; Schneider, G.; Väänänen, H. K.; Vihko, P. *Biochem. Biophys. Res. Commun.* **2002**, *292*, 128.
- [54] Smoukov, S. K.; Quaroni, L.; Wang, X.; Doan, P. E.; Hoffman, B. M.; Que, L., Jr. *J. Am. Chem. Soc.* **2002**, *124*, 2595.
- [55] Guddat, L. W.; McAlpine, A. S.; Hume, D.; Hamilton, S.; de Jersey, J.; Martin, J. L. *Structure* **1999**, *7*, 757.
- [56] Lindqvist, Y.; Johansson, E.; Kaija, H.; Vihko, P.; Schneider, G. *J. Mol. Biol.* **1999**, *291*, 135.
- [57] Wang, X.; Que, L. *Biochemistry* **1998**, *37*, 7813.
- [58] Hur S.; Brulce, T. C.; *Proc. Natl. Acad. Sci. U.S.A.* **2003**, *100*, 12015.
- [59] Schenk, G.; Gahan, L. R.; Carrington, L. E.; Mitić, N.; Valizadeh, M.; Hamilton, S. E.; de Jersey, J.; Guddat, L. W. *Proc. Natl. Acad. Sci. U.S.A.* **2005**, *102*, 273.
- [60] Voegtli, W. C.; White, D. J.; Reiter N. J.; Rusnak, F.; Rosenzweig, A. C.; *Biochemistry* **2000**, *39*, 15365.
- [61] Benini, S.; Rypniewski, W. R.; Wilson, K. S.; Ciurli, S.; Mangani, S.; *J Biol Inorg Chem* **2001**, *6*, 778.
- [62] Sousa, S.F.; Fernandes, P.A., Ramos, M.J.; *J. Phys. Chem. A*, **2007**, *111*, 10439.
- [63] Cox, R.S.; Schenk, G.; Mitić, N.; Gahan, L. R.; Hengge, A. C.; *J. Am. Chem. Soc.* **2007**, *129*, 9550.
- [64] Myara, I.; Charpentier, C.; Lemonnier, A. *Life Sci.* **1984**, *34*, 1985–1998.
- [65] Vanhoof, G.; Goossens, F.; De Meester, I.; Hendriks, D.; Scharpe, S. *FASEB J.* **1995**, *9*, 736–744.
- [66] Yaron, A.; Naider, F. *Crit. Rev. Biochem. Mol. Biol.* **1993**, *28*, 31–81.
- [67] Royce, P.M.; Steinmann, B. Royce PM & Steinmann B, eds, **2002**, pp. 727–743. Wiley-Liss, New York.
- [68] Fernandez-Espla, M. D.; Martin-Hernandez, M. C.; Fox, P. F. *Appl. Environ. Microbiol.* **1997**, *63*, 314–316.
- [69] Suga, K.; Kabashima, T.; Ito, K.; Tsuru, D.; Okamura, H.; Kataoka, J.; Yoshimoto, T. *Biosci. Biotechnol. Biochem.* **1995**, *59*, 2087–2090.
- [70] Ghosh, M.; Grunden, A. M.; Dunn, D. M.; Weiss, R.; Adams, M. W. *J. Bacteriol.* **1998**, *180*, 4781–4789.

- [71] Forlino, A.; Lupi, A.; Vaghi, P.; Icaro Cornaglia, A.; Calligaro, A.; Campari, E.; Cetta, G. *Hum. Genet.* **2002**, *111*, 314-22.
- [72] Endo, F.; Tanoue, A.; Hata, A.; Kitano, A.; Matsuda, I. *J. Inherited Metab. Disease* **1989**, *12*, 351-354.
- [73] Browne, P.; O'Cuinn, G. *J. Biol. Chem.* **1983**, *258*, 6147-6154.
- [74] Fujii, M.; Nagaoka, Y.; Imamura, S.; Shimizu, T. *Biosci. Biotechnol. Biochem.* **1996**, *60*, 1118-1122.
- [75] Lowther, W.T.; Matthews, B.W. *Chem. Rev.* **2002**, *102*, 4581-4608.
- [76] Cunningham, D. F.; O'Connor, B. *Biochim. Biophys. Acta* **1997**, *1343*, 160-186
- [77] Kobayashi, M.; Shimizu, S. *Eur. J. Biochem.* **1999**, *261*, 1-9.
- [78] Yang, S. I.; Tanaka, T. *FEBS J.* **2008**, *275*, 271-280.
- [79] Du, X.; Tove, S.; Kast-Hutcherson, K.; Grunden, A. M. *FEBS Lett.* **2005**, *579*, 6140-6146.
- [80] Maher, M. J.; Ghosh, M.; Grunden, A.M.; Menon, A.L.; Adams, M.W.; Freeman, H.C.; Guss, J.M. *Biochemistry* **2004**, *43*, 2771-2783.
- [81] Lupi, A.; Tenni, R.; Rossi, A.; Cetta, G.; Forlino, A. *Amino Acids* **2008**, *35*, 739-752.
- [82] Besio, R.; Alleva, S.; Forlino, A.; Lupi, A.; Meneghini, C.; Minicozzi, V.; Profumo, A.; Stellato, F.; Tenni, R.; Morante, S. *Eur. Biophys. J.* **2009**, DOI 10.1007/s00249-009-0459-4.
- [83] Roderick, S. L.; Matthews, B. W. *Biochemistry* **1993**, *32*, 3907-3912.
- [84] Wilce, M. C. J.; Bond, C. S.; Dixon, N. E.; Freeman, H. C.; Guss, J. M.; Lilley, P. E.; Wilce, J. A. *Proc. Natl. Acad. Sci., U.S.A.* **1998**, *95*, 3472-3477.
- [85] Leopoldini, M.; Russo, N.; Toscano, M. *J. Phys. Chem. B* **2006**, *110*, 1063-1072.
- [86] Abashkin, Y. G.; Burt, S. K. ; Collins, J. R. ; Cachau, R. E. ; Russo, N. ; Erickson, J. W. In *Metal-Ligand Interactions: Structure and Reactivity* **1996**, N. Russo, D. R. Salahub (Eds), Kluwer, Dordrecht, Nato Science Series, *474*, 1-22.
- [87] Bertini, I.; Luchinat, C. in *Bioinorganic Chemistry*; Bertini, I., Gray, H. B., Lippard, S. J., Valentine, J. S., Eds.; University Science Books: Mill Valley, CA, **1994**.
- [88] Olsen, L.; Anthony, J.; Ryde, U.; Adolph, H. W.; Hemmingsen, L. *J. Phys. Chem. B* **2003**, *107*, 2366-2375.
- [89] Marino, T.; Russo, N.; Toscano, M. *J. Am. Chem. Soc.* **2005**, *127*, 4242-4253.
- [90] Mueller, U., Niesen, F. H., Roske, Y., Goetx, F., Behlke, J., Buessow, K., Heinemann, U. **2007**, to be published, DOI:10.2210/pdb2okn/pdb.
- [91] Leopoldini, M.; Russo, N.; Toscano, M. *J. Am. Chem. Soc.* **2007**, *129*, 7776-7784.

Appendix B

Paper VII

“Atomistic details of the Catalytic Mechanism of
Fe(III)-Zn(II) Purple Acid Phosphatase”

Marta E. Alberto, Tiziana Marino, Maria J. Ramos and Nino Russo

J. Chem. Theory Comput. **2010**, *6*, 2424–2433

Atomistic details of the Catalytic Mechanism of Fe(III)–Zn(II) Purple Acid Phosphatase

Marta E. Alberto,[†] Tiziana Marino,[†] Maria J. Ramos,[‡] and Nino Russo^{*,†}

Dipartimento di Chimica, Università della Calabria, Via P. Bucci, cubo 14c, 87036 Arcavacata di Rende (CS), Centro di Calcolo ad Alte Prestazioni per Elaborazioni Parallele e Distribuite—Centro d’Eccellenza MIUR, Italy and REQUIMTE, Departamento de Química, Faculdade de Ciências, Universidade do Porto, Rua do Campo Alegre, 687, 4169-007 Porto, Portugal

Received April 08, 2010

Abstract: In the present work, we performed a theoretical investigation of the reaction mechanism of the Fe(III)–Zn(II) purple acid phosphatase from red kidney beans (rkbPAP), using the hybrid density functional theory and employing different exchange–correlation potentials. Characterization of the transition states and intermediates involved and the potential energy profiles for the reaction in different environments (gas phase, protein environment, and water) are reported. Our results show that the Fe(III)–Zn(II)PAP catalyzes the hydrolysis of methylphosphate via direct attack by a bridging metals-coordinated hydroxide leading to the cleavage of the ester bond. From our study emerges that the rate-limiting step of the reaction is the nucleophilic attack followed by the less energetically demanding release of the leaving group. Furthermore, we provide insights into some important points of contention concerning the precatalytic complex and the substrate coordination mode into the active site prior to hydrolysis. In particular: (i) Two models of enzyme–substrate with different orientations of the substrate into the active site were tested to evaluate the possible roles played by the conserved histidine residues (His 202 and His 296); (ii) Different protonation states of the substrate were taken into account in order to reproduce different pH values and to verify its influence on the catalytic efficiency and on the substrate binding mode; (iii) The metals role in each step of the catalytic mechanism was elucidated. We were also able to ascertain that the activation of the leaving group by the protonated His 296 is decisive to reach an optimal catalytic efficiency, while the bond scission without activation requires higher energy to occur.

1. Introduction

Purple acid phosphatases (PAPs)^{1–3} belong to binuclear metallohydrolases, an interesting family of enzymes that have received in the last years considerable attention.^{4–11} Binuclear sites in enzymes appear to have several potentially useful properties, not found in mononuclear centers, which play essential roles in catalysis. Members of this class have been recognized as potential targets for the development of chemotherapeutics and for drug design against a wide variety

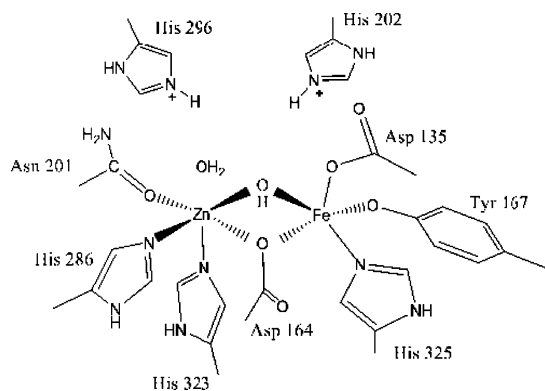
of human disorders^{12–20} and represent also promising candidates in bioremediation.²¹

PAPs are the only binuclear metallohydrolases that use a heterovalent active site Fe(III)–M(II) to catalyze the hydrolysis of monophosphates at acidic to neutral pH.^{1–3,22–26} The identity of the divalent metal ion varies with the source of the enzyme. Mammalian PAPs contain an antiferromagnetically coupled binuclear iron center Fe(III)–Fe(II) in the active site,^{27–33} while plant PAPs most typically have Fe(III)–Zn(II) centers,^{26,34–36} but an interesting example of an enzymatically active binuclear Fe(III)–Mn(II) center was found in the case of PAP from the sweet potato.^{24,25,37} In spite of the scarce similarity in their primary sequences, the

* Corresponding author. E-mail: nrusso@unical.it.

[†] Università della Calabria.

[‡] Universidade do Porto.

Scheme 1. Red Kidney Bean PAP Active Site

active site structure and the residues coordinating the metal ions in the active site are identical in mammalian and plant PAPs, displaying similar enzymatic and spectroscopic properties.³⁸ For example, the intense purple color that distinguishes PAPs from the other phosphatases is due to a charge-transfer transition ($\lambda_{\max} = 510\text{--}560\text{ nm}$) in the active site from a conserved tyrosinate to the Fe(III) ion.^{39–41} Nevertheless, while plant PAPs have a chromophoric center similar to that of their animal counterparts ($\lambda_{\max} = 550\text{ nm}$), their activity cannot be regulated by reversible oxidation/reduction, as it indeed occurs for mammalian PAPs which are reversibly inactivated by the oxidation of the divalent iron ion, suggesting that PAP may be regulated by changes in redox potential within animal cells.^{42,43} The identity of their active sites has been demonstrated in several studies by using metal ion replacement^{44–52} and by spectroscopic and magnetochemical measurements,^{53,54} giving evidence that they employ a similar working mechanism. Moreover other studies suggest that rkbPAP is a good model for the structure and mechanism of other acid phosphatases, such as the human one.⁵⁷ PAP from red kidney beans, the object of our investigation, was the first member of this family for which a crystal structure became available^{55,56} and is by far the most explored so far. The metal atoms first-shell ligands include seven invariant aminoacid residues: three histidines, two aspartates, a tyrosine, and an asparagine (Scheme 1).⁵⁶ The presence of the water molecule terminally coordinated to the divalent metal ion was supported by ENDOR measurements⁵⁸ as well as electron density maps,^{59,60} and EXAFS⁶¹ studies sustained the presence of the bridging hydroxide, the most likely candidate as the nucleophile.⁵⁸ Although in many earlier studies the presence of a terminal Fe(III)-bound water molecule as a nucleophile candidate has been proposed,^{62–64} ENDOR measurements of pig PAP and rkbPAP–SO₄ crystal structures indicate that there is no water ligand at the iron site, suggesting also that the trivalent metal ion is five coordinated.⁵⁸ Such evidence lead to the exclusion of a mechanism in which a terminal Fe(III)-bound hydroxide acts as nucleophile. Moreover, experimentally it was observed that the reduced nucleophilicity of the bridging hydroxide is compensated by an increased electrophilicity of the substrate when comparing the possibilities of: (i) a terminally coordinated nucleophile and terminally coordinated substrate, with (ii) a bridging nucleophile and bridging substrate.⁵⁸ In addition, the crystal structures of PAPs,

determined in the presence of a phosphate group,⁵⁶ show a network of hydrogen bonds with uncoordinated and conserved histidine residues of the second shell of the ligands (His 202 and His 296 for rkbPAP), which, therefore, could play essential roles in catalysis. Although the importance of these conserved histidines has been demonstrated by site-directed mutagenesis studies,^{14,65,66} it is still not clear the effective role of each one in the stabilization of the substrate in the catalytic cavity.

Despite the presence in the literature of structural spectroscopic and kinetic data, the individual steps of the PAPs-catalyzed hydrolysis reaction remain a matter of controversy. The general mechanism proposed in the literature for PAP-catalyzed reactions involves a nucleophilic attack performed by the bridging hydroxide to the phosphorus center leading to hydrolytic cleavage of the phosphate–ester bond.^{4,67} Nevertheless, several crucial aspects are still uncertain, such as the binding mode of the substrate in the active site prior to the hydrolysis, the effective role of each metal atom, and also the function of the two histidine residues located in the second-shell ligands (His 202 and His 296).^{4,5,7,37,46,48,58,64,67}

In order to better characterize the several steps of the catalytic mechanism of the Fe(III)–Zn(II)–PAP (from rkbPAP), for the first time a detailed theoretical exploration of the hydrolysis process is reported in this work, providing characterization of the transition states and intermediates involved and presenting the potential energy profiles for the reaction in different environments (gas phase, protein environment, and water). Moreover our computations can give insights into some interesting aspects. In particular: (i) Two models of enzyme–substrate (ES) with different orientations of the substrate into the active site were tested to evaluate the possible roles played by the conserved histidine residues (His 202 and His 296); (ii) Different protonation states of the substrate were taken into account in order to reproduce different pH values and to verify its influence on the catalytic efficiency and on the substrate binding mode; (iii) The metals role in each step of the catalytic mechanism was elucidated.

2. Computational Details and Models

The theoretical investigation of the catalytic mechanism of the Fe(III)–Zn(II)–PAP was performed at density functional theory (DFT) level by means of GAUSSIAN 03⁶⁸ suite of programs. Geometry optimizations in the gas phase were carried out using the hybrid B3LYP functional, composed by Becke's⁶⁹ three-parameter hybrid exchange functional (B3), and the correlation functional of Lee, Yang and Parr (LYP)⁷⁰ using 6-31G(d,p) basis sets for all atoms except the iron and Zn ions, which were described by the quasi-relativistic Stuttgart–Dresden pseudopotentials.⁷¹ In order to confirm proper convergence to equilibrium and transition-state geometries, vibrational frequency analysis was done based on analytical second derivatives of the Hamiltonian at the same level of theory. Solvent effects were introduced in the framework of the self-consistent reaction field conductor-like polarizable continuum model (SCRF-CPCM),^{72,73} using two dielectric constants to simulate water and reproduce the protein environment. For the latter, an empirical

value of $\epsilon = 4$ accounts for the average effect of both the protein and the water medium surrounding the protein. For the water, $\epsilon = 80$ was used. In the CPCM method, the continuum is modeled as a conductor, instead of a dielectric. This simplifies the electrostatic computations, and corrections are made a posteriori for dielectric behavior. The UA0 radii were used to build the cavity.⁷⁴ In order to obtain more accurate energies in the gas phase, in the protein environment, and in water, single points calculations were performed on the optimized geometries using the larger basis set 6-311+G(2d,2p) and testing several exchange–correlation functionals (B3LYP,^{69,70} PBE0PBE,⁷⁵ BB1K,⁷⁶ MPWB1K,⁷⁷ and MW1B95).⁷⁷ Our benchmark reported in Section 3.3, shows that the meta-hybrid functional (BB1K, MPWB1K, MW1B95) reproduces with good accuracy experimental values found on similar reactions catalyzed by PAPs enzymes.^{24,78,79} In addition, many studies have demonstrated that the hybrid-meta generalized gradient approximation (GGA) methods give more reliable results in the reproduction of the reaction kinetics showing great ability in the calculation of barrier heights with high accuracy, also compared to higher-level post-Hartree–Fock methods, supporting our evidence.^{80,81} The energy values discussed in the text are those obtained with the hybrid-meta MPWB1K functional, previously employed successfully also in other enzymatic studies.^{80–82} The crystal structure of red kidney bean PAP, determined in the presence of phosphate acting as an inhibitor (PDB code 4kbp, chain A),⁵⁶ was used to devise a model of the active site of the enzyme. The latter contains the metal ions Fe(III) and Zn(II) and the seven amino acids of their first-shell ligands. In particular, the Fe(III) ion is coordinated to Asp 135, Tyr 167, His 325, and Asp 164 that bridges both of the metals, while the Asn 201, His 286, and His 323 represent the divalent metal ion Zn(II) ligands. In order to study their roles in the catalytic cycle, two histidine residues (His 296 and His 202) of the second shell of the ligands were also included in the model. No water molecule was introduced to complete the coordination environment of the Zn ion because the formation of the precatalytic complex has been suggested to cause the expulsion of this labile terminal water ligand.⁶⁷ Only the side chains of the residues were kept in our model. Moreover the carbon atoms where truncation was done were kept fixed to their X-ray crystal positions during the optimizations to avoid an unrealistic expansion of the cluster during the calculations. This procedure gives rise to smaller imaginary frequencies, but the latter does not significantly contribute to the zero point energies (ZPE) and can thus be tolerated. A bridging hydroxide as a nucleophile was included in the cluster model, in agreement with previous studies that support the presence of this group.^{58,61} In the absence of crystallographic data for the ES complex, the latter was modeled in the active site as methyl-phosphate since this kind of enzyme catalyzes the hydrolysis of monophosphates. The resulting cluster contains 114 atoms. In order to establish the most stable spin multiplicity of the system, preliminary calculations on the ES complex with different values of spin multiplicity ($2S + 1 = 2, 4, 6, \text{ and } 8$) were performed. The lowest energy was obtained with a value of 6, which arises from a high-spin

configuration of the Fe(III) center, in agreement with electron paramagnetic resonance (EPR) measurements that support our result.²⁵ The doublet, quartet, and octet electronic states lie at 36.3, 23.8, and 98.3 kcal/mol with respect to the same structure obtained with sextet multiplicity, respectively. For the quartet spin state, the entire catalytic cycle was reproduced in order to consider eventual involvement of different spin states along the potential energy surface (PES). The results clearly show that no crossing occurs between the two energetic profiles. (See Figure S1 in the Supporting Information). Spin density distribution and molecular orbital pictures for all the stationary points along the PES are reported in Figures S2 and S3 of the Supporting Information, respectively. As expected, from these data, it is clear that the higher spin densities are localized on the iron center.

3. Results and Discussion

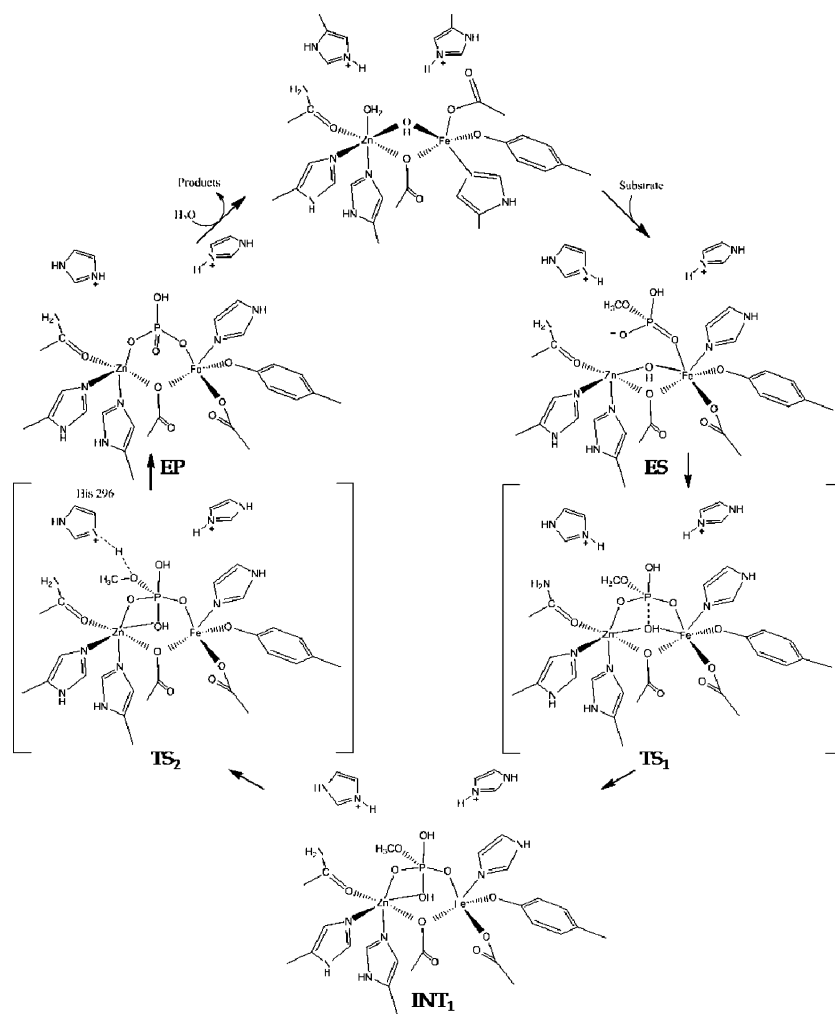
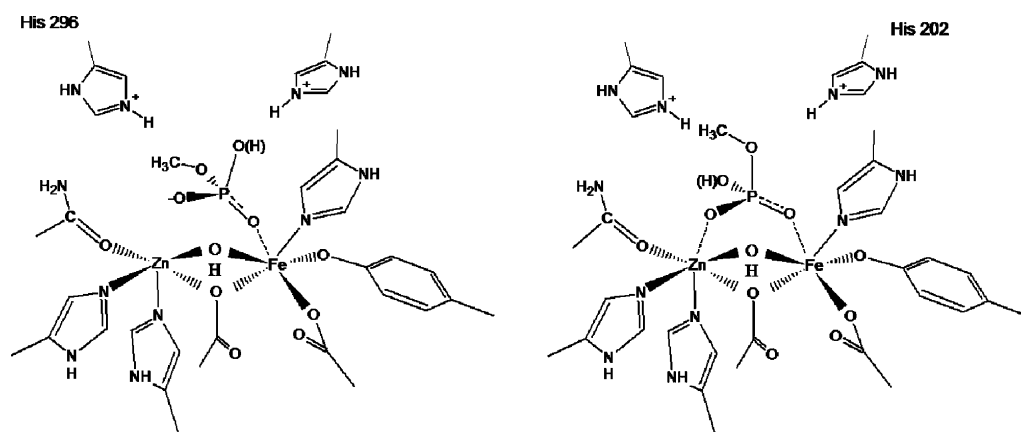
The steps involved in the whole process and determined through our calculations are sketched in Scheme 2. According to our results, a mechanism in which the metal-bridging hydroxide performs a nucleophilic attack on the phosphorus atom leading to the cleavage of the ester bond, activated by a proton shift from the histidine residue 296, is proposed. The potential energy profiles for the considered reaction cycle are depicted in Figure 5 of Section 3.3.

The possibility of a concerted $\text{S}_{\text{N}}2$ mechanism has also been considered in our investigation, but we found that two transition states are required to complete the catalytic process.

3.1. ES Complex. Since the X-ray structure of rkbPAP used to devise the cluster model of the active site was determined in the presence of an inhibitor, to obtain a valid initial structure for our exploration of the catalytic mechanism, we evaluated several crucial aspects in the construction of our model. First of all, the substrate's orientation into the active site, and then its protonation state and the coordination binding mode to the dimetallic center. In order to consider the right orientation of the substrate into the catalytic cavity, we took into account some experimental indications suggesting that the His 296 may be responsible for the proton shift to the leaving group during the catalytic cycle, while a second conserved residue His 202 should be involved only in the transition-state stabilization.^{14,65,66} According to this evidence, the substrate was modeled in the catalytic cavity with the methoxy group oriented toward the His 296 (Scheme 3a). In addition, we tried to study a mechanism in which the His 202 worked as proton carrier to the leaving group, considering the other stereoisomer of the methyl phosphate (Scheme 3b), but all the efforts to locate the saddle points for the reaction with that model failed.

From geometric point of view, the results obtained using models (a) and (b) show an important difference. The substrate binds in a different manner the dimetallic center in the optimized structures inducing different electronic distributions, probably responsible of the different activity of the two stereoisomers. The optimized ES complex for model (b) is reported in Figure S4 of the Supporting Information.

Another point of conjecture is the mode of substrate binding. Although several studies of this kind of enzyme

Scheme 2. Proposed Mechanism for the Hydrolysis of Methyl-Phosphate Promoted by Red Kidney Bean PAP**Scheme 3.** Considered Substrate Orientations into the Catalytic Cavity

exists, the exact coordination of the substrate to the dimetallic center it is still uncertain. It has been previously proposed that the precise substrate coordination may be pH dependent.⁴ In order to better understand this aspect, we took into consideration that the Fe–Zn–PAP from red kidney beans display a maximum catalytic rate at $\text{pH} \approx 6$.⁷⁸ At that value of pH ($4.5 < \text{pH} < 6.5$), our substrate is likely in its monoanionic form ($\text{CH}_3\text{HPO}_4^-$). At pH slightly higher, the substrate could be present in its dianionic form. In order to provide insight into this important point of controversy, we

tested two different protonation states of the substrate into the active site. We were able to verify that the activation barrier associated with the model containing $\text{CH}_3\text{OPO}_3^{2-}$ as the substrate is higher by more than 10 kcal/mol with respect to the other one relative to the monoanionic species, confirming that the reaction proceeds faster at a lower pH . Moreover, we prove that the pH influences the coordination mode. The $(\text{CH}_3)\text{HPO}_4^-$ substrate binds in a monodentate-like manner the bimetallic center, while the dianionic form of the substrate $\text{CH}_3\text{OPO}_3^{2-}$ results in a bicoordinated ES

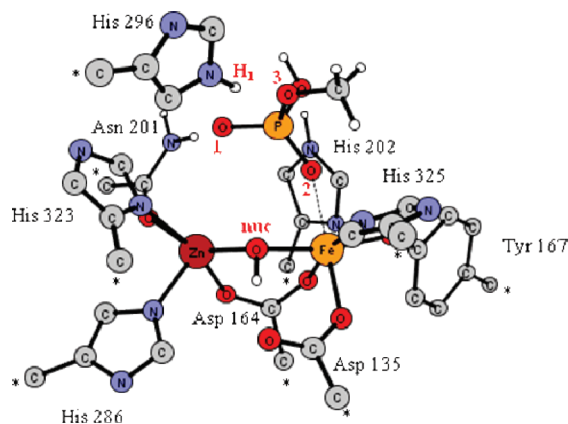


Figure 1. Optimized structure of the ES complex. Only the most significant hydrogen atoms are reported. Stars indicate the atoms kept fixed to their crystallographic positions during optimizations.

Table 1. Main Bond Lengths (Å) of the Optimized Stationary Points along the Reaction Path

	ES	TS ₁	INT ₁	TS ₂	EP
Zn–O ₁	3.47	2.10	2.03	2.03	1.97
Fe–O ₂	2.30	2.11	2.00	2.01	2.07
Zn–Onuc	1.98	2.28	2.17	2.17	–
Fe–Onuc	2.01	2.24	3.36	3.43	–
P–Onuc	3.64	2.00	1.85	1.80	1.55
Fe–Zn	3.54	4.00	4.58	4.83	4.36
O ₃ –H ₁	1.74	1.66	1.76	1.20	0.98

complex (see Figure S5 of the Supporting Information). As a result of this preliminary investigation, we report in Figure 1 the optimized structure of the ES complex. Main geometrical parameters of ES, together with those for the other stationary points encountered along the reaction path, are collected in Table 1.

As shown in Figure 1, the overall geometry of the metal centers predicted by our calculation is of a distorted square pyramidal geometry for the pentacoordinated Zn(II) cation, while the iron center adopts an octahedral geometry. The internuclear distance between the two metal ions is 3.54 Å. In the optimized complex, the substrate is stabilized in the active site by a network of hydrogen-bonding interactions with the Asn 201 and with conserved histidine residues located in the second coordination sphere (His 202 and His 296). The distance between the bridging hydroxide and the phosphorus atom of the incoming substrate is 3.64 Å. Thanks to this disposition in the active site, the substrate is in an ideal near-attack configuration.⁸³ During the optimization, the substrate orients the methoxy group toward the protonated His 296, resulting in a monodentate coordination to the Fe(III) ion. In such a complex, the leaving group is optimally oriented along the axis of the access channel to easily leave the active site after the hydrolysis process. In Figure 2 is shown the orientation of the methoxy group with respect to the whole chain A of the enzyme.

3.2. Reaction Mechanism. The nucleophilic attack of the bridging hydroxide (O_{nuc}) to the substrate phosphorus atom (TS₁) induces a cascade of geometric changes leading to the first enzyme–intermediate complex (INT₁). The subsequent proton shift from the His 296 to the leaving group (TS₂)

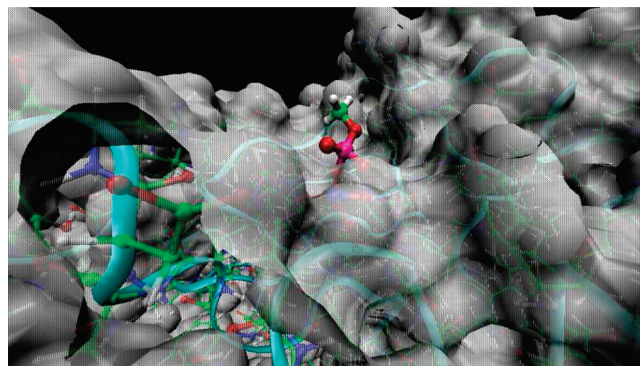


Figure 2. Orientation of the methyl phosphate group into the enzymatic channel. The B3LYP-optimized coordinates of the active site were introduced in the crystallographic data of the rkbPAP (pdb code 4kbp) by superimposition of the carbon atoms kept fixed to their X-ray crystal positions during the optimizations.

culminates in the enzyme–product complex (EP). The geometries of the optimized stationary points (see Table 1) are displayed in Figure 3.

The first transition state (TS₁) involves not only the shortening of the P–O_{nuc} distance, which in the ES varies from 3.64 to 2.00 Å but implies also important changes in the substrate coordination mode to the active site. The methyl-phosphate group binds now in a bidentate manner the dimetallic center, displaying distances of 2.10 and 2.11 Å from Zn and Fe, respectively. The bridging coordination geometry adopted led to an elongation of the Zn–Fe distance from 3.54 Å in the ES complex to 4.00 Å in the TS₁, consenting to increase the nucleophilicity of the metal-bound hydroxide by lengthening the distances Zn–O_{nuc} and Fe–O_{nuc} to 2.28 and 2.24 Å, respectively. In addition, modification in the substrate geometry was observed. The three oxygen atoms of the substrate (O₁, O₂, and O₃) occupy equatorial positions with respect to P, adopting a pentacoordinate geometry. The analysis of the vibrational mode clearly indicates the stretching of the incoming P–O_{nuc} bond, as a result of the nucleophilic attack of the bridging hydroxide to the phosphorus atom, and was confirmed to be a first-order saddle point with only one imaginary frequency (88 cm^{−1}). The hydrogen-bonding network found in the enzyme–substrate complex is still retained in the transition state. In particular the distance between the leaving group's oxygen atom and the hydrogen of the conserved His 296 (O₃–H₁) decreases in the transition state, reaching a distance of 1.66 Å. The latter not only contributes to stabilize the transition state but allows an optimal orientation of the leaving group toward the subsequent protonation step. TS₁ lies at 15.6 kcal/mol above ES, as can be observed from Figure 5. Upon addition of solvent effects, the barrier becomes slightly lower (13.1 and 13.3 kcal/mol for protein environment and water, respectively).

A trigonal bipyramidal geometry was found for the phosphorus atom in the intermediate complex (INT₁) in which the P–O_{nuc} bond is completely formed being 1.85 Å. This mode of coordination has been observed in the crystal

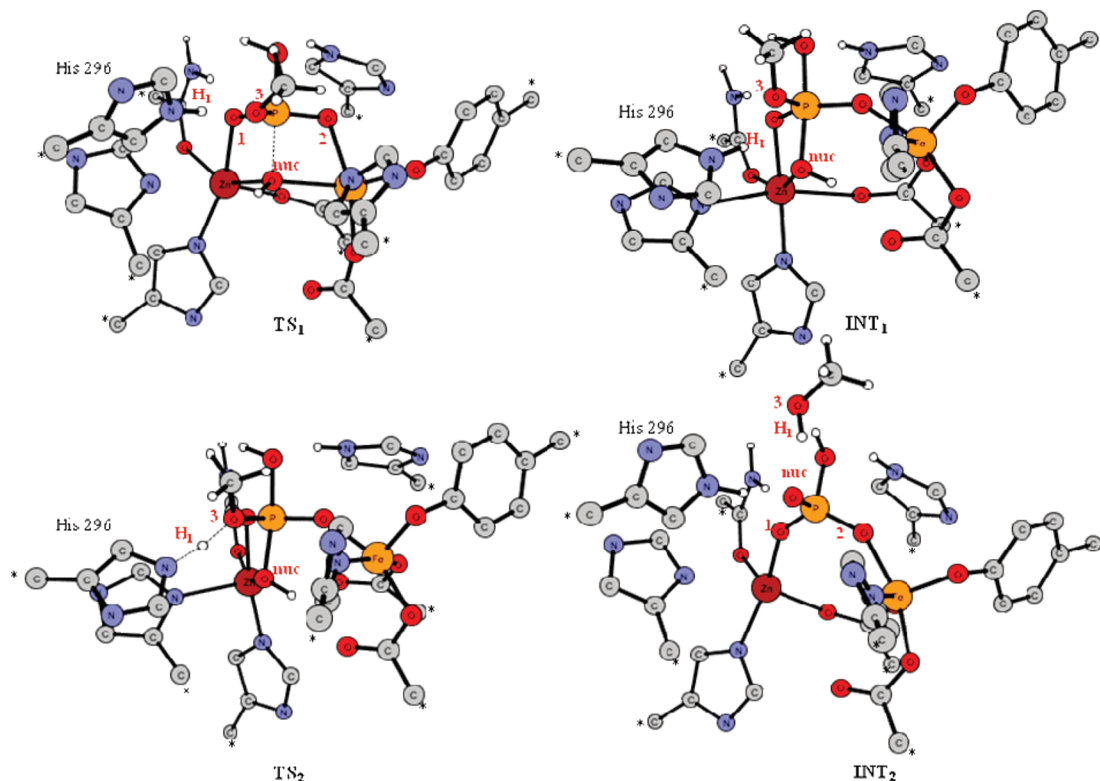


Figure 3. Optimized structures of the stationary points TS_1 , INT_1 , TS_2 , and EP for the hydrolysis of the methyl phosphate promoted by the rkbPAP enzyme. Stars indicate the atoms kept fixed to their crystallographic positions during optimizations. Only the most significant hydrogen atoms are reported in the figure.

structures of sweet potato PAP⁷⁸ and di-Ni(II) urease,⁸⁴ both with bound phosphate, and of di-Mn(II) λ PP,⁸⁵ with bound sulfate.

Although the substrate remains still bicoordinated to the dimetallic center, the distance between the Zn and Fe ions increases significantly becoming 4.58 Å. The lengthening of the metal–metal distance was already suggested in a previous work, in which the binding of the substrate has been shown to decrease the coupling interaction between the two metal centers, as indicated by a decrease in J from 20 to 6 cm^{-1} .⁵⁸ The bridging hydroxide is completely shifted away from the trivalent metal ion toward the divalent one, showing distances of 3.36 and 2.17 Å from them, respectively. From an energetic point of view, in both the gas phase and the solvent, the intermediate INT_1 shows only a small difference in the energy values with respect to TS_1 .

To get the final product, a proton shift from the His 296 to the substrate's methylated oxygen atom was observed in the second transition state TS_2 . An imaginary frequency of $376i \text{ cm}^{-1}$ confirms its nature as first-order saddle point. The vibrational mode indicates the motion of the N–H₁ and H₁–O₃ couple of bonds with critical lengths of 1.27 and 1.20 Å, respectively. In such a transition state, the proton shift happens before the just formed methanol group leaves the substrate. This stationary point lies at 19.3 kcal/mol above ES in the gas phase, while solvation effects increase this difference becoming 21.0 and 22.7 kcal/mol in protein environment and water, respectively. The requirement of an activated leaving group to reach an optimal catalytic efficiency has been the subject of previous studies.^{78,24} For red kidney bean and pig PAP, it was demonstrated that

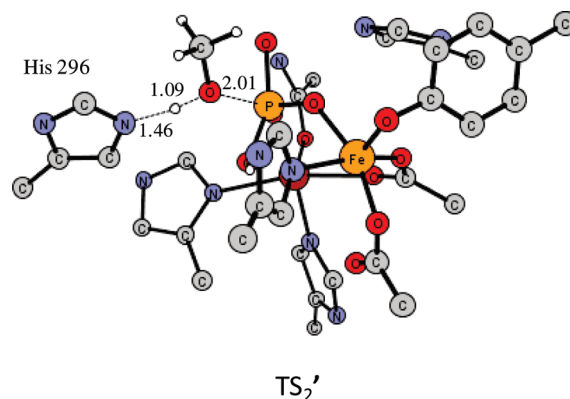


Figure 4. Concerted transition state in which the release of the methoxy group occurs at the same time of the proton shift from the His 296

reactivity declines as the leaving group's pK_a increases, while no dependence of catalytic parameters from the leaving group's pK_a was found from the sweet potato PAP. This evidence suggests that sweet potato PAP can catalyze efficiently a range of activated and inactivated phosphate esters in contrast to red kidney bean and pig PAPs. The possibility that the bond between the phosphorus atom and the methoxy group breaks without activation was also considered in our investigation. We were able to characterize a further transition state (TS_2') in which no activation takes place before the leaving group leaves and in which a shift from the His 296 occurs in a concerted manner with the scission (Figure 4). The analysis of the obtained vibrational frequency ($138i \text{ cm}^{-1}$) clearly indicates the rupture of the

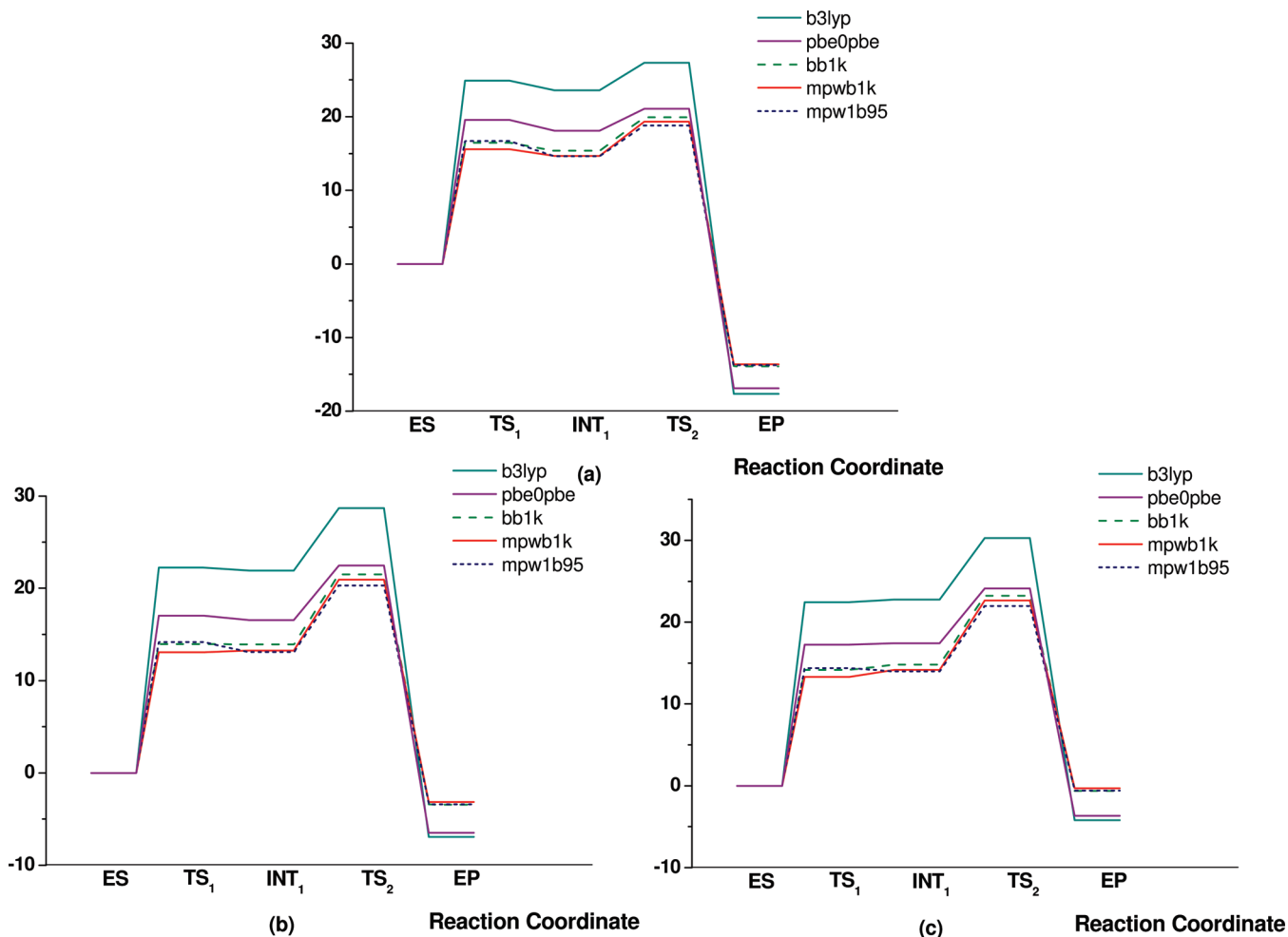


Figure 5. Potential energy profiles for the reaction in: (a) gas phase, (b) protein environment ($\epsilon = 4$), and (c) water.

P–O₃ bond and the formation of the O₃–H₁ one. Nevertheless, this hypothesis of a concerted transition state is energetically unfavorable requiring a higher amount of energy with respect to the other transition state TS₂. This stationary point lies at 32.0 kcal/mol with respect to the ES in the gas phase, while with the introduction of solvent effects, the differences become 36.8 and 39.0 kcal/mol in protein environment and water. According to our calculation for red kidney bean PAP, we can observe that the activation of the leaving group is crucial to get the final enzyme–product complex.

The last point encountered along the reaction path corresponds to the enzyme–product complex (EP). The release of the leaving group induces significant structural rearrangements. The phosphorus atom is likely to regenerate its optimal tetrahedral geometry requiring a reorganization of the active site. During the optimization, a rotation of the bond between the phosphorus atom and the native nucleophile (P–O_{nuc}) occurs to reach a reasonable tetra-coordination. The phosphate remains tightly bound to the dimetallic center by the oxygen atoms O₁ and O₂ and with distances of 1.97 and 2.07 Å from Zn and Fe, respectively. The OH_{nuc} group oriented toward the His 296 spontaneously transfers the proton to the His 296, regenerating the active site. The distance between the metal ions decreases in the EP complex reaching 4.36 Å, from 4.83 Å in the previous TS₂ geometry.

Such a complex is stabilized by a network of hydrogen bonding involving the His 296 and His 202 of the second coordination sphere, the His 325 Fe(III)-bound, and Asn 201 Zn(II)-bound. The EP complex is obtained exothermically with a great energy gain (13.6 kcal/mol in gas phase). Interestingly, the solvent effect seems to destabilize the product of reaction that is found at –3.1 and –0.3 kcal/mol lower in energy than the reactants.

3.3. Energetic of the Reaction. Different exchange–correlation functionals were used to estimate the energies of the stationary points located on the paths in the gas phase and in different environments (water and protein). This benchmark could be interesting since a large number of density functionals at different levels of sophistication have become available, and a well-established computation protocol for the enzymatic reaction is still lacking.

A detailed analysis of the performance of the popular B3LYP functional in the reproduction of a large variety of chemical properties and system types was performed in a recent study.⁸⁰ The latter shows that the B3LYP performance in the prediction of geometrical structures including closed- and open-shell structures is satisfactory and is able to compete in accuracy with the other proposed XC functional as well as with other ab initio methods.

On the contrary, for some properties several new density functionals significantly outperform this popular hybrid

Table 2. Energies (kcal/mol) of the Stationary Points along the Reaction Paths^a

		ES	TS ₁	INT ₁	TS ₂	EP
Gas phase	B3LYP	0	24.93	23.58	27.33	−17.65
	PBE0PBE	0	19.58	18.11	21.07	−16.87
	BB1K	0	16.47	15.36	19.92	−13.91
	MPWB1K	0	15.59	14.66	19.34	−13.64
	MPW1B95	0	16.68	14.61	18.83	−13.76
$\epsilon = 4$	B3LYP	0	22.26	21.94	28.67	−6.94
	PBE0PBE	0	17.03	16.55	22.48	−6.48
	BB1K	0	13.94	13.92	21.52	−3.45
	MPWB1K	0	13.06	13.24	20.96	−3.14
	MPW1B95	0	14.16	13.09	20.32	−3.39
$\epsilon = 80$	B3LYP	0	22.44	22.77	30.27	−4.18
	PBE0PBE	0	17.24	17.42	24.11	−3.67
	BB1K	0	14.17	14.82	23.22	−0.62
	MPWB1K	0	13.3	14.15	22.67	−0.3
	MPW1B95	0	14.39	13.97	21.98	−0.57

^a In the gas phase, in the protein environment ($\epsilon = 4$), and in water ($\epsilon = 80$).

functional. Many studies have demonstrated that the hybrid-meta GGA methods give more reliable results in the reproduction of the reaction kinetics showing great ability in the calculation of barrier heights with high accuracy.⁸⁰ Taking these aspects under consideration, in our investigation we chose the B3LYP functional for the optimizations of all the stationary points along the reaction path and, to obtain energetic values, we performed single point calculation with a larger basis set testing the hybrids B3LYP and PBE0PBE and the meta-hybrids BB1K, MPWB1K, and MW1B95. The results are shown in Figure 5.

From Table 2 and Figure 5 it is possible to observe that the hybrid-meta GGA functionals (BB1K, MPWB1K, and MPW1B95) give very similar results concerning the energy of the stationary points along the paths in the gas phase, in the protein environment, and in water. In addition, the calculated values well agree with the energy barriers extracted from the k_{cat} experimentally obtained for reactions catalyzed by PAPs enzymes (13–15 kcal/mol depending on the substrate).^{24,78,79}

On the contrary, the profiles obtained at B3LYP and PBE0PBE levels of theory show higher energy results. Furthermore, we can observe that the protein environment has a slightly higher stabilization effect on the structures than the more polar water environment, and moreover only the first part of the mechanism results stabilized. The TS₂ and the product of the reaction seem to be destabilized with the introduction of the environment.

Conclusion

The catalytic mechanism of the Fe(III)–Zn(II) purple acid phosphatase (PAP) enzyme was investigated at the density functional (DF) level of theory. The model cluster used to simulate the active site of the enzyme, made up of 114 atoms, was large enough to reliably reproduce the hydrolysis of the methyl-phosphate monoanionic substrate ($\text{CH}_3\text{OHPO}_3^-$).

The main results can be summarized as follows:

- The PAP hydrolysis reaction involves the formation of the trigonal bipyramidal intermediate, arising from nucleophilic addition of the bridging hydroxide molecule

to the substrate phosphorus atom, followed by the protonation of the substrate methoxy group leading to the final P–O bond cleavage.

- The role of the two conserved histidine residues was elucidated. The protonated His 296 has been confirmed to play a fundamental role acting as a proton carrier and activating the methoxy leaving group, while the His 202 takes part in the optimal orientation of the substrate during the catalysis by establishing a hydrogen bond with it.
- From our study emerges that the rate-limiting step of the reaction is the nucleophilic attack followed by the less energetically demanding release of the leaving group.
- We were able to establish that the activation of the leaving group by the His 296 is actually crucial in order to reach an optimal catalytic efficiency. A transition state (TS₂[′]) in which no activation takes place before the leaving group leaves and in which a shift from the His 296 occurs in a concerted manner with the scission was further characterized, but it requires a higher amount of energy to be overcome than TS₂.
- The dianionic form of the substrate was also considered in our investigation. We found that the activation barrier for the nucleophilic attack associated with that model is considerably higher than the other one relative to the monoanionic species, confirming that the reaction proceeds faster at lower pH. This result is in agreement with the experimental indications that support a monoanionic substrate being pH = 6, the optimum value for the achievement of the maximum catalytic rate for rkbPAP.⁷⁸
- We found that the monoanionic form of methylphosphate binds in a monodentate-like manner, the bimetallic center in the precatalytic complex, while the dianionic form $\text{CH}_3\text{OPO}_3^{2-}$ results in a bicoordinated ES complex. Our evidence supports the hypothesis that the mode of substrate binding is pH dependent, as it has been previously suggested in other works.⁴
- Different XC functionals were used to calculate the barrier heights in the gas phase, in the protein environment, and in water. The meta-hybrid functionals give results that better agree with the energy barriers calculated from the k_{cat} obtained for similar reactions catalyzed by PAPs enzymes, confirming their ability in the reproduction of the reaction kinetics.

Acknowledgment. The University of Calabria, the Regione Calabria (FSE-POR 2000/2006, misura 3.7), the MIUR PRIN 2008, and the University of Porto are gratefully acknowledged.

Supporting Information Available: Further information regarding the chosen spin state along the PES, spin density distribution, and molecular orbital picture for the all stationary points, optimized structure, and selected geometrical parameters of the ES complex using Model (b), and the ES and TS₁ containing $\text{CH}_3\text{OPO}_3^{2-}$ substrates are provided. This information are available free of charge via the Internet at <http://pubs.acs.org/>.

References

- (1) Twitchett, M. B.; Sykes, A. G. *Eur. J. Inorg. Chem.* **1999**, 2105.
- (2) Klabunde, T.; Krebs, B. *Struct. Bonding (Berlin, Ger.)* **1997**, 89, 177.
- (3) Oddie, G. W.; Schenk, G.; Angel, N. Z.; Walsh, N.; Guddat, L. W.; de Jersey, J.; Cassady, A. I.; Hamilton, S. E.; Hume, D. A. *Bone* **2000**, 27, 575.
- (4) Mitić, N.; Smith, S. J.; Neves, A.; Guddat, L. W.; Gahan, L. R.; Schenk, G. *Chem. Rev.* **2006**, 106, 3338.
- (5) Wilcox, D. E. *Chem. Rev.* **1996**, 96, 2435.
- (6) Sträter, N.; Lipscomb, W. N.; Klabunde, T.; Krebs, B. *Angew. Chem., Int. Ed. Engl.* **1996**, 35, 2024.
- (7) Dismukes, G. C. *Chem. Rev.* **1996**, 96, 2909.
- (8) Barford, D.; Das, A. K.; Egloff, M. P. *Annu. Rev. Biophys. Biomol. Struct.* **1998**, 27, 133.
- (9) Rusnak, F.; Mertz, P. *Physiol. Rev.* **2000**, 80, 1483.
- (10) Jackson, M. D.; Denu, J. M. *Chem. Rev.* **2001**, 101, 2313.
- (11) Lowther, W. T.; Matthews, B. W. *Biochim. Biophys. Acta* **2000**, 1477, 157.
- (12) Nuttleman, P. R.; Roberts, R. M. *J. Biol. Chem.* **1990**, 265, 12192.
- (13) Sibille, J. C.; Doi, K.; Aisen, P. *J. Biol. Chem.* **1987**, 262, 59.
- (14) Kaija, H.; Alatalo, S. L.; Halleen, J. M.; Lindqvist, Y.; Schneider, G.; Väänänen, H. K.; Vihko, P. *Biochem. Biophys. Res. Commun.* **2002**, 292, 128.
- (15) Räisänen, S. R.; Alatalo, S. L.; Ylipahkala, H.; Halleen, J. M.; Cassady, A. I.; Hume, D. A.; Väänänen, H. K. *Biochem. Biophys. Res. Commun.* **2005**, 331, 120.
- (16) Moss, D. W.; Raymond, F. D.; Wile, D. B. *Crit. Rev. Clin. Lab. Sci.* **1995**, 32, 431.
- (17) Angel, N. Z.; Walsh, N.; Forwood, M. R.; Ostrowski, M. C.; Cassady, A. I.; Hume, D. A. *J. Bone Miner. Res.* **2000**, 15, 103.
- (18) Hayman, A. R.; Jones, S. J.; Boyde, A.; Foster, D.; Colledge, W. H.; Carlton, M. B.; Evans, M. J.; Cox, T. M. *Development* **1996**, 122, 3151.
- (19) Ek-Rylander, B.; Flores, M.; Wendel, M.; Heinegard, D.; Andersson, G. *J. Biol. Chem.* **1994**, 269, 14853.
- (20) Valizadeh, M.; Schenk, G.; Nash, K.; Oddie, G. W.; Guddat, L. W.; Hume, D. A.; de Jersey, J.; Burke, T. R., Jr.; Hamilton, S. *Arch. Biochem. Biophys.* **2004**, 424, 154.
- (21) Cashikar, A. G.; Kumaresan, R.; Rao, N. M. *Plant Physiol.* **1997**, 114, 907.
- (22) Antanaitis, B. C.; Aisen, P. *J. Biol. Chem.* **1982**, 257, 5330.
- (23) Doi, K.; Bradley, C.; Aisen, P. *Struct. Bonding (Berlin, Ger.)* **1988**, 70, 1.
- (24) Schenk, G.; Ge, Y.; Carrington, L. E.; Wynne, C. J.; Searle, I. R.; Carroll, B. J.; Hamilton, S.; de Jersey, J. *Arch. Biochem. Biophys.* **1999**, 370, 183.
- (25) Durmus, A.; Eicken, C.; Sift, B. H.; Kratel, A.; Kappi, R.; Hütterman, J.; Krebs, B. *Eur. J. Biochem.* **1999**, 260, 709.
- (26) Merckx, M.; Averill, B. A. *Biochemistry* **1998**, 37, 8490.
- (27) Chen, T. T.; Bazer, F. W.; Cetorelli, J. J.; Pollard, W. E.; Roberts, R. M. *J. Biol. Chem.* **1973**, 248, 8560.
- (28) Campbell, H. D.; Zerner, B. *Biochem. Biophys. Res. Commun.* **1973**, 54, 1493.
- (29) Campbell, H. D.; Dionysius, D. A.; Keough, D. T.; Wilson, B. E.; de Jersey, J.; Zerner, B. *Biochem. Biophys. Res. Commun.* **1978**, 82, 615.
- (30) Robinson, D. B.; Glew, R. H. *J. Biol. Chem.* **1980**, 255, 5864.
- (31) Hayman, A. R.; Warburton, M. J.; Pringle, J. A.; Coles, B.; Chambers, T. J. *Biochem. J.* **1989**, 261, 601.
- (32) Allen, S. H.; Nuttleman, P. R.; Ketcham, C. M.; Roberts, R. M. *J. Bone Miner. Res.* **1989**, 4, 47.
- (33) Janckila, A. J.; Woodford, T. A.; Lam, K. W.; Li, C. Y.; Yam, L. T. *Leukemia* **1992**, 6, 199.
- (34) Beck, J. L.; McConachie, L. A.; Summors, A. C.; Arnold, W. N.; de Jersey, J.; Zerner, B. *Biochim. Biophys. Acta* **1986**, 869, 61.
- (35) Bozzo, G. G.; Raghothama, K. G.; Plaxton, W. C. *Biochem. J.* **2004**, 377, 419.
- (36) Bozzo, G. G.; Raghothama, K. G.; Plaxton, W. C. *Eur. J. Biochem.* **2002**, 269, 6278.
- (37) Schenk, G.; Boutchard, C. L.; Carrington, L. E.; Noble, C. J.; Moubaraki, B.; Murray, K. S.; de Jersey, J.; Hanson, G. R.; Hamilton, S. *J. Biol. Chem.* **2001**, 276, 19084.
- (38) Schenk, G.; Guddat, L. W.; Ge, Y.; Carrington, L. E.; Hume, D. A.; Hamilton, S.; de Jersey, J. *Gene* **2000**, 250, 117.
- (39) Antanaitis, B. C.; Aisen, P.; Lilienthal, H. R. *J. Biol. Chem.* **1983**, 258, 3166.
- (40) Averill, B. A.; Davis, J. C.; Burman, S.; Zirino, T.; Sanders-Loehr, J.; Loehr, T. M.; Sage, J. T.; Debrunner, P. G. *J. Am. Chem. Soc.* **1987**, 109, 3760.
- (41) Yang, Y.-S.; McCormick, J. M.; Solomon, E. I. *J. Am. Chem. Soc.* **1997**, 119, 11832.
- (42) Wang, D. L.; Holz, R. C.; David, S. S.; Que, L.; Stankovich, M. T. *Biochemistry* **1991**, 30, 8187.
- (43) Bernhardt, P. V.; Schenk, G.; Wilson, G. J. *Biochemistry* **2004**, 43, 10387.
- (44) Beck, J. L.; Keough, D. T.; de Jersey, J.; Zerner, B. *Biochim. Biophys. Acta* **1984**, 791, 357.
- (45) Funhoff, E. G.; Ljusberg, J.; Wang, Y.; Andersson, G.; Averill, B. A. *Biochemistry* **2001**, 40, 11614.
- (46) Funhoff, E. G.; Klaassen, C. H. W.; Samyn, B.; Van Beeumen, J.; Averill, B. A. *ChemBioChem* **2001**, 2, 355.
- (47) Merckx, M.; Averill, B. A. *Biochemistry* **1998**, 37, 11223.
- (48) Merckx, M.; Pinkse, M. W. H.; Averill, B. A. *Biochemistry* **1999**, 38, 9914.
- (49) Pinkse, M. W. H.; Merckx, M.; Averill, B. A. *Biochemistry* **1999**, 38, 9926.
- (50) Funhoff, E. G.; Bollen, M.; Averill, B. A. *J. Inorg. Biochem.* **2005**, 99, 521.
- (51) Beck, J. L.; McArthur, M. J.; de Jersey, J.; Zerner, B. *Inorg. Chim. Acta* **1988**, 153, 39.
- (52) Beck, J. L.; de Jersey, J.; Zerner, B. *J. Am. Chem. Soc.* **1988**, 110, 3317.
- (53) Gehring, S.; Fleischhauer, P.; Behlendorf, M.; Huber, M.; Lorösch, J.; Haase, W.; Dietrich, M.; Witzel, H.; Locke, R.; Krebs, B. *Inorg. Chim. Acta* **1996**, 252, 13.

- (54) Battistuzzi, G.; Dietrich, M.; Locke, R.; Witzel, H. *Biochem. J.* **1997**, *323*, 593.
- (55) Sträter, N.; Klabunde, T.; Tucker, P.; Witzel, H.; Krebs, B. *Science* **1995**, *268*, 1489.
- (56) Klabunde, T.; Sträter, N.; Fröhlich, R.; Witzel, H.; Krebs, B. *J. Mol. Biol.* **1996**, *259*, 737.
- (57) Klabunde, T.; Sträter, N.; Krebs, B.; Witzel, H. *FEBS Lett.* **1995**, *367*, 56.
- (58) Smoukov, S. K.; Quaroni, L.; Wang, X.; Doan, P. E.; Hoffman, B. M.; Que, L., Jr. *J. Am. Chem. Soc.* **2002**, *124*, 2595.
- (59) Guddat, L. W.; McAlpine, A. S.; Hume, D.; Hamilton, S.; de Jersey, J.; Martin, J. L. *Structure* **1999**, *7*, 757.
- (60) Lindqvist, Y.; Johansson, E.; Kaija, H.; Vihko, P.; Schneider, G. *J. Mol. Biol.* **1999**, *291*, 135.
- (61) Wang, X.; Que, L. *Biochemistry* **1998**, *37*, 7813.
- (62) Merckx, M.; Averill, B. A. *J. Am. Chem. Soc.* **1999**, *121*, 6683.
- (63) Merckx, M.; Averill, B. A. *Biochemistry* **1998**, *37*, 8490.
- (64) Twitchett, M. B.; Schenk, G.; Aquino, M. A. S.; Yiu, D. T. Y.; Lau, T. C.; Sykes, A. G. *Inorg. Chem.* **2002**, *41*, 5787.
- (65) Funhoff, E. G.; Wang, Y.; Andersson, G.; Averill, B. A. *FEBS J.* **2005**, *272*, 2968.
- (66) Truong, N. T.; Naseri, J. I.; Vogel, A.; Rompel, A.; Krebs, B. *Arch. Biochem. Biophys.* **2005**, *440*, 38.
- (67) Schenk, G.; Elliott, T. W.; Leung, L.; Carrington, L. E.; Mitić, N.; Gahan, L. R.; Guddat, L. W. *BMC Struct. Biol.* **2008**, *8*, 6.
- (68) Frisch, M. J.; Trucks, G. W.; Schlegel, H. B.; Scuseria, G. E.; Robb, M. A.; Cheeseman, J. R.; Montgomery, J. A., Jr.; Vreven, T.; Kudin, K. N.; Burant, J. C.; Millam, J. M.; Iyengar, S. S.; Tomasi, J.; Barone, V.; Mennucci, B.; Cossi, M.; Scalmani, G.; Rega, N.; Petersson, G. A.; Nakatsuji, H.; Hada, M.; Ehara, M.; Toyota, K.; Fukuda, R.; Hasegawa, J.; Ishida, M.; Nakajima, T.; Honda, Y.; Kitao, O.; Nakai, H.; Klene, M.; Li, X.; Knox, J. E.; Hratchian, H. P.; Cross, J. B.; Bakken, V.; Adamo, C.; Jaramillo, J.; Gomperts, R.; Stratmann, R. E.; Yazyev, O.; Austin, A. J.; Cammi, R.; Pomelli, C.; Ochterski, J. W.; Ayala, P. Y.; Morokuma, K.; Voth, G. A.; Salvador, P.; Dannenberg, J. J.; Zakrzewski, V. G.; Dapprich, S.; Daniels, A. D.; Strain, M. C.; Farkas, O.; Malick, D. K.; Rabuck, A. D.; Raghavachari, K.; Foresman, J. B.; Ortiz, J. V.; Cui, Q.; Baboul, A. G.; Clifford, S.; Cioslowski, J.; Stefanov, B. B.; Liu, G.; Liashenko, A.; Piskorz, P.; Komaromi, I.; Martin, R. L.; Fox, D. J.; Keith, T.; Al-Laham, M. A.; Peng, C. Y.; Nanayakkara, A.; Challacombe, M.; Gill, P. M. W.; Johnson, B.; Chen, W.; Wong, M. W.; Gonzalez, C.; Pople, J. A. *Gaussian 03*, revision A.1; Gaussian, Inc.: Pittsburgh, PA, 2003.
- (69) Becke, A. D. *J. Chem. Phys.* **1993**, *98*, 5648.
- (70) Lee, C. T.; Yang, W. T.; Parr, R. G. *Phys. Rev. B: Condens. Matter Mater. Phys.* **1988**, *37*, 785.
- (71) Andrae, D.; Haussermann, U.; Dolg, M.; Stoll, H.; Preuss, H. *Theor. Chim. Acta* **1990**, *77*, 123.
- (72) Barone, V.; Cossi, M. *J. Phys. Chem. A* **1998**, *102*, 1995.
- (73) Cossi, M.; Rega, N.; Scalmani, G.; Barone, V. *J. Comput. Chem.* **2003**, *24*, 669.
- (74) Rappe, A. K.; Casewit, C. J.; Colwell, K. S.; Goddard, W. A., III; Skiff, W. M. *J. Am. Chem. Soc.* **1992**, *114*, 10024.
- (75) Adamo, C.; Barone, V. *J. Chem. Phys.* **1999**, *110*, 6158.
- (76) Zhao, Y.; Lynch, B. J.; Truhlar, D. G. *J. Phys. Chem. A* **2004**, *108*, 2715.
- (77) Zhao, Y.; Truhlar, D. G. *J. Phys. Chem. A* **2004**, *108*, 6908.
- (78) Schenk, G.; Gahan, L. R.; Carrington, L. E.; Mitić, N.; Valizadeh, M.; Hamilton, S. E.; de Jersey, J.; Guddat, L. W. *Proc. Natl. Acad. Sci. U.S.A.* **2005**, *102*, 273.
- (79) Cox, R. S.; Schenk, G.; Mitić, N.; Gahan, L. R.; Hengge, A. C. *J. Am. Chem. Soc.* **2007**, *129*, 9550.
- (80) Sousa, S. F.; Fernandes, P. A.; Ramos, M. J. *J. Phys. Chem. A* **2007**, *111*, 10439.
- (81) Bras, N. F.; Moura-Tamames, S. A.; Fernandes, P. A.; Ramos, M. J. *J. Comput. Chem.* **2008**, *29*, 2565.
- (82) Leopoldini, M.; Russo, N.; Toscano, M. *Chem.—Eur. J.* **2009**, *15*, 8026.
- (83) Hur, S.; Brulce, T. C. *Proc. Natl. Acad. Sci. U.S.A.* **2003**, *100*, 12015.
- (84) Voegtli, W. C.; White, D. J.; Reiter, N. J.; Rusnak, F.; Rosenzweig, A. C. *Biochemistry* **2000**, *39*, 15365.
- (85) Benini, S.; Rypniewski, W. R.; Wilson, K. S.; Ciurli, S.; Mangani, S. *J. Biol. Inorg. Chem.* **2001**, *6*, 778.

-Supporting Information-

Atomistic details of the Catalytic Mechanism of Fe(III)-Zn(II) Purple Acid Phosphatase

Marta E. Alberto¹, Tiziana Marino¹, Maria J. Ramos² and Nino Russo^{1}*

¹ Dipartimento di Chimica Università della Calabria, Via P. Bucci, cubo 14c, 87036 Arcavacata di Rende (CS), Centro di Calcolo ad Alte Prestazioni per Elaborazioni Parallele e Distribuite – Centro d’Eccellenza MIUR, Italy;

² REQUIMTE, Departamento de Química, Faculdade de Ciências, Universidade do Porto, Rua do Campo Alegre, 687, 4169-007 Porto, Portugal

AUTHOR EMAIL ADDRESS: nrusso@unical.it

- **Comparison between energetic profiles obtained at quartet and sextet spin multiplicities;** -S1-
- **Spin Density distribution;** -S2-
- **Molecular orbital picture for (a) ES (b) TS₁ (c) INT₁ (d) TS₂ (e) EP geometries;** -S3-
- **Optimized structure and selected geometrical parameters of the ES complex using Model (b);** -S4-
- **Model (a) - CH₃OPO₃²⁻ substrate;** -S5-

Comparison between energetic profiles obtained at quartet and sextet spin multiplicities

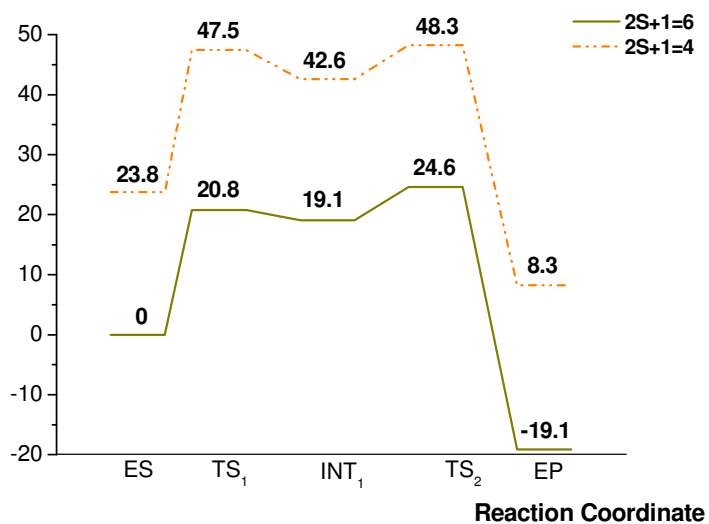


Figure S1. Comparison between energetic profiles obtained at different spin multiplicities. The reported values arise from single point calculation on the optimized geometries obtained with sextet spin state, in gas phase with 6-31G(d,p)/SDD bases.

Spin Density distribution

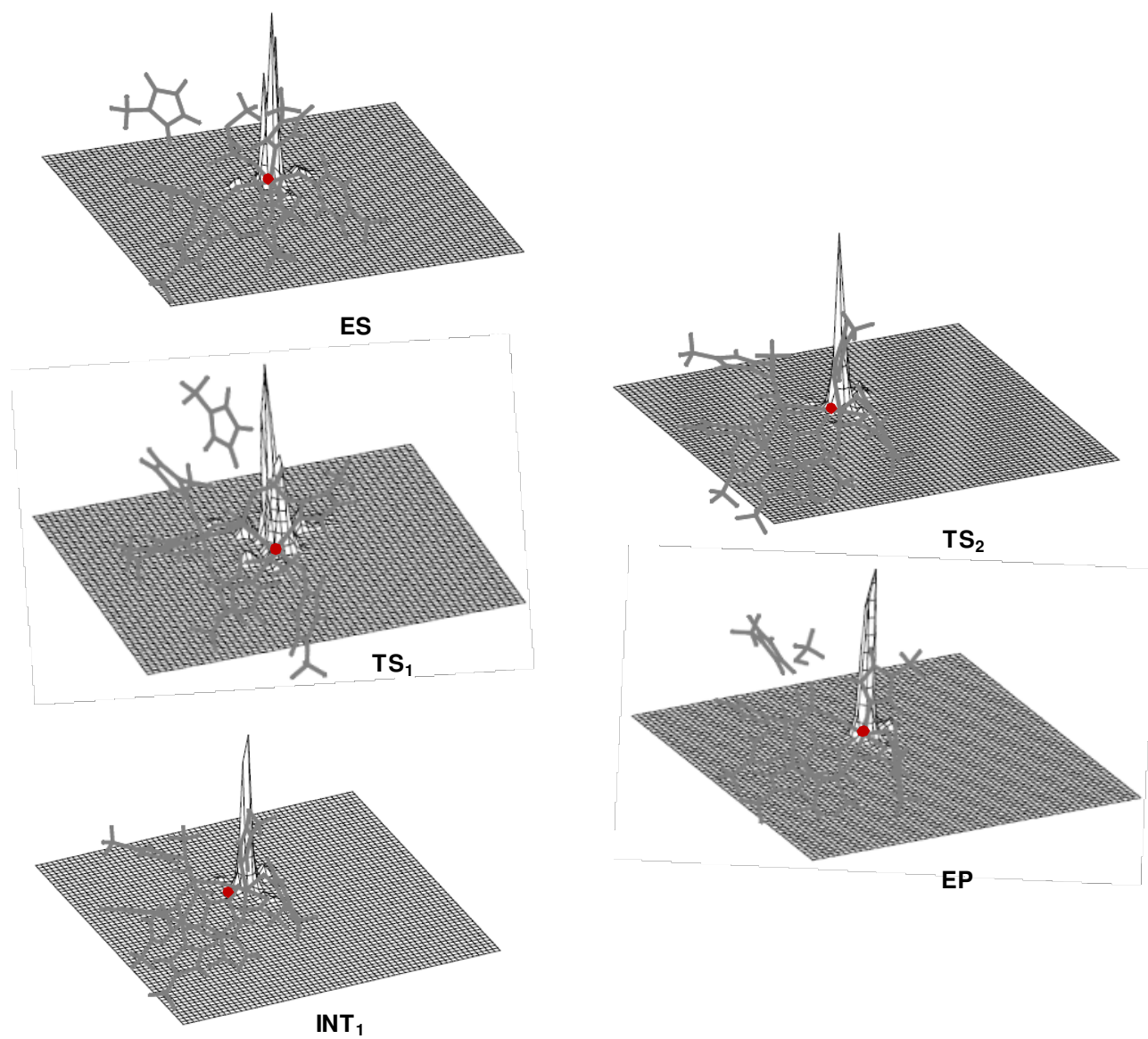


Figure S2. Spin Density distribution in each stationary point along the energetic profile. Red points are located on the iron ion.

Molecular orbital picture for (a) ES (b) TS₁ (c) INT₁ (d) TS₂ (e) EP geometries.

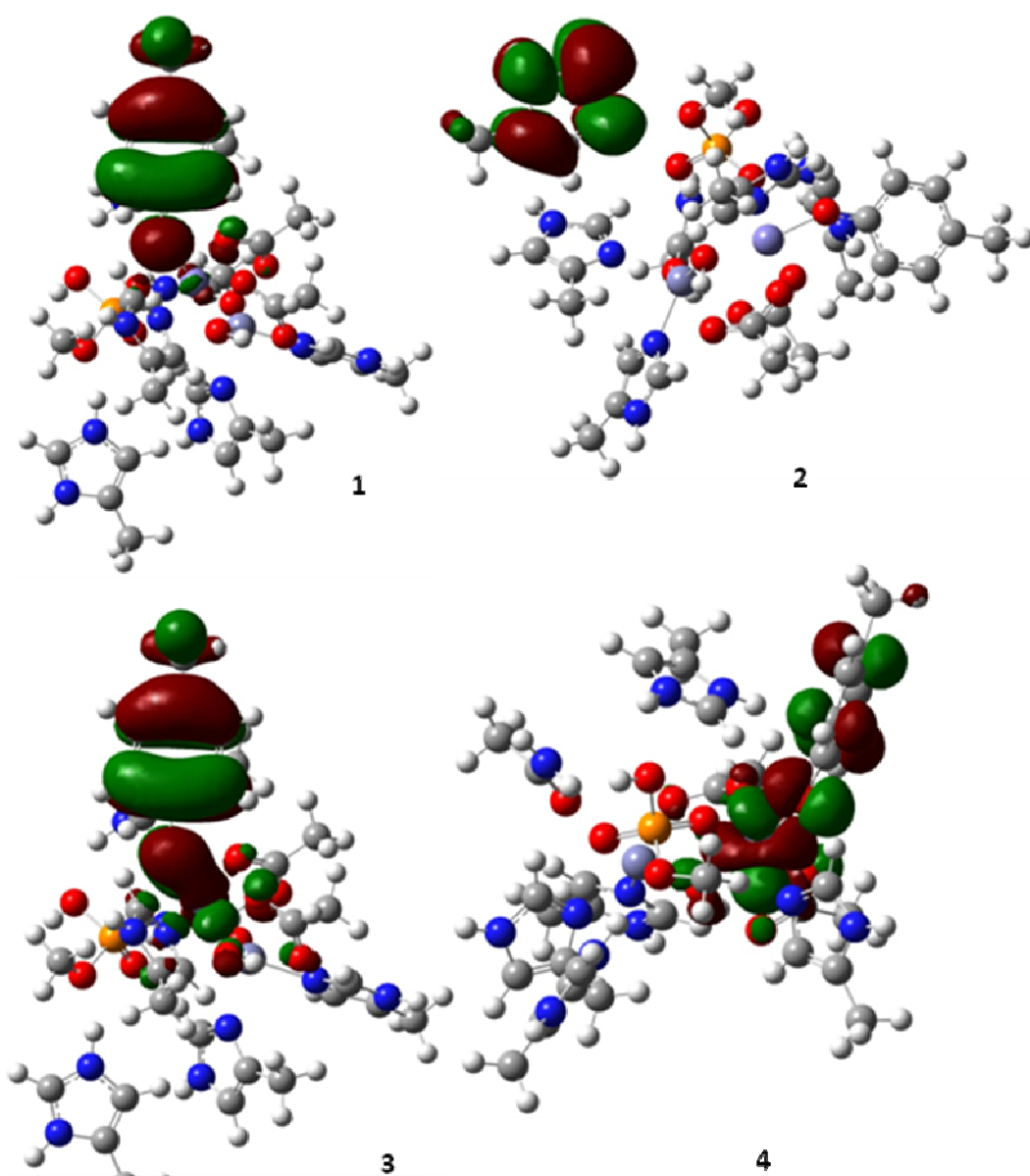


Figure S3(a). Molecular orbital picture for ES geometry. 1) α HOMO 2) α LUMO 3) β HOMO 4) β LUMO.

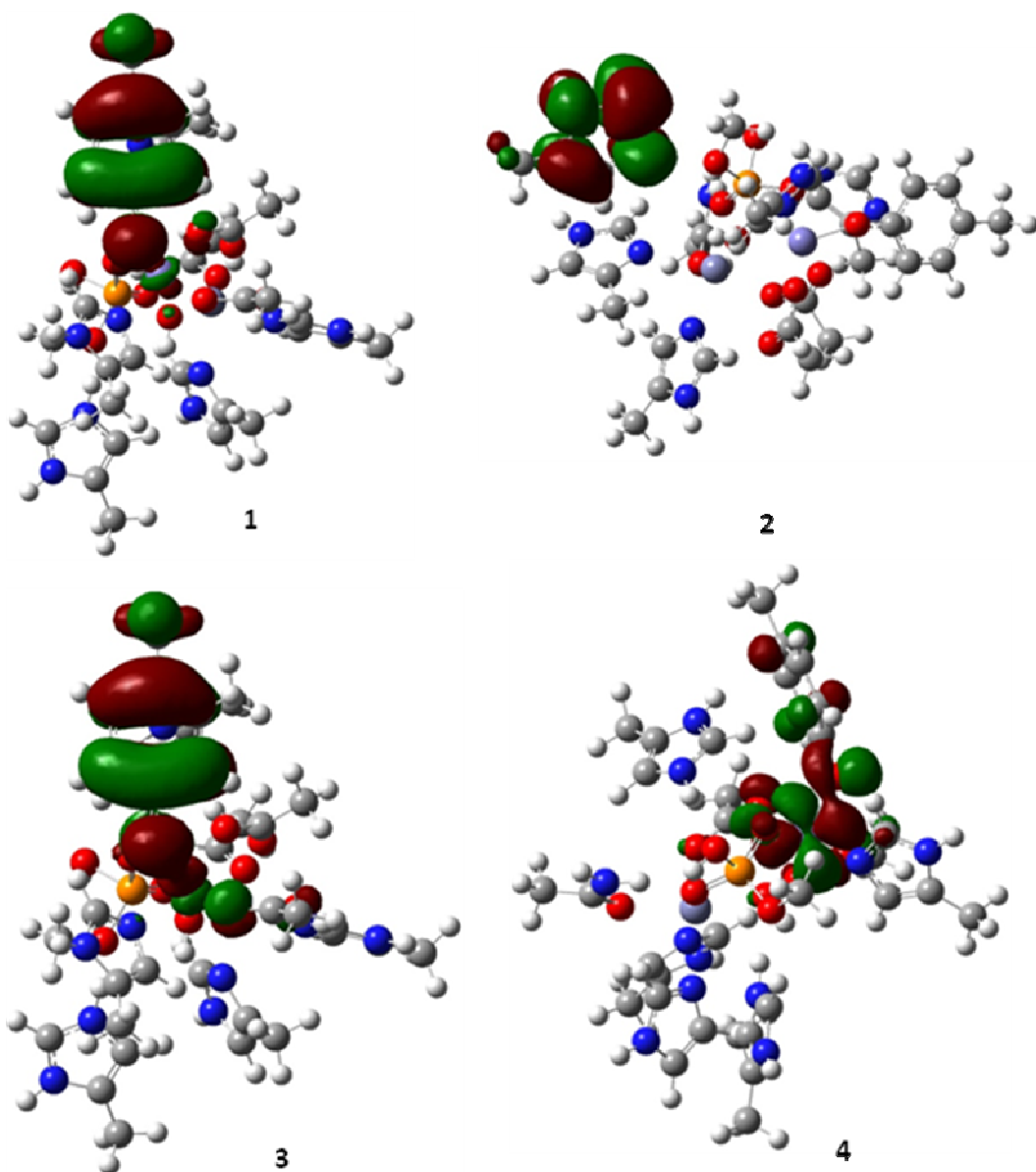


Figure S3(b). Molecular orbital picture for TS_1 geometry; 1) α HOMO 2) α LUMO 3) β HOMO 4) β LUMO.

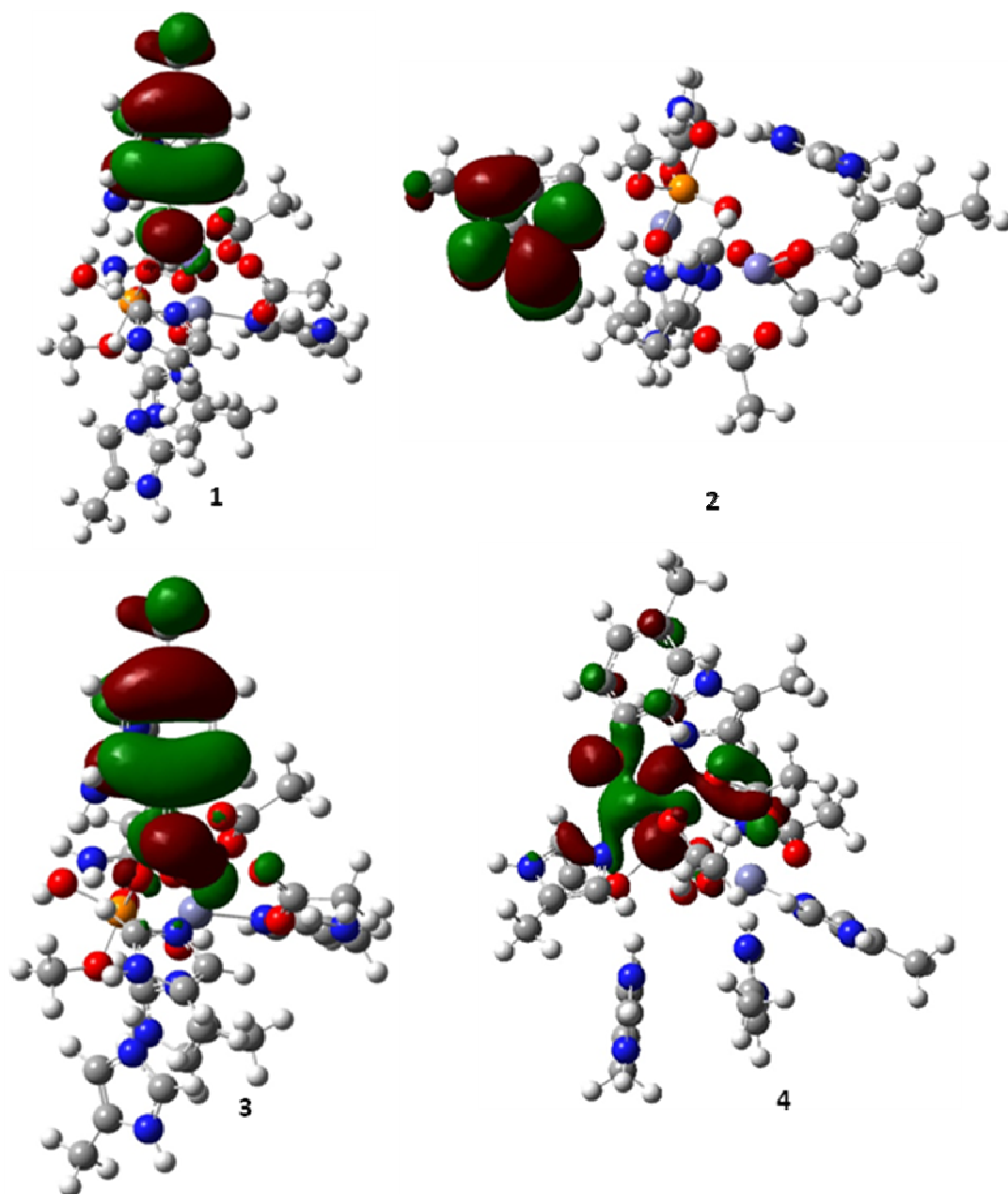


Figure S3(c). Molecular orbital picture for INT₁ geometry; 1) α HOMO 2) α LUMO 3) β HOMO
4) β LUMO

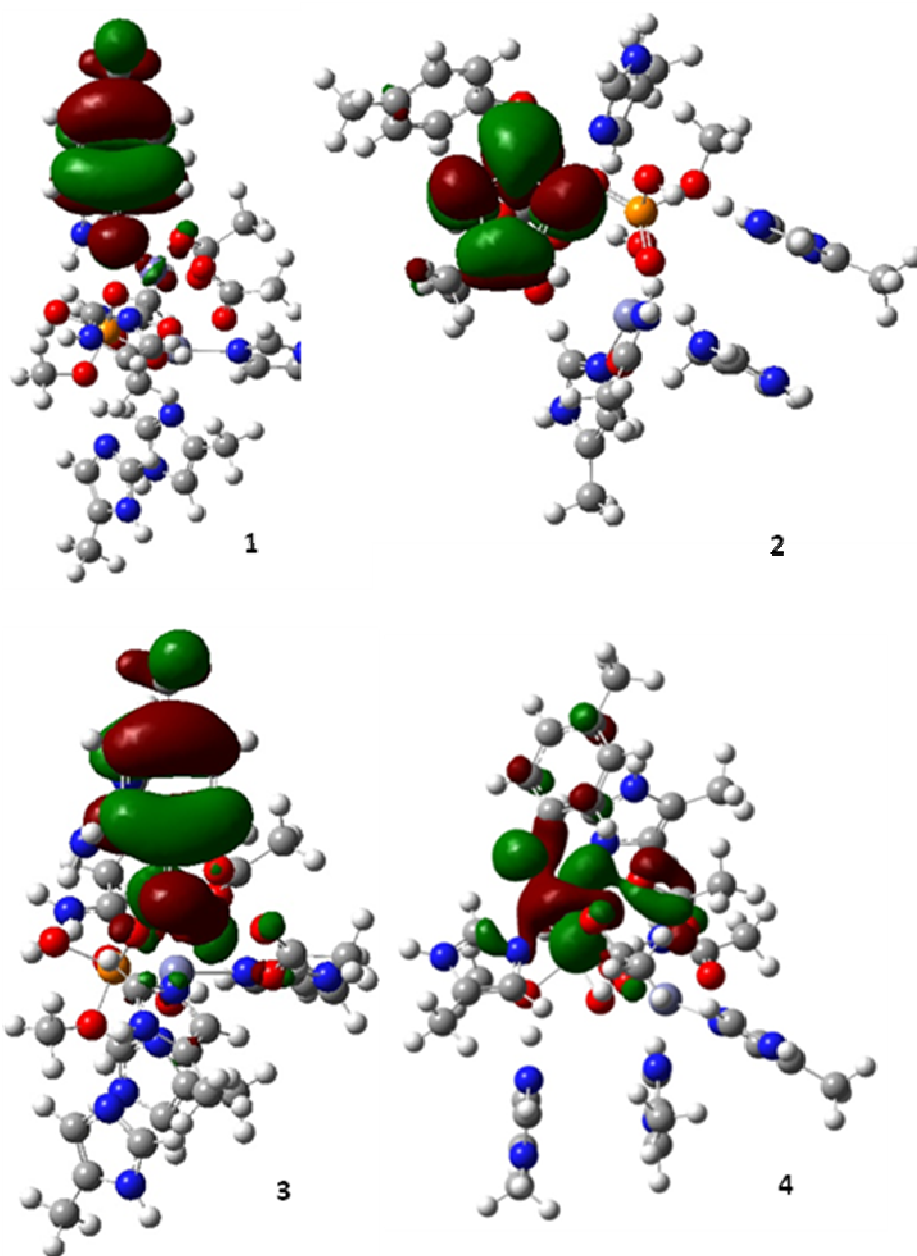


Figure S3(d). Molecular orbital picture for TS_1 geometry; 1) α HOMO 2) α LUMO 3) β HOMO
4) β LUMO

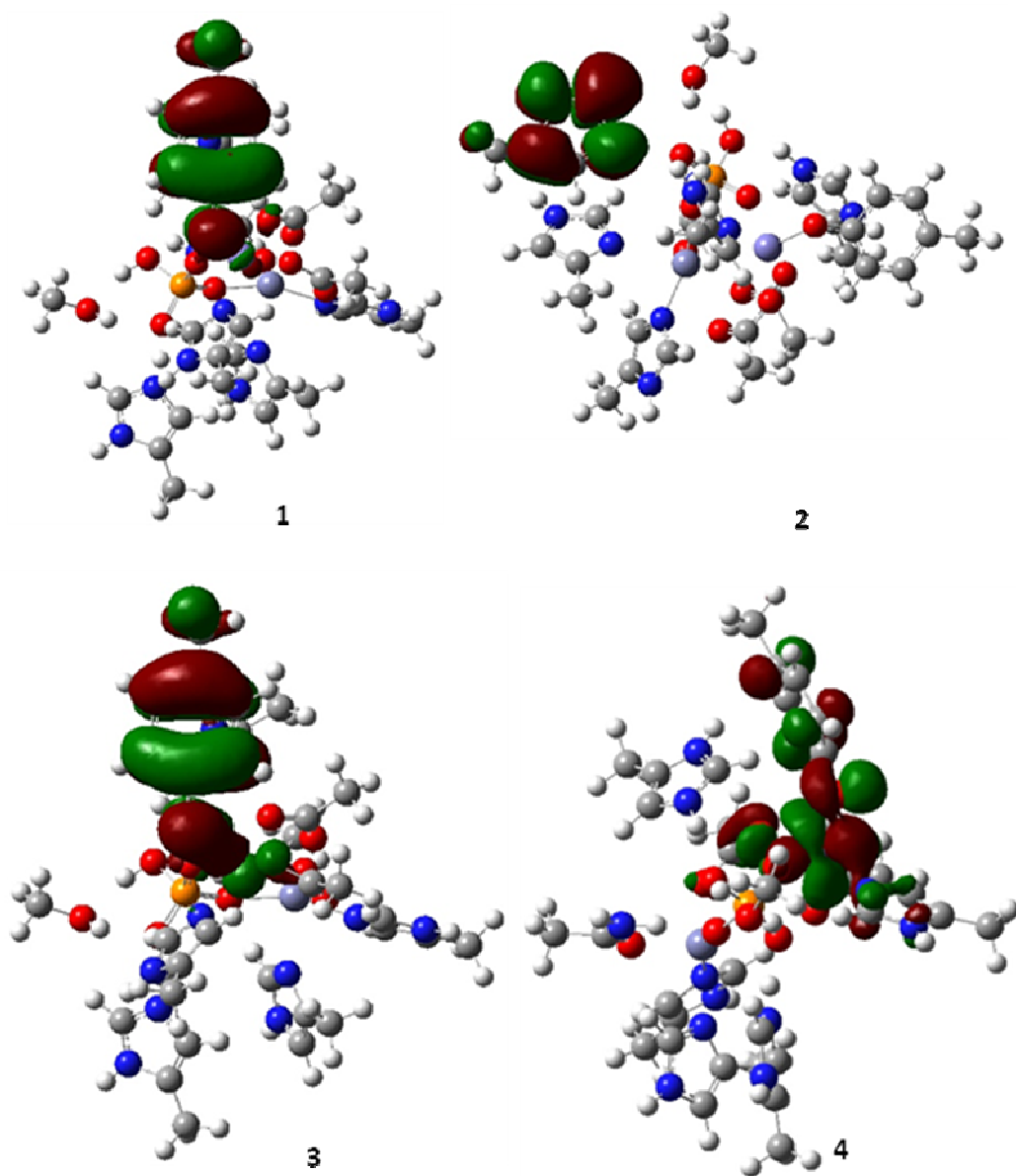
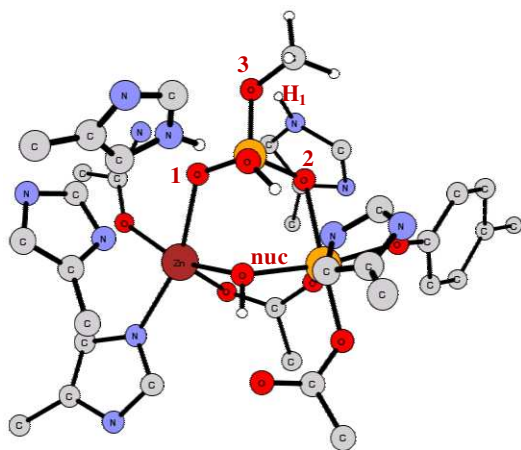


Figure S3(e). Molecular orbital picture for EP geometry; 1) α HOMO 2) α LUMO 3) β HOMO 4) β LUMO

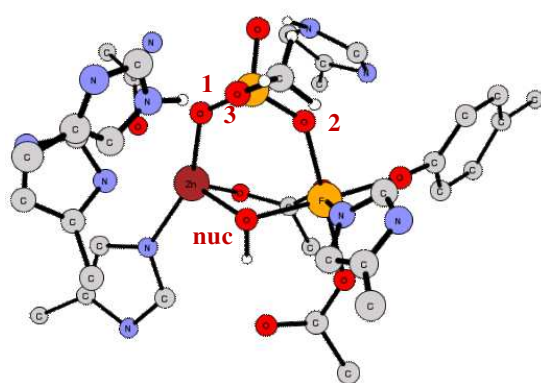
Optimized structure and selected geometrical parameters of the ES complex using Model (b)



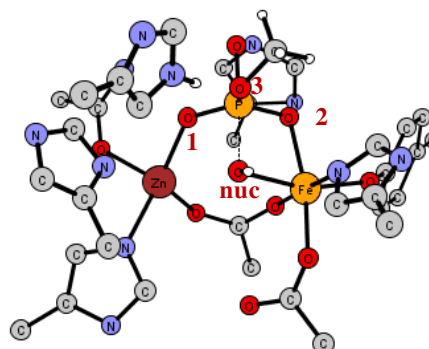
ES

Model (b)	ES
<i>Zn-O₁</i>	2.24
<i>Fe-O₂</i>	2.17
<i>Zn-Onuc</i>	2.04
<i>Fe-Onuc</i>	2.03
<i>P-Onuc</i>	2.94
<i>Fe-Zn</i>	3.65
<i>O₃-H₁</i>	2.47

Model (a) - $\text{CH}_3\text{OPO}_3^{2-}$ substrate-

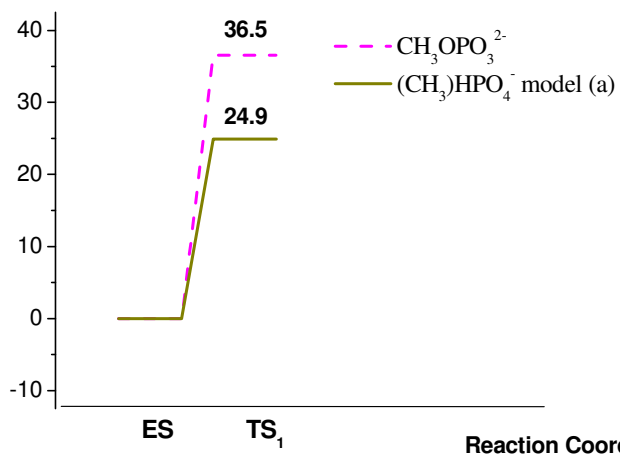


ES



TS₁

imaginary frequency (88.3 cm⁻¹)



$\text{CH}_3\text{OPO}_3^{2-}$	ES	TS ₁
<i>Zn-O₁</i>	2.09	1.95
<i>Fe-O₂</i>	2.07	2.04
<i>Zn-Onuc</i>	2.01	2.72
<i>Fe-Onuc</i>	2.00	2.18
<i>P-Onuc</i>	3.30	1.99
<i>Fe-Zn</i>	3.51	4.08
<i>O₃-H₁</i>	1.51	1.58

Paper VIII

“Can human prolidase enzyme use different metals for
full catalytic activity ?”

Marta E. Alberto, Monica Leopoldini and Nino Russo

submitted

Can human prolidase enzyme use different metals for full catalytic activity?

*Marta E. Alberto, Monica Leopoldini, Nino Russo**

Dipartimento di Chimica and Centro di Calcolo ad Alte Prestazioni per Elaborazioni Parallele e Distribuite-Centro d'Eccellenza MIUR, Universita' della Calabria, I-87030 Arcavacata di Rende (CS), Italy.

* corresponding author: nrusso@unical.it

Abstract

The catalytic hydrolysis of the Gly-Pro substrate by the bimetallic prolidase active site model cluster has been investigated at the DF/B3LYP level of theory, in order to provide fundamental insights into the still poorly understood mechanism of prolidase catalysis. To date, the majority of prolidasases exhibit metal-dependent activity, requiring two divalent cations such as Zn^{2+} , Mn^{2+} or Co^{2+} for maximal activity. In addition, it has been recently proved the coexistence of two different metal ions in the active site of human prolidase (Zn and Mn) with the protein remaining partially active.

With the purpose to identify which is the most efficient dimetallic centre for the prolidase catalyzed reaction, Zn(II), Co(II) and Mn(II) have been examined as the potential catalytic metals of this enzyme. Furthermore, in order to better elucidate the exact roles played by the metals occupying the site 1 and site 2 positions, the heterobimetallic active site having Zn and Mn cations has been also investigated, considering the two derivatives Mn1-Zn2 and Zn1-Mn2.

The rate-determining step of the hydrolysis reaction is found to be always the nucleophilic addition of the hydroxide ion on the carbonyl carbon of the scissile peptide bond, followed by the less energetically demanding proline-peptide C-N bond scission. The analysis of the involved energy barriers does not enable to indicate clearly the preference of a particular metal rather than another by prolidase enzyme. Instead, we may point out a slightly better behavior of the cobalt containing cluster as far as both tetrahedral formation and its decomposition are concerned, due to a greater

degree of ligands-to-metals charge transfer. The mixed Mn-Zn heterodimetallic clusters appear to be also able to perform the hydrolysis of the Pro-Gly substrate, with a slight preference for the Mn1-Zn2 configuration.

Introduction

Prolidases (EC 3.4.13.9) are metalloenzymes that catalyze the hydrolysis of the imide bond between an α -carboxyl group and a proline or hydroxyproline residue at the C-terminal end. These bonds are not susceptible to generic peptidase cleavage, having proline its side chain cycling back to the backbone amino group and generating a pyrrolidine ring not easy to be hydrolysed.¹ Only a limited number of mammalian peptidases are known to be able to hydrolyse proline adjacent bonds and their activity is influenced by the isomeric state (cis-trans) as well as by the position of proline in the peptide chain. All the known proline-specific peptidases cleave only when the peptide bond preceding proline has trans conformation.^{2,3} Due to its peculiarity, the presence of this aminoacid strongly influences the conformation, properties and biological functions of several molecules such as peptides involved in immunomodulation and coagulation, cytokines, growth factors, neuro- and vasoactive peptides.³ Members of this class have been isolated from different mammalian tissues⁴ as well as from bacteria^{5,6} and archaea (*Pyrococcus furiosus*).⁷ While the physiological role of prolidase in bacteria and archaea is unclear, in humans it is relevant in the latest stage of protein catabolism particularly of those molecules rich in imino acids such as collagens, thus being involved in matrix remodelling. A deficiency of this enzyme in humans causes a recessive connective tissue disorder (prolidase deficiency) characterized by abnormalities of the skin, mental retardation and respiratory tract infections.^{8,9} The enzyme could play also an important role in biotechnological applications. It has a potential use in the dairy industry as a cheese-ripening agent since the release of proline from peptides in cheese reduces bitterness.¹⁰ In addition, it was recently reported¹¹ that prolidase is able to hydrolyze highly toxic, organophosphorus, acetylcholinesterase inhibitors, which include various chemical warfare agents and pesticides and recently it has been used as target enzyme for specific melanoma prodrug activation. Its main activity is Gly-Pro dipeptides hydrolysis,^{5,12,13} although the enzyme is also active against Ala-Pro, Met-Pro, Phe-Pro, Leu-Pro and Val-Pro. In addition, some prolidase proteins were found to be able to cleave dipeptides with proline at the N-terminal end

or dipeptides that do not contain a proline residue.¹³ To date, the majority of prolidases that have been studied exhibit metal-dependent activity, requiring divalent cations such as Zn²⁺, Mn²⁺, or Co²⁺ for maximal activity.^{14,15} They have been purified either as monomers or as dimers depending on the enzyme.¹⁶⁻¹⁸ The best characterized prolidase in terms of structure and catalytic site composition is the one isolated from the archaeon *Pyrococcus furiosus* (Pfp_{prol}) for which the complete structure and active site organization have been described in details by crystallographic and site directed mutagenesis studies, both in native and *E. Coli* recombinant enzyme.¹⁹ The latter displays a 28% identity with human prolidase for which, on the contrary, information on the structure, the organization of the active site and the catalytic mechanism are still lacking. X-ray crystal structure analysis of *P. furiosus* cobalt containing prolidase has identified five amino acids that function as the metal-binding residues in this enzyme. Histidine-284 and glutamate-313 solely bind to the first Co center (Co1), aspartate-209 to the second Co center (Co2), and aspartate-220 and glutamate-327 are ligands to both cobalt cations.^{20,21} The corresponding residues in human prolidase are His371, Glu413, Asp277, Asp288 and Glu453. Interestingly, strong structural homologies among prolidase and other proteins such as methionine aminopeptidases and proline aminopeptidase have been recognized. The dinuclear metal clusters in these enzymes are coordinated by identical sets of residues.¹⁵ Due to these homologies, prolidase, together with methionine aminopeptidase (MetAP)²² and proline aminopeptidase (APPro),²³ becomes a member of a group of enzymes whose most distinctive shared feature is a “pita-bread” fold of the C-terminal catalytic domain and they are suggested to share a common reaction mechanism in which the metals coordinated hydroxide group performs a nucleophilic attack on the carbonyl carbon of the scissile peptide bond.²⁰ The cleavage of the amide bond is provided by a proton shift played by a conserved Glu residue which acts as a proton shuttle, first abstracting an H⁺ from the bridging nucleophile water molecule/hydroxide ion and then transferring it to the nitrogen atom of the substrate (see Scheme 1).¹⁵ Such a role as proton carrier is similar to that proposed for Glu133 in peptide deformylase,²⁴ Glu270 in carboxypeptidase A,^{25,26} Asp120 in β -lactamase²⁷ and Glu106 in carbonic anhydrase.²⁸ Like the human enzyme, Pfp_{prol} is a homodimer with two subunits. Each monomer has a dinuclear metal cluster requiring Co(II) for full activity.²⁰ The enzyme activity could also be supported by the presence of Mn²⁺ as demonstrated by the results concerning the human prolidase synthesized in prokaryotic and eukaryotic hosts. The recombinant

enzyme was found to require Mn(II) for full activity identical to the endogenous human fibroblasts prolidase.²⁹ The effects of various bivalent ions (Ca^{2+} , Mg^{2+} , Cu^{2+} , Fe^{2+} , Ni^{2+}) on prolidase activity were tested in several works, all resulting in lowering the catalytic efficiency. The influence of the Zn(II) ions was also evaluated and it's almost generally accepted in the literature^{4,19,20} that the presence of Zn in the active site significantly reduces prolidase activity. Actually, there are also indirect evidences that in prolidase the binding site is not highly selective against the nature of the bonded divalent ion. A typical case in this respect is represented by prolidase in *Pyrococcus furiosus* (Pfp) for which, during the crystallization process, it was observed that Zn(II) substituted native Co(II) ions,²⁰ supposedly necessary for full enzymatic activity.

In addition, it was recently reported the first experimental evidence for the coexistence of two different metal ions in the active site of recombinant human prolidase (Zn and Mn) with the protein remaining partially active.³⁰ So the Zn(II) cation in the active site seems to lead toward a decreasing of activity although the enzyme preserves a significant activity. The heterobimetallic center could be required for distinct functions either structural or catalytic, or alternatively, catalyzing different steps in a multistep sequence. This kind of enzymes seems to employ the two metals in different functions, thus the positions of the individual metals are crucial in determining the catalytic efficiency. Despite the numerous studies done to characterize prolidase structures, questions remain in regards to the exact roles played by the metals occupying the M1 and M2 positions, and the exact nature of the metal centers. With the purpose of identifying the catalytic metal dication among zinc, cobalt, manganese, we have performed a computational study on the hydrolysis of a Gly-Pro substrate by a dinuclear cluster as a model for the prolidase active site. Furthermore we have considered also the heterobimetallic active site having Zn and Mn cations as the two derivatives Mn1-Zn2 and Zn1-Mn2, in order to better understand the individual roles played by the metallic center.

Methods

The quantum mechanical (QM) studies performed on metalloenzymes use chemical models for the active sites since proteins are macromolecules not possible to be studied on the whole by theoretical methods. Using available X-ray structures, the active site is divided into two parts, the quantum mechanical cluster and the environment, that is the

portion surrounding the catalytic region not involved in catalysis. The quantum mechanical cluster is usually made up by the metal ion and its first coordination sphere, to which some nearby residues recognized as fundamental in catalysis are added. Ligands are represented by the functional part of the side-chains only (imidazole rings for histidines, acetates for aspartates or glutamates). An atom of each amino acidic residue is usually kept frozen at its crystallographic position in order to mimic the steric effects produced by the surrounding protein and to avoid an unrealistic expansion of the cluster during the optimization procedure.³¹ The environment not explicitly included in the quantum cluster has a double steric and electrostatic effect. The first one can be brutally reproduced by fixing some crystallographic positions. The electrostatic effect is introduced assuming it being a homogeneous polarizable medium with a dielectric constant usually chosen to be equal to 4. The active site model cluster used in this work has been built starting from the 2.45 Å X-ray structure of the recombinant human prolidase produced in *E. Coli* (PDB code = 2OKN).³² The cluster is made up by two metallic cations (Zn, Co, Mn) and their first coordination sphere, i.e. four CH₃COO⁻ groups, that mimic the Asp277, Asp288, Glu413 and Glu453, and a methylimidazole ring for the His371 amino acid. Outer sphere residues included in the cluster are Phe227, His256, His378 and Arg451 modeled by methylbenzene, methylimidazole and [CH₃NHC(NH₂)₂]⁺, respectively. Pro-Gly substrate is modeled in the active site according to the binding mode of substrates of enzymes of the same family.³³ All the computations have been carried out with the Gaussian 03 code.³⁴ The hybrid Becke exchange and Lee, Yang and Parr correlation (B3LYP) functional has been used to perform geometry optimization.³⁵⁻³⁸ The 6-31G* basis set has been chosen for the C, N, O, P and H atoms,³⁹⁻⁴² while for the metal the LANL2DZ pseudopotential in connection with the relative orbital basis set,⁴³ has been used. Electronic ground states have been singlet for Zn-, septet for Co-, and undecaplet for Mn-homodimetallic clusters, and sextet for the mixed Zn-Mn ones. Geometry optimization has been followed by frequency calculations, performed on all stationary points of the reaction paths, to evaluate their character as minima or saddle points, and to compute zero point energy corrections, that have been then included in all the relative energy values. Intrinsic reaction coordinate (IRC) calculations^{44,45} have been performed with the aim to confirm that a given transition state connects a particular couple of consecutive minima.

Single point energy calculations using the 6-311++G** basis set have been performed on the B3LYP/6-31G* optimized geometries, and used to build the potential energy surfaces (PESs). The performance of the B3LYP functional in predicting properties of transition metals containing systems is supported by a large number of publications, especially concerning enzymatic catalysis^{24,33,46-53} in which also hydrolysis reactions are involved.^{24,33,48,50-53} Solvent effects have been introduced as single point computations on the optimized gas phase structures in the framework of Self Consistent Reaction Field Polarizable Continuum Model (SCRF-PCM)⁵⁴⁻⁵⁶ in which the cavity is created *via* a series of overlapping spheres, using the PCM approach. The United Atom (UA0) Topological Model applied on the atomic radii of the UFF force field⁵⁷ has been used to build the cavity, in the gas-phase equilibrium geometry. The dielectric constant value $\epsilon = 4$ has been chosen by taking into account the coupled effect of the protein itself and the water medium surrounding the protein, according to previous suggestions.^{24,33,46-53} Natural Bond Orbital (NBO) analysis⁵⁸ has been carried out to determine net charges and some electronic properties.

Results and discussion

➤ *Zn-, Co-, Mn-homodimetallic clusters*

The optimized geometries of the stationary points belonging to the reaction sequence of scheme 1 and referred to the homodimetallic clusters containing Zn, Co and Mn dications, respectively, are presented in the Figure 1. Distances are given without parenthesis for zinc, and in bracket and square parenthesis for cobalt and manganese, respectively. The complex between the enzyme active site and the substrate, ES, is obtained when the Pro-Gly substrate interacts with Me2 metal centre through the glycine amide NH₂ lone pair (Me2-N distances are 2.28, 2.23 and 2.36 Å, for zinc, cobalt and manganese, respectively). The carbonyl oxygen of the substrate seems to do not establish with Me1 any interaction, for all considered metal species (O-Me1 distance is 4.91, 4.95 and 5.22 Å, for zinc, cobalt and manganese, respectively). This is mainly due to the fact that the carbonyl oxygen of the substrate is involved in a strong H-bond with the N δ of His256 residue (1.88 Å for both zinc and manganese, and 1.86 Å for cobalt). The nucleophilic attack by the bridging OH on the substrate carbon atom (TS1) occurs when the O---C distance assumes the critical value of 1.77 (zinc), 1.76 (cobalt) and 1.80 (manganese) Å. Its nature of saddle point is clearly indicated by the

imaginary frequency at 179, 170 and 185 cm^{-1} , for zinc, cobalt and manganese, respectively, whose visual inspection proposes the stretching of $\text{O}_{\text{OH}}-\text{C}_{\text{substrate}}$ bond. The incoming negative charge of the oxygen of the $\text{C}=\text{O}$ bond is stabilized, in addition to the H-bond with the N-H of the His256 residue, by the its coordination to the Me1 centre (at 2.17, 2.11 and 2.20 Å, for Zn, Co and Mn, respectively), as can be seen from the TS1 structure reported in the Figure 1. TS1 evolves into the tetrahedral intermediate INT1, in which the C-OH bond is completely formed at 1.52 Å, for both Zn and Mn, and 1.56 Å, for Co. The OH is involved into a strong H-bond with the oxygen coming from the Glu413 residue (1.78 Å, in all three cases), that has to perform the proton shift from the OH to the intraring nitrogen of the proline, in order to be the C-N bond broken, leading to products. First, the proton moves from the OH to the oxygen of Glu413 residue, through the transition state TS2 (imaginary frequency at 597, 525 and 444 cm^{-1} , for Zn^{2+} , Co^{2+} and Mn^{2+} , respectively). It leads to the INT2 intermediate, in which the Glu413 is protonated and establishes a strong H-bond with the nitrogen of the proline ring, at 1.58 (Zn^{2+}), 1.64 (Co^{2+}) and 1.63 (Mn^{2+}) Å. The coordination bond of Glu413 with the Me1 site is elongated from 2.13, 2.10 and 2.16 Å in the INT1 up to 2.39, 2.37 and 2.38 Å, in the INT2, for zinc, cobalt and manganese, respectively. Protonation of the proline nitrogen by Glu413 occurs through the transition state TS3, in which the $\text{O}_{\text{Glu}}\text{---H}$ and $\text{H}\text{---N}_{\text{proline}}$ bond distances assume the values of 1.13 and 1.44 Å (zinc), 1.13 and 1.47 Å (cobalt), and 1.16 and 1.43 Å (manganese). Visual inspection of the imaginary frequency at 751, 327 and 646 cm^{-1} mainly shows the stretching of these two bonds. The C-N bond results to be quite short (1.57 Å for zinc and manganese, and 1.56 Å, for cobalt) for a transition state in which the nitrogen is being protonated, so that this TS is mainly governed by the motion of the H^+ particle. The next step encountered on the potential energy profile after the TS3 is the final complex between products, EP. Once the intraring nitrogen of proline is protonated by Glu413 in the TS3, the cleavage of the C-N bond occurs simultaneously. In fact, all attempts to localize on the potential energy profile a stationary point characterized by a protonated proline and an intact C-N bond failed. In the EP, the glycine results to be bound to both the metals through one oxygen of the carboxylic group (Me1-O and Me2-O distances are 2.05 and 2.13 Å (zinc), 2.18 and 2.03 Å (cobalt), and 2.23 and 2.13 Å (manganese)), and to the Me2 site with the NH_2 (2.29, 2.30 and 2.41 Å, for zinc, cobalt and manganese, respectively). Proline instead is hydrogen bound to the Glu413 residue at 2.31, 2.06 and 2.21 Å, for zinc, cobalt and

manganese, respectively. The Potential Energy Surfaces (PESs) for the hydrolysis in the protein like environment of the Pro-Gly substrate by the prolidase model cluster are reported in Figure 2, for zinc (black line), cobalt (red line) and manganese (blue line).

The energy cost (TS1) to pass from the initial ES complex to the tetrahedral intermediate INT1 is computed to be 13.1, 11.1 and 10.8 kcal/mol, for the Zn^{2+} , Co^{2+} and Mn^{2+} , respectively. These values indicate that the nucleophilic attack that seems to determine the reaction kinetics proceeds with a reasonable rate for all dications. The INT1 is found to be isoenergetic with the TS1 stationary point in all examined cases, along the potential energy profile. TS2 relative energy is 20.5, 18.2 and 19.8 kcal/mol, and therefore the energy barrier to pass from INT1 to INT2, the latter found at 20.3, 19.1 and 18.0 kcal/mol, is computed to be 7.4, 6.6 and 8.9 kcal/mol, for the Zn^{2+} , Co^{2+} and Mn^{2+} , respectively. TS3 lies at 19.7, 18.6 and 23.4 kcal/mol with respect to the ES reference, so that the last step requires a barrier of 5.4 kcal/mol in the case of manganese containing cluster, whereas for zinc and cobalt it has a negative barrier. The slightly negative barrier predicted for zinc and cobalt clusters is mainly due to the well known B3LYP/DFT underestimation of barriers especially concerning H transfer processes,⁵⁹ i.e. if the reaction barrier is very low, reactions are sometimes found to be barrierless or even have a negative barrier. This does not change our conclusions that this last step occurs very easily in the case of Zn(II) and Co(II) metals. The final complex EP between the enzyme active site and the glycine and proline products is found at 5.9, 1.8 and 8.0 kcal/mol above the reactants ES, in the case of Zn(II), Co(II) and Mn(II). Thus, the catalyzed reaction results to be thermoneutral in the case of cobalt cation and slightly thermodynamically unfavoured for Zn^{2+} and Mn^{2+} (Figure 2).

All the examined divalent metals appear to well perform the tetrahedral intermediate formation in the hydrolysis reaction of Pro-Gly substrate. The second step in the catalysed reaction, i.e. the protonation of the proline amide nitrogen and thus the collapse of the tetrahedral intermediate into products, seems to proceed very easily for zinc and cobalt. Manganese cluster indeed requires a certain amount of energy to perform this last step. The analysis of the involved energy barriers for all the studied cases does not enable to indicate clearly the preference of a transition metal rather than another by prolidase enzyme. Instead, we may point out a slightly better behavior of the cobalt containing cluster as far as both tetrahedral formation and its decomposition are concerned.

Additionally, zinc cation in the active site seems to be also able to perform Pro-Gly hydrolysis, departing from the experimental suggestions indicating that the presence of Zn in the active site significantly reduces prolidase activity. In the Table 1, the natural charges obtained through NBO analysis are collected for all the stationary points encountered on the potential energy profiles of the Zn-, Co- and Mn-containing clusters. The natural charges exhibited by the metals in all the seven stationary points indicate that in the case of cobalt, a certain charge transfer from ligands to cation seems to occur. For example, in the Co-ES species, natural charges on site 1 and 2 are 1.141 and 1.156 |e|. The charge transfer seems to occur mainly from the bridging OH (-1.107 |e|) and from the oxygen atom of the Glu413 residue, directly coordinated to the Co1 (-0.782 |e|). This charge distribution is retained from the beginning to the end of the reaction (see Table 1). In the Zn and Mn containing clusters, this behavior is less pronounced. By taking again the first species encountered as reference, the charges on Zn1 and Zn2, and Mn1 and Mn2 are 1.435 and 1.433 |e|, and 1.577 and 1.576 |e|, respectively. This situation results in a natural charge on the oxygen atoms of the OH and of the Glu413 ligands of -1.268 and -0.826 |e|, and -1.278 and -0.848 |e|, in the case of Zn²⁺ and Mn²⁺, respectively. Ligands-to-metals charge transfer seems to be responsible for the slightly better performance of the cobalt cation as compared to zinc and manganese ions. The results support the reaction mechanism reported in the Scheme 1, involving the OH attack on substrate and the protonation of amide nitrogen by Glu/Asp residue, usually established for the metallohydrolases class of enzymes. However, prolidase seems to be to some extent different from the other peptidases, as far as the decomposition of the tetrahedral intermediate is concerned. In fact, most of computational studies^{24,33,51,52} have generally predicted a single step reaction path for the reactions catalyzed by these enzymes, that is once the nucleophilic addition takes place, the collapse into products occurs very easily without further energy cost. This has been found for peptide deformylase,²⁴ methionine aminopeptidase,³³ thermolysin,⁶⁰ insulin-degrading enzyme (IDE).⁵² The presence of the five-membered pyrrolidine ring causes a lesser reactivity of the amide nitrogen towards protonation, as well as a steric effect on the interaction of the substrate with the enzyme, leading to a relatively low amount of energy for the tetrahedral intermediate decomposition, through proton shift performed by glutamate residue.

➤ *Zn-Mn heterodimetallic clusters*

In a recent study on recombinant human prolidase produced in *E. Coli*,³⁰ it has been established the first experimental existence that two different kinds of metals, Mn and Zn, can be simultaneously present in the active site, with the protein maintaining its catalytic activity. Actually, there are also some evidences that in prolidase the binding site is not highly selective against the nature of the bonded divalent ion. A typical case in this respect is prolidase from *Pyrococcus furiosus* where in the crystal Zn(II) substitutes Co(II), supposedly necessary for full enzymatic activity.²⁰ Even in the presence of over-concentrated Zn(II) ions, the protein partially retains its enzymatic activity if at least one out of the four metal binding sites in the dimeric protein is occupied by a Mn(II) ion.³⁰ The optimized geometries of the stationary points belonging to the reaction sequence of scheme 1 and referred to the heterodimetallic clusters containing Zn and Mn dications at both sites 1 and 2, are presented in the Figure 3. The two clusters are indicated as Zn1-Mn2 and Mn1-Zn2, depending on the occurrence of the metal at site 1, characterized by the His ligand, and site 2. Distances are given without and with parenthesis, for Mn1-Zn2 and Zn1-Mn2 clusters, respectively. Substrate approaches the active site through glycine NH₂ coordination to Me2 (at 2.27 and 2.36 Å, for the Mn1-Zn2 and Zn1-Mn2 clusters, respectively). No interaction is found between the substrate carbonyl oxygen and the Me1 (distances are 4.88 (Mn1-Zn2) and 5.12 (Zn1-Mn2) Å), being the oxygen involved into a strong H-bond with Nδ of the His256 aminoacid (see Figure 3). The O_{OH} and C_{substrate} distances assume the values of 3.27 and 3.38 Å, whereas the bridging OH is hydrogen bonded to the Glu413 at 2.25 and 2.18 Å, as far as the Mn1-Zn2 and Zn1-Mn2 clusters are concerned. Both metals appear to be five coordinated in both the two configurations. The optimized transition state (TS1) structures for nucleophilic attack by the OH shows a critical distance for the O--C bond of 1.78 and 1.77 Å, for the Mn1-Zn2 and Zn1-Mn2 clusters, respectively. As a consequence, the substrate carbonyl oxygen interacts with the site 1, also thanks to its incoming increased negative charge, at 2.20 (Mn1-Zn2) and 2.17 (Zn1-Mn2) Å. It receives a H-bond from His256, of length of 1.75 Å in both cases. Hessian calculations show one imaginary frequency at 181 and 182 cm⁻¹, for the Mn1-Zn2 and Zn1-Mn2, respectively, and it corresponds to the reaction coordinate describing the C-O bond formation. After the TS1, the tetrahedral intermediate INT1 originates. It shows a C-O_{OH} σ bond of 1.53 and 1.51 Å, a O--Me1 coordination bond of 2.10 and 2.04 Å, and a H-bonding interaction between the Glu413

and the bridging OH of 1.79 and 1.77 Å, in the case of the Mn1-Zn2 and Zn1-Mn2, in the order. The hydroxyl group is now not a ligand at the site 1 (distances are 2.53 and 2.61 Å) whereas it is retained at the site 2 in both cases. The OH group is being deprotonated through the transition state TS2, characterized by an imaginary frequency at 375 and 436 cm⁻¹ corresponding to the normal mode associated to the H⁺ shift from the OH to the oxygen of the Glu413 residue. A neutral Glu413 is found in the next optimized intermediate INT2. The oxygen of the initial OH is again bridging the two metals because of its increased negative charge, at 2.17 and 2.04 Å, and at 2.10 and 2.06 Å, for sites 1 and 2, as far as the two Mn1-Zn2 and Zn1-Mn2 clusters are involved. Proline nitrogen with an approximately sp³ hybridization is interacting with the Glu413 through a H-bond whose length is found to be 1.64 (Mn1-Zn2) and 1.61 (Zn1-Mn2) Å. Through the transition state TS3 (imaginary frequency at 192 and 283 cm⁻¹) protonation of the proline nitrogen occurs. Visual inspection of the vibrational normal mode provides the stretching of the O_{Glu}--H and H--N_{pro} couple of bonds, whose critical distances are 1.11 and 1.51 Å, and 1.12 and 1.48 Å, respectively, as far as the Mn1-Zn2 and Zn1-Mn2 configurations are concerned. As occurred in the case of the homometallic cluster, the C-N bond in the substrate is quite short (1.56 Å in both cases), indicating again that this saddle point is mainly governed by the proton shift rather than by the C-N bond rupture. Finally, the complex between products, EP, is identified along the reaction profile. Glycine is bound at the active site with the NH₂ group at the site 2, at 2.35 Å in both cases, and with the carboxylic oxygen at both sites (Me1--O and Me2--O distances are 2.20 and 2.07 Å, and 2.08 and 2.28 Å, for the Mn1-Zn2 and Zn1-Mn2, respectively). Proline remains in the active site by establishing a hydrogen bonding interaction with Glu413 at 2.11 (Mn1-Zn2) and 2.16 (Zn1-Mn2) Å.

The Potential Energy Surfaces (PES) in the protein like environment for the Mn1-Zn2 and Zn1-Mn2 clusters are illustrated in the Figure 4, as black and red line, respectively. The nucleophilic attack occurs with a very feasible energy barrier, of 11.3 and 13.8 kcal/mol, and it leads to the intermediate INT1 lying at 11.6 and 14.4 kcal/mol, as far as Mn1-Zn2 and Zn1-Mn2 clusters are concerned. TS2 relative energy is computed to be 18.4 and 19.9 kcal/mol, so that an energy cost of 6.8 and 5.5 kcal/mol (computed with respect to the INT1 species), for the Mn1-Zn2 and Zn1-Mn2 clusters, respectively, is required. INT2 is found at 17.3 (Mn1-Zn2) and 19.9 (Zn1-Mn2) kcal/mol along the PES. The last transition state TS3 relative energy is 17.5 and 20.4 kcal/mol, so that INT2 → TS3 conversion seems to occur very easily. Products EP

are isoenergetic with respect to the reference ES (-0.4 and 0.2 kcal/mol), so reaction appears to be again quite thermoneutral. The overall energy diagrams show some differences in energetics between the models. Particularly, the Zn1-Mn2 potential energy profile lies slightly over the one of the Mn1-Zn2 cluster. A look at the natural charges of the stationary points, reported in the Table 2, indicates again a correlation between the better performance and the charge transfer from ligands to metals, occurring in the Mn1-Zn2 cluster rather than in the Zn1-Mn2 one. Mn when presents at the site 1 exhibits an average natural charge of ≈ 1.434 |e| whereas Zn at the site 2 has a natural charge of ≈ 1.234 |e|. Ligands responsible for this charge transfer are the nucleophile OH and the site 1 coordinated Glu413 oxygen atom. In the case of the Zn1-Mn2 cluster, indeed, the charges exhibited by the two metals are, as average values, 1.739 and 1.573 |e|. at sites 1 and 2, respectively. Mn and Zn substitution reveals the role of the metal positions in the catalysis. Site 1 seems to be involved in the first step of the reaction, that is the nucleophilic addition on the substrate carbonyl carbon, since Mn \rightarrow Zn substitution at this position entails an increase in the energy barrier of 2.5 kcal/mol and also a destabilization of the INT1 of 2.8 kcal/mol. Site 2 indeed is implicated in the collapse of the tetrahedral intermediate into the products. In fact, Zn \rightarrow Mn replacement entails slightly higher energies in this step of the reaction. The PESs obtained with the heterodimetallic clusters are also very feasible. The contemporaneous presence of Mn and Zn at the active site at both sites in fact gives two clusters that are able to perform the hydrolysis of the Pro-Gly substrate, with a slight preference for the Mn1-Zn2 configuration.

Conclusions

In this paper, the catalytic mechanism of the prolidase, a bimetallic enzyme involved in the hydrolysis of iminodipeptides containing a proline or hydroxyproline residue at the C-terminal end, has been investigated through DFT methods.

The model cluster used to simulate the active site of the enzyme, made up by 121 atoms, has been large enough to reliably reproduce the hydrolysis of the Pro-Gly model for the substrate.

Three metal cations, Zn, Co and Mn have been examined as probable catalytically active cations.

The simultaneous presence of two different kinds of metals (Mn and Zn) in the active site has been also examined.

On the basis on the obtained results, we can summarize the following conclusions.

Independently of the particular divalent metal, the hydrolysis reaction is made up by two steps, the nucleophilic addition by the metals-bridging hydroxide ion on the peptide carbonyl carbon atom, leading to a tetrahedral intermediate. Protonation of the proline nitrogen in this intermediate, performed by the Glu413 residue, entails the release of the two products, glycine and proline.

The rate-determining step may be identified in the nucleophilic attack step. The protonation step seems to require lower energies in all examined cases.

The proposed role of the Glu413 aminoacid in the active site as a proton shuttle is also confirmed.

Obtained potential energy profiles for the homodimetallic clusters containing zinc, cobalt and manganese seem to be very feasible in all three cases, with very small differences in energetics. A clear dependence of the catalytic activity on a particular transition metal is not revealed.

A slightly better performance of the cobalt containing cluster appears to be associated to the occurrence of a charge transfer from ligands to metals, not observed for zinc and manganese divalent metals.

The simultaneous presence in the active site of two different kinds of metals, Mn and Zn, reveals the role of the metal positions in the catalysis. Site 1 seems to be involved in the first step of the reaction, that is the nucleophilic addition on the substrate carbonyl carbon, since Mn \rightarrow Zn substitution at this position entails a slight increase in the energy barrier. Site 2 indeed is implicated in the collapse of the tetrahedral intermediate into the products, because Zn \rightarrow Mn replacement entails slightly higher energies in this step of the reaction. However, also these clusters are able to perform the hydrolysis of the Pro-Gly substrate, with a slight preference for the occurrence of Mn at site 1 and Zn at site 2.

Results obtained in this study reveal that prolidase catalytic activity seem to be not highly selective against the nature of the bonded divalent ion. Prolidase may incorporate in the active site different metals, depending on the ambient levels of ions within the organism, and fully perform the hydrolysis of Xaa-Pro substrates.

Acknowledgments

The University of Calabria and MIUR (PRIN 2008) are gratefully acknowledged for financial support.

References

- (1) Myara, I.; Charpentier, C.; Lemonnier, A. *Life Sci.* **1984**, *34*, 1985–1998.
- (2) Vanhoof, G.; Goossens, F.; De Meester, I.; Hendriks, D.; Scharpe, S. *FASEB J.* **1995**, *9*, 736–744
- (3) Yaron, A.; Naider, F. *Crit. Rev. Biochem. Mol. Biol.* **1993**, *28*, 31–81.
- (4) Royce, P.M.; Steinmann, B. Royce PM & Steinmann B, eds, **2002**, pp. 727–743. Wiley-Liss, New York.
- (5) Fernandez-Espla, M. D.; Martin-Hernandez, M. C.; Fox, P. F. *Appl. Environ. Microbiol.* **1997**, *63*, 314–316.
- (6) Suga, K.; Kabashima, T.; Ito, K.; Tsuru, D.; Okamura, H.; Kataoka, J.; Yoshimoto, T. *Biosci. Biotechnol. Biochem.* **1995**, *59*, 2087–2090.
- (7) Ghosh, M.; Grunden, A. M.; Dunn, D. M.; Weiss, R.; Adams, M. W. *J. Bacteriol.* **1998**, *180*, 4781–4789.
- (8) Forlino, A.; Lupi, A.; Vaghi, P.; Icaro Cornaglia, A.; Calligaro, A.; Campari, E.; Cetta, G. *Hum. Genet.* **2002**, *111*, 314–22.
- (9) Endo, F.; Tanoue, A.; Hata, A.; Kitano, A.; Matsuda, I. *J. Inherited Metab. Disease* **1989**, *12*, 351–354.
- (10) Bockelmann, W. *Int. Dairy J.* **1995**, *5*, 977–994.
- (11) Cheng, T. C.; Harvey, S. P.; Chen, G. L. *Appl. Environ. Microbiol.* **1996**, *62*, 1636–1641.
- (12) Browne, P.; O’Cuinn, G. *J. Biol. Chem.* **1983**, *258*, 6147–6154.
- (13) Fujii, M.; Nagaoka, Y.; Imamura, S.; Shimizu, T. *Biosci. Biotechnol. Biochem.* **1996**, *60*, 1118–1122
- (14) Wilcox, D.E. *Chem. Rev.* **1996**, *96*, 2435–2458.
- (15) Lowther, W.T.; Matthews, B.W. *Chem. Rev.* **2002**, *102*, 4581–4608.
- (16) Cunningham, D. F.; O’Connor, B. *Biochim. Biophys. Acta* **1997**, *1343*, 160–186
- (17) Kobayashi, M.; Shimizu, S. *Eur. J. Biochem.* **1999**, *261*, 1–9.
- (18) Yang, S. I.; Tanaka, T. *FEBS J.* **2008**, *275*, 271–280.
- (19) Du, X.; Tove, S.; Kast-Hutcherson, K.; Grunden, A. M. *FEBS Lett.* **2005**, *579*, 6140–6146.
- (20) Maher, M. J.; Ghosh, M.; Grunden, A.M.; Menon, A.L.; Adams, M.W.; Freeman, H.C.; Guss, J.M. *Biochemistry* **2004**, *43*, 2771–2783.

- (21) Willingham, K.; Maher, M. J.; Grunden, A.M.; Ghosh, M.; Adams, M.W.; Freeman, H.C.; Guss, J.M. *Acta Crystallogr. D Biol. Crystallogr.* **2001**, *57*, 428–430.
- (22) Roderick, S. L.; Matthews, B. W. *Biochemistry* **1993**, *32*, 3907-3912.
- (23) Wilce, M. C. J.; Bond, C. S.; Dixon, N. E.; Freeman, H. C.; Guss, J. M.; Lilley, P. E.; Wilce, J. A. *Proc. Natl. Acad. Sci., U.S.A.* **1998**, *95*, 3472-3477.
- (24) Leopoldini, M.; Russo, N.; Toscano, M. *J. Phys. Chem. B* **2006**, *110*, 1063-1072.
- (25) Abashkin, Y. G.; Burt, S. K. ; Collins, J. R. ; Cachau, R. E. ; Russo, N. ; Erickson, J. W. In *Metal-Ligand Interactions: Structure and Reactivity* **1996**, N. Russo, D. R. Salahub (Eds), Kluwer, Dordrecht, Nato Science Series, *474*, 1-22.
- (26) Bertini, I.; Luchinat, C. in *Bioinorganic Chemistry*, Bertini, I., Gray, H. B., Lippard, S. J., Valentine, J. S., Eds.; University Science Books: Mill Valley, CA, **1994**.
- (27) Olsen, L.; Anthony, J.; Ryde, U.; Adolph, H. W.; Hemmingsen, L. *J. Phys. Chem. B* **2003**, *107*, 2366-2375.
- (28) Marino, T.; Russo, N.; Toscano, M. *J. Am. Chem. Soc.* **2005**, *127*, 4242-4253.
- (29) Lupi, A.; Tenni, R.; Rossi, A.; Cetta, G.; Forlino, A. *Amino Acids* **2008**, *35*, 739–752.
- (30) Besio, R.; Alleva, S.; Forlino, A.; Lupi, A.; Meneghini, C.; Minicozzi, V.; Profumo, A.; Stellato, F.; Tenni, R.; Morante, S. *Eur. Biophys. J.* **2009**, DOI 10.1007/s00249-009-0459-4.
- (31) Siegbahn, P. E. M.; Blomberg, M. R. A. *Chem. Rev.* **2000**, *100*, 421-437.
- (32) Mueller, U., Niesen, F. H., Roske, Y., Goetx, F., Behlke, J., Buessow, K., Heinemann, U. **2007**, to be published, DOI:10.2210/pdb2okn/pdb.
- (33) Leopoldini, M.; Russo, N.; Toscano, M. *J. Am. Chem. Soc.* **2007**, *129*, 7776-7784.
- (34) Frisch, M. J. et al. Gaussian, Inc., Pittsburgh PA, **2003**.
- (35) Becke, A. D. *J. Chem. Phys.* **1993**, *98*, 5648-5652.
- (36) Lee, C.; Yang, W.; Parr, R. G. *Phys. Rev. B* **1988**, *37*, 785-789.
- (37) Becke, A. D. *J. Chem. Phys.* **1993**, *98*, 1372-1377.
- (38) Becke, A. D. *Phys. Rev. A* **1988**, *38*, 3098-3100.
- (39) Ditchfield, R.; Hehre, W. J.; Pople, J. A. *J. Chem. Phys.* **1971**, *54*, 724-728.
- (40) Hehre, W. J.; Ditchfield, R.; Pople, J. A. *J. Chem. Phys.* **1972**, *56*, 2257-2262.
- (41) Hariharan, P. C.; Pople, J. A. *Mol. Phys.* **1974**, *27*, 209-214.
- (42) Gordon, M. S. *Chem. Phys. Lett.* **1980**, *76*, 163-168.
- (43) Dolg, M.; Wedig, U.; Stoll, H.; Preuss, H. *J. Chem. Phys.* **1987**, *86*, 866-872.
- (44) Gonzalez, C.; Schlegel, H. B. *J. Chem. Phys.* **1989**, *90*, 2154-2161.
- (45) Gonzalez, C.; Schlegel, H. B. *J. Phys. Chem.* **1990**, *94*, 5523-5527.
- (46) Leopoldini, M.; Russo, N.; Toscano, M.; Dulak, M.; Wesoloski, A. T. *Chem. A Eur. J.* **2006**, *12*, 2532-2541.
- (47) Leopoldini, M.; Russo, N.; Toscano, M. *Chem. A Eur. J.* **2007**, *13*, 2109-2117.

- (48) Leopoldini, M.; Marino, T.; Russo, N.; Toscano, M. *Int. J. Quantum Chem.*, **2008**, *108*, 2023-2029.
- (49) Leopoldini, M.; Chiodo, S. G.; Toscano, M.; Russo, N. *Chem. Eur. J.* **2008**, *14*, 8674-8681.
- (50) Leopoldini M.; Marino, T.; Toscano, M. *Theor. Chem. Acc.*, **2008**, *120*, 459-466.
- (51) Leopoldini, M.; Russo, N.; Toscano, M. *Chem. Eur. J.* **2009**, *15*, 8674-8681.
- (52) Amata, O.; Marino, T.; Russo, N.; Toscano, M. *J. Am. Chem. Soc.* **2009**, *131*, 14804-14811.
- (53) Alberto, M. E.; Marino, T.; Ramos, M. J.; Russo, N. *J. Chem. Theory Comput.* **2010**, *6*, 2424-2433
- (54) Miertus, S.; Scrocco, E.; Tomasi, J. *Chem. Phys.* **1981**, *55*, 117-129.
- (55) Miertus, S.; Tomasi, J. *Chem. Phys.* **1982**, *65*, 239-245.
- (56) Cossi, M.; Barone, V.; Commi, R.; Tomasi, J. *Chem. Phys. Lett.* **1996**, *255*, 327-335.
- (57) Barone, V.; Cossi, M.; Menucci, B.; Tomasi, J. *J. Chem. Phys.* **1997**, *107*, 3210-3221.
- (58) Glendening; E. D.; Reed, A. E.; Carpenter, J. E.; Weinhold, F. *NBO*, version 3.1.
- (59) Ramos, M. J.; Fernandes, P. A. *Acc. Chem. Res.*, **2008**, *41*, 689-698.
- (60) Pelmeshnikov, V.; Blomberg, M. R. A.; Siegbahn, P. E. M. *J. Biol. Inorg. Chem.* **2002**, *7*, 284-298.

Table 1

	Mn-Mn						
	ES	TS1	INT1	TS2	INT2	TS3	EP
O_{nuc}	-1.278	-1.072	-0.926	-1.005	-1.034	-1.023	-0.862
H_{nuc}	0.485	0.519	0.526	0.507	0.522	0.502	0.412
C_{sub}	0.722	0.768	0.753	0.750	0.747	0.752	0.826
O_{sub}	-0.710	-0.902	-0.926	-0.987	-0.992	-0.988	-0.752
N_{sub}	-0.480	-0.554	-0.587	-0.597	-0.631	-0.619	-0.707
O1_{glu}	-0.781	-0.796	-0.792	-0.734	-0.737	-0.740	-0.765
O2_{glu}	-0.848	-0.845	-0.832	-0.734	-0.703	-0.729	-0.867
Mn1	1.577	1.600	1.586	1.579	1.583	1.586	1.590
Mn2	1.576	1.573	1.574	1.572	1.571	1.578	1.579

	Zn-Zn						
	ES	TS1	INT1	TS2	INT2	TS3	EP
O_{nuc}	-1,268	-1,044	-0,904	-0,959	-1,023	-1,015	-0,870
H_{nuc}	0,487	0,526	0,532	0,512	0,524	0,508	0,401
C_{sub}	0,729	0,771	0,756	0,754	0,749	0,753	0,825
O_{sub}	-0,715	-0,893	-0,965	0,980	-0,982	-0,978	-0,704
N_{sub}	-0,480	-0,553	-0,582	-0,591	-0,629	-0,621	-0,702
O1_{glu}	-0,785	-0,791	-0,787	-0,741	-0,742	-0,744	0,764
O2_{glu}	-0,826	-0,821	-0,811	-0,727	-0,666	-0,687	-0,852
Zn1	1,435	1,437	1,433	1,432	1,444	1,444	1,437
Zn2	1,433	1,421	1,416	1,401	1,412	1,412	1,430

	Co-Co						
	ES	TS1	INT1	TS2	INT2	TS3	EP
O_{nuc}	-1,107	-0,948	-0,869	-0,914	-0,895	-0,891	-0,756
H_{nuc}	0,490	0,532	0,538	0,520	0,528	0,511	0,419
C_{sub}	0,729	0,779	0,768	0,763	0,757	0,762	0,834
O_{sub}	-0,714	-0,852	-0,886	-0,902	-0,915	-0,912	-0,701
N_{sub}	-0,482	-0,552	-0,576	-0,587	-0,629	-0,622	-0,726
O1_{glu}	-0,775	-0,789	-0,784	-0,738	-0,743	-0,748	-0,758
O2_{glu}	-0,782	-0,770	-0,763	-0,666	-0,637	-0,657	-0,770
Co1	1,141	1,141	1,143	1,134	1,145	1,146	1,160
Co2	1,156	1,120	1,111	1,090	1,121	1,122	1,127

Table 2

	Mn1-Zn2						
	ES	TS1	INT1	TS2	INT2	TS3	EP
O_{nuc}	-1,210	-1,020	-0,893	-0,972	-0,988	-0,983	-0,820
H_{nuc}	0,490	0,526	0,533	0,515	0,530	0,516	0,417
C_{sub}	0,728	0,775	0,762	0,759	0,750	0,755	0,825
O_{sub}	-0,714	-0,862	-0,920	-0,935	-0,945	-0,943	-0,710
N_{sub}	-0,481	-0,552	-0,582	-0,590	-0,628	-0,623	-0,720
O1_{glu}	-0,784	-0,793	-0,790	-0,731	-0,742	-0,743	-0,762
O2_{glu}	0,794	-0,784	-0,775	-0,686	-0,649	-0,666	-0,796
Mn1	1,428	1,433	1,432	1,428	1,440	1,440	1,435
Zn2	1,268	1,233	1,225	1,205	1,227	1,228	1,252

	Zn1-Mn2						
	ES	TS1	INT1	TS2	INT2	TS3	EP
O_{nuc}	-1.323	-1.081	-0.924	-1.024	-1.065	-1.062	-0.871
H_{nuc}	0.482	0.521	0.525	0.509	0.520	0.508	0.362
C_{sub}	0.725	0.764	0.748	0.745	0.743	0.746	0.824
O_{sub}	-0.714	-0.928	-1.010	-1.022	-1.013	-1.013	-0.776
N_{sub}	-0.480	-0.558	-0.588	-0.595	-0.632	-0.628	-0.704
O1_{glu}	-0.784	-0.797	-0.588	-0.742	-0.740	-0.744	-0.745
O2_{glu}	-0.879	-0.866	-0.856	-0.744	-0.708	-0.728	-0.924
Zn1	1.752	1.744	1.738	1.732	1.727	1.736	1.747
Mn2	1.569	1.570	1.570	1.569	1.567	1.582	1.585

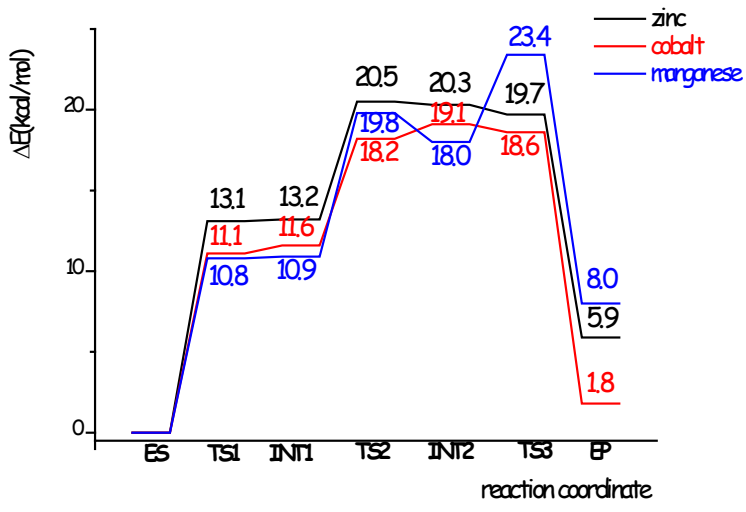


Figure 2

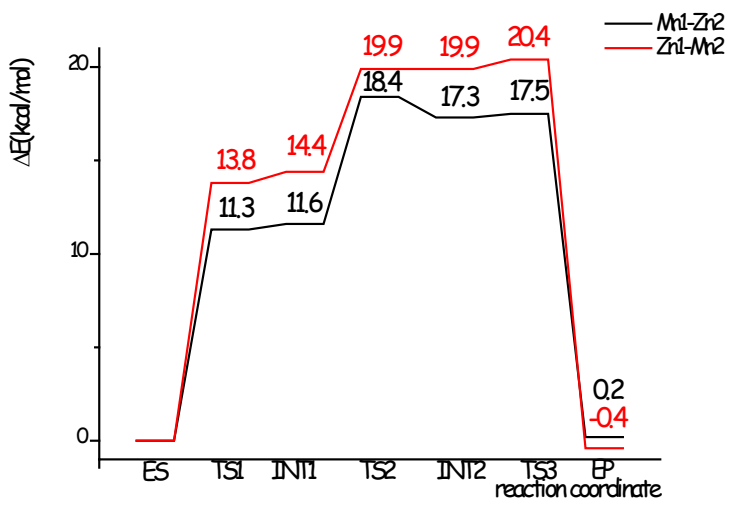
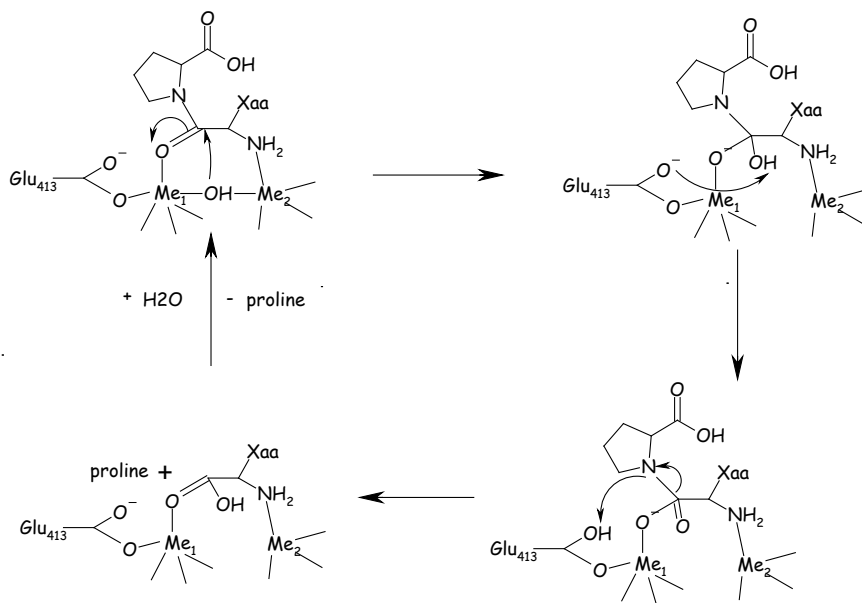
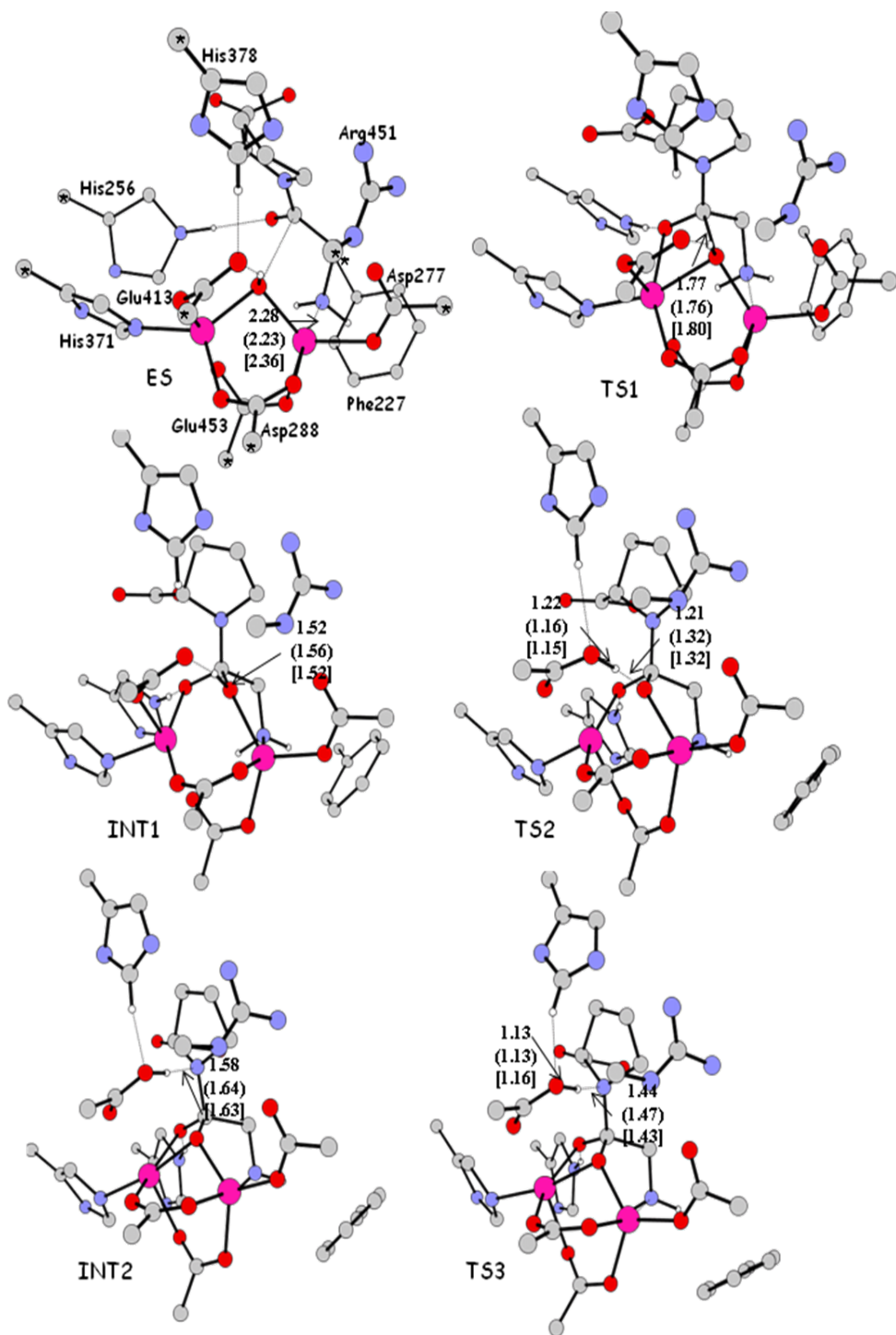


Figure 4



Scheme 1

Figure 1



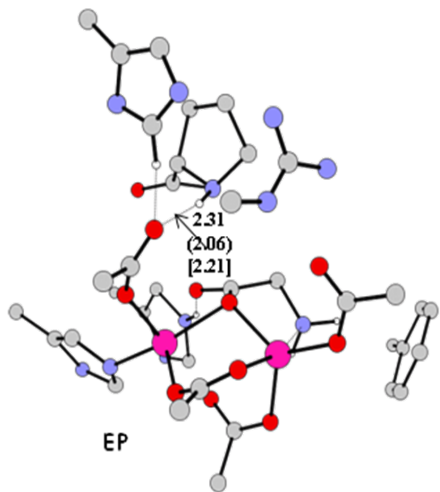
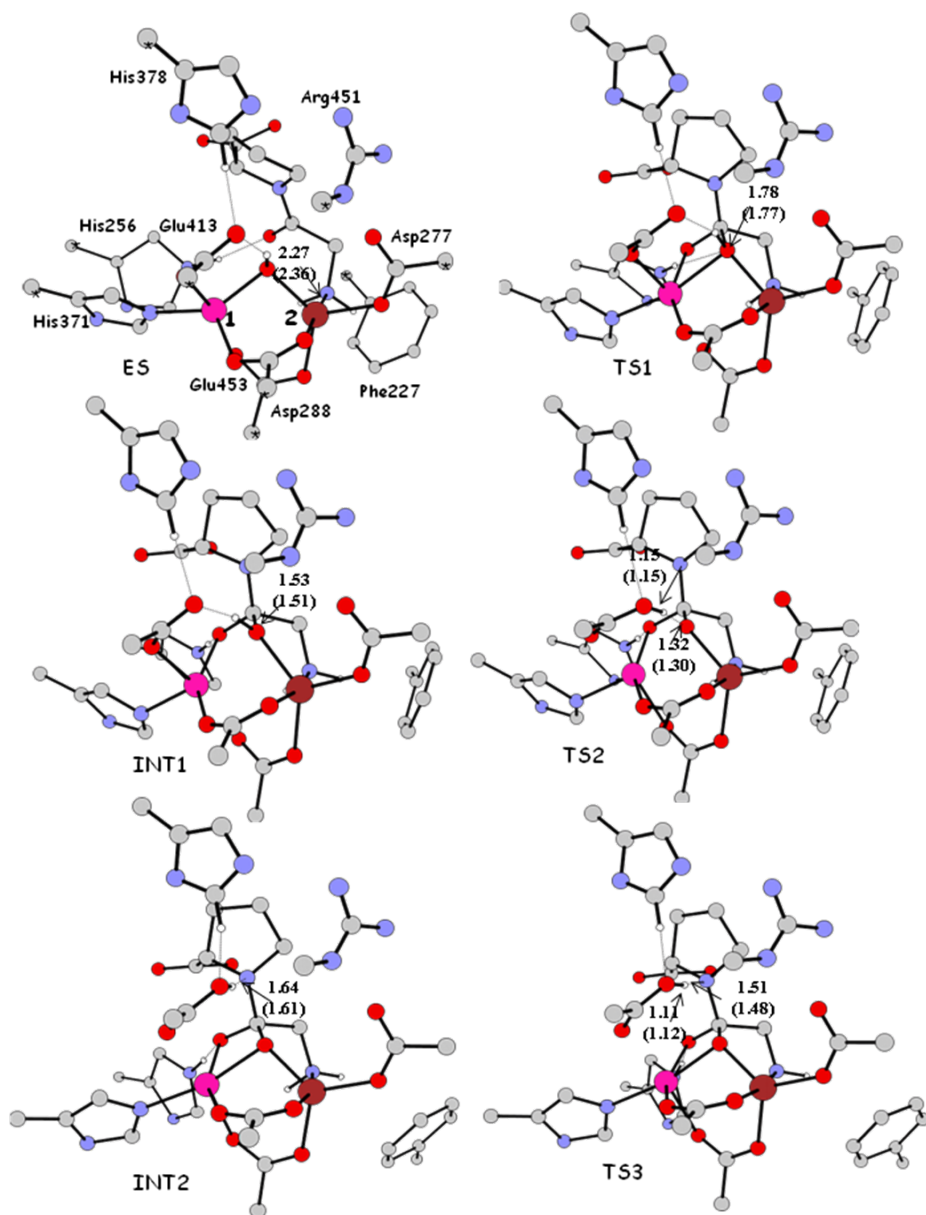
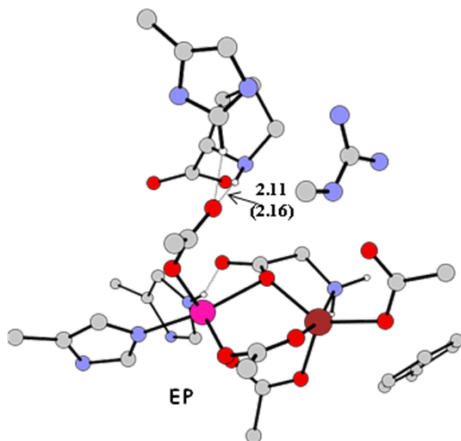


Figure 3





SCHEMES LEGENDS

Scheme 1. Prolidase proposed catalytic mechanism.

FIGURES LEGENDS

Figure 1. B3LYP optimized geometries of the points ES, TS1, INT1, TS2, INT2, TS3, EP. Distances are given without and with bracket and square parenthesis for Zn-Zn, Co-Co and Mn-Mn clusters, respectively.

Figure 2. Potential energy surfaces in the protein like environment for the hydrolysis of Gly-Pro by prolidase, for Zn-Zn (black), Co-Co (red) and Mn-Mn (blue) clusters.

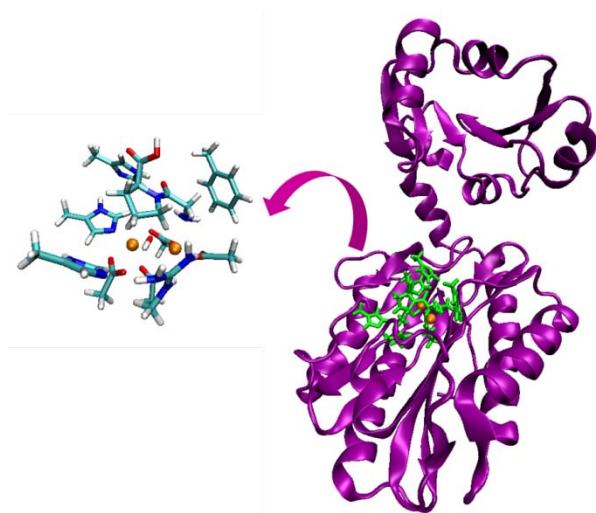
Figure 3. B3LYP optimized geometries of the points ES, TS1, INT1, TS2, INT2, TS3, EP. Distances are given without and with parenthesis, for Mn1-Zn2 and Zn1-Mn2 clusters, respectively.

Figure 4. Potential energy surfaces in the protein like environment for the hydrolysis of Gly-Pro by prolidase, for Mn1-Zn2 (black) and Zn1-Mn2 (red) clusters.

TABLES LEGENDS

Table 1. Atomic net charges (in $|e|$) of the stationary points along the potential energy profile of prolidase, for Zn-Zn, Co-Co and Mn-Mn clusters.

Table 2. Atomic net charges (in $|e|$) of the stationary points along the potential energy profile of prolidase, for Mn1-Zn2 and Zn1-Mn2 clusters.



Synopsis TOC. Human prolidase may use different metal cations in the active site as to catalyse reaction.